



MONASH University

**Multivalent Ligands as Chemical Probes  
for the Investigation of Dopamine D<sub>2</sub>  
Receptor Pharmacology**

Anitha Kopinathan

*B. Med. Chem., B. Pharm. Sci. (Hons)*

A thesis submitted for the degree of Doctor of Philosophy at

Monash University in 2017

Medicinal Chemistry, Monash Institute of Pharmaceutical Sciences

---

## **Copyright notice**

© Anitha Kopinathan (2017).

*I certify that I have made all reasonable efforts to secure copyright permissions for third-party content included in this thesis and have not knowingly added copyright content to my work without the owner's permission.*

---

*“So remember to look up at the stars and not down at your feet. Try to make sense of what you see and wonder about what makes the universe exist. Be curious. And however difficult it may seem, there is always something you can do and succeed at. It matters that you don't just give up.”*

-Stephen Hawking

---

## Table of Contents

<b>Declaration</b> .....	<b>1</b>
<b>Thesis including published works declaration</b> .....	<b>2</b>
<b>Acknowledgements</b> .....	<b>4</b>
<b>Abbreviations</b> .....	<b>6</b>
<b>Abstract</b> .....	<b>9</b>
<b>Chapter 1: General Introduction and Thesis Aims</b> .....	<b>11</b>
Chapter 1.1: Multivalent Approaches and Beyond: Novel Tools for the Investigation of Dopamine D <sub>2</sub> Receptor Pharmacology .....	12
Chapter 1.2: Thesis Aims .....	37
<b>Chapter 2: Probing Efficacy at the Dopamine D<sub>2</sub> Receptor</b> .....	<b>43</b>
Chapter 2.1: Fragmentation of the Antipsychotic Aripiprazole Reveals the 1,2,3,4-Tetrahydroquinolin-2-one Moiety to be the Key Determinant of Efficacy and Affinity for Agonists at the Dopamine D <sub>2</sub> Receptor .....	44
Chapter 2.2: Efforts towards the Investigation of Modulating Efficacy at the Dopamine D <sub>2</sub> Receptor using Extended Structures .....	68
<b>Chapter 3: Probing Allostery at the Dopamine D<sub>2</sub> Receptor</b> .....	<b>105</b>
An SAR Investigation of ‘Next Generation’ Analogues of the Drug-like Dopamine D <sub>2</sub> Receptor Negative Allosteric Modulator SB269652.....	106
<b>Chapter 4: Probing Receptor-Ligand Interactions at the Dopamine D<sub>2</sub> Receptor</b> .....	<b>164</b>
The Development of a Photoactivatable Bitopic Negative Allosteric Modulator for the Dopamine D <sub>2</sub> Receptor .....	165
<b>Chapter 5: Thesis Outcomes and Future Directions</b> .....	<b>197</b>
<b>Appendices</b> .....	<b>203</b>
Chapter 2 Supplementary Information .....	204
Chapter 3 Supplementary Information .....	206
List of Publications, Awards and Conference Presentations.....	211

---

## **Declaration**

I hereby declare that this thesis contains no material which has been accepted for the award of any other degree or diploma at any university or equivalent institution and that, to the best of my knowledge and belief, this thesis contains no material previously published or written by another person, except where due reference is made in the text of the thesis.

Signature:



Print Name: Anitha Kopinathan

Date: 30/06/2017

## Thesis including published works declaration

I hereby declare that this thesis contains no material which has been accepted for the award of any other degree or diploma at any university or equivalent institution and that, to the best of my knowledge and belief, this thesis contains no material previously published or written by another person, except where due reference is made in the text of the thesis.

This thesis includes 1 original paper published in a peer reviewed journal. The core theme of the thesis is Medicinal Chemistry and Drug Discovery Biology. The ideas, development and writing up of all the papers in the thesis were the principal responsibility of myself, the student, working within the Medicinal Chemistry and Drug Discovery Biology Themes under the supervision of Dr Ben Capuano, Dr J. Robert Lane and Prof. Peter Scammells.

The inclusion of co-authors reflects the fact that the work came from active collaboration between researchers and acknowledges input into team-based research.

In the case of 1 my contribution to the work involved the following:

Thesis Chapter	Publication Title	Status (published, in press, accepted or returned for revision, submitted)	Nature and % of student contribution	Co-author name(s) Nature and % of Co-author's contribution	Co-author(s), Monash student Y/N
1	<i>Multivalent approaches and beyond: novel tools for the investigation of dopamine D<sub>2</sub> receptor pharmacology</i>	<i>Published</i>	<i>Primary author of manuscript. Preparation of figures and final manuscript. 85%.</i>	1) <i>J. Robert Lane: Co-author of manuscript, 5%</i>	<i>No</i>
				2) <i>Ben Capuano: Co-author of manuscript, 5%</i>	<i>No</i>
				3) <i>Peter J. Scammells: Co-author of manuscript, 5%</i>	<i>No</i>

---

I have not renumbered sections of published papers in order to generate a consistent presentation within the thesis. Every chapter stands on its own and therefore the numbering of the chemical structures, figures, schemes, tables and references commences in each Chapter from 1.

**Student signature:**



**Date:** 30/06/2017

The undersigned hereby certify that the above declaration correctly reflects the nature and extent of the student's and co-authors' contributions to this work. In instances where I am not the responsible author I have consulted with the responsible author to agree on the respective contributions of the authors.

**Main Supervisor signature:**



**Date:** 30/06/2017

---

## Acknowledgements

Navigating your PhD often requires a great deal of persistence, patience and resilience. When I reflect on how much I've learnt and how far I've come, I know that this would not have been possible without the guidance and support of some important people.

I would like to express my sincere gratitude to my three supervisors Dr Ben Capuano, Dr Robert Lane and Prof. Peter Scammells. Ben thank you for your belief in me way back when I was an honours student, for sharing your chemistry wisdom with me and for all the assistance you've provided me with in the lab (e.g. fixing things out of my reach and opening the occasional bottle) throughout my PhD. Your positive outlook towards research (especially when things do not go as planned, as they so often do), encouragement and meticulous attention to detail have always been qualities that I've admired and appreciated. I also hope these are attributes that I will have as I move forward to my next phase in life. Rob thank you for sharing your wealth of knowledge about the dopamine receptors with me, and for all of your guidance in the pharmacology lab. Your ideas, feedback and expertise in manuscript writing have really enabled me to take my research to a higher level which would have not been possible without your help. Peter thank you for your support and mentorship in all things chemistry-related. Your insights, feedback and encouragement have been sincerely appreciated and have also enhanced my work immeasurably.

To all the members of labs 103/106 and the Scammells Group past and present, thank you for the great memories I have shared with all of you. From conference attendances (in Australia and overseas), trivia nights, postgrad balls, lunchtimes in the sun, and much more. Having the opportunity to trouble-shoot chemistry ideas, or just to have a laugh (or a beer) with you after a stressful day made PhD life easier. To my fellow MedChem PhD cohort thank you for games nights, epic screenings of the Star Wars Trilogy and the many lunch times spent together. My PhD experience would not have been the same without you. To all the post-docs and researchers within the Theme of Medicinal Chemistry, thank you for your advice and friendship. I would like to thank Dr Monika Szabo for the synthesis of the methoxy derivatives mentioned in Chapter 3. Thank you also to Dr Jason Dang, for all your technical support (NMR, HRMS, HPLC and LCMS) and for letting me be privy to all the secret codes for the instruments in the mass-spec lab. I would especially like to thank my friends Kelsang Tara, Monika, Manuela and Natalie for being there throughout this journey with words of advice, encouragement and for all the moral support that you've provided me with over cups of tea/coffee/chai lattes.

There are also a number of PhD students and post-docs in the DDB lab that I would also like to thank. You all made me feel welcome and were always willing to lend a helping hand. I would particularly like to thank members of Team Dopamine: Dr Herman Lim, Chris Draper-Joyce, Dr Carmen Klein Herenbrink and Alastair Keen for all of their assistance in the pharmacology lab, for teaching me how to conduct assays and for helping me trouble-shoot when problems arose. I would like to also thank Chris for conducting the biological testing shown in

---

Chapter 3. To the members of the Halls and Canals groups, thank you for your feedback and suggestions during our combined group meetings.

I would also like to extend my thanks to my PhD panel members: Dr David Chalmers, Dr Meritxell Canals and Prof Jonathan Baell for your advice and input regarding my projects over the course of my PhD.

To all my family and friends, there are far too many of you to name, thank you for all of your love, encouragement and support. I am blessed to have such a vast support network of people who never fail to remind me to enjoy all the little things in life and have always been there when I've needed help.

Last, but by no means least, my utmost heartfelt thanks go to my husband Aaron. You've been by my side through thick, thin and everything in-between. None of this would have been possible without your encouragement and support. Thank you for putting up with my highs and lows throughout the course of this PhD, for being a very thorough first-pass proof reader of my work, for managing to put a smile on my face and for always being there no matter what.

---

## Abbreviations

°C	degrees celcius
µg	microgram
µL	microlitre
µm	micrometre
µM	micromolar
7CN-THIQ	1,2,3,4-tetrahydroisoquinoline-7-carbonitrile
Å	angstrom
AcOH	acetic acid
aq.	aqueous
boc	<i>tert</i> -butyloxycarbonyl
cAMP	cyclic adenosine monophosphate
CHCl <sub>3</sub>	chloroform
CHO	Chinese hamster ovary
CNS	central nervous system
CO <sub>2</sub>	carbon dioxide
CuSO <sub>4</sub>	copper (II) sulfate
d	day
D <sub>2</sub> R	dopamine D <sub>2</sub> receptor
1,2-DCE	1,2-dichloroethane
DCM	dichloromethane
DIBAL-H	diisobutylaluminium hydride
DIPEA	<i>N,N</i> -diisopropylethylamine
DMEM	Dulbecco's modified eagle medium
DMF	<i>N,N</i> -dimethylformamide
DMSO	dimethyl sulfoxide
EDC	<i>N</i> -(3-dimethylaminopropyl)- <i>N'</i> -ethylcarbodiimide hydrochloride
EDTA	ethylenediaminetetraacetic acid
EGTA	ethylene glycol-bis(2-aminoethylether)- <i>N,N,N',N'</i> -tetraacetic acid
EPS	extrapyramidal side effects
eq.	equivalent
Et <sub>2</sub> O	diethylether
EtI	ethyl iodide
EtOAc	ethyl acetate
EtOH	ethanol
FSK	forskolin
g	gram
GPCR	G protein-coupled receptor
h	hour
H <sub>2</sub> O	water
HATU	1-[ <i>bis</i> (dimethylamino)methylene]-1 <i>H</i> -1,2,3-triazolo[4,5- <i>b</i> ]pyridinium 3-oxid hexafluorophosphate
HCl	hydrochloric acid
HCOOH	formic acid
HEPES	2-[4-(2-hydroxyethyl)piperazin-1-yl]ethanesulfonic acid
HOBt	1 <i>H</i> -benzo[ <i>d</i> ][1,2,3]triazol-1-ol
HPLC	high performance liquid chromatography

---

Hz	hertz
I <sub>2</sub>	iodine
K	kelvin
K <sub>2</sub> CO <sub>3</sub>	potassium carbonate
KMnO <sub>4</sub>	potassium permanganate
LCMS	liquid chromatography-mass spectrometry
LiAlH <sub>4</sub>	lithium aluminium hydride
M	molar
<i>m/z</i>	mass-to-charge ratio
MeCN	acetonitrile
MeI	methyl iodide
MeOH	methanol
mg	milligram
MgCl <sub>2</sub>	magnesium chloride
min	minute
mL	millilitre
mm	millimetre
MsCl	methanesulfonyl chloride
Na <sub>2</sub> SO <sub>4</sub>	sodium sulfate
NaBH(OAc) <sub>3</sub>	sodium triacetoxyborohydride
NaCl	sodium chloride
NaH	sodium hydride
NaHCO <sub>3</sub>	sodium bicarbonate
NaI	sodium iodide
NAM	negative allosteric modulator
NaOH	sodium hydroxide
NH <sub>3</sub>	ammonia
NH <sub>4</sub> Cl	ammonium chloride
nm	nanometre
nM	nanomolar
NMR	nuclear magnetic resonance
PBS	phosphate-buffered saline
pERK	phosphorylated extracellular signal-regulated kinase
Pet. Spirits	petroleum spirits
PPh <sub>3</sub>	triphenylphosphine
rbf	round bottom flask
rt	room temperature
SAR	structure-activity relationship
sat.	saturated
SCZ	schizophrenia
SEM	standard error of the mean
TBAF	tetra- <i>n</i> -butylammonium fluoride
TBS-Cl	<i>tert</i> -butyldimethylsilyl chloride
TEA	triethylamine
TFA	trifluoroacetic acid
THF	tetrahydrofuran
THIQ	1,2,3,4-tetrahydroisoquinoline
THQ	1,2,3,4-tetrahydroquinolin-2-one

---

TLC	thin layer chromatography
TM	transmembrane helix
$t_R$	retention time
UV	ultraviolet
WT	wild-type

---

## Abstract

The dopamine D<sub>2</sub> receptor (D<sub>2</sub>R) is a G protein-coupled receptor (GPCR) that is strongly implicated in the symptoms of neurological disorders such as schizophrenia (SCZ) and Parkinson's disease. To date, our structural and pharmacological understanding of the D<sub>2</sub>R have generally been restricted to ligands which interact with the orthosteric binding site which is highly conserved amongst aminergic GPCRs. Despite the development of a number of extended (or bitopic) ligands for the D<sub>2</sub>R, our understanding of the pharmacological implications of receptor-ligand interactions at the less structurally-homologous allosteric site is still in its infancy. This thesis explores the utility of multivalent ligands as chemical probes of secondary binding interactions at the D<sub>2</sub>R and their impact upon D<sub>2</sub>R pharmacology.

Chapter 2 demonstrates the use of multivalent ligands for the investigation of the molecular determinants of efficacy at the D<sub>2</sub>R. Sub-chapter 2.1 describes the synthesis and pharmacological evaluation of a series of chemically truncated analogues of aripiprazole, the first FDA-approved D<sub>2</sub>R partial agonist for the treatment of schizophrenia. From this research, it was determined that the 1,2,3,4-tetrahydroquinolin-2-one (THQ) tail of aripiprazole was a key determinant of functional affinity ( $K_A$ ) and efficacy ( $\tau$ ) at the D<sub>2</sub>R. This was confirmed by the synthesis and evaluation of a series of THQ-containing hybrid molecules which showed enhancements in affinity and a trend towards improved efficacy. Subsequently, mutagenesis studies of the D<sub>2</sub>R centred on both aripiprazole and the hybrid molecules revealed that interactions with extracellular residues of transmembrane helices (TMs) 1 and 2 can direct affinity and efficacy at the D<sub>2</sub>R. This work suggested that it may be possible to direct efficacy using differing tail moieties. Consequently, Sub-chapter 2.2 details the synthesis and pharmacological evaluation of a second series of hybrid molecules containing the tail moiety of a high affinity derivative of SB269652, a D<sub>2</sub>R negative allosteric modulator (NAM). This work added further evidence to the notion that the nature of the tail moiety and its positioning within the extracellular regions of the TMs 1 and 2 is able to direct the affinity and efficacy of extended D<sub>2</sub>R structures.

Chapter 3 details the use of multivalent ligands as chemical probes of allostery at the D<sub>2</sub>R. Herein a series of analogues which focussed on the modification to the indole-2-carboxamide tail of SB269652 were synthesised and pharmacologically profiled in a structure-activity relationship (SAR) study of negative cooperativity at the D<sub>2</sub>R. From this research it was evident that negative cooperativity was strongly influenced by the nature of the tail moiety and yielded a suite of compounds with a spectrum of negative cooperativities. This work also led to the discovery of a

---

first-in-class SB269652 analogue (**15e**, Chapter 3) that acts to modulate both dopamine's affinity and efficacy.

Chapter 4 demonstrates the utility of multivalent ligands as irreversible probes for the D<sub>2</sub>R. This chapter outlines the synthesis and pharmacological characterisation of photoactivatable derivatives of SB269652. This study yielded a novel photoactivatable irreversible ligand (**7**, Chapter 4) which may be used for the investigation of bitopic and allosteric receptor-ligand interactions at the D<sub>2</sub>R.

A toolbox of multivalent ligands were synthesised and pharmacologically evaluated to probe a variety of pharmacological parameters at the D<sub>2</sub>R. The work described within this thesis further validates their use in future investigations of the D<sub>2</sub>R.

---

# **Chapter 1**

## General Introduction and Thesis Aims

---

**1.1 Multivalent Approaches and Beyond: Novel Tools for the Investigation of Dopamine D<sub>2</sub> Receptor Pharmacology**

**Anitha Kopinathan**, Peter J. Scammells, J. Robert Lane, Ben Capuano

*Future Medicinal Chemistry*, **2016**, 8 (11), 1349-1372.

## Multivalent approaches and beyond: novel tools for the investigation of dopamine D<sub>2</sub> receptor pharmacology

The dopamine D<sub>2</sub> receptor (D<sub>2</sub>R) has been implicated in the symptomology of disorders such as schizophrenia and Parkinson's disease. Multivalent ligands provide useful tools to investigate emerging concepts of G protein-coupled receptor drug action such as allosteric, bitopic binding and receptor dimerization. This review focuses on the approaches taken toward the development of multivalent ligands for the D<sub>2</sub>R recently and highlights the challenges associated with each approach, their utility in probing D<sub>2</sub>R function and approaches to develop new D<sub>2</sub>R-targeting drugs. Furthermore, we extend our discussion to the possibility of designing multitarget ligands. The insights gained from such studies may provide the basis for improved therapeutic targeting of the D<sub>2</sub>R.

First draft submitted: 15 January 2016; Accepted for publication: 22 March 2016; Published online: 30 June 2016

**Keywords:** allosteric • bitopic • bivalent • D<sub>2</sub>R • designed multiple ligands • dopamine D<sub>2</sub> receptor • multivalent • orthosteric

G protein-coupled receptors (GPCRs) are the largest family of membrane receptor proteins found within the human genome [1]. They are structurally characterized by seven transmembrane (7TM) helices linked by three intracellular and three extracellular loops, and are further clustered into five sub-families based on their sequence homology [2] (Figure 1). GPCRs are important targets in pharmaceutical research given the unrivalled number of physiological processes in which they are involved, and the variety of stimuli to which they respond including, ions, neurotransmitters, peptides and proteins. Therefore, it is not surprising that almost 40% of all commercially available pharmaceuticals target GPCR activity in some manner [3].

The class A (rhodopsin-like) family of GPCRs includes the dopamine receptor family, of which, there are five subtypes (D<sub>1</sub>-D<sub>5</sub>). These five subtypes are further classified into two groups: D<sub>1</sub>-like (D<sub>1</sub> and D<sub>5</sub>) and D<sub>2</sub>-like (D<sub>2</sub>, D<sub>3</sub> and D<sub>4</sub>), based on their excitatory

(G<sub>s</sub>) or inhibitory (G<sub>i/o</sub>) effects on adenylate cyclase (AC). Sequence homology within the transmembrane domains are highly conserved amongst the dopamine receptor subtypes [5]. The D<sub>1</sub>-like receptors have 78% homology, while the D<sub>3</sub> and D<sub>4</sub> receptors share 75% and 53% homology, respectively, with the D<sub>2</sub> receptor [6]. Dopaminergic innervations are predominantly located within the brain and are divided into four major dopaminergic pathways called the mesolimbic, mesocortical, nigrostriatal and tuberoinfundibular pathways. Dopaminergic neurons play a crucial role in executing central nervous system (CNS) functions including movement, reward, sleep, affect, feeding, memory and learning. While in the periphery, dopamine regulates physiological functions such as emesis, hormone regulation, retinal processes, olfaction, cardiovascular and renal functions [7–13]. Historically, dopamine receptors have been of great interest in the study of diseases that affect the CNS. In particular, the dopamine D<sub>2</sub> recep-

Anitha Kopinathan<sup>1,2</sup>,  
Peter J Scammells<sup>1</sup>,  
J Robert Lane<sup>\*2</sup>  
& Ben Capuano<sup>\*\*1</sup>

<sup>1</sup>Medicinal Chemistry, Monash Institute of Pharmaceutical Sciences, Monash University, 381 Royal Parade, Parkville, Victoria, 3052, Australia

<sup>2</sup>Drug Discovery Biology, Monash Institute of Pharmaceutical Sciences, Monash University, 381 Royal Parade, Parkville, Victoria, 3052, Australia

\*Author for correspondence:

[REDACTED]

\*\*Author for correspondence:

[REDACTED]

**FUTURE  
SCIENCE** part of

**fsg**

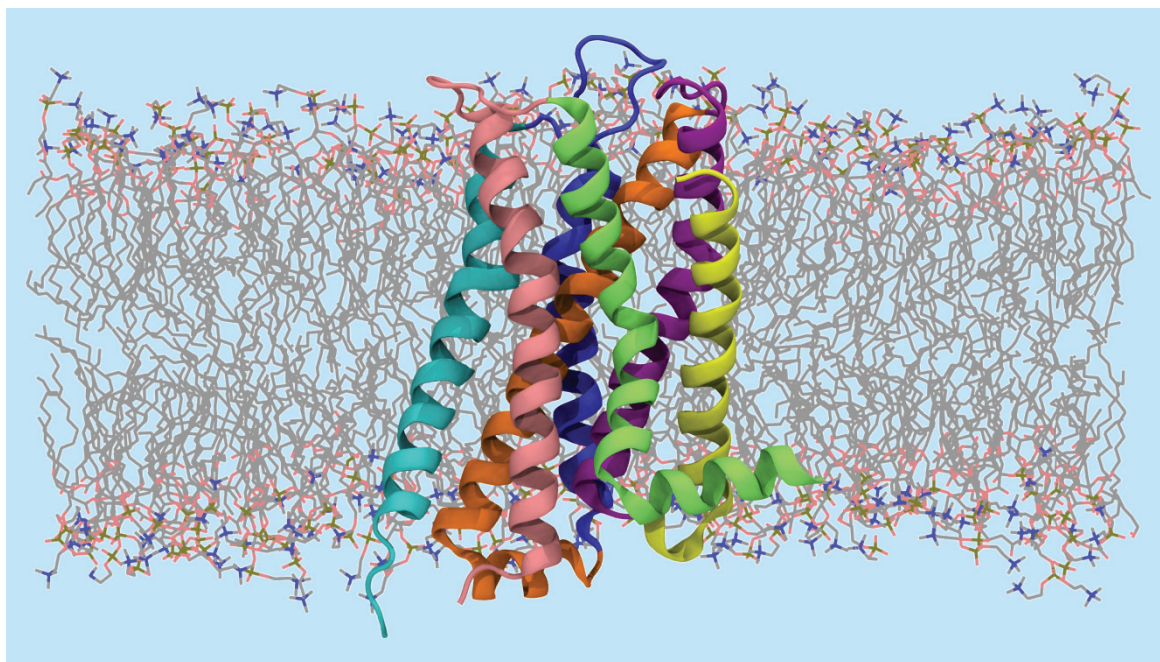


**Figure 1. A crystal structure of the dopamine  $D_3$  receptor highlighting the general structure of a class A G protein-coupled receptor embedded within a lipid bilayer. Seven transmembrane helices are linked by three pairs of intracellular and extracellular loops.**

Data taken from [4].

tor ( $D_2R$ ) is an attractive target for the treatment of the symptoms of schizophrenia (SCZ) and Parkinson's disease (PD) [14–20]. At present,  $D_2R$  antagonists and partial agonists are amongst the most efficacious drugs available for the treatment of SCZ, while  $D_2R$  agonists are primarily used to treat the symptoms of PD.

### Schizophrenia

Early observations of psychostimulant-induced psychoses, and the discovery of nonselective dopamine receptor antagonists (neuroleptics) which alleviated psychoses in SCZ sufferers, led to the hypothesis that the causes of SCZ were attributed to hyperdopaminergic activity in the brain [21]. Further investigations into the underlying cause for the symptoms of SCZ, however, revealed a far more complex and intricate relationship between dopaminergic neurotransmission and the symptoms of the disease state. The notion of 'regional imbalance' has led to the evolution of the dopamine hypothesis whereby, dopamine dysfunction in the brain is implicated in the symptomatology of SCZ without focusing on excessive dopamine transmission as a prime cause of the disease state [21,22]. Subsequently, it has been suggested that hyperdopaminergic activity at the mesolimbic pathway may be responsible for the positive symptoms (i.e., hallucinations, delusions, paranoia), while a hypodopaminergic state in the mesocortical pathway could be attributed to the negative symptoms (i.e., emotional and social withdrawal, blunted affect and motor

retardation) and cognitive deficits (i.e., difficulties with memory and learning) of SCZ [23,24]. Although the dopamine hypothesis addresses the symptomology of SCZ in most cases, there are approximately 30% of sufferers whose symptoms are resistant to treatment with dopamine antagonists [25]. This anomaly has led to the development of alternative hypotheses which implicate different neurotransmitter pathways such as the serotonin [26], glutamate [27] and muscarinic acetylcholine [28] receptors. It has also been proposed that SCZ may be a neurodevelopmental disorder which begins in pre- or peri-natal life and finally manifests itself as psychoses in late adolescence [29]. The number of theories proposed for the symptomology of SCZ, highlights the complexity of this disease state and the obvious need for further research in this field.

The first generation antipsychotics (FGAs) (e.g., haloperidol (**1**) and chlorpromazine (**2**)) are potent  $D_2R$  antagonists that provide sufferers of SCZ relief from the positive symptoms of the disease. Although effective at treating the positive symptoms of SCZ,  $D_2R$  antagonists are also believed to trigger movement disorders (commonly known as extrapyramidal side effects or, EPS), prolactin elevation and neuroleptosis. These side effects are believed to be caused by the indiscriminate antagonism of  $D_2Rs$  at the nigrostriatal, tuberoinfundibular and mesocortical dopaminergic pathways, respectively [30]. The subsequent discovery of second generation antipsychotics (SGAs, e.g., clozapine (**3**))

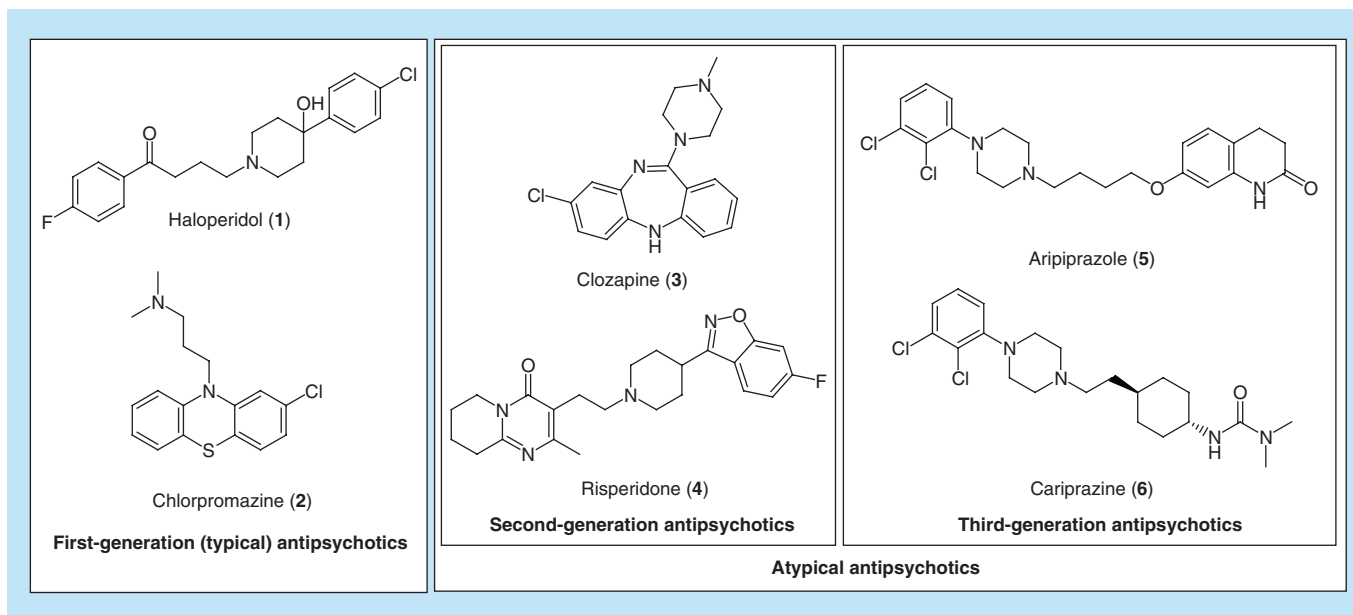


**Figure 2. Antipsychotic drugs for the treatment of schizophrenia grouped by their classifications.**

and risperidone (4) and third generation antipsychotics (TGAs, e.g., aripiprazole (5) and cariprazine (6)) has provided SCZ sufferers with treatments that have a lower propensity for EPS. These improvements have

been attributed to a number of different mechanisms including their poly-pharmacological profile (antagonism at the 5-HT<sub>2A</sub>R has been highlighted as particularly important) [31], differing receptor occupancy

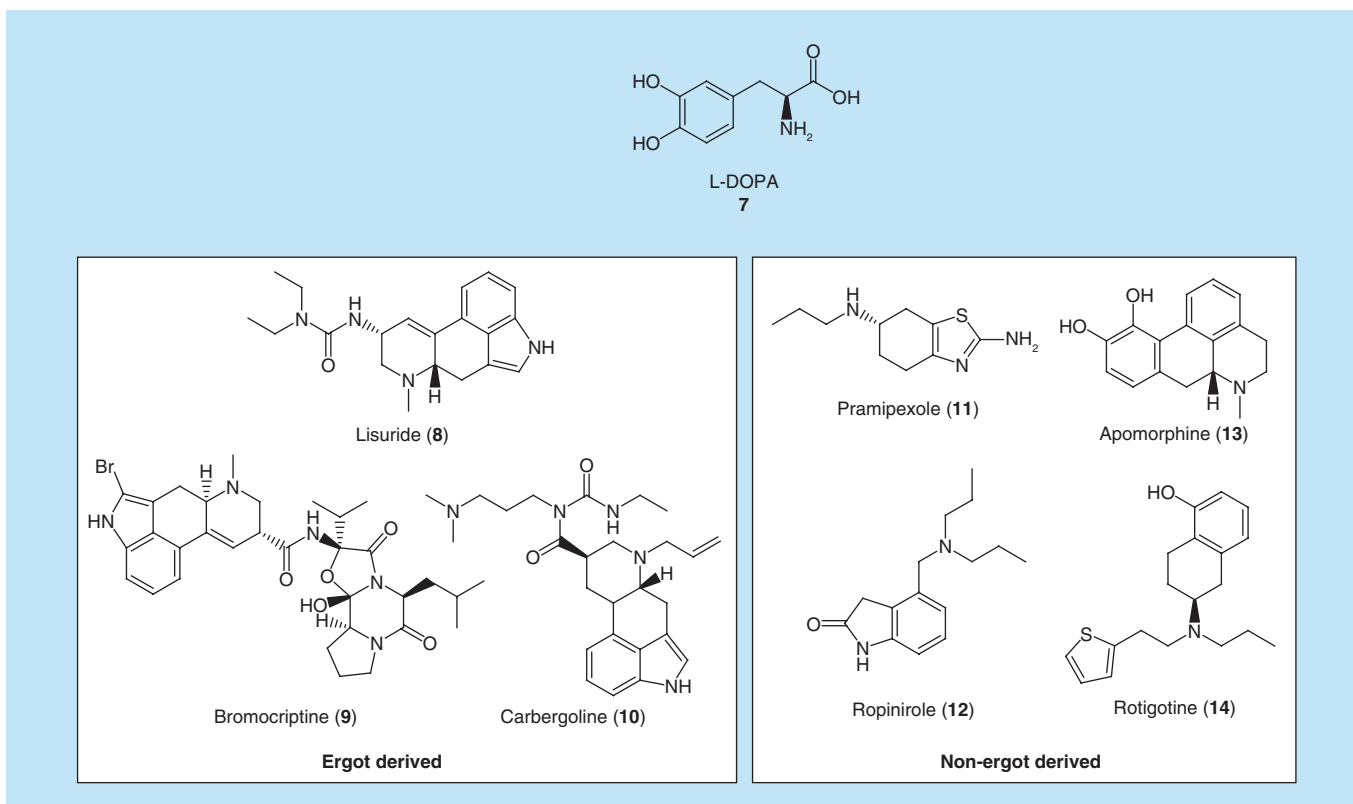


**Figure 3. Structures of levodopa and common ergot- and nonergot-derived D<sub>2</sub>R agonists used for the treatment of Parkinson's disease.**

L-DOPA: Levodopa.

levels at high- and low-affinity receptor states [32], and fast dissociation kinetics from the D<sub>2</sub>R compared with FGAs such as **1** [33]. Although more recently, the fast-off theory proposed by Seeman and colleagues has recently been challenged by Sahlholm and colleagues who, using a functional kinetic assay, found no correlation between the atypicality of antipsychotics and their apparent off-rate [34]. Despite these benefits, SGAs are also associated with a variety of cardiovascular and metabolic side effects as a consequence of their polypharmacology [35,36]. For example, **3** has a high propensity to cause weight gain and other metabolic side effects due to its affinity for the serotonin 5-HT<sub>2C</sub> receptor (5-HT<sub>2C</sub>R) [36]. Additionally, almost 3% of clozapine-users will be prone to agranulocytosis, a potentially fatal blood disorder, which restricts its widespread use [37,38]. Consequently, the search for novel antipsychotic therapies with further improved side effect profiles continues (Figure 2).

### Parkinson's disease

PD is a progressive neurodegenerative disorder characterized by symptoms such as loss of movement, depression, rigidity and dementia. The motor symptoms of PD are attributed to dopaminergic cell loss within the substantia nigra (SN) pars compacta, and ultimately leads to dysfunction of the basal ganglia (a group of deep nuclei involved in the initiation and execution of movement) [39]. Levodopa (L-DOPA), a biological precursor and prodrug of dopamine, was first determined to be an effective treatment for PD in the 1950s after it was used by Carlsson *et al.* to reverse parkinsonian-like symptoms in rabbits [40,41]. Although L-DOPA was approved by the US FDA in the 1970s, and is still classified as the gold standard for the treatment of motor symptoms of PD, it is associated with a range of side effects including: L-DOPA-induced dyskinesias or hyperkinetic movement, the re-emergence of PD symptoms prior to the next scheduled dose of L-DOPA (or 'wearing off') [42], fluctuations of psychomotor state (known as 'on-off oscillations') [43], nausea and vomiting [44]. To combat its poor pharmacokinetic profile and the side effects associated with its administration at high doses, L-DOPA was subsequently co-administered with: (i) DOPA decarboxylase (DDC) inhibitors to slow the peripheral degradation of L-DOPA prior to CNS penetration [45]; (ii) monoamine oxidase-B (MAO-B) inhibitors to prevent the metabolism of dopamine in the CNS [46], and (iii) inhibitors of catechol *O*-methyl transferase (COMT) to reduce the clearance and improve bioavailability of L-DOPA both peripherally and centrally [47,48].

Given the poor bioavailability and extremely short plasma half-life of L-DOPA (**7**), D<sub>2</sub>R agonists were

viewed as a viable alternative since presynaptic dopamine synthesis could be bypassed and D<sub>2</sub>Rs could be stimulated directly [45,49]. Although these compounds have lower efficacy compared with L-DOPA, D<sub>2</sub>R agonists are longer-lasting and have greatly improved bioavailability [50]. D<sub>2</sub>R agonists for the treatment of PD can be divided into ergot derived (e.g., lisuride (**8**), bromocriptine (**9**) and carbergoline (**10**)) and nonergot derived (e.g., pramipexole (**11**), ropinirole (**12**), apomorphine (**13**) and rotigotine (**14**)) compounds based on their structural properties [45] (Figure 3). The dopamine receptor selectivity profiles of these agonists have been observed to vary, and thus, provide some insight into the therapeutic benefits of targeting individual dopamine receptor subtypes. For instance, D<sub>2</sub>R stimulation is known to ease motor symptoms, while the high D<sub>3</sub>R affinity of pramipexole demonstrated antidepressant effects in PD and non-PD patients [51–53]. The physiological outcome of D<sub>1</sub>-like receptor activation is less well understood; however, there is some evidence to suggest that D<sub>1</sub>-like receptors have some neuroprotective function in PD [54]. The side effects triggered by the use of D<sub>2</sub>R agonists include: hallucinations, fluid retention, impulse control disorders and somnolence [55]. Despite the prolonged half-life of D<sub>2</sub>R agonists (65 h, in the case of **10**) compared with that of L-DOPA (0.77–1.08 h as single administration, 1.5 h when co-administered with DCC inhibitors) [56], the majority of PD sufferers will inevitably be treated with L-DOPA due to its superior efficacy. As such, there is still an unmet need for improved therapies for the treatment of PD.

### Multivalent approaches

Chemical probes enable the investigation of receptor structure and function in order to consolidate the gaps in our current understanding of GPCRs. These chemical tools allow us to examine questions about the D<sub>2</sub>R including whether D<sub>2</sub>Rs are able to form homo- or hetero-dimers, or if an allosteric approach could lead to the development of a clinically relevant drug for the treatment of SCZ or PD, and whether we are able to use biased agonism as a means to avoid on-target side effects. From probing the various binding sites on a receptor and their function, to the investigation of signal transduction, chemical probes have an important role to play in pharmaceutical research [57,58]. Multivalency has been defined as the operation of multiple molecular recognition events of the same kind occurring simultaneously between two entities [59,60]. Multivalent ligands that can occupy more than one binding site, simultaneously. Such a mode of interaction means that multivalent ligands can be very useful tools for the investigation of the pharmacological concepts above.

Herein, we examine two distinct classes of multivalent ligands (Figure 4):

- Bivalent ligands that target the orthosteric sites of two separate receptors and are useful tools for the investigation of receptor dimerization and the function of such dimers in biological systems [61,62];
- Bitopic ligands which target both the orthosteric and allosteric sites within a single receptor, and enable the probing of pharmacological outcomes exhibited by bitopic binding interactions [63,64];
- Finally, in light of the potential advantages of polypharmacology for the treatment of schizophrenia, we extend our review to the concept of designed multiple ligands (DMLs). In particular, we discuss approaches to design DMLs through the incorporation of structural elements of ligands that selectively bind to particular receptor targets into one molecule with the aim of generating a new chemical entity that displays selectivity across multiple targets. As such, DMLs provide an approach to rationally design drugs with a desired profile of polypharmacology that are useful for the treatment of complex disease states such as schizophrenia [65]. While DMLs are not multivalent ligands *per se*, the design of DMLs are subject to some of the particular challenges that applies to the design of multivalent ligands, namely the incorporation of multiple pharmacophores into a single molecule while retaining the desired pharmacological activity.

The orthosteric binding site is the region of the receptor to which the endogenous ligand (dopamine, in the case of the D<sub>2</sub>R) binds. Ligands that compete directly with the endogenous ligand, known as the

orthosteric ligand, are exemplified by the previously described treatments for SCZ and PD. The orthosteric binding site of the D<sub>2</sub>R has been well defined using affinity labeling studies, substituted cysteine accessibility studies, structure–activity studies, molecular modeling studies and combinations thereof [66]. Subsequently, this has aided the discovery of both high affinity agonists and antagonists [66,67]. More recently, further insight has been gained from the crystal structure of the highly homologous dopamine D<sub>3</sub> receptor in complex with the orthosteric antagonist eticlopride [4]. In contrast, an allosteric pocket is a binding site that is topographically distinct to the orthosteric binding site (Figure 3). Targeting the allosteric site of a receptor can yield ligands which have efficacy in their own right, or modulate the affinity and/or the efficacy of an orthosterically bound ligand. As such, these ligands are sometimes termed allosteric modulators [68]. Allosterically binding ligands are not faced with the same selectivity challenges as orthosterically binding ligands since allosteric sites may be less conserved between receptor subtypes compared with the orthosteric site [69]. Clinically, two FDA-approved allosteric modulators have been proven to be useful in the treatment of human immunodeficiency virus (maraviroc) and parathyroid carcinoma (cinacalcet) [70]. Thus far, a drug-like allosteric D<sub>2</sub>R ligand has yet to be discovered.

Although GPCRs have traditionally been considered to function as single (monomeric) units, recent studies suggest that they may also exist as homo- and hetero-dimers, and even higher order oligomers [71–74]. While these discoveries add further complexities to our current understanding of GPCR function and their biological outcomes, they provide new avenues for exploration and exploitation in drug discovery and

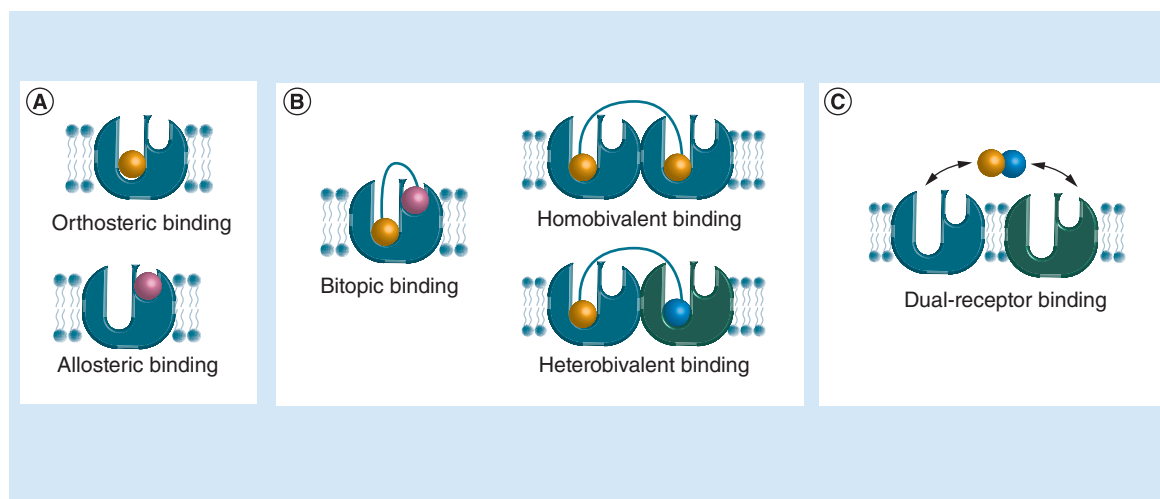


**Figure 4. Schematic representations of univalent and multivalent binding modes. (A)** Classical orthosteric and allosteric binding. **(B)** Multivalent ligand binding. **(C)** Dual-receptor binding mode of designed multiple ligands.

design. This has led to the synthesis of homo- and heterobivalent ligands as pharmacological tools to probe receptor dimers through the concomitant engagement of two receptors in an orthosteric manner. While the existence of D<sub>2</sub>R homodimers and a number of D<sub>2</sub>R heterodimers (e.g., D<sub>2</sub>R/adenosine A<sub>2A</sub> receptors [73], D<sub>2</sub>R/D<sub>1</sub>R [75] and D<sub>2</sub>R/serotonin 5-HT<sub>2A</sub> receptors [76]) have been supported by qualitative and quantitative studies. However, it should be noted that a recent study by Frederick *et al.* has presented evidence against the existence of D<sub>2</sub>R/D<sub>1</sub>R heteromers *in vivo* [77]. This example highlights the key challenges associated with the study of GPCR heteromers; that of providing definitive evidence of their existence *in vivo* and determining the physiological role of such heteromers. In light of this challenge, bivalent ligands may be useful tools with which to investigate whether receptor homo- or hetero-dimers possess distinct biological functions that may be exploited in order to treat diseases such as SCZ and PD.

The dual occupation of both the orthosteric and allosteric sites of a receptor with a single ligand, termed bitopic binding, can lead to the development of molecules with improved selectivity and affinity [64]. Another advantage of bitopic binding is that specific receptor conformations may be stabilized which may selectively trigger receptor signaling to the relative exclusion of others, so called biased agonism. Biased agonists may enable us to distinguish distinct signaling pathways which mediate on-target side effects from those which mediate on-target therapeutic effects [78,79].

Multivalent approaches for the investigation of GPCRs provide new avenues to further our knowledge of receptor function. This review focuses on the approaches taken toward the development of three distinct classes of multivalent ligands; namely, bivalent ligands, bitopic ligands and DMLs. Through this review we aim to discuss the promise and challenges

associated with these multivalent ligand approaches to explore D<sub>2</sub>R function.

### Bivalent ligands

Evidence for the existence of homo- and heteromeric receptor dimers have been presented through a variety of *in vitro* and *in vivo* pharmacological studies [71,73,74,80,81], which has had a number of implications for medicinal chemistry endeavors. First, receptor dimers could potentially have restricted tissue distribution; second, they may induce novel receptor signaling; and third, dimers may possess novel binding properties that may be harnessed in drug design efforts [82]. The concept of the bivalent ligand was initially developed by Portoghese *et al.* in the hope of probing dimeric opioid receptors [83,84] (Figure 5). Bivalent ligands are defined as two pharmacophore units attached, via a linker, to a spacer of adequate length to span across a receptor dimer and enable simultaneous binding at two receptors [85]. These ligands may be developed as either the homobivalent or heterobivalent variants, where two of the same, or two distinct pharmacophores, are attached to the spacer, respectively. In the instances where direct attachment of a spacer to the pharmacophore proves detrimental to the binding of the pharmacophore, a linker may be added to join both the pharmacophore and spacer together. The work conducted by Portoghese and colleagues in order to gain an understanding of receptor dimers of the opioid receptor subtypes ( $\mu$ ,  $\kappa$  and  $\delta$ ) has provided a guide for the subsequent development and pharmacological evaluation of bivalent ligands for other receptor dimers [83,86,87]. However, research conducted by Erbs *et al.* has demonstrated that although  $\mu$  and  $\delta$  opioid receptors exist in close physical proximity to one another in neuronal cells, their co-expression may only occur in a small number of neuronal cells in subcortical networks [88]. These findings highlight the difficulty in the interpretation of data relating to receptor dimers and also have implications on the applications for which bivalent ligands are utilized as probes.

The dual targeting of two individual binding sites of a receptor dimer requires a number of considerations to be taken into account, particularly when developing bivalent ligands for the investigation of said receptor dimer. Bivalent ligands are required to possess the following attributes for their successful development: a pharmacophore that has a suitable attachment point for either the spacer or linker; a linker that does not diminish receptor–ligand interactions and maintains a suitable degree of aqueous solubility and a spacer that is of suitable length which links the two pharmacophoric units and is able to bridge the span of the two receptors [61] (Figure 6). Achieving these attributes, how-

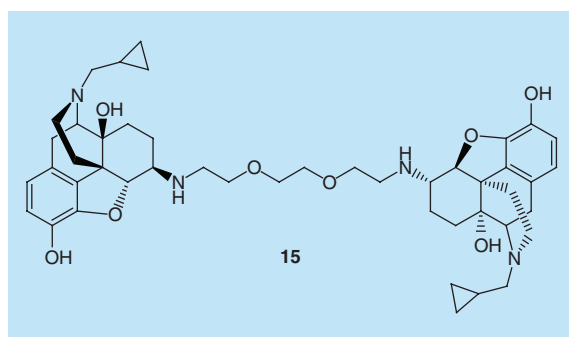


**Figure 5. An example of a  $\beta$ -naltrexamine homobivalent ligand initially synthesized by Portoghese *et al.* to probe the opioid receptors.** Data taken from [84].

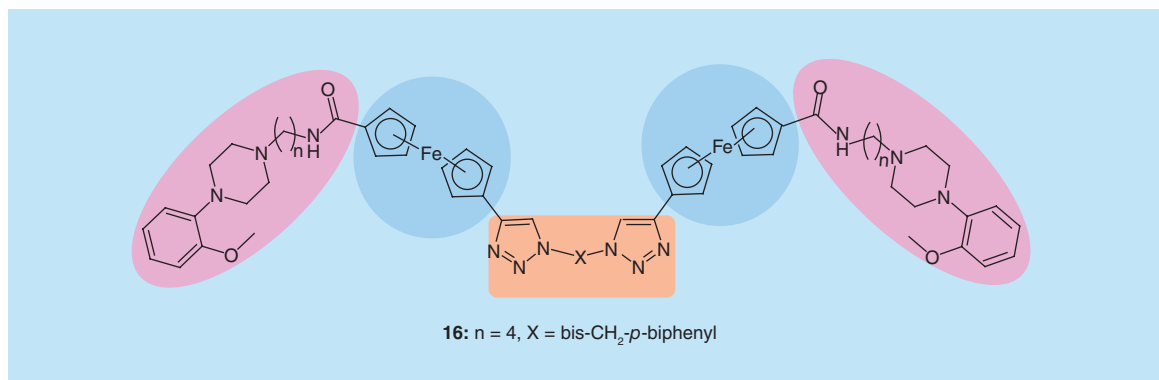


**Figure 6.** A schematic of the bivalent ligand synthesized by Huber *et al.* with the highest affinity at the D<sub>2</sub>R (comprising of two pharmacophores [lilac], two linkers [blue] and a spacer [orange]).

Data taken from [89].

ever, typically result in ligands with high molecular weights, poor solubility and high lipophilicity, which, in turn, make them unfavorable for use in a clinical setting. Despite this, bivalent ligands may have utility as probes for investigating the presence and function of homo- and hetero-dimers of the D<sub>2</sub>R and other receptors in native tissues [62].

### Homobivalent ligands

The use of homobivalent ligands to investigate homodimeric D<sub>2</sub>Rs has become an area of research interest since D<sub>2</sub>R homodimers were observed through pharmacological and histochemical techniques [71,90–92]. Initial work in D<sub>2</sub>R homobivalent ligands conducted by Huber *et al.* demonstrated the importance of a suitable linker, through their investigation of ferrocene-linked homobivalent ligands. Through the incorporation of a ferrocene ‘hinge’ it was hypothesized that conformational flexibility would be beneficial in guiding orthosteric binding of the phenylpiperazine pharmacophores while providing subtype selectivity for the D<sub>2</sub>R. The hypothesis regarding conformational flexibility was upheld by the homobivalent ligand, **16** (Figure 6), which was observed to have the highest binding affinity for the D<sub>2</sub>R ( $K_i = 15$  nM) compared with a reference set of homobivalent ligands lacking the ferrocene ‘hinge’ ( $K_i > 1000$  nM). Subtype selectivity for the D<sub>2</sub>R was not achieved. However, this could be anticipated given the use of orthosteric pharmacophores which inherently interact with the most conserved region amongst the dopamine receptor subtypes. As a consequence of the additional bulk of the ferrocene hinges, **16** was also observed to have a minor loss in affinity compared with its monovalent counterpart ( $K_i = 4$  nM) [89]. Although only minor, the loss in affinity between the monovalent compound and **16** might be considered counterintuitive given that bivalent ligands are thought to have improved affinity due to favorable enthalpic factors which would localize the

second pharmacophore within the region of its binding pocket upon binding of the first pharmacophore to its receptor [61]. This slight loss in affinity highlights the importance of considering thermodynamic factors when developing these types of molecules. Based on the work by Mohr *et al.*, the loss in affinity observed between **16** and its monovalent counterpart may be due to a conformational change in the receptor dimer that may have occurred upon binding of the first pharmacophore which makes binding of the second pharmacophore less favorable, termed negative cooperativity [93]. Alternatively, noncomplementary spatial geometry of the bivalent ligand upon binding of the first pharmacophore may also be another plausible reason for diminished binding [93]. However, this may be considered less likely given the rotational freedom provided by the ferrocene hinges.

Spacer length is also considered a crucial factor in enabling a homobivalent ligand to span across, and bind the orthosteric sites of receptor dimers. In a study of ropinirole-based homobivalent ligands by Jörg *et al.* (**17**), as the spacer lengths were extended beyond the functionally optimal 22–26-atom spacer lengths, a twofold loss of functional potency was observed [94]. This is further supported by a series of (*R*)-apomorphine-based homobivalent ligands (**18**) that were found to show a spacer length-dependent decrease in affinity before and after the optimal spacer length was achieved [95]. Although these compounds showed increases in potency or affinity upon achieving optimal linker lengths (16- to 26-atom spacer lengths) within their synthesized series, none were observed to be more efficacious than their parent pharmacophores [94,95]. Again this lack in improved affinity may be attributed to thermodynamic factors such as translational and rotational entropy as well as spatial geometry. Although the tethering of two ligands will reduce the overall entropic cost of receptor binding, as the length and flexibility of a spacer increases, the conformational entropic cost when one

pharmacophore is bound to a protomer increases considerably. Consequently, highly flexible spacers tethering two pharmacophores together may reduce binding affinities due to entropic factors. An exception to this was observed in a series of clozapine-based homobivalent ligands synthesized by McRobb *et al.* (19), where homobivalent ligands with spacer lengths of 16 and 18-atom units were observed to display a 75- to

79-fold increase in affinity in comparison to the parent pharmacophore 3 [96] (Figure 7).

Homobivalent ligands have been observed to have novel binding profiles. In a study evaluating homobivalent ligands as pharmacological tools for the D<sub>2</sub>R by Kühhorn *et al.* (20), a distinct steepening of the Hill slopes (the gradient of curves obtained in experiments measuring concentration-dependent competi-

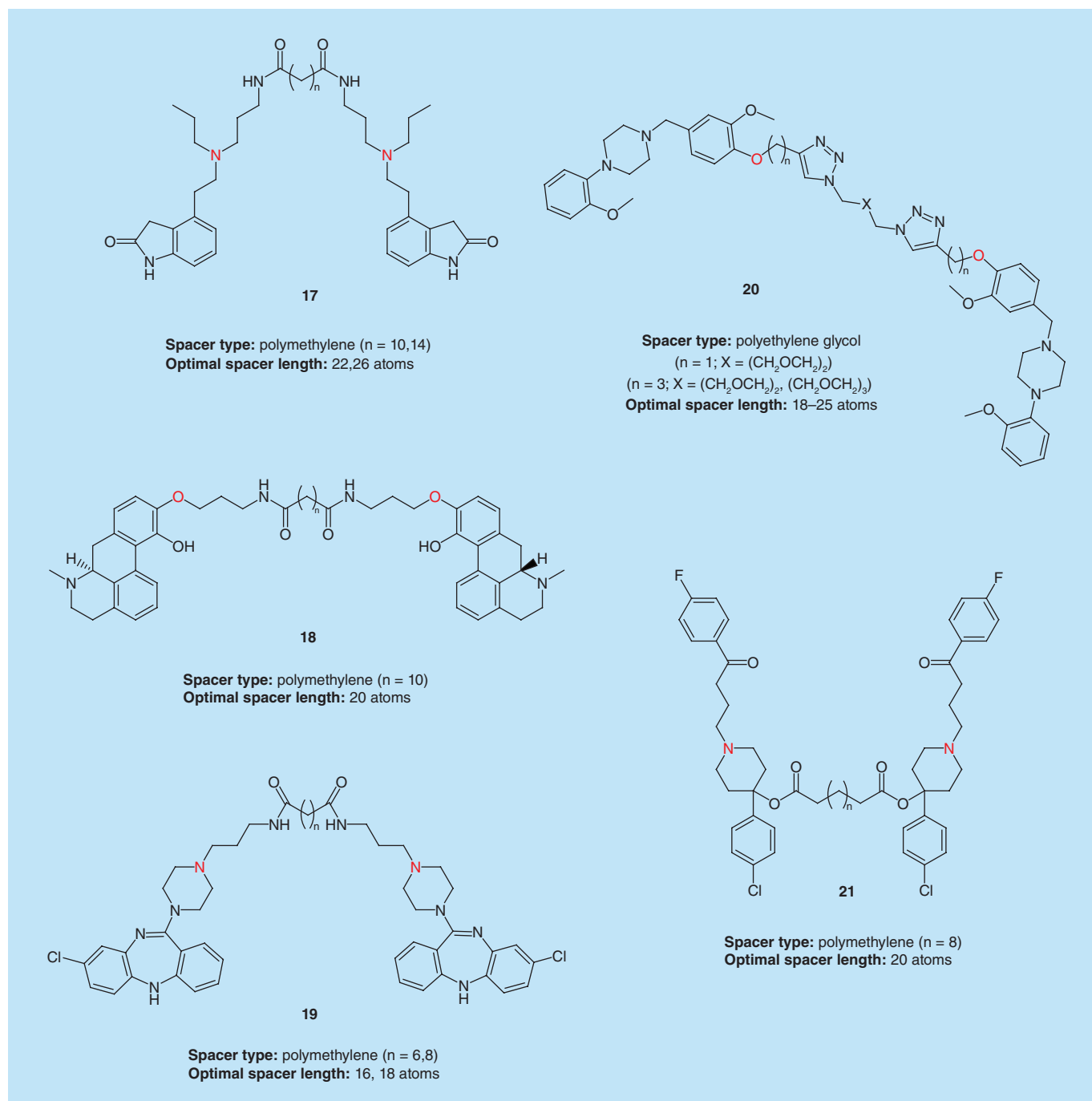
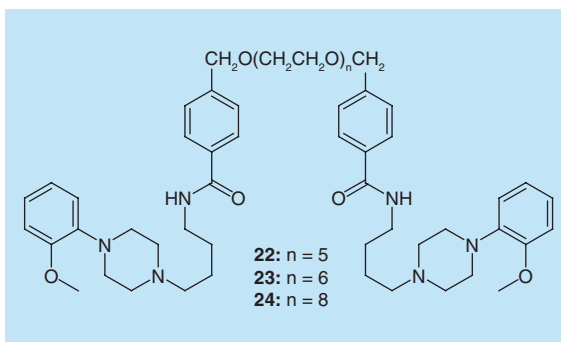


Figure 7. General structures of various homobivalent ligands including their spacer types and optimal spacer lengths as indicated from the highlighted atoms (red).

tive inhibition of an orthosteric radioligand) for homobivalent ligands was noted versus their monovalent counterparts. The authors suggested that Hill slopes of 2 were indicative of dual occupancy of the orthosteric sites of dimerized D<sub>2</sub>R<sub>s</sub>. This was rationalized by the fact that the binding of one bivalent ligand should cause the displacement of two equivalents of the radioligand, which, would lead to a steepening of competition curves. These findings were further corroborated by the observation that the monovalent and asymmetric variants (i.e., one pharmacophore is able to bind to the D<sub>2</sub>R while the other has little to no affinity for the receptor) displayed Hill slopes of unity, suggesting that these molecules appear to only bind a single protomer [97]. Similar observations were made in a recent study of haloperidol-based homobivalent ligands by Salama *et al.* (21). Additionally, Salama *et al.* suggested that Hill slopes greater than unity could be an indication of positive cooperativity between receptor protomers which could result from a receptor-bridging binding mode and was not solely a characteristic of allosterically modulated receptor–receptor interactions [98]. In contrast, Huber *et al.* synthesized a series of arylamidoalkyl substituted phenylpiperazine homobivalent ligands that were observed to produce Hill slopes approaching unity (Figure 8) [99]. This anomaly was rationalized by the suggestion that these homobivalent ligands adopt an alternative bitopic binding mode rather than binding to two adjacent orthosteric binding sites. Hence, the occupation of both the orthosteric and allosteric sites of a single protomer would only cause displacement of a single radioligand, giving rise to a Hill slope close to unity. It is evident that there are a number of challenges associated with the accurate evaluation and interpretation of pharmacological results obtained from the study of homobivalent ligands. The primary challenge in evaluating such ligands pharmacologically is the difficulty in demonstrating unequivocally that the receptors exist as dimers both *in vitro* model systems and, in particular, *in vivo*. Although techniques such as bioluminescence resonance energy transfer (BRET) have been employed to demonstrate the existence of GPCR oligomers in living cells [100], the interpretation of such approaches has been questioned. As such, it can be challenging to provide definitive proof of GPCR dimer/oligomerization. It follows then that it is also difficult to determine whether the novel properties exhibited by bivalent ligands are the consequence of engaging a receptor dimer or a monomeric receptor. This is further complicated by the fact that affinities of bivalent ligands are commonly compared with the affinity of a monovalent ligand or the parent pharmacophore which does not allow us to adequately compare the dual occupa-



**Figure 8. Arylamidoalkyl-substituted phenylpiperazine homobivalent ligands synthesized by Huber *et al.***

Data taken from [99].

tion of orthosteric sites of both protomers [89,94–96]. ‘Dummy’ bivalent ligands (where one pharmacophore of the bivalent is replaced with a structurally similar, nonbinding motif) would provide a better comparator. This is because the ‘dummy’ ligand would orientate the pharmacophore and its spacer in a similar fashion to that of the bivalent ligand and reduce some of the ambiguity surrounding the contribution made by the spacer and its orientation upon binding the first protomer. This is exemplified by the work of Kühhorn *et al.* where ‘dummy’ bivalent ligands were used as a comparator to evaluate their homobivalent ligands at the D<sub>2</sub>R [101].

### Heterobivalent ligands

Given the complex pathophysiology of CNS disorders such as SCZ and PD, it is now widely accepted that improved therapeutic benefits can be gained through the targeting of additional receptors in combination with the D<sub>2</sub>R [102–104]. The targeting of D<sub>2</sub>R heterodimers, which generally have a more discrete distribution compared with monomeric receptors, provides an opportunity to develop ligands that are more selective in their actions and may show greater efficacy but avoid side effects. This is exemplified by two series of heterobivalent ligands that have been developed to probe D<sub>2</sub>R/adenosine A<sub>2A</sub> receptor (A<sub>2A</sub>AR) receptor dimers. A<sub>2A</sub>AR antagonists were hypothesized to slow the degeneration of dopaminergic neurons and the progression of PD [105]. Thus, in targeting D<sub>2</sub>R/A<sub>2A</sub>AR dimers it was hoped that both the motor symptoms and the progression of the disease might be controlled. In a study conducted by Soriano *et al.*, heterobivalent ligands containing XCC (A<sub>2A</sub>AR antagonist) and (±)-PPHT-NH<sub>2</sub> (D<sub>2</sub>R agonist) were synthesized and their utility in detecting heteromeric dimers of the A<sub>2A</sub>AR and D<sub>2</sub>R was evaluated (structure not shown) [106]. The results indicated that dopamine-adenosine heterobivalent ligands were useful tools in determining the presence of heteromers in striatal

tissue. The authors also asserted that an appreciable increase in affinity of the heterobivalent ligands, in the presence of both receptors, was a strong indication of binding across the heteromer [106]. Subsequently, in a study by Jörg *et al.*, an  $A_{2A}AR/D_2R$  heterobivalent ligand (**25**) was synthesized and demonstrated minor improvements in inhibitory potency at the  $A_{2A}AR$  and functional potency at the  $D_2R$  (Figure 9). However, given the labor intensive process required to synthesize these ligands and their unlikelihood of being utilized as CNS therapeutics, Jörg and colleagues saw greater utility in these compounds as a starting point for the development of DMLs (discussed further below) and as potential probes for the elucidation of heteromeric receptors [107].

### Bitopic ligands

The concept of the bitopic ligand [63,64] is considered an extension of the bivalent ligand model developed by Portoghese. Rather than targeting two adjacent orthosteric sites of receptor dimers, bitopic ligands target two topographically distinct sites on a single receptor. A bitopic ligand can be defined as a chemical entity comprising of an orthosteric and allosteric pharmacophore that are tethered together via a linker, which enables the simultaneous binding of two binding sites on a single receptor [63,93,108]. Bitopic ligands present three distinct advantages as an approach: first bitopic

ligands may provide improvements in affinity compared with classical orthosteric-targeting ligands; second, they may engender greater selectivity over receptor subtypes and third, bitopic ligands may exhibit signaling bias. An additional advantage of bitopic ligands is that, unlike allosteric ligands, bitopic ligands do not require the presence of an endogenous ligand in order to elicit an effect at their biological target. This may be particularly useful in neurodegenerative illnesses, such as PD, where there is a lack of endogenous tone [63].

The optimal dual interaction of both an orthosteric and allosteric site by a bitopic ligand may enhance the affinity and subtype selectivity compared with the parent orthosteric ligand. In addition to subtype selectivity, it may also be possible for bitopic ligands to stabilize unique receptor conformations that differ from that of the parent orthosteric ligand that may be linked to a distinct profile of biased agonism. This is exemplified by the bitopic muscarinic  $M_2$  acetylcholine receptor ( $M_2$  mAChR) ligands synthesized by Antony *et al.* (**26**) which incorporated oxotremorine-like orthosteric agonists (iperoxo, **27**) with  $M_2$ -selective bis(ammonio) alkane-type allosteric (W84, **28**) (Figure 10). Antony and colleagues also found that the engagement of the orthosteric site was affinity providing while subtype selectivity and biased agonism was a factor of allosteric engagement by their bitopic ligands [109]. At the adenosine  $A_1$  receptor ( $A_1AR$ ), Narlawar *et al.* devel-

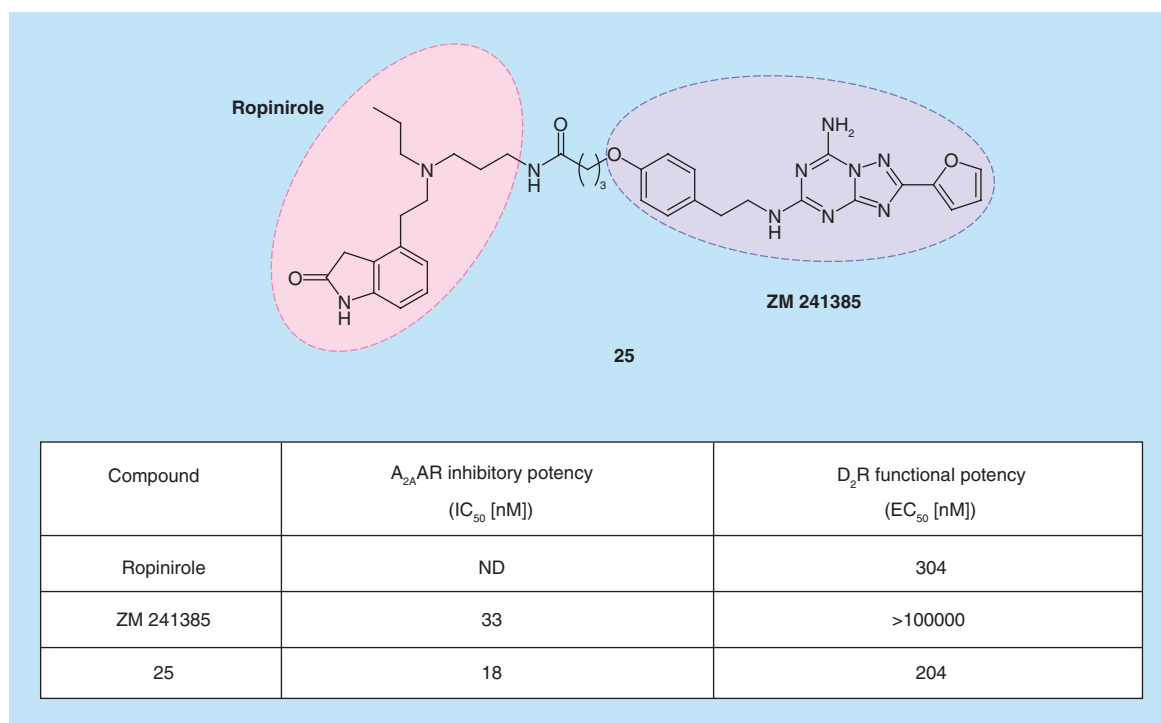


**Figure 9.** Compound **25**, an  $A_{2A}AR/D_2R$  heterobivalent ligand, and its improved relative  $A_{2A}AR$  inhibitory and  $D_2R$  functional potency compared with its parent pharmacophores. ND: Not determined.

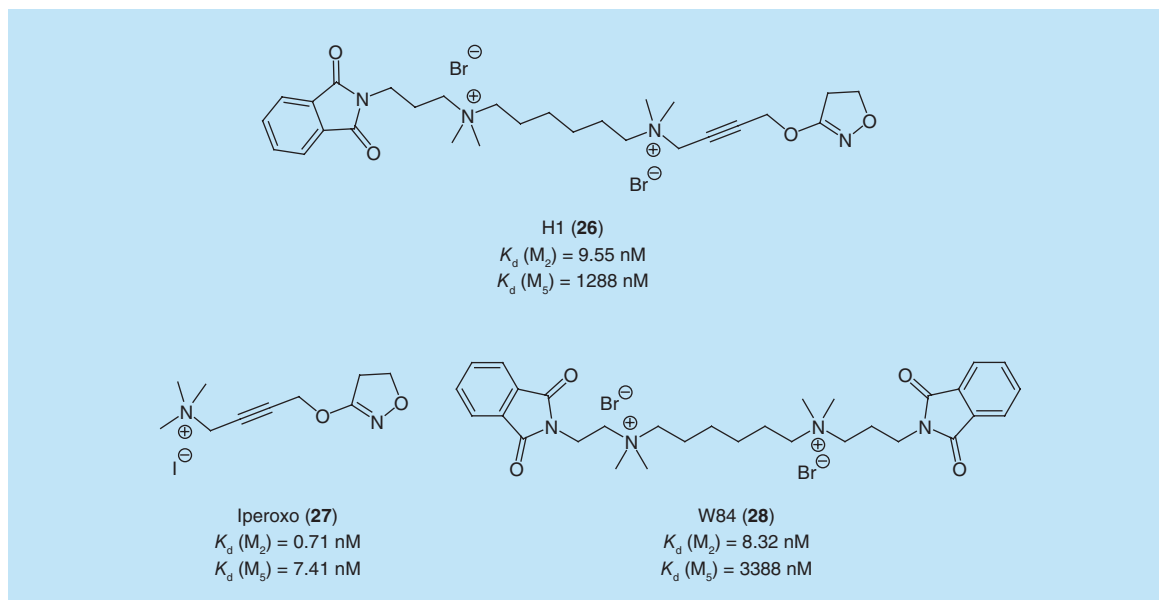


**Figure 10.** The structure and apparent muscarinic M<sub>2</sub> receptor binding affinities of H1 (26) and its parent fragments, iperoxo (27) and W84 (28).

oped a series of bitopic ligands to probe the allosteric regions of the receptor. The affinity and potency of N<sup>6</sup>-[2-amino-3-(3,4-dichlorobenzoyl)-4,5,6,7-tetrahydrothieno[2,3-*c*]-pyridin-6-yl-9-nonyloxy-4-phenyl]-adenosine (LUF6258, **29**) demonstrated no significant changes in the presence of PD81,723 (**30**),

an allosteric enhancer, providing some evidence that the ligand may engage both the orthosteric and an allosteric site of the A<sub>1</sub>AR which may be in close proximity [110]. Similarly, Valant *et al.* developed an A<sub>1</sub>AR bitopic ligand, VCP746 (**31**), following a rational design process. Not only were they able to demonstrate

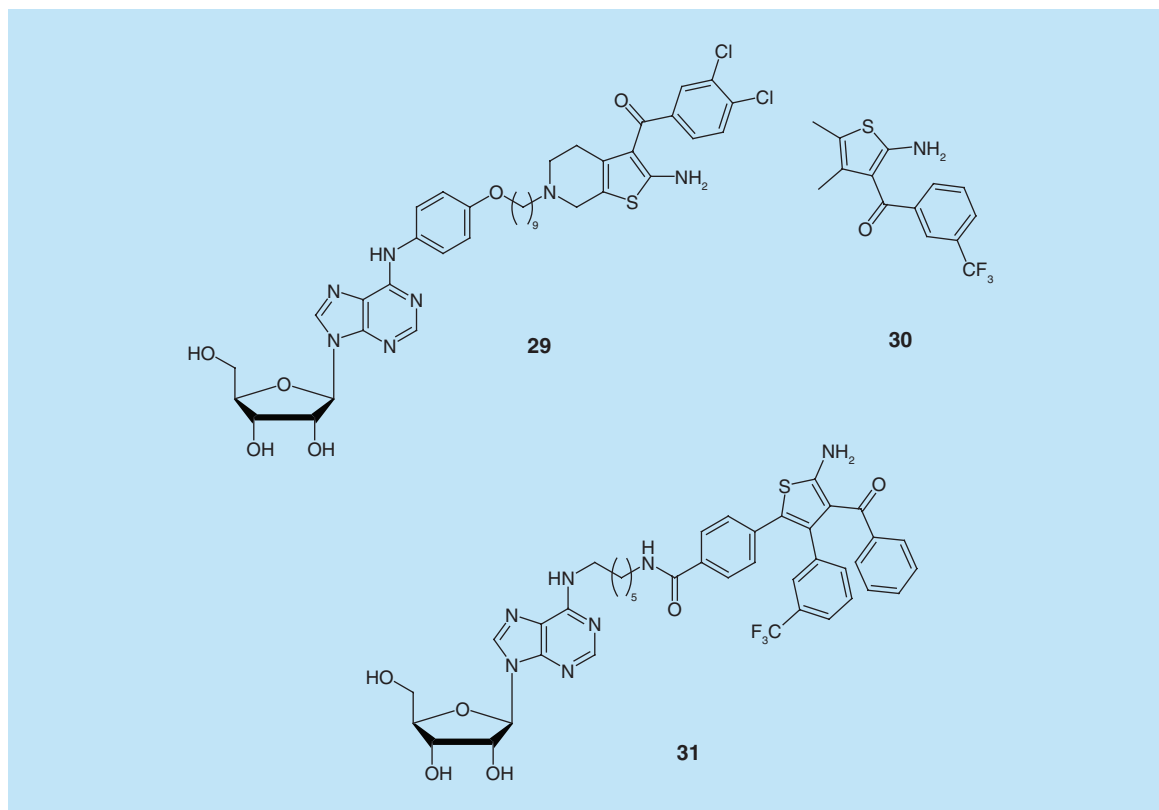


**Figure 11.** A<sub>1</sub>AR bitopic ligands LUF6258 (29) and VCP746 (31), and the A<sub>1</sub>AR allosteric enhancer PD81,723 (30).

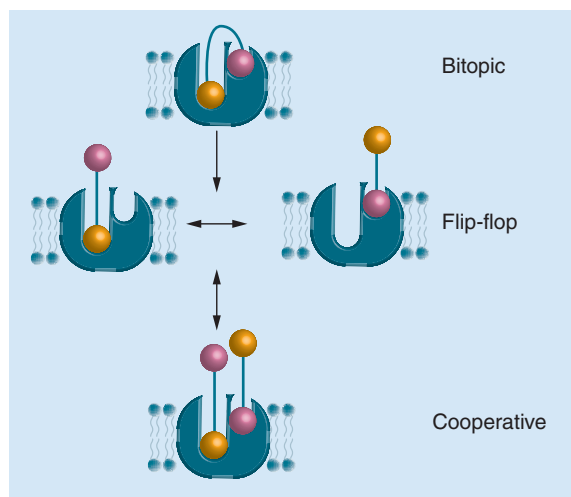


**Figure 12.** The potential binding modes that may be adopted by bitopic ligands.

that **31** bound in a bitopic fashion to the  $A_1AR$ , but also verified its cardio-protective actions *in vitro* [111] (Figure 11). Additionally, much like bivalent ligands, it is difficult to conclusively demonstrate that bitopic ligands engage in a purely bitopic mode [63]. An alternative binding mode that may be engaged by bitopic ligands is the “flip-flop” mechanism where the bitopic ligand binds solely to either the orthosteric or allosteric site but does not occupy both binding sites concomitantly. This “flip-flop” mechanism would be difficult to distinguish, pharmacologically, from a ligand with a purely bitopic binding mode. It is possible, however, to determine the distribution of these two binding modes by the relative affinity of the ligand for these two distinct orientations [63,64]. Similarly, it may also be possible for two bitopic ligands to simultaneously adopt the separate poses in the one receptor (i.e., one ligand interacts orthosterically, while the other engages allosterically) [63,112] (Figure 12). In this regard, a combined approach of site directed mutagenesis and molecular dynamic simulations has been used to provide further evidence of a bitopic mode of interaction as exemplified by the work of both Antony *et al.* and Keov *et al.* [109,113]. For example in the study by Antony *et al.*, radioligand binding assays, in wild-type and mutant receptors, in addition to receptor docking simulations were used to validate a bitopic mode of interaction of **26** at the  $M_2R$  [109].

#### Allosteric modulation at the $D_2R$ by a bitopic mechanism

SB269652 (**32**) was described as the first drug-like negative allosteric modulator of the  $D_2R$  by Silvano *et al.* [114] in 2010. Subsequently, in an extensive characterization study, Lane *et al.* provided evidence to suggest that **32** interacts with the  $D_2R$  via a novel bitopic mode of inter-

action that confers its allosteric activity across a  $D_2R$  receptor dimer [115]. The presence of common structural orthosteric  $D_2R$  ligand motifs such as an ionisable nitrogen, and an aliphatic linker within the structure of **32** alluded to the fact that it may interact with the orthosteric site of the  $D_2R$ . The subsequent evaluation of a series of 1,2,3,4-tetrahydroisoquinolin-7-carbonitrile (THIQ7CN) fragments provided evidence that the THIQ7CN moiety of **32** interacts orthosterically at the  $D_2R$ . Intriguingly, **32** exhibited allosteric pharmacology rather than a competitive mode of interaction which would be typified by orthosteric engagement. Bitopic engagement of the receptor was deemed a critical factor in the ability of **32** to elicit negative cooperativity at the  $D_2R$ . A loss of negative cooperativity was noted when **32** was synthesized as the *cis* variant. This led to the hypothesis that bitopic engagement of the  $D_2R$  was crucial to the negative cooperativity exerted by **32**, with the indole-2-carboxamide moiety extending into a putative allosteric pocket at the top of TM2. Molecular modeling predicted a hydrogen bond interaction between the indolic NH of the indole-2-carboxamide moiety and Glu95<sup>2.65</sup> located at the top of the TM2 helix of the  $D_2R$ . These findings were confirmed by a loss of negative cooperativity upon the mutation of the Glu95<sup>2.65</sup> residue to an alanine. Furthermore, methylation of the indolic NH converted the pharmacology of **32** from a negative allosteric modulator to a competitive orthosteric antagonist. A novel functional complementation system was employed to determine whether **32** was able to modulate the effect of dopamine across a  $D_2R$  dimer. This enabled Lane *et al.* not only to reconcile their initial observation that **32** bound in a bitopic fashion, but that this bitopic mode of interaction confers allostery across a dimer. This discovery extends the range of pharmacology that can be triggered by a bitopic mode of interaction. Subsequently, in rat striatal tissue, **32** demonstrated modulatory activity and, given the proposed mechanism of action, suggested the presence of  $D_2R$  dimers within this tissue [115] (Figure 13). Furthermore, the identification of this putative allosteric  $D_2R$  binding site at the top of TM2 has led to the synthesis of the first series of allosteric  $D_2R$  fragments [116]. Interestingly, Kühhorn (**33**, **34**) (Figure 14), Salama (**21**) and their colleagues similarly proposed that their homobivalent ligands could be binding in a bitopic fashion to one protomer of a  $D_2R$  dimer and, through a cooperative mechanism, cause displacement of the radioligand in the other, thus causing a distinct steepening of Hill slopes [97,98]. Allostery is typically defined as the specific interaction between a ligand and a topologically distinct binding site of a receptor which differs from its orthosteric site [117]. However, the allosteric behavior of SB269652 likely differs from other

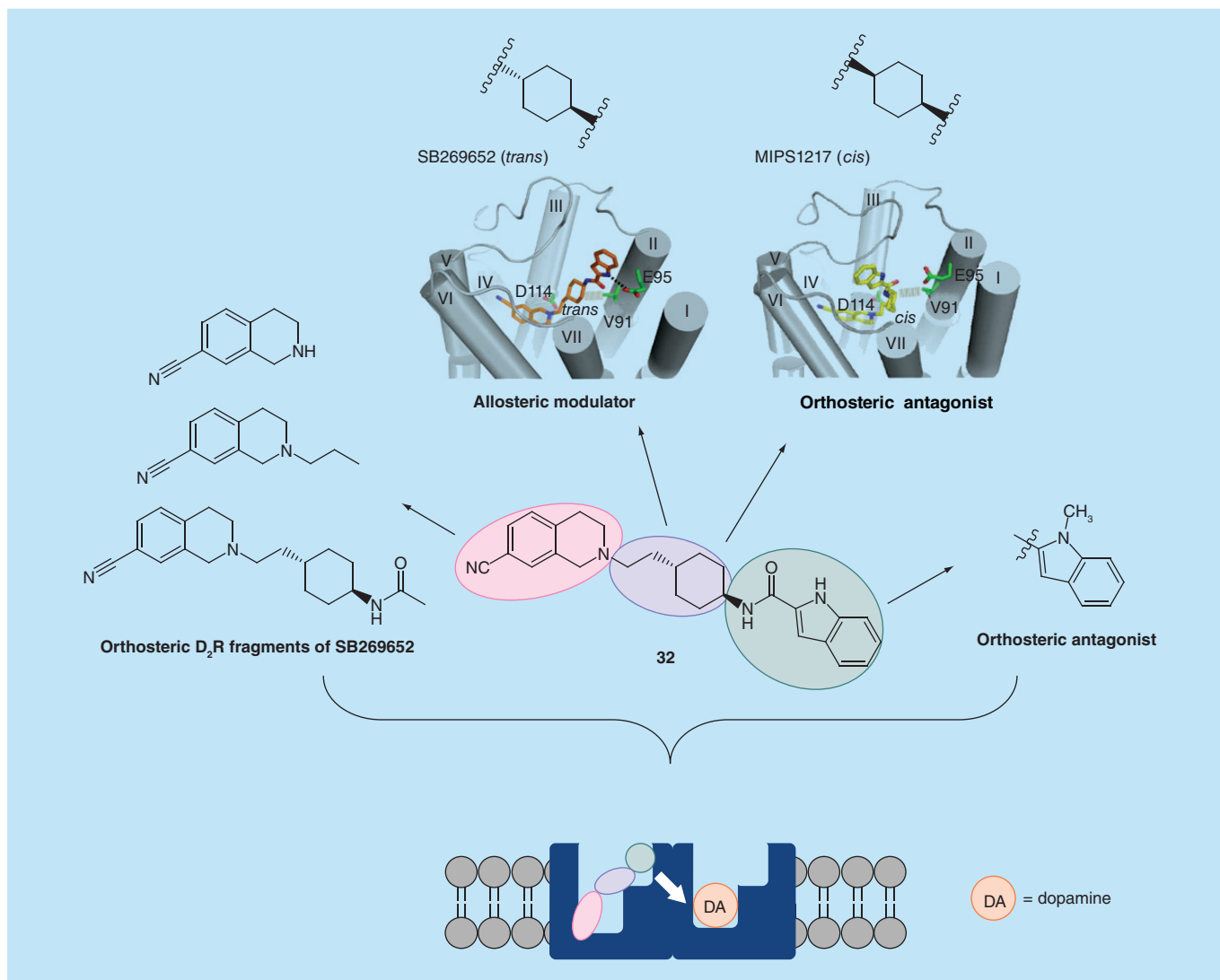


**Figure 13. A schematic representation of the extensive structure–activity relationship study conducted on SB269652.** **32** is highlighted by its various structural regions; the THIQ7CN (pink), the cyclohexylene spacer (blue) and the indole-2-carboxamide tail (green). Synthesis and pharmacological evaluation of a series of fragments and analogs led to the proposal of a bitopic binding mode that confers a novel mechanism of allostery at a D<sub>2</sub>R dimer.

Reproduced with permission from [115] © Macmillan Publishers Ltd (2014).

prototypical allosteric modulators of aminergic GPCRs. Indeed, many allosteric modulators described for the muscarinic acetylcholine receptors have a pharmacology that can be theoretically accommodated within a monomeric receptor model. Such a ternary complex between an orthosteric ligand and an allosteric ligand simultaneously bound to a single receptor was demonstrated directly by the solution of the crystal structure of the M<sub>2</sub> muscarinic receptor bound to both an agonist and a positive allosteric modulator [118].

Bitopic ligands that act to modulate ligand binding and activity across receptor dimers present a new avenue for further research. A subsequent structure–activity relationship (SAR) study of **32** carried out by Shonberg *et al.* has provided further insights into the

chemical determinants of **32** which underlie allostery at the D<sub>2</sub>R [119]. As we gain a better understanding of the structural, chemical and pharmacological intricacies of this novel mechanism for targeting the D<sub>2</sub>R, it will provide the basis for the development of improved modulators of the D<sub>2</sub>R.

#### Putative bitopic ligands that demonstrate biased agonism

Biased agonism refers to the ability of a ligand to preferentially activate a specific signaling pathway over another upon binding to a receptor, by stabilizing a ligand-specific conformation [120–122] (Figure 15). The advantage of biased agonism is the notion that ligands can selectively activate therapeutically relevant signaling pathways while

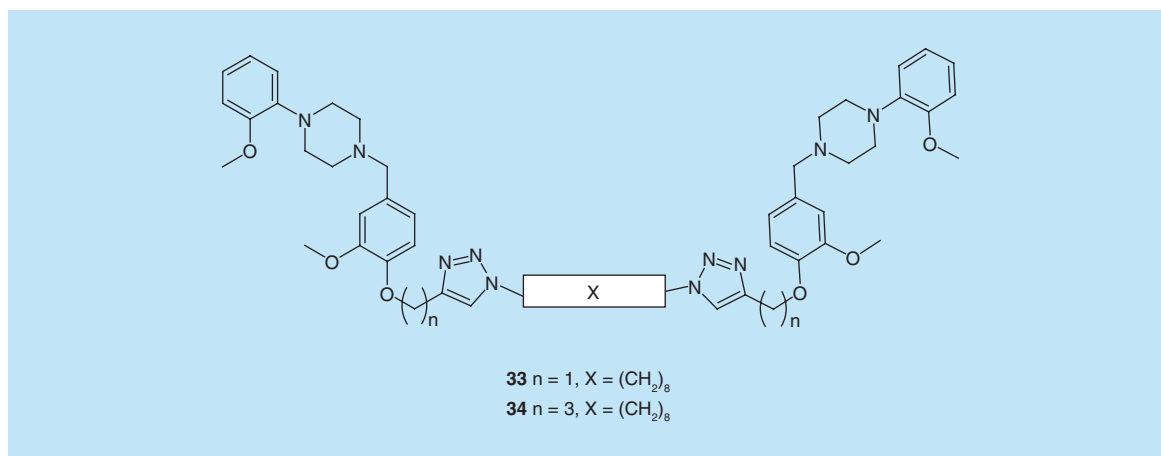


**Figure 14.**  $D_2R$  homobivalent ligands developed by Kühhorn *et al.*

Data taken from [97].

avoiding those that contribute to unwanted side effects by stabilizing specific receptor conformations. Over time, structural investigations of ligands such as McN-A-343 (an  $M_2$  muscarinic acetylcholine receptor partial agonist, structure not shown) and **31** (an  $A_1AR$  bitopic ligand), have highlighted the possibility that bitopic binding modes may confer biased agonism [63,111]. This idea has been corroborated by the work of Bock *et al.* which demonstrated that synthesized bitopic ligands were able to stabilize ligand-specific receptor conformations via interactions within an allosteric vestibule of the  $M_2$  muscarinic acetylcholine receptor to elicit biased agonist responses [123].

As of yet, the link between biased agonism at the  $D_2R$  and bitopic modes has not been demonstrated. However, a number of studies have suggested that the antipsychotic aripiprazole (**5**), a partial agonist of the  $D_2R$ , may be a biased agonist and that its antipsychotic efficacy may relate to this biased action [124,125]. A number of functionally selective  $D_2R$  ligands have been developed based on the template of **5** by Chen *et al.* (UNC9975 (**35**) and UNC9994 (**36**)) [126,127], Vangveravong *et al.* (SV-III-130s (**37**)) [128,129], Möller *et al.* (**38**) [130] and Szabo *et al.* (**39**) [131] (Figure 16). Of interest, **5** and other function-

ally selective ligands have been observed to occupy both the orthosteric and an extended binding region within the  $D_2R$  via computational modeling [132], and it is therefore tempting to speculate that the biased actions of such ligands may result from a bitopic mode of interaction.

Preliminary investigations into the molecular determinants of biased agonism at the  $D_2R$  have recently been conducted. Weichert *et al.* synthesized two series of enantiomerically pure biased agonists using a conjugated enyne moiety (**40a**, **40b**) and an aminotetraline moiety (**41**) as the proposed orthosteric portion of the ligand. Subsequent pharmacological investigation of these ligands found that the enyne-containing ligands were observed to have similar biased agonism profiles regardless of their enantiomeric form. The aminotetraline derivatives, however, showed enantiomer-specific biased agonism. The (*R*)-enantiomer showed selectivity toward  $\beta$ -arrestin recruitment, while the (*S*)-enantiomer was not observed to be functionally selective. This was rationalized by molecular modeling which suggested that two distinct extended binding pockets of the  $D_2R$  may be occupied by the lipophilic appendages of each aminotetraline derivative, thus, giving rise to their distinctly different pharmacologies [133] (Figure 17).

Biased bitopic ligands are an interesting prospect that warrant further investigation. As discussed above, however, providing definitive proof of a bitopic mode of interaction can be challenging. Through the synthesis and evaluation of novel functionally selective bitopic ligands for the  $D_2R$ , however, it may be possible to address some of these questions and aid the progression toward developing treatments for SCZ and PD which are less prone to causing on-target side effects.

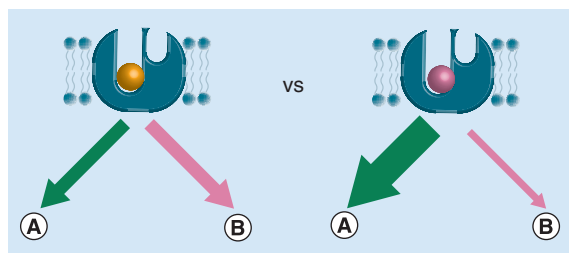


**Figure 15.** A non-functionally selective ligand which activates both signaling pathways (A & B) equally, compared with a functionally selective ligand which can favor the triggering of one signalling pathway over the other.

### DMLs

DMLs are compounds that are designed to have a specific profile of multitarget affinity and efficacy and provide an

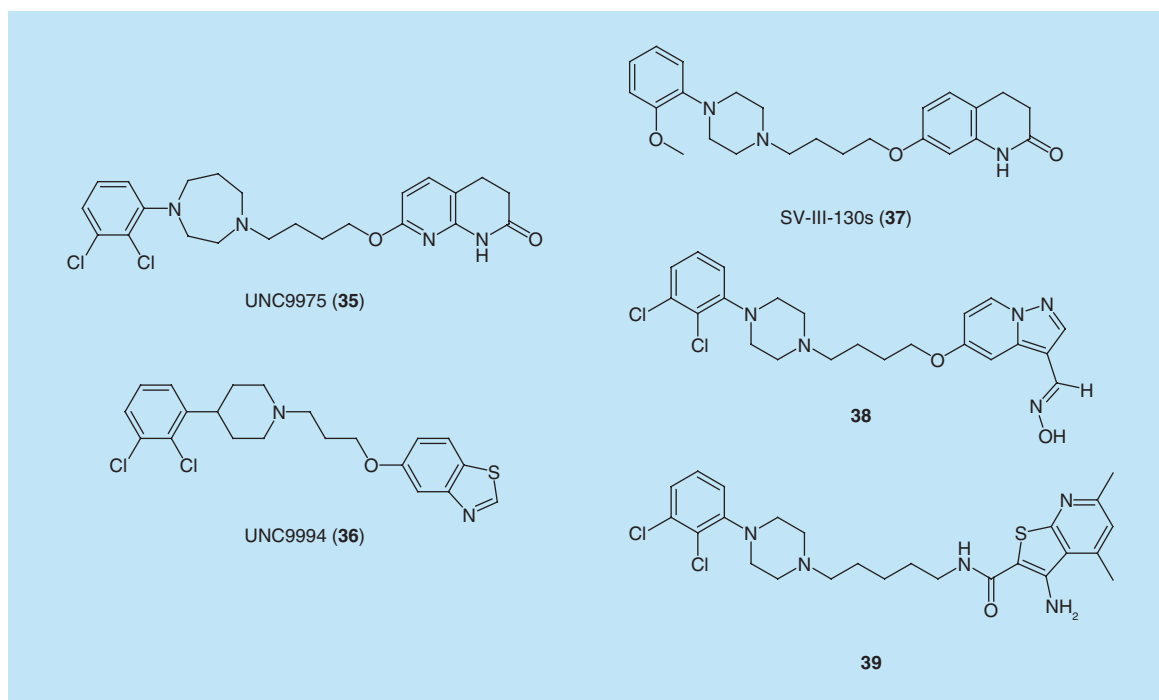


**Figure 16.** The chemical structures of putative bitopic ligands which exhibit biased agonism at the D<sub>2</sub>R.

alternative strategy for the development of treatments for complex disease states [65,104,134]. The development of DMLs for the treatment of CNS disorders is by no means a novel concept. The atypical antipsychotic, ziprasidone (45), was developed using a DML approach. Dopamine

(42) and the lipophilic appendage of a serotonin (5-HT) (43) receptor ligand were merged, and subsequently optimized, to yield a D<sub>2</sub>R/serotonin 5-HT<sub>2A</sub> receptor (5-HT<sub>2A</sub>R) antagonist that is currently used to treat SCZ [134] (Figure 18). While poly-pharmacology has been

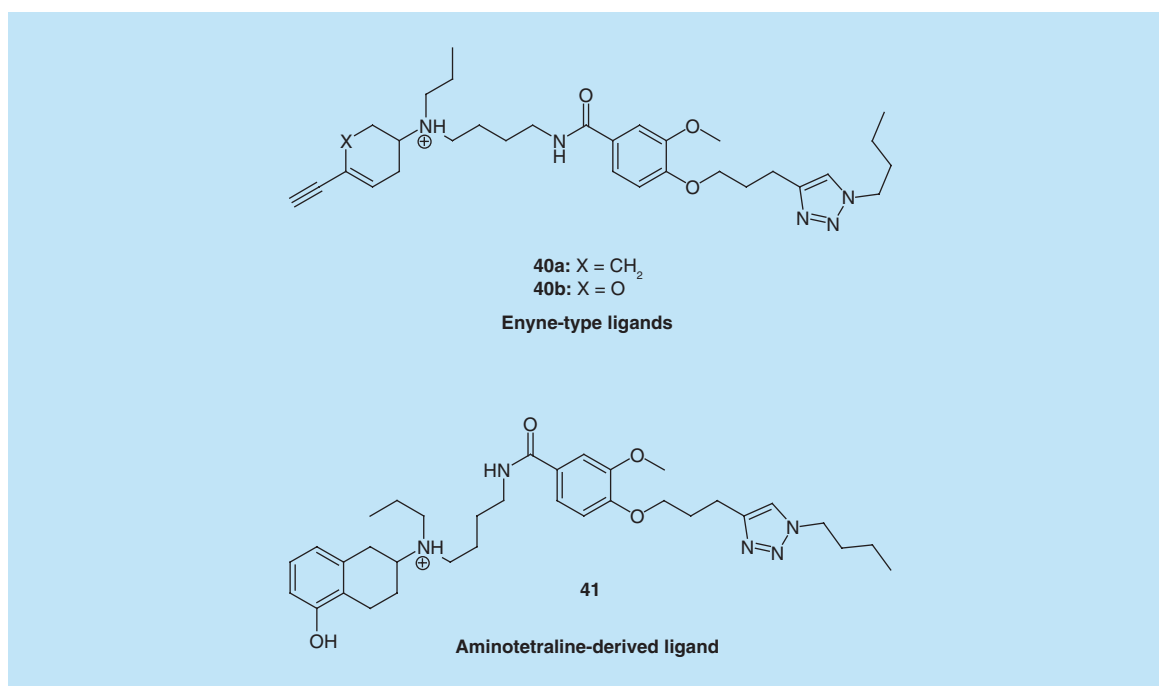


**Figure 17.** A general schematic of the bitopic ligands synthesized by Weichert *et al.* to investigate the molecular determinants of biased agonism at the D<sub>2</sub>R.

Data taken from [133].

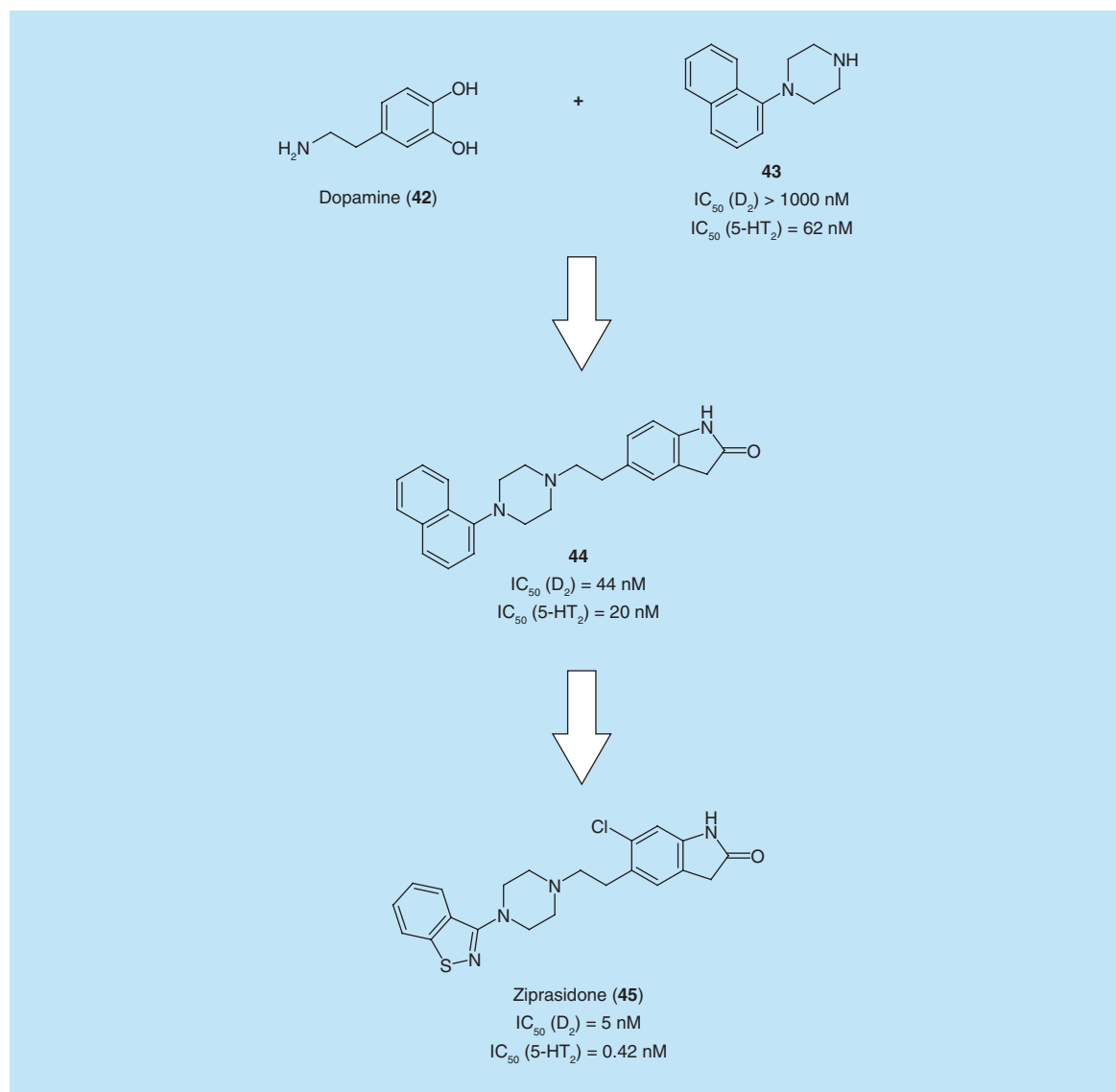


**Figure 18.** The development of ziprasidone (45) from dopamine (42) and 43 using a designed multiple ligand and optimization approach.

suggested to underlie the efficacy of some clinically effective drugs, for example, the superior antipsychotic efficacy of clozapine, such profiles of multiple-receptor targeting were the result of serendipity rather than design [104]. In contrast, efforts in developing DMLs are more focused toward the rational and selective ‘building-in’ of beneficial pharmacological profiles through the integrative use of structural, computational and pharmacological information to guide ligand design. Although DMLs do not function in a multivalent fashion, as for multivalent ligands, their design requires the integration of multiple pharmacophores into a single molecule while retaining the activity of the parent molecules. Furthermore, the design of DMLs often follows an evolutionary path from ligands in which the pharmacophores are separated by a linker to more drug-like, integrated structures.

A common approach used in the rational design of DMLs has been described by Morphy *et al.* where two individual pharmacophores each with their own distinct pharmacology, are integrated into one molecule that possesses attributes of both parent molecules. The extent of integration is methodically increased until the structure is merged and drug-like [65] (Figure 19). DMLs are considered advantageous in complex, multifaceted disease states where multiple receptors are implicated in disease progression. It has also been asserted that drugs that bind multiple receptor targets simultaneously, not only improve efficacy, but may also be safer than drugs that only target a single receptor [65,135]. It has been proposed that DMLs could be safer alternatives to selective drugs, particularly when dealing with CNS disorders such as SCZ and PD, where co-morbid symptoms require mul-

multiple drugs to treat various aspects of the disease. The development of DMLs which retain their core mechanism of action while incorporating complementary components of action may generate therapeutics which have reduced remission rates and which ameliorate drug resistance issues, and unfavorable drug–drug interactions [135]. DMLs are also considered to be advantageous given that the merging of two known drug-like molecules may lead to the ‘designing-out’ of unfavorable structural characteristics of a compound which may be associated with side-effects [65]. Additionally, unlike new chemical entities, DMLs are generally derived from chemical structures that have been investigated in SAR analyses and, generally, already have favorable drug-like properties which makes them ideal candidates for development and optimization. Like with most multivalent approaches, the design and development of DMLs can have its challenges. Attaining the desired affinity and receptor selectivity profiles required to yield therapeutic benefits can be a difficult and slow process; especially, when SAR of the parent ligands are not available, or there is little data on the structure of the targeted receptors [134].

Investigations into D<sub>2</sub>R partial agonist/serotonin reuptake inhibitor (SRI) DMLs by Yan *et al.* demonstrate the

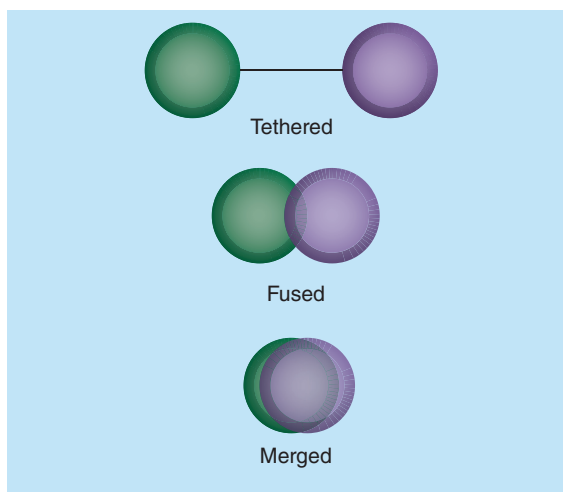


**Figure 19. The progression of integrating two pharmacophores into a designed multiple ligand as described by Morphy *et al.***

Data taken from [55].

advantages that can be gained through taking an integrative approach to DML design. Previous work on tetrahydrocarbazole-based DMLs yielded two lead compounds which showed *in vivo* promise in animal models but little

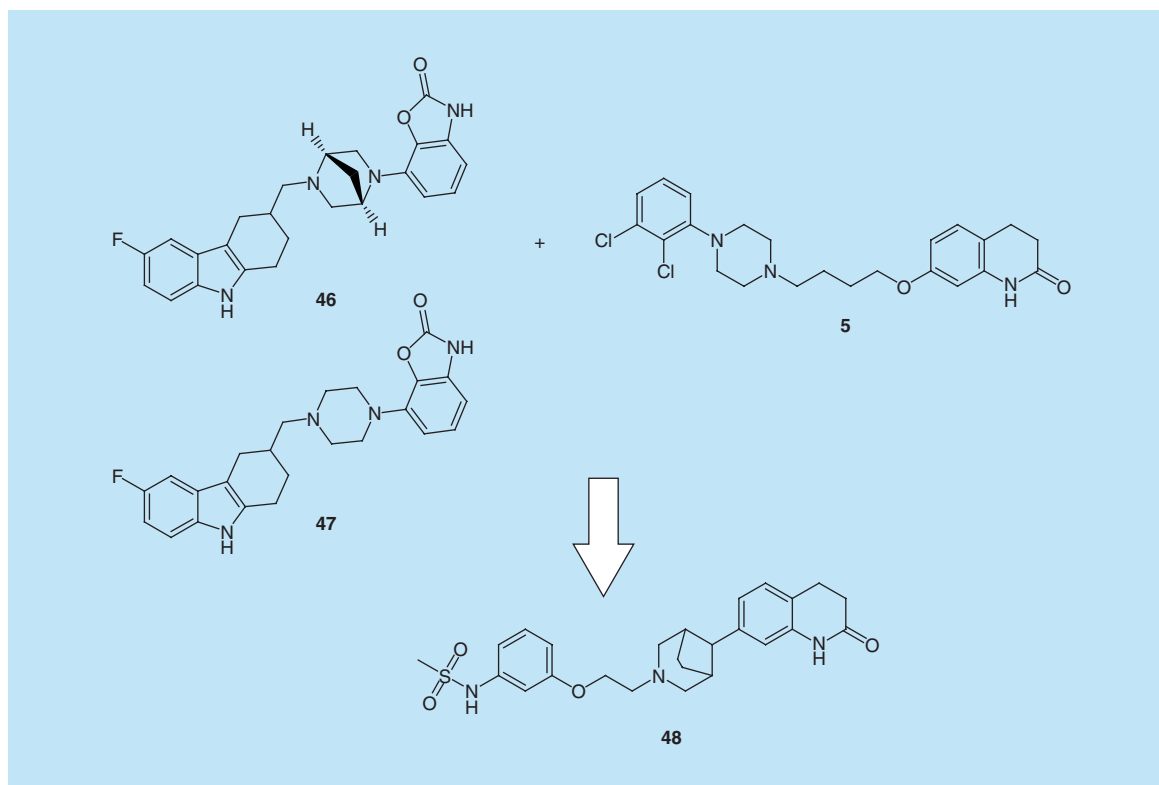


**Figure 20. A dihydroquinolinone/sulfonamide designed multiple ligand synthesized by Yan *et al.* using previously discovered D<sub>2</sub>R partial agonist/SRI designed multiple ligands (46 and 47) and aripiprazole (5) as a starting template to yield 48.**

A similar approach was taken by Carro *et al.* in the development of 49.

Data taken from [136,137].

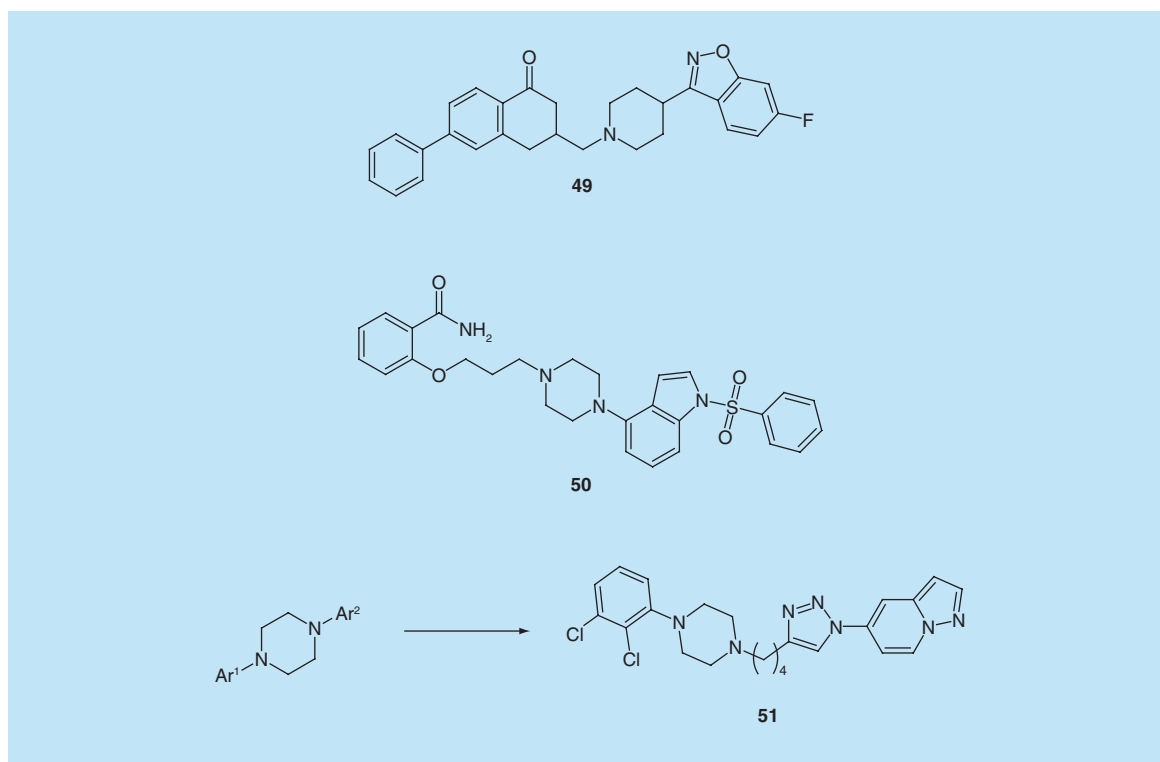


**Figure 21. Computationally derived designed multiple ligands.** Kolaczowski *et al.* used computational modeling to guide their development of **50** [139]. Similarly, Möller *et al.* investigated a training set of 1,4-disubstituted arylpiperazines (including **5**) to derive **51** using 3D QSSR and predictive modeling programs [140].

difference in affinity for the primary targets (SRI and  $D_2R$ ) over off-target receptors *in vitro*. Through rational parent molecule choice based on existing  $D_2R$  ligands (**5**, **46**, **47**) with their desired pharmacological profile, subsequent investigation of linker types and length, Yan and colleagues uncovered a dihydroquinolinone/sulfonamide-based DML (**48**) that had preferential affinity for SRI and the  $D_2R$  over undesired receptors [136] (Figure 20). Similarly, Carro *et al.* investigated a series of aminoalkyl-tetralones and tetralols as dual  $D_2R/5-HT_{2A}R$  ligands for the treatment of SCZ (**49**). In a similar fashion to Yan *et al.*, Carro *et al.* investigated the effects of substitution around the structures in order to gain an understanding of their effects on function and affinity at the target receptors [137]. Similarly, Szabo *et al.* demonstrated that DMLs could be developed by merging two parent molecules with obvious structural overlap. Through the merging of Lu AE51090 ( $M_1$  mAChR agonist), and ziprasidone ( $5-HT_{2A}/D_2R$  antagonist), a novel  $M_1$  mAChR/ $D_2R/5-HT_{2A}R$  merged ligand was developed as a lead molecule for further development [138].

Structural information about target receptors, the binding modes and SAR of parent molecules and the determination of ideal regions for linkage or overlap provides invaluable insights which aid rational DML design. This is best exemplified by the work carried out by Kolaczowski *et al.*, which used computational mod-

eling to guide their choice of parent molecules, and the design of their  $D_2/5-HT_6$  DMLs using two libraries of structurally similar  $D_2R$  partial agonists and  $5-HT_6$  receptor antagonists (not shown). This led to the discovery of 2-(3-(4-(1-(phenylsulfonyl)-1H-indol-4-yl)piperazin-1-yl)propoxy)benzamide (**50**), a DML with nanomolar affinity for its target receptors in rat models, and showed potent antidepressant and anxiolytic like effects [139]. More recently, in a computationally intensive study conducted by Möller *et al.*, 3D quantitative structure selectivity relationship (3D QSSR) in conjunction with CoMFA and CoMSIA prediction models to develop and design a series of  $5-HT_{2A}/D_2R$  DMLs. Möller's study yielded a library of synthesized GPCR ligands containing a pyrazolo[1,5-*a*]pyridine head group and a 1,2,3-triazole based linker unit (**51**) (Figure 21). This study yielded one highly potent DML that showed sub-nanomolar affinity for the  $5-HT_{2A}$  and appreciable affinity for the  $D_2R$  also [140]. Structural information also enabled Jörg *et al.* to convert a series of  $D_2R/A_{2A}AR$  heterobivalent ligands into DMLs. Using structural information such as the crystal structure of the  $A_{2A}AR$  [141] and the structure–activity relationship (SAR) analysis of ZM 241385 [142], Jörg *et al.* were able to remove the tyrosine moiety from ZM 241385 and attach it to ropinirole without the need for a spacer (**52**) (Figure 22) [107].

DMLs are an emerging field in the quest toward the development of novel CNS therapies with favorable pharmacological profiles. The ability to ‘design-in’ favorable pharmacological attributes of parent molecules while ‘designing-out’ their unfavorable attributes may allow for the repurposing of effective treatments that were discontinued based on unfavorable side effect profiles. While this idea makes DMLs an exciting prospect, a great deal of SAR information about the parent molecules, and a detailed understanding of receptor binding sites are required in order to accurately guide rational drug design. Additional challenges may also be faced by medicinal chemists including; attempting to determine disease-specific target combinations that provide highly efficacious clinical outcomes, and attempting to instill the correct balance of desired activities for each target while maintaining greater selectivity over undesired targets [65]. The increasing insights into GPCR–drug interactions provided by x-ray crystallography may enhance our ability to rationally design DMLs. In this regard, while we have gained some insight from the D<sub>3</sub>R crystal structure bound to eticlopride [4] (Figure 1), a structure of the D<sub>2</sub>R would be of significant value.

### Conclusion

The research presented in this review demonstrates that multivalent ligands have utility as chemical tools

and probes for the study of GPCR structure and function. Bivalent ligands provide an opportunity to probe the SAR and function of D<sub>2</sub>R dimers and higher order oligomers. The difficulties in correctly interpreting these data, however, stems from an inability to conclusively determine whether receptors truly form dimers in native tissues and whether these molecules bind in a truly bivalent fashion. Similarly, bitopic ligands provide a novel way to explore concepts such as biased agonism and allostery. However, careful planning of experiments and the subsequent analysis of the data obtained is necessary in truly determining whether these ligands concomitantly interact with both the orthosteric and allosteric site of a receptor. Finally, DMLs provide promise for the development of drug-like molecules that display a specific profile of polypharmacology at different therapeutically implicated receptors as an approach to treat complex disease states such as SCZ and PD.

### Future perspective

Multivalent ligands have utility as chemical tools and probes for the study of receptor structure and function at the D<sub>2</sub>R and other GPCRs of interest. It is envisioned that difficulties in the interpretation of data obtained through their use may only be addressed upon the development of crystallization methods which enable the structure of the D<sub>2</sub>R to be elucidated. From this, it is anticipated that bound crystal structures of these classes of ligands may be obtained in order to eliminate

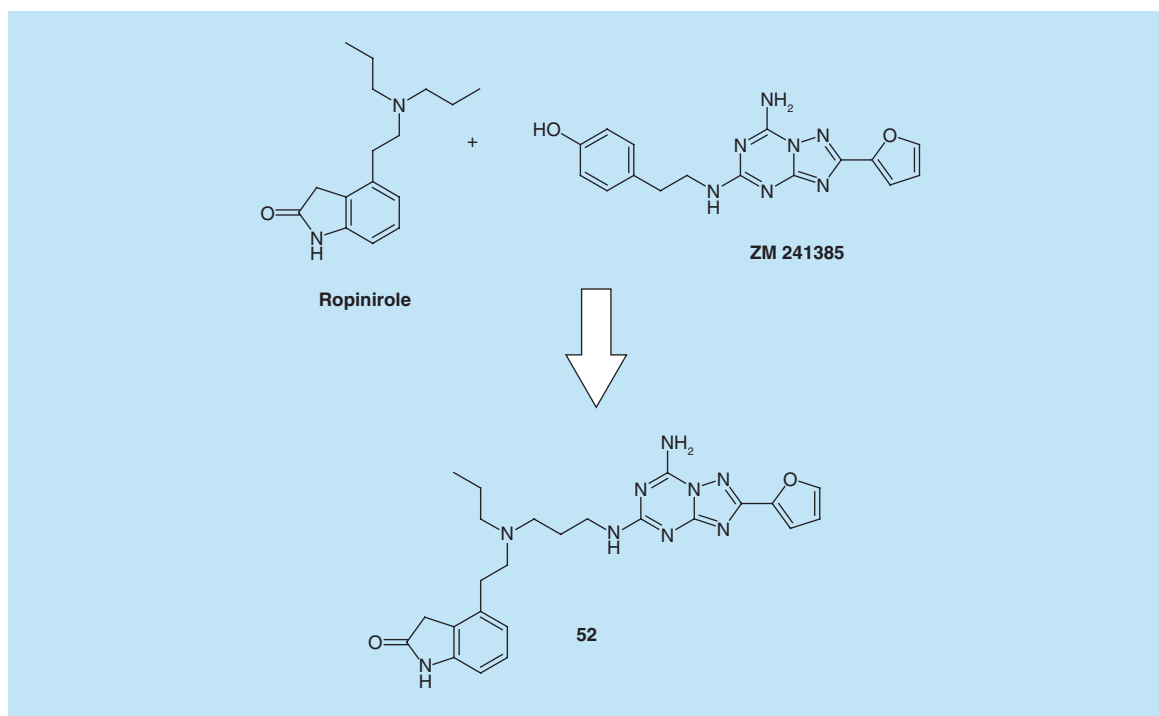


**Figure 22.** The chemical structure of the D<sub>2</sub>R/A<sub>2A</sub>AR designed multiple ligand (52) resulting from the progressive integration of ropinirole and ZM 241385.

the ambiguities that surround the interpretation of the results that they produce. While hetero- and homo-bivalent ligands have utility in the study of GPCR oligomers, their use must be accompanied by complementary biophysical or biochemical approaches that allow us to define the nature of the receptor complexes.

### Acknowledgements

The authors wish to thank Tamir Dingjan for computational assistance in generating **Figure 1** for this paper.

### Financial & competing interests disclosure

A Kopinathan gratefully acknowledges the Faculty of Pharmacy and Pharmaceutical Sciences, Monash University for financial support. The authors have no other relevant affiliations or financial involvement with any organization or entity with a financial interest in or financial conflict with the subject matter or materials discussed in the manuscript apart from those disclosed.

No writing assistance was utilized in the production of this manuscript.

### Executive summary

- The development of tool compounds and chemical probes using multivalent approaches has enabled the investigation of concepts such as allosterism, bitopic binding, bivalent binding and dual receptor binding to aid the development of novel D<sub>2</sub>R treatments.
- Bivalent ligands are useful tool compounds in studying the function of D<sub>2</sub>R homodimers, heterodimers and oligomers.
- Bitopic ligands enable the investigation of allostery via a novel mode of interaction and may also enable the study of biased agonism and ways to avoid on-target side effects that affect current treatments for SCZ and PD.
- DMLs provide us with structural insights into the chemical requirements for the development of multitarget drugs for treatment of complex disease states.
- These probes are useful in the investigation of pharmacological concepts at the D<sub>2</sub>R; however, caution should be exercised in interpreting the results obtained given the ambiguity surrounding their mechanisms of interaction.

### References

Papers of special note have been highlighted as:

• of interest; •• of considerable interest

- 1 Kobilka BK. G protein coupled receptor structure and activation. *Biochim. Biophys. Acta* 1768(4), 794–807 (2007).
- 2 Fredriksson R, Lagerstrom MC, Lundin LG, Schiöth HB. The G-protein-coupled receptors in the human genome form five main families: phylogenetic analysis, paralogon groups, and fingerprints. *Mol. Pharmacol.* 63(6), 1256–1272 (2003).
- 3 Rask-Andersen M, Almén MS, Schiöth HB. Trends in the exploitation of novel drug targets. *Nat. Rev. Drug Discov.* 10(8), 579–590 (2011).
- 4 Chien EY, Liu W, Zhao Q *et al.* Structure of the human dopamine D<sub>3</sub> receptor in complex with a D<sub>2</sub>/D<sub>3</sub> selective antagonist. *Science* 330(6007), 1091–1095 (2010).
- 5 Mcallister G, Knowles MR, Ward-Booth SM *et al.* Functional coupling of human D<sub>2</sub>, D<sub>3</sub>, and D<sub>4</sub> dopamine receptors in HEK293 cells. *J. Recept. Signal Transduction* 15(1–4), 267–281 (1995).
- 6 Gingrich JA, Caron MG. Recent advances in the molecular biology of dopamine receptors. *Annu. Rev. Neurosci.* 16(1), 299–321 (1993).
- 7 Beaulieu JM, Gainetdinov RR. The physiology, signaling, and pharmacology of dopamine receptors. *Pharmacol. Rev.* 63(1), 182–217 (2011).
- 8 Carlsson A. A paradigm shift in brain research. *Science* 294(5544), 1021–1024 (2001).
- 9 Iversen SD, Iversen LL. Dopamine: 50 years in perspective. *Trends Neurosci.* 30(5), 188–193 (2007).
- 10 Missale C, Nash SR, Robinson SW, Jaber M, Caron MG. Dopamine receptors: from structure to function. *Physiol. Rev.* 78(1), 189–225 (1998).
- 11 Snyder SH, Taylor KM, Coyle JT, Meyerhoff JL. The role of brain dopamine in behavioral regulation and the actions of psychotropic drugs. *Am. J. Psychiatry* 127(2), 199–207 (1970).
- 12 Sibley DR. New insights into dopaminergic receptor function using antisense and genetically altered animals. *Annu. Rev. Pharmacol. Toxicol.* 39 313–341 (1999).
- 13 Ibrahim NaE. Nausea and vomiting in cancer patients: topic review. *J. Palliat. Care Med.* 5(1), 203 (2014).
- 14 Rinne UK, Lonnberg P, Koskinen V. Dopamine receptors in the Parkinsonian brain. *J. Neural Transm.* 51(1–2), 97–106 (1981).
- 15 Guttman M, Seeman P. L-dopa reverses the elevated density of D<sub>2</sub> dopamine receptors in Parkinson's diseased striatum. *J. Neural Transm.* 64(2), 93–103 (1985).
- 16 Wong DF, Wagner HN, Tune LE *et al.* Positron emission tomography reveals elevated D<sub>2</sub> dopamine-receptors in drug-naïve schizophrenics. *Science* 234(4783), 1558–1563 (1986).
- 17 German DC, Manaye K, Smith WK, Woodward DJ, Saper CB. Midbrain dopaminergic cell loss in Parkinson's disease: computer visualization. *Ann. Neurol.* 26(4), 507–514 (1989).
- 18 Tune LE, Wong DF, Pearlson G *et al.* Dopamine D-2 receptor density estimates in schizophrenia: a positron

- emission tomography study with C-11 N-methylspiperone. *Psychiatry Res.* 49(3), 219–237 (1993).
- 19 Hietala J, Syvalahti E, Vuorio K *et al.* Striatal D2 dopamine receptor characteristics in neuroleptic-naïve schizophrenic patients studied with positron emission tomography. *Arch. Gen. Psychiatry* 51(2), 116–123 (1994).
  - 20 Goldsmith SK, Shapiro RM, Joyce JN. Disrupted pattern of D2 dopamine receptors in the temporal lobe in schizophrenia: a postmortem study. *Arch. Gen. Psychiatry* 54(7), 649–658 (1997).
  - 21 Jucaite A, Nyberg S. Dopaminergic hypothesis of schizophrenia: a historical perspective. In: *Targets and Emerging Therapies for Schizophrenia*. Albert JS, Wood MW (Eds). John Wiley & Sons, Inc., NJ, USA, 5–35 (2012).
  - 22 Davis KL, Kahn RS. Dopamine in schizophrenia: a review and reconceptualization. *Am. J. Psychiatry* 148(11), 1474 (1991).
  - 23 Sesack SR, Carr DB. Selective prefrontal cortex inputs to dopamine cells: implications for schizophrenia. *Physiol. Behav.* 77(4–5), 513–517 (2002).
  - 24 Bruder GE, Keilp JG, Xu H *et al.* Catechol-O-methyltransferase (COMT) genotypes and working memory: associations with differing cognitive operations. *Biol. Psychiatry* 58(11), 901–907 (2005).
  - 25 Lindenmayer JP. Treatment refractory schizophrenia. *Psychiatric Quart.* 71(4), 373–384 (2000).
  - 26 Meltzer HY, Li Z, Kaneda Y, Ichikawa J. Serotonin receptors: their key role in drugs to treat schizophrenia. *Prog. Neuro-Psychopharmacol. Biol. Psychiatry* 27(7), 1159–1172 (2003).
  - 27 Aghajanian GK, Marek GJ. Serotonin model of schizophrenia: emerging role of glutamate mechanisms. *Brain Res. Rev.* 31(2–3), 302–312 (2000).
  - 28 Raedler TJ, Bymaster FP, Tandon R, Copolov D, Dean B. Towards a muscarinic hypothesis of schizophrenia. *Mol. Psychiatry* 12(3), 232–246 (2006).
  - 29 Insel TR. Rethinking schizophrenia. *Nature* 468(7321), 187–193 (2010).
  - 30 Stahl SM. Psychosis and schizophrenia. In: *Stahl's Essential Psychopharmacology: Neuroscientific Basis and Practical Applications*. Stahl SM (Ed.). Cambridge University Press, London, UK, 79–128 (2013).
  - 31 Newman-Tancredi A. Biased agonism at serotonin 5-HT<sub>1A</sub> receptors: preferential postsynaptic activity for improved therapy of CNS disorders. *Neuropsychology* 1(2), 149–164 (2011).
  - 32 Mukherjee J. Evaluation of dopamine D-2 receptor occupancy by clozapine, risperidone, and haloperidol *in vivo* in the rodent and nonhuman primate brain using 18F-fallypride. *Neuropsychopharmacology* 25(4), 476–488 (2001).
  - 33 Kapur S, Seeman P. Does fast dissociation from the dopamine D-2 receptor explain the action of atypical antipsychotics? A new hypothesis. *Am. J. Psychiatry* 158(3), 360–369 (2001).
  - 34 Sahlholm K, Zeberg H, Nilsson J, Ögren SO, Fuxe K, Århem P. The fast-off hypothesis revisited: a functional kinetic study of antipsychotic antagonism of the dopamine D2 receptor. *Eur. Neuropsychopharmacol.* 26(3), 467–476 (2016).
  - 35 Reynolds GP, Kirk SL. Metabolic side effects of antipsychotic drug treatment: pharmacological mechanisms. *Pharmacol. Ther.* 125(1), 169–179 (2010).
  - 36 De Hert M, Detraux J, Van Winkel R, Yu W, Correll CU. Metabolic and cardiovascular adverse effects associated with antipsychotic drugs. *Nat. Rev. Endocrinol.* 8(2), 114–126 (2012).
  - 37 Iqbal MM, Rahman A, Husain Z, Mahmud SZ, Ryan W, Feldman J. Clozapine: a clinical review of adverse effects and management. *Ann. Clin. Psychiatry* 15(1), 33–48 (2003).
  - 38 Cohen D, Bogers JP, Van Dijk D, Bakker B, Schulte PF. Beyond white blood cell monitoring: screening in the initial phase of clozapine therapy. *J. Clin. Psychiatry* 73(10), 1307–1312 (2012).
  - 39 Shulman JM, De Jager PL, Feany MB. Parkinson's disease: genetics and pathogenesis. *Annu. Rev. Pathol.* 6 193–222 (2011).
  - 40 Carlsson A, Lindqvist M, Magnusson TOR. 3,4-dihydroxyphenylalanine and 5-hydroxytryptophan as reserpine antagonists. *Nature* 180(4596), 1200–1200 (1957).
  - 41 Carlsson A. The occurrence, distribution and physiological role of catecholamines in the nervous system. *Pharmacol. Rev.* 11(2, Part 2), 490–493 (1959).
  - 42 Stocchi F. The levodopa wearing-off phenomenon in Parkinson's disease: pharmacokinetic considerations. *Expert Opin. Pharmacother.* 7(10), 1399–1407 (2006).
  - 43 Lees AJ. The on-off phenomenon. *J. Neurol. Neurosurg. Psychiatry* 52(Suppl.), 29–37 (1989).
  - 44 Fahn S. The history of dopamine and levodopa in the treatment of Parkinson's disease. *Mov. Disord.* 23(Suppl. 3), S497–S508 (2008).
  - 45 Jorg M, Scammells PJ, Capuano B. The dopamine D2 and adenosine A2A receptors: past, present and future trends for the treatment of Parkinson's disease. *Curr. Med. Chem.* 21(27), 3188–3210 (2014).
  - 46 Fernandez HH, Chen JJ. Monoamine oxidase-B inhibition in the treatment of Parkinson's disease. *Pharmacotherapy* 27(12P2), S174–S185 (2007).
  - 47 Kurth MC, Adler CH, Hilaire MS *et al.* Tolcapone improves motor function and reduces levodopa requirement in patients with Parkinson's disease experiencing motor fluctuations: a multicenter, double-blind, randomized, placebo-controlled trial. Tolcapone Fluctuator Study Group I. *Neurology* 48(1), 81–87 (1997).
  - 48 Nutt JG, Woodward WR, Beckner RM *et al.* Effect of peripheral catechol-O-methyltransferase inhibition on the pharmacokinetics and pharmacodynamics of levodopa in parkinsonian patients. *Neurology* 44(5), 913–919 (1994).
  - 49 Nutt JG. Pharmacokinetics and pharmacodynamics of levodopa. *Mov. Disord.* 23(Suppl. 3), S580–S584 (2008).
  - 50 Stacy M, Galbreath A. Optimizing long-term therapy for Parkinson disease: options for treatment-associated dyskinesia. *Clin. Neuropharmacol.* 31(2), 120–125 (2008).
  - 51 Keyser JD. Subtypes and localization of dopamine receptors in human brain. *Neurochem. Int.* 22(2), 83–93 (1993).

- 52 Barone P, Scarzella L, Marconi R *et al.* Pramipexole versus sertraline in the treatment of depression in Parkinson's disease. *J. Neurol.* 253(5), 601–607 (2006).
- 53 Maj J, RogóZ Z, Skuza G, Kołodziejczyk K. Antidepressant effects of pramipexole: a novel dopamine receptor agonist. *J. Neural Transm.* 104(4–5), 525–533 (1997).
- 54 Lewis M, Huang X, Nichols D, Mailman R. D1 and functionally selective dopamine agonists as neuroprotective agents in Parkinson's disease. *CNS Neurol. Disord. Drug Targets* 5(3), 345–353 (2006).
- 55 Antonini A, Tolosa E, Mizuno Y, Yamamoto M, Poewe WH. A reassessment of risks and benefits of dopamine agonists in Parkinson's disease. *Lancet Neurol.* 8(10), 929–937 (2009).
- 56 Nutt JG, Fellman JH. Pharmacokinetics of levodopa. *Clin. Neuropharmacol.* 7(1), 35–49 (1984).
- 57 Kiessling LL, Gestwicki JE, Strong LE. Synthetic multivalent ligands as probes of signal transduction. *Angew. Chem. Int. Ed. Engl.* 45(15), 2348–2368 (2006).
- 58 Bunnage ME. Getting pharmaceutical R&D back on target. *Nat. Chem. Biol.* 7(6), 335–339 (2011).
- 59 Mammen M, Choi SK, Whitesides GM. Polyvalent interactions in biological systems: implications for design and use of multivalent ligands and inhibitors. *Angew. Chem. Int. Ed. Engl.* 37(20), 2755–2794 (1998).
- 60 Krishnamurthy VM, Estroff LA, Whitesides GM. Multivalency in ligand design. In: *Fragment-Based Approaches in Drug Discovery*. Jahnke W, Erlanson DA (Eds). Wiley-VCH Verlag GmbH & Co. KGaA 11–53 (2006).
- 61 Shonberg J, Scammells PJ, Capuano B. Design strategies for bivalent ligands targeting GPCRs. *ChemMedChem* 6(6), 963–974 (2011).
- 62 Berque-Bestel I, Lezoualc'h F, Jockers R. Bivalent ligands as specific pharmacological tools for G protein-coupled receptor dimers. *Curr. Drug Disc. Technol.* 5(4), 312–318 (2008).
- 63 Lane JR, Sexton PM, Christopoulos A. Bridging the gap: bitopic ligands of G-protein-coupled receptors. *Trends Pharmacol. Sci.* 34(1), 59–66 (2013).
- **A comprehensive review of current knowledge in the field of bitopic ligands.**
- 64 Valant C, Robert Lane J, Sexton PM, Christopoulos A. The best of both worlds? Bitopic orthosteric/allosteric ligands of G protein-coupled receptors. *Annu. Rev. Pharmacol. Toxicol.* 52 153–178 (2012).
- 65 Morphy R, Rankovic Z. Design of multitarget ligands. In: *Lead Generation Approaches in Drug Discovery*. Morphy R, Rankovic Z (Eds). John Wiley & Sons, Inc., NJ, USA, 141–164 (2010).
- **A useful resource for the design and development of designed multiple ligands.**
- 66 Shi L, Javitch JA. The binding site of aminergic G protein-coupled receptors: the transmembrane segments and second extracellular loop. *Annu. Rev. Pharmacol. Toxicol.* 42, 437–467 (2002).
- 67 Sukalovic V, Soskic V, Kostic-Rajacic S. Modeling of dopamine D2 receptor: overview of 35-year evolution. *Curr. Med. Chem.* 22(25), 2972–2990 (2015).
- 68 Conn PJ, Christopoulos A, Lindsley CW. Allosteric modulators of GPCRs: a novel approach for the treatment of CNS disorders. *Nat. Rev. Drug Discov.* 8(1), 41–54 (2009).
- 69 Christopoulos A. Advances in GPCR allostery: from function to structure. *Mol. Pharmacol.* 86(5), 463–478 (2014).
- 70 Wang L, Martin B, Brennehan R, Luttrell LM, Maudsley S. Allosteric modulators of G protein-coupled receptors: future therapeutics for complex physiological disorders. *J. Pharmacol. Exp. Ther.* 331(2), 340–348 (2009).
- 71 Zawarynski P, Talerico T, Seeman P, Lee SP, O'dowd BF, George SR. Dopamine D2 receptor dimers in human and rat brain. *FEBS Lett.* 441(3), 383–386 (1998).
- 72 Maggio R, Scarselli M, Novi F, Corsini GU. Heterodimerization of G-protein-coupled receptors reveals an unexpected level of pharmacological diversity. *Med. Chem. Res.* 13(1–2), 25–33 (2004).
- 73 Canals M, Marcellino D, Fanelli F *et al.* Adenosine A2A-dopamine D2 receptor–receptor heteromerization: qualitative and quantitative assessment by fluorescence and bioluminescence energy transfer. *J. Biol. Chem.* 278(47), 46741–46749 (2003).
- 74 Armstrong D, Strange PG. Dopamine D2 receptor dimer formation: evidence from ligand binding. *J. Biol. Chem.* 276(25), 22621–22629 (2001).
- 75 Pei L, Li S, Wang M *et al.* Uncoupling the dopamine D1–D2 receptor complex exerts antidepressant-like effects. *Nat. Med.* 16(12), 1393–1395 (2010).
- 76 Lukasiewicz S, Polit A, Kedracka-Krok S, Wedzony K, Mackowiak M, Dziedzicka-Wasylewska M. Heterodimerization of serotonin 5-HT(2A) and dopamine D(2) receptors. *Biochim. Biophys. Acta* 1803(12), 1347–1358 (2010).
- 77 Frederick AL, Yano H, Trifilieff P *et al.* Evidence against dopamine D1/D2 receptor heteromers. *Mol. Psychiatry* 20(11), 1373–1385 (2015).
- 78 Kenakin TP. Biased signalling and allosteric machines: new vistas and challenges for drug discovery. *Br. J. Pharmacol.* 165, 1659–1669 (2012).
- 79 Shonberg J, Lopez L, Scammells PJ, Christopoulos A, Capuano B, Lane JR. Biased agonism at G protein-coupled receptors: the promise and the challenges: a medicinal chemistry perspective. *Med. Res. Rev.* 34(6), 1286–1330 (2014).
- 80 Perreault ML, O'dowd BF, George SR. Dopamine receptor homooligomers and heterooligomers in schizophrenia. *CNS Neurosci. Ther.* 17(1), 52–57 (2011).
- 81 Palczewski K. Oligomeric forms of G protein-coupled receptors (GPCRs). *Trends Biochem. Sci.* 35(11), 595–600 (2010).
- 82 George SR, O'dowd BF, Lee SP. G-protein-coupled receptor oligomerization and its potential for drug discovery. *Nat. Rev. Drug Discov.* 1(10), 808–820 (2002).
- 83 Portoghese PS, Ronsisvalle G, Larson DL, Yim CB, Sayre LM, Takemori AE. Opioid agonist and antagonist bivalent ligands as receptor probes. *Life Sci.* 31(12–13), 1283–1286 (1982).

- 84 Erez M, Takemori AE, Portoghese PS. Narcotic antagonistic potency of bivalent ligands which contain beta-naltrexamine: evidence for simultaneous occupation of proximal recognition sites. *J. Med. Chem.* 25(7), 847–849 (1982).
- 85 Portoghese PS. From models to molecules: opioid receptor dimers, bivalent ligands, and selective opioid receptor probes. *J. Med. Chem.* 44(14), 2259–2269 (2001).
- 86 Portoghese PS, Larson DL, Sayre LM *et al.* Opioid agonist and antagonist bivalent ligands: the relationship between spacer length and selectivity at multiple opioid receptors. *J. Med. Chem.* 29(10), 1855–1861 (1986).
- 87 Portoghese PS. Bivalent ligands and the message-address concept in the design of selective opioid receptor antagonists. *Trends Pharmacol. Sci.* 10(6), 230–235 (1989).
- 88 Erbs E, Faget L, Scherrer G *et al.* A mu-delta opioid receptor brain atlas reveals neuronal co-occurrence in subcortical networks. *Brain Struct. Funct.* 220(2), 677–702 (2015).
- 89 Huber D, Hübner H, Gmeiner P. 1,1'-disubstituted ferrocenes as molecular hinges in mono- and bivalent dopamine receptor ligands. *J. Med. Chem.* 52(21), 6860–6870 (2009).
- 90 Ng GYK, O'dowd BF, Caron M, Dennis M, Brann MR, George SR. Phosphorylation and palmitoylation of the human D2L dopamine receptor in Sf9 cells. *J. Neurochem.* 63(5), 1589–1595 (1994).
- 91 Ng GYK, Odowd BF, Lee SP *et al.* Dopamine D2 receptor dimers and receptor-blocking peptides. *Biochem. Biophys. Res. Co.* 227(1), 200–204 (1996).
- 92 Lee SP, O'dowd BF, Ng GY *et al.* Inhibition of cell surface expression by mutant receptors demonstrates that D2 dopamine receptors exist as oligomers in the cell. *Mol. Pharmacol.* 58(1), 120–128 (2000).
- 93 Mohr K, Trankle C, Kostenis E, Barocelli E, De Amici M, Holzgrabe U. Rational design of dualsteric GPCR ligands: quests and promise. *Br. J. Pharmacol.* 159(5), 997–1008 (2010).
- 94 Jörg M, Kaczor AA, Mak FS *et al.* Investigation of novel ropinirole analogues: synthesis, pharmacological evaluation and computational analysis of dopamine D2 receptor functionalized congeners and homobivalent ligands. *MedChemComm* 5(7), 891 (2014).
- 95 Shonberg J, Lane JR, Scammells PJ, Capuano B. Synthesis, functional and binding profile of (R)-apomorphine based homobivalent ligands targeting the dopamine D2 receptor. *MedChemComm* 4(9), 1290–1296 (2013).
- 96 Mcrobb FM, Crosby IT, Yuriev E, Lane JR, Capuano B. Homobivalent ligands of the atypical antipsychotic clozapine: design, synthesis, and pharmacological evaluation. *J. Med. Chem.* 55(4), 1622–1634 (2012).
- 97 Kühhorn J, Hübner H, Gmeiner P. Bivalent dopamine D2 receptor ligands: synthesis and binding properties. *J. Med. Chem.* 54(13), 4896–4903 (2011).
- 98 Salama I, Löber S, Hübner H, Gmeiner P. Synthesis and binding profile of haloperidol-based bivalent ligands targeting dopamine D2-like receptors. *Bioorg. Med. Chem. Lett.* 24(16), 3753–3756 (2014).
- 99 Huber D, Löber S, Hübner H, Gmeiner P. Bivalent molecular probes for dopamine D2-like receptors. *Bioorg. Med. Chem.* 20(1), 455–466 (2012).
- 100 Angers S, Salahpour A, Joly E *et al.* Detection of beta 2-adrenergic receptor dimerization in living cells using bioluminescence resonance energy transfer (BRET). *Proc. Natl Acad. Sci. USA* 97(7), 3684–3689 (2000).
- 101 Kühhorn J, Götz A, Hübner H, Thompson D, Whistler J, Gmeiner P. Development of a bivalent dopamine D2 receptor agonist. *J. Med. Chem.* 54(22), 7911–7919 (2011).
- 102 Newman-Tancredi A, Kleven MS. Comparative pharmacology of antipsychotics possessing combined dopamine D2 and serotonin 5-HT1A receptor properties. *Psychopharmacology* 216(4), 451–473 (2011).
- 103 Armentero MT, Pinna A, Ferre S, Lanciego JL, Muller CE, Franco R. Past, present and future of A(2A) adenosine receptor antagonists in the therapy of Parkinson's disease. *Pharmacol. Ther.* 132(3), 280–299 (2011).
- 104 Roth BL, Sheffler DJ, Kroeze WK. Magic shotguns versus magic bullets: selectively non-selective drugs for mood disorders and schizophrenia. *Nat. Rev. Drug Discov.* 3(4), 353–359 (2004).
- 105 Schwarzschild MA, Agnati L, Fuxe K, Chen JF, Morelli M. Targeting adenosine A2A receptors in Parkinson's disease. *Trends Neurosci.* 29(11), 647–654 (2006).
- 106 Soriano A, Ventura R, Molero A *et al.* Adenosine A2A receptor-antagonist/dopamine D2 receptor-agonist bivalent ligands as pharmacological tools to detect A2A-D2 receptor heteromers. *J. Med. Chem.* 52(18), 5590–5602 (2009).
- 107 Jörg M, May LT, Mak FS *et al.* Synthesis and pharmacological evaluation of dual acting ligands targeting the adenosine A2A and dopamine D2 receptors for the potential treatment of Parkinson's disease. *J. Med. Chem.* 58(2), 718–738 (2015).
- **A good example of the evolution of DMLs from heterobivalent ligands.**
- 108 Valant C, Sexton PM, Christopoulos A. Orthosteric/allosteric bitopic ligands: going hybrid at GPCRs. *Mol. Interv.* 9(3), 125–135 (2009).
- 109 Antony J, Kellershohn K, Mohr-Andra M *et al.* Dualsteric GPCR targeting: a novel route to binding and signaling pathway selectivity. *FASEB J.* 23(2), 442–450 (2009).
- 110 Narlawar R, Lane JR, Doddareddy M, Lin J, Brussee J, Ijzerman AP. Hybrid ortho/allosteric ligands for the adenosine A(1) receptor. *J. Med. Chem.* 53(8), 3028–3037 (2010).
- 111 Valant C, May LT, Aurelio L *et al.* Separation of on-target efficacy from adverse effects through rational design of a bitopic adenosine receptor agonist. *Proc. Natl Acad. Sci. USA* 111(12), 4614–4619 (2014).
- 112 Schwartz TW, Holst B. Allosteric enhancers allosteric agonists and ago-allosteric modulators: where do they bind and how do they act? *Trends Pharmacol. Sci.* 28(8), 366–373 (2007).
- 113 Keov P, López L, Devine SM *et al.* Molecular mechanisms of bitopic ligand engagement with the M1 muscarinic acetylcholine receptor. *J. Biol. Chem.* 289(34), 23817–23837 (2014).
- 114 Silvano E, Millan MJ, Mannoury La Cour C *et al.* The tetrahydroisoquinoline derivative SB269,652 is an allosteric

- antagonist at dopamine D3 and D2 receptors. *Mol. Pharmacol.* 78(5), 925–934 (2010).
- 115 Lane JR, Donthamsetti P, Shonberg J *et al.* A new mechanism of allostery in a G protein-coupled receptor dimer. *Nat. Chem. Biol.* 10(9), 745–752 (2014).
- **Describes a mechanism of allostery via a bitopic binding interaction.**
- 116 Mistry SN, Shonberg J, Draper-Joyce CJ *et al.* Discovery of a novel class of negative allosteric modulator of the dopamine D2 receptor through fragmentation of a bitopic ligand. *J. Med. Chem.* 58(17), 6819–6843 (2015).
- 117 Langmead CJ, Christopoulos A. Functional and structural perspectives on allosteric modulation of GPCRs. *Curr. Opin. Cell Biol.* 27, 94–101 (2014).
- 118 Kruse AC, Ring AM, Manglik A *et al.* Activation and allosteric modulation of a muscarinic acetylcholine receptor. *Nature* 504(7478), 101–106 (2013).
- 119 Shonberg J, Draper-Joyce C, Mistry SN *et al.* Structure–activity study of N-((trans)-4-(2-(7-Cyano-3,4-dihydroisoquinolin-2(1H)-yl)ethyl)cyclohexyl)-1H-indole-2-carboxamide (SB269652): a bitopic ligand that acts as a negative allosteric modulator of the dopamine D2 receptor. *J. Med. Chem.* 58(13), 5287–5307 (2015).
- 120 Kenakin T, Miller LJ. Seven transmembrane receptors as shapeshifting proteins: the impact of allosteric modulation and functional selectivity on new drug discovery. *Pharmacol. Rev.* 62(2), 265–304 (2010).
- 121 Kenakin T, Christopoulos A. Signalling bias in new drug discovery: detection, quantification and therapeutic impact. *Nat. Rev. Drug Discov.* 12(3), 205–216 (2013).
- 122 Stallaert W, Christopoulos A, Bouvier M. Ligand functional selectivity and quantitative pharmacology at G protein-coupled receptors. *Expert Opin. Drug Discov.* 6(8), 811–825 (2011).
- 123 Bock A, Merten N, Schrage R *et al.* The allosteric vestibule of a seven transmembrane helical receptor controls G-protein coupling. *Nat. Commun.* 3, 1044 (2012).
- 124 Shapiro DA, Renock S, Arrington E *et al.* Aripiprazole, a novel atypical antipsychotic drug with a unique and robust pharmacology. *Neuropsychopharmacology* 28(8), 1400–1411 (2003).
- 125 Urban JD, Vargas GA, Von Zastrow M, Mailman RB. Aripiprazole has functionally selective actions at dopamine D-2 receptor-mediated signaling pathways. *Neuropsychopharmacology* 32(1), 67–77 (2007).
- 126 Chen X, Sassano MF, Zheng L *et al.* Structure-functional selectivity relationship studies of beta-arrestin-biased dopamine D(2) receptor agonists. *J. Med. Chem.* 55(16), 7141–7153 (2012).
- 127 Allen JaY JM, Setola V, Chen X *et al.* Discovery of  $\beta$ -arrestin-biased dopamine D2 ligands for probing signal transduction pathways essential for antipsychotic efficacy. *Proc. Natl Acad. Sci. USA* 108(45), 18488–18493 (2011).
- 128 Luedtke RR, Mishra Y, Wang Q *et al.* Comparison of the binding and functional properties of two structurally different D2 dopamine receptor subtype selective compounds. *ACS Chem. Neurosci.* 3(12), 1050–1062 (2012).
- 129 Vangveravong S, Zhang Z, Taylor M *et al.* Synthesis and characterization of selective dopamine D2 receptor ligands using aripiprazole as the lead compound. *Bioorg. Med. Chem.* 19(11), 3502–3511 (2011).
- 130 Moller D, Kling RC, Skultety M, Leuner K, Hubner H, Gmeiner P. Functionally selective dopamine D(2), D(3) receptor partial agonists. *J. Med. Chem.* 57(11), 4861–4875 (2014).
- 131 Szabo M, Klein Herenbrink C, Christopoulos A, Lane JR, Capuano B. Structure–activity relationships of privileged structures lead to the discovery of novel biased ligands at the dopamine D2 receptor. *J. Med. Chem.* 57(11), 4924–4939 (2014).
- 132 Kling RC, Tschammer N, Lanig H, Clark T, Gmeiner P. Active-state model of a dopamine D2 receptor – G $\alpha$ i complex stabilized by aripiprazole-type partial agonists. *PLoS ONE* 9(6), e100069 (2014).
- 133 Weichert D, Banerjee A, Hiller C, Kling RC, Hübner H, Gmeiner P. Molecular determinants of biased agonism at the dopamine D2 receptor. *J. Med. Chem.* 58(6), 2703–2717 (2015).
- 134 Morphy R, Rankovic Z. Designing multiple ligands – medicinal chemistry strategies and challenges. *Curr. Pharm. Des.* 15(6), 587–600 (2009).
- 135 Millan MJ. Multi-target strategies for the improved treatment of depressive states: conceptual foundations and neuronal substrates, drug discovery and therapeutic application. *Pharmacol. Ther.* 110(2), 135–370 (2006).
- 136 Yan Y, Zhou P, Rotella DP *et al.* Potent dihydroquinolinone dopamine D2 partial agonist/serotonin reuptake inhibitors for the treatment of schizophrenia. *Bioorg. Med. Chem. Lett.* 20(9), 2983–2986 (2010).
- 137 Carro L, Torrado M, Raviña E *et al.* Synthesis and biological evaluation of a series of aminoalkyl-tetralones and tetralols as dual dopamine/serotonin ligands. *Eur. J. Med. Chem.* 71 237–249 (2014).
- 138 Szabo M, Lim HD, Klein Herenbrink C, Christopoulos A, Lane JR, Capuano B. Proof of concept study for designed multiple ligands targeting the dopamine D2, serotonin 5-HT2A, and muscarinic M1 acetylcholine receptors. *J. Med. Chem.* 58(3), 1550–1555 (2015).
- 139 Kołaczkowski M, Marcinkowska M, Bucki A *et al.* Novel 5-HT6 receptor antagonists/D2 receptor partial agonists targeting behavioral and psychological symptoms of dementia. *Eur. J. Med. Chem.* 92 221–235 (2015).
- 140 Möller D, Salama I, Kling RC, Hübner H, Gmeiner P. 1,4-Disubstituted aromatic piperazines with high 5-HT2A/D2 selectivity: quantitative structure–selectivity investigations, docking, synthesis and biological evaluation. *Bioorg. Med. Chem.* 23(18), 6195–6209 (2015).
- 141 Jaakola V-P, Griffith MT, Hanson MA *et al.* The 2.6 angstrom crystal structure of a human A2A adenosine receptor bound to an antagonist. *Science* 322(5905), 1211–1217 (2008).
- 142 Federico S, Paoletta S, Cheong SL *et al.* Synthesis and biological evaluation of a new series of 1,2,4-triazolo[1,5-a]-1,3,5-triazines as human A(2A) adenosine receptor antagonists with improved water solubility. *J. Med. Chem.* 54(3), 877–889 (2011).

## 1.2 Thesis Aims

Multivalent ligands demonstrate a great deal of potential to act as chemical probes for the investigation of receptor structure and function, particularly at the D<sub>2</sub>R. A number of studies investigating D<sub>2</sub>R extended structures have postulated that these ligands bind the receptor via an extended or bitopic binding mode.<sup>1-4</sup> Although orthosteric interactions at the D<sub>2</sub>R have been thoroughly investigated using a variety of techniques,<sup>5,6</sup> very little is understood about allosteric binding interactions. Herein we present the use of extended D<sub>2</sub>R structures that engage the D<sub>2</sub>R in a multivalent fashion to probe the effects of concomitant orthosteric and allosteric binding on efficacy, negative cooperativity and receptor-ligand interactions at the D<sub>2</sub>R. As such, the overarching aim of this thesis is to demonstrate the utility of multivalent ligands as chemical probes for the pharmacological and structural evaluation of both orthosteric and allosteric interactions at the D<sub>2</sub>R. The published article entitled “Multivalent approaches and beyond: novel tools for the investigation of dopamine D<sub>2</sub> receptor pharmacology”, presented at the beginning of Chapter 1, provides a detailed review which forms the foundations of the ensuing chapters.

Chapter 2 focuses on the use of multivalent ligands to probe the determinants of efficacy at the D<sub>2</sub>R. A spectrum of D<sub>2</sub>R-acting ligands, ranging from inverse to full agonists, are currently used to treat a variety of central nervous system (CNS) disorders such as schizophrenia and Parkinson’s disease. Our understanding of the molecular basis which drives the efficacy of these ligands, however, is still in its infancy. Sub-chapter 2.1 aims to explore the determinants of efficacy at the D<sub>2</sub>R through the synthesis and pharmacological evaluation of truncated synthons of aripiprazole, the first FDA-approved partial agonist for the treatment of schizophrenia. To determine whether efficacy was driven by orthosteric or putative allosteric interactions at the D<sub>2</sub>R, synthons comprising of either the 1-(2,3-dichlorophenyl)piperazine (DCPP) “head” or the 1,2,3,4-tetrahydroquinolin-2-one (THQ) “tail” were synthesised (Figure A). The synthons were characterised pharmacologically to determine measures of binding affinity ( $K_i$ ), potency ( $EC_{50}$ ), functional affinity ( $K_A$ ) and efficacy ( $\tau$ ) using either an operational model of partial agonism or agonism. Next to determine whether similar changes in efficacy could be mediated upon attachment of the THQ “tail” of aripiprazole to a series of structurally diverse orthosteric D<sub>2</sub>R ligands, a series of hybrid molecules were synthesised (Figure A). The hybrid molecules and their precursors were then pharmacologically evaluated at the wild-type and a series of mutant receptors. The aim of this work was to determine whether it may be possible to elucidate key receptor interactions that may be important for the efficacy of these extended structures at the D<sub>2</sub>R. As a preliminary investigation Sub-chapter 2.2, drawing on the observations made in Sub-chapter 2.1,

aimed to investigate whether structurally differing tail moieties could direct the modulation of efficacy at the D<sub>2</sub>R. Herein a series of hybrid molecules which contain the *N*-cyclohexyl-7-azaindole-2-carboxamide moiety of a potent SB269652 analogue (a bitopic D<sub>2</sub>R negative allosteric modulator (NAM)), were synthesised and pharmacologically evaluated (Figure B).<sup>4,7</sup>

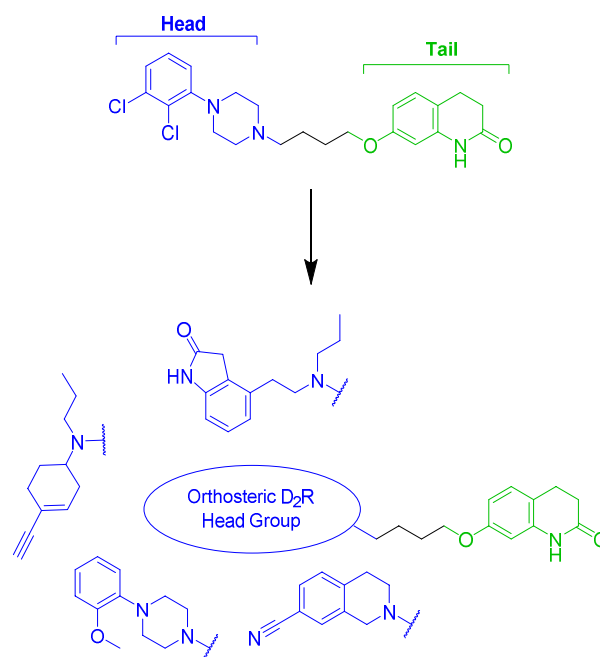


**Figure A.** The structure of aripiprazole highlighting the head (blue) and tail (green) moieties of its structure and the subsequent hybrid molecules developed.

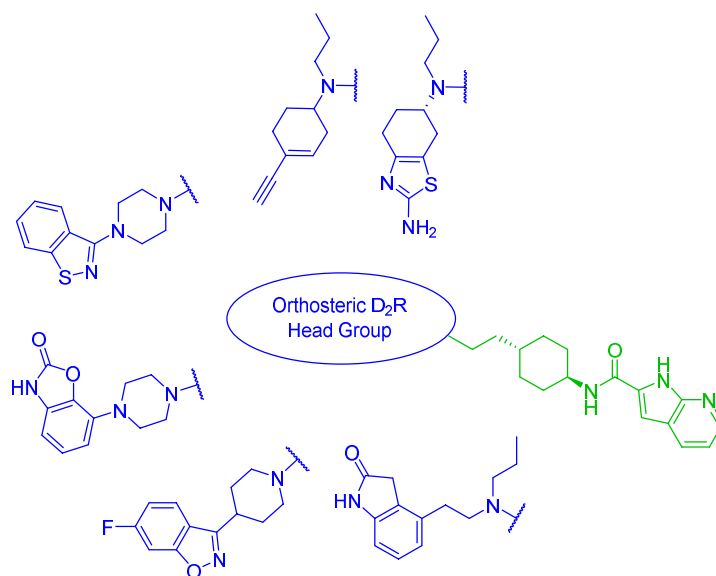


**Figure B.** The general structure of hybrid molecules synthesised in Sub-chapter 2.2 highlighting the orthosterically-binding head groups (blue) and the putative allosteric *N*-cyclohexyl-7-azaindole-2-carboxamide appendage (green).

Chapter 3 illustrates the utility of multivalent ligands as a probe for gaining insights into allostery at the D<sub>2</sub>R. SB269652 is the first drug-like D<sub>2</sub>R NAM described in the literature.<sup>7</sup> Subsequent SAR investigations of its structure, within our group, revealed that SB269652 engaged the D<sub>2</sub>R in a bitopic fashion and was able to modulate the potency of dopamine across a D<sub>2</sub>R homodimer.<sup>4</sup> An initial SAR investigation within our group observed that the indole-2-carboxamide tail of SB269652 was a key determinant of its negative cooperativity at the D<sub>2</sub>R.<sup>8</sup> In order to gain a greater appreciation of the molecular determinants of allostery at the D<sub>2</sub>R an SAR investigation of SB269652 was conducted which primarily focussed on making modifications to the indole-2-carboxamide tail (Figure C). To determine the effects on negative cooperativity caused by these modifications, the compounds were to be characterised using an operational model of allosterism to obtain values of functional affinity ( $K_B$ ), and cooperativity ( $\alpha\beta$ ) in the presence of dopamine. In conducting this SAR investigation, the aim was to also develop a suite of analogues with a range of negative cooperativities (from high to low). This would enable us to eventually probe the behavioural effects of these molecules in an *in vivo* setting and, ultimately, allow us to determine whether NAMs with varying cooperativity have the potential for therapeutic utility in a clinical setting.

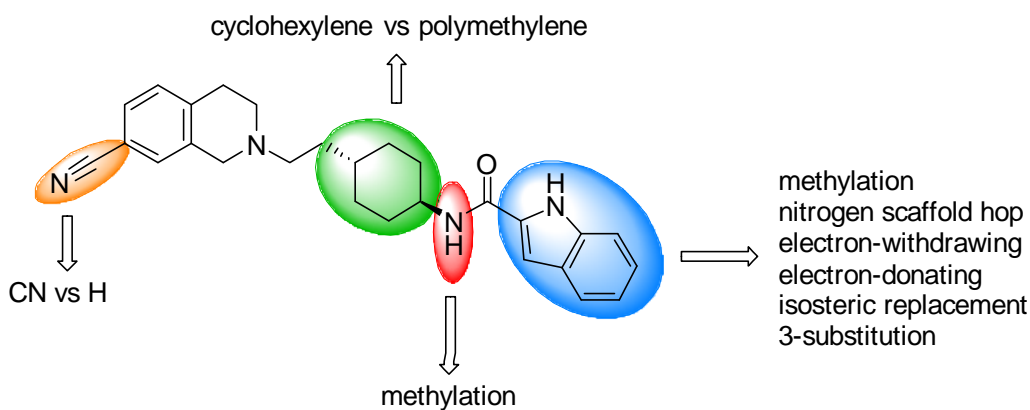


**Figure C.** Structural diversification of SB269652.

Chapter 4 showcases the use of multivalent ligands as irreversible probes for the investigation of receptor-ligand interactions at the D<sub>2</sub>R. Orthosteric binding at the D<sub>2</sub>R is a well understood phenomenon as a consequence of numerous investigations and the recent procurement of the highly homologous D<sub>3</sub>R crystal structure.<sup>5</sup> Allosteric binding at the D<sub>2</sub>R, however, is poorly understood as this region of GPCRs are less structurally conserved amongst receptor subtypes. Despite this, numerous extended D<sub>2</sub>R structures are postulated to engage the D<sub>2</sub>R via an “extended” or bitopic mode of binding.<sup>1-3,9</sup> Affinity labelling has been extensively utilised for the *in vitro* and *in vivo* examinations of GPCR structure, function, localisation and their interaction with ligands.<sup>10,11</sup> Additionally, the ability of some irreversible probes to also facilitate the crystallisation of GPCRs,<sup>12</sup> makes their development an attractive prospect particularly for the D<sub>2</sub>R. As such, a small series of SB269652 derivatives containing a photoactivatable azide moiety were devised as potential chemical tools that could be used to study allosteric or bitopic receptor-ligand interactions at the D<sub>2</sub>R. *In vitro* pharmacological methods were used to ensure that the two probes (Figure D) captured the binding site of interest, and were then evaluated for their ability to bind the D<sub>2</sub>R irreversibly upon photoactivation.

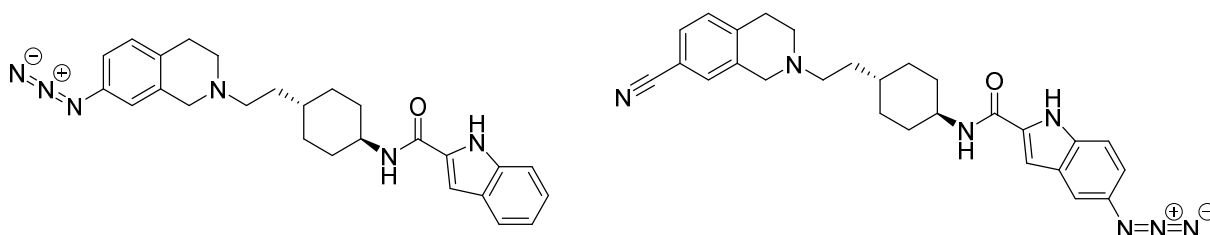


**Figure D.** The chemical structures of the proposed SB269652-derived photoactivatable irreversible D<sub>2</sub>R probes

### 1.2.1 References

1. Weichert, D.; Banerjee, A.; Hiller, C.; Kling, R. C.; Hübner, H.; Gmeiner, P. Molecular Determinants of Biased Agonism at the Dopamine D<sub>2</sub> Receptor. *J. Med. Chem.* **2015**, *58*, 2703-2717.
2. Szabo, M.; Klein Herenbrink, C.; Christopoulos, A.; Lane, J. R.; Capuano, B. Structure–Activity Relationships of Privileged Structures Lead to the Discovery of Novel Biased Ligands at the Dopamine D<sub>2</sub> Receptor. *J. Med. Chem.* **2014**, *57*, 4924-4939.
3. Shonberg, J.; Herenbrink, C. K.; Lopez, L.; Christopoulos, A.; Scammells, P. J.; Capuano, B.; Lane, J. R. A structure-activity analysis of biased agonism at the dopamine D<sub>2</sub> receptor. *J. Med. Chem.* **2013**, *56*, 9199-9221.
4. Lane, J. R.; Donthamsetti, P.; Shonberg, J.; Draper-Joyce, C. J.; Dentry, S.; Michino, M.; Shi, L.; Lopez, L.; Scammells, P. J.; Capuano, B.; Sexton, P. M.; Javitch, J. A.; Christopoulos, A. A new mechanism of allosterism in a G protein-coupled receptor dimer. *Nat. Chem. Biol.* **2014**, *10*, 745-752.
5. Chien, E. Y.; Liu, W.; Zhao, Q.; Katritch, V.; Han, G. W.; Hanson, M. A.; Shi, L.; Newman, A. H.; Javitch, J. A.; Cherezov, V.; Stevens, R. C. Structure of the human dopamine D<sub>3</sub> receptor in complex with a D<sub>2</sub>/D<sub>3</sub> selective antagonist. *Science*. **2010**, *330*, 1091-1095.
6. Shi, L.; Javitch, J. A. The binding site of aminergic G protein-coupled receptors: the transmembrane segments and second extracellular loop. *Annu. Rev. Pharmacol. Toxicol.* **2002**, *42*, 437-467.
7. Silvano, E.; Millan, M. J.; Mannoury la Cour, C.; Han, Y.; Duan, L.; Griffin, S. A.; Luedtke, R. R.; Aloisi, G.; Rossi, M.; Zazzeroni, F.; Javitch, J. A.; Maggio, R. The tetrahydroisoquinoline derivative SB269,652 is an allosteric antagonist at dopamine D<sub>3</sub> and D<sub>2</sub> receptors. *Mol. Pharmacol.* **2010**, *78*, 925-934.
8. Shonberg, J.; Draper-Joyce, C.; Mistry, S. N.; Christopoulos, A.; Scammells, P. J.; Lane, J. R.; Capuano, B. Structure–Activity Study of N-((trans)-4-(2-(7-Cyano-3,4-dihydroisoquinolin-2(1H)-yl)ethyl)cyclohexyl)-1H-indole-2-carboxamide (SB269652), a Bitopic Ligand That Acts as a Negative Allosteric Modulator of the Dopamine D<sub>2</sub> Receptor. *J. Med. Chem.* **2015**, *58*, 5287-5307.
9. Newman, A. H. B., T.; Banala, A. K.; Donthamsetti, P.; Pongetti, K.; LaBounty, A.; Levy, B.; Cao, J.; Michino, M.; Luedtke, R. R.; Javitch, J. A.; Shi, L. Molecular Determinants of Selectivity and Efficacy at the Dopamine D<sub>3</sub> Receptor. *J. Med. Chem.* **2012**, *55*, 6689-6699.
10. Weichert, D.; Gmeiner, P. Covalent molecular probes for class A G protein-coupled receptors: advances and applications. *ACS Chem. Biol.* **2015**, *10*, 1376-1386.

11. Jorg, M.; Scammells, P. J. Guidelines for the Synthesis of Small-Molecule Irreversible Probes Targeting G Protein-Coupled Receptors. *ChemMedChem* **2016**, 11, 1488-1498.
12. Weichert, D.; Kruse, A. C.; Manglik, A.; Hiller, C.; Zhang, C.; Hübner, H.; Kobilka, B. K.; Gmeiner, P. Covalent agonists for studying G protein-coupled receptor activation. *PNAS* **2014**, 111, 10744-10748.

---

## **Chapter 2**

# **Probing Efficacy at the Dopamine D<sub>2</sub> Receptor**

---

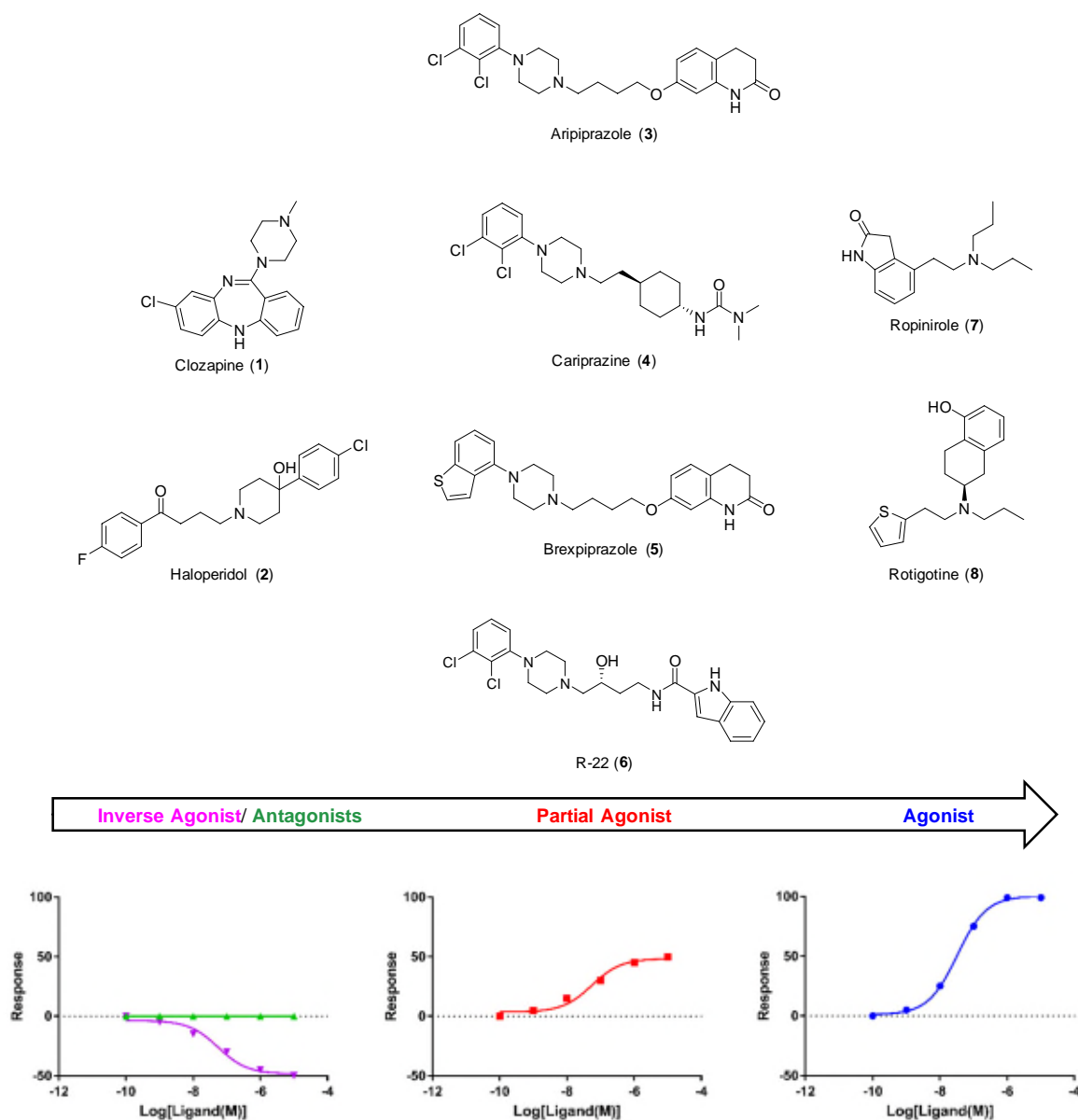
## **Chapter 2.1**

**Fragmentation of the Antipsychotic Aripiprazole Reveals the 1,2,3,4-Tetrahydroquinolin-2-one Moiety to be the Key Determinant of Efficacy and Affinity for Agonists at the Dopamine D<sub>2</sub> Receptor**

### 2.1.1 Introduction

The dopamine D<sub>2</sub> receptor (D<sub>2</sub>R) is a well-established therapeutic target for the treatment of disorders affecting the central nervous system (CNS). A broad spectrum of D<sub>2</sub>R-targeting ligands ranging from inverse agonists (or antagonists)<sup>1-3</sup> (e.g. clozapine (**1**) and haloperidol (**2**)) to agonists (e.g. ropinirole (**7**) and rotigotine (**8**))<sup>4</sup> are commonly used to treat the symptoms of diseases such as schizophrenia (SCZ) and Parkinson's disease, respectively (Figure 1). In more recent times, D<sub>2</sub>R-targeting partial agonists have also become a therapeutic approach for treating schizophrenia. Whilst their mechanism of action is not fully understood, the therapeutic utility of partial agonists (particularly in treating the symptoms of SCZ) is believed to result from their ability to attenuate or increase neurotransmission in dopaminergic pathways which are believed to be hyper- or hypoactive, respectively. As a consequence of this stabilising effect, partial agonists are also thought to be particularly beneficial in avoiding the undesirable extrapyramidal side effects (EPS) and hyperprolactinemia associated with typical antipsychotics.<sup>4</sup> Aripiprazole (**3**) was the first D<sub>2</sub>R partial agonist to gain FDA approval in 2002 for the treatment of SCZ,<sup>5</sup> however, it remains unclear why aripiprazole displays antipsychotic efficacy whilst other D<sub>2</sub>R partial agonists have failed to do so. Consequently, it has taken more than a decade for a second generation of D<sub>2</sub>R partial agonists (i.e. cariprazine (**4**)<sup>6</sup> and brexpiprazole (**5**)<sup>7</sup> (Figure 1)) to obtain FDA approval.

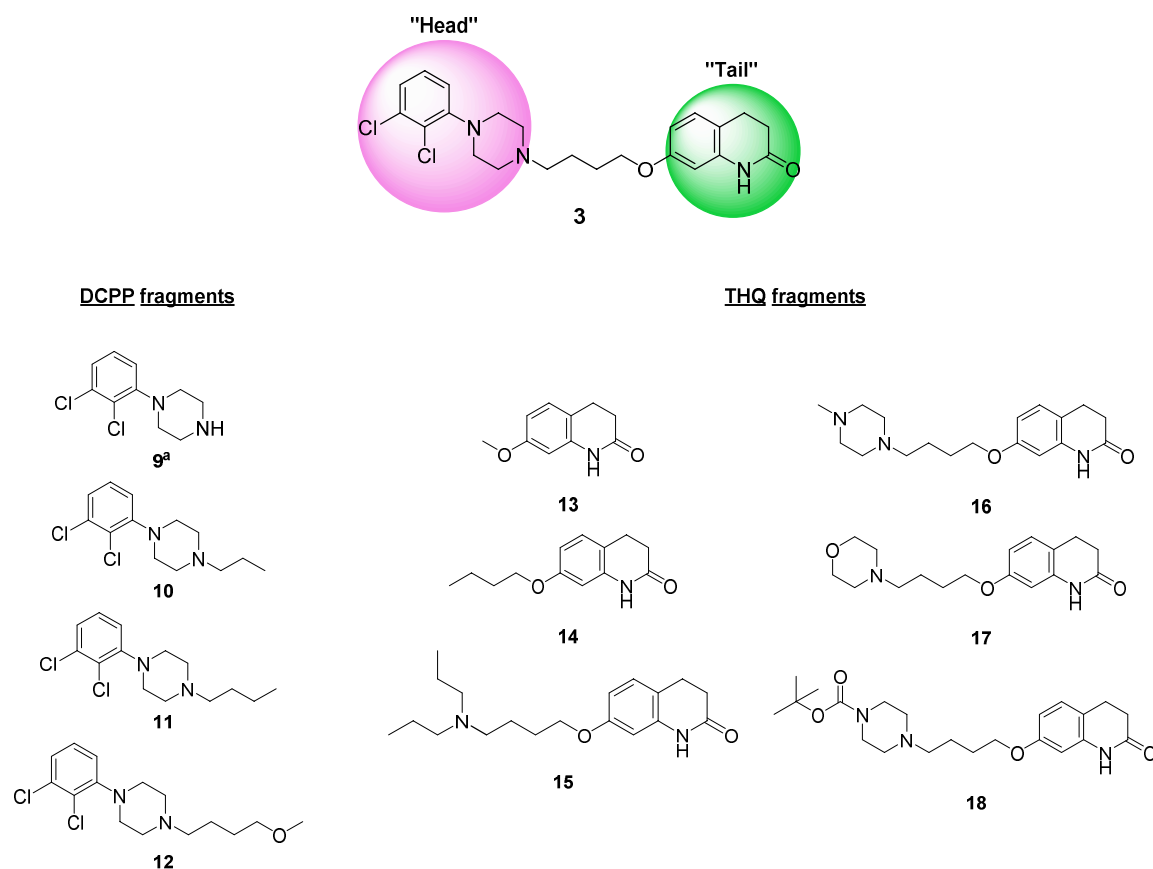
Based on our current understanding, it is evident that there is therapeutic utility for D<sub>2</sub>R ligands with a spectrum of efficacies to treat a variety of CNS disorders. Whilst our knowledge of orthosteric binding at the D<sub>2</sub>R have been furthered through affinity labelling studies, substituted cysteine accessibility studies and the resolution of the highly homologous D<sub>3</sub>R crystal structure,<sup>8-10</sup> our understanding of the molecular basis of efficacy at the D<sub>2</sub>R (which yields this spectrum of clinically relevant ligands) is still in its infancy. In a study conducted by Newman and colleagues, the structural determinants of gaining D<sub>3</sub>R selectivity over the D<sub>2</sub>R were investigated using deconstructed synthons of R-22 (**6**)<sup>11</sup> (Figure 1). Newman *et al.* noted that whilst the extended alkyl chain-containing synthons caused an enhancement of affinity at the D<sub>2</sub>R as a consequence of gaining additional receptor interactions, affinity and efficacy was decreased upon incorporation of the indole-2-carboxamide tail of **6**. Additionally, investigations of extended D<sub>2</sub>R partial agonists within our own research group demonstrated that modifications to the “tail” moiety which extends towards a secondary binding pocket of the D<sub>2</sub>R modulated efficacy and influenced their apparent biased agonism profiles.<sup>12,13</sup> Similar findings were also observed by the groups of Gmeiner and Li.<sup>14-16</sup> Taken together, it is apparent that an extended binding mode is an important determinant of affinity and efficacy of D<sub>2</sub>R partial agonists and other ligands, and may suggest that a bitopic mode of interaction may be consistent with these observations.



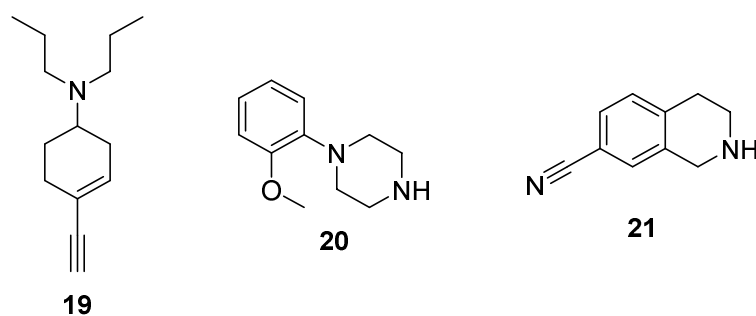
**Figure 1.** The structures of a variety of D<sub>2</sub>R-targeting ligands in the order of their relative increasing efficacies (LHS to RHS); inverse agonists (clozapine **1**) and haloperidol **2**), partial agonists (aripiprazole **3**), cariprazine **4**), brexpiprazole **5**) and R-22 **6**) and full agonists (ropinirole **7**) and rotigotine **8**)).

In order to gain a better understanding of structural determinants of agonist efficacy at the D<sub>2</sub>R, we chose to investigate the structural characteristics of **3**. A structure-activity relationship (SAR) study was conducted through the synthesis and pharmacological characterisation of a series of progressively fragmented synthons of **3** incorporating either the orthosterically-binding 1-(2,3-dichlorophenyl)piperazine (DCPP, and or “head”) or the 1,2,3,4-tetrahydroquinolin-2-one (THQ, and or “tail”) moieties of its structure (Figure 2). *In vitro* assays were used to evaluate the synthesised fragments to determine their ability to displace [<sup>3</sup>H]spiperone or [<sup>3</sup>H]raclopride binding at the D<sub>2</sub>R and their ability to stimulate the inhibition of forskolin (FSK)-induced cyclic

adenosine monophosphate (cAMP) production as a measure of D<sub>2</sub>R mediated G $\alpha_{i/o}$  G protein activation. Based on the pharmacological results obtained in the fragmented SAR of **3**, a series of hybrid molecules were synthesised by attaching the 7-butoxy-1,2,3,4-tetrahydroquinolin-2-one “tail”-containing moiety (fragment **14**) to a series of known orthosterically-binding D<sub>2</sub>R ligands (i.e. **7**, FAUC73 (**19**), 1-(2-methoxyphenyl)piperazine (**20**) and 1,2,3,4-tetrahydroisoquinoline-7-carbonitrile (**21**)) (Figures 1 and 3). These compounds were also evaluated using *in vitro* pharmacological profiling and provided further insights into the structural determinants of affinity and efficacy of elongated structures at the D<sub>2</sub>R.



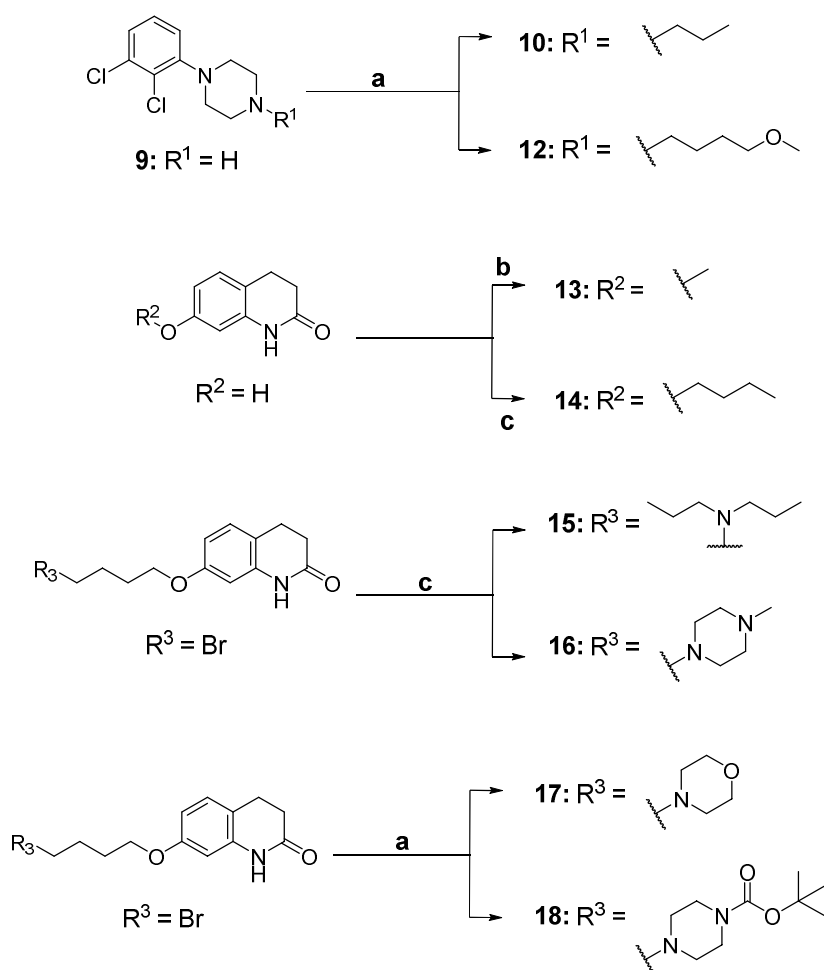
**Figure 2.** Progressively fragmented synthons of **3** incorporating either the DCP “head” or THQ “tail”. <sup>a</sup>Compound was commercially sourced as the hydrochloride salt.



**Figure 3.** Orthosterically-binding D<sub>2</sub>R ligands used in hybrid ligand synthesis; FAUC73 (**19**, D<sub>2</sub>R agonist), 1-(2-methoxyphenyl)piperazine (**20**, weak D<sub>2</sub>R partial agonist) and 1,2,3,4-tetrahydroisoquinoline-7-carbonitrile (**21**, D<sub>2</sub>R antagonist).

### 2.1.2 Synthesis

Fragments comprising either the “head” or “tail” moiety of **3** were synthesised using a series of nucleophilic substitution reactions (Scheme 1). The devised “head”-containing (DCPP) analogues (**9-12**) were progressively elongated towards the “tail” (THQ), whilst the THQ-containing compounds (**13-18**) were progressively extended towards the ionisable nitrogen of the “head” moiety. DCPP-containing synthons (**10** and **12**) were synthesised using commercially available 1-(2,3-dichlorophenyl)piperazine hydrochloride (**9**) and the necessary alkyl or methoxyalkyl halide to furnish the final products in yields of up to 54%. The alkyl chain-containing “tail” fragments, **13** and **14**, were similarly synthesised using 7-hydroxy-1,2,3,4-tetrahydroquinolin-2-one and the necessary alkyl halide which were left to stir at reflux for up to 5 d. **13** was synthesised in the presence of potassium carbonate (K<sub>2</sub>CO<sub>3</sub>) in DMF, whilst **14** was synthesised in the presence of both K<sub>2</sub>CO<sub>3</sub> and sodium iodide (NaI) in acetonitrile (MeCN), giving respective yields of 72% and 47%. THQ fragments incorporating an ionisable nitrogen to mimic that of the DCPP “head” group were devised such that only one ionisable nitrogen was present within their structures to ensure chemical similarity with **3**. Synthons **15** and **16** were synthesised in a similar fashion to fragment **14** and garnered in respective yields of 97% and 52%. Fragments **17** and **18** were synthesised by reacting 7-(4-bromobutoxy)-1,2,3,4-tetrahydroquinolin-2-one with either morpholine or *tert*-butyl piperazine-1-carboxylate, respectively, and obtained in respectable yields. Fragment **11** was previously synthesised following literature procedures and was included in our SAR study given its structural relevance to **3**.<sup>11</sup>

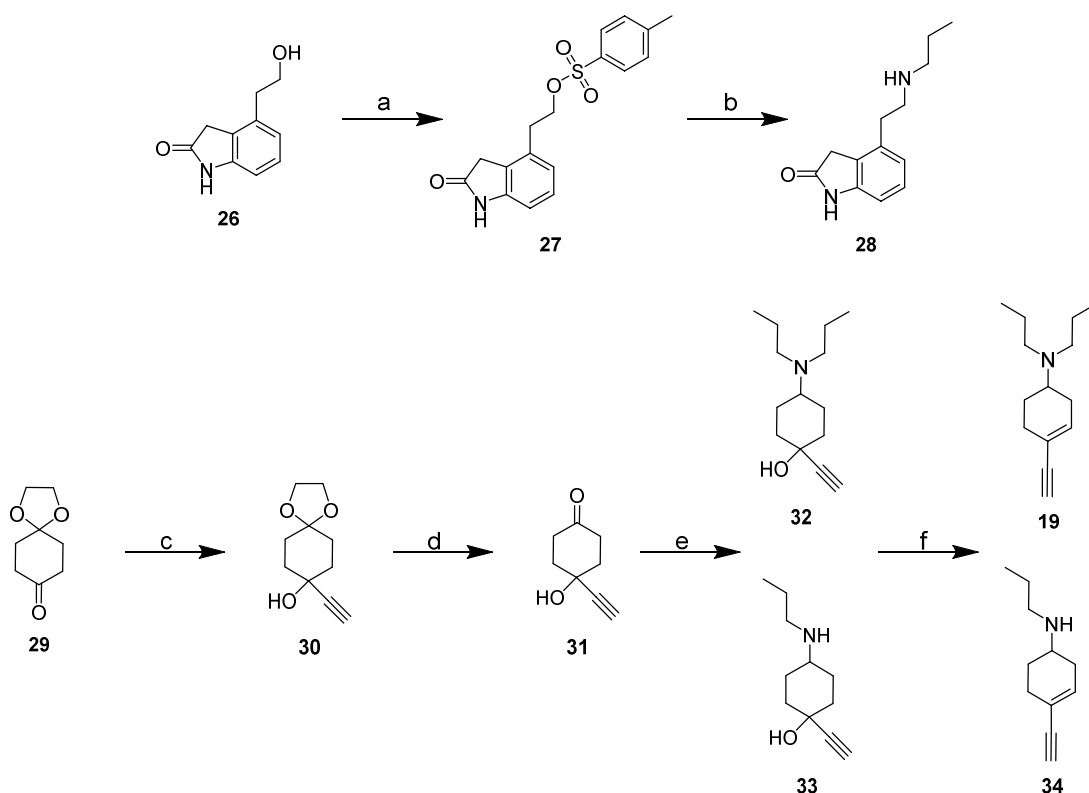
**Scheme 1.** Synthesis of DCPD and THQ-containing fragment synthons of 5<sup>a</sup>

<sup>a</sup>Reagents and conditions: (a) 1-bromopropane (for **10**), 1-bromo-4-methoxybutane (for **12**), morpholine (for **17**) or *tert*-butyl piperazine-1-carboxylate (for **18**), DIPEA, acetone, reflux, 13 h, 40-73%; (b) MeI, K<sub>2</sub>CO<sub>3</sub>, DMF, rt, 16 h, 72%; (c) 1-bromobutane (for **14**), di-*n*-propylamine (for **15**) or 1-methylpiperazine (for **16**), K<sub>2</sub>CO<sub>3</sub>, MeCN or acetone, NaI, reflux, 16 h-5 d, 47-97%.

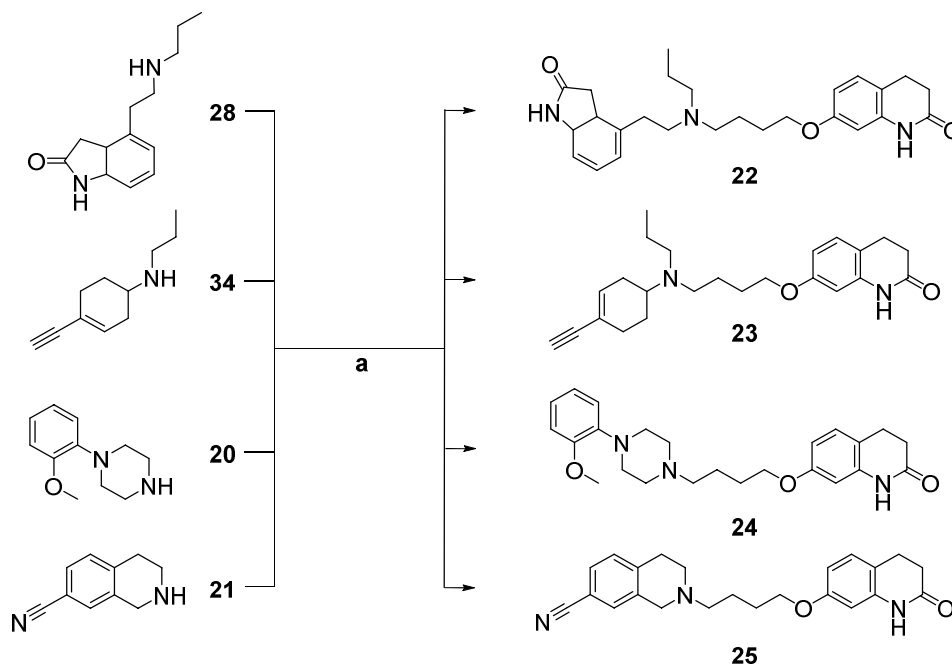
Next, to test whether a similar increase of affinity and efficacy could be observed upon the attachment of fragment **14** to other orthosteric D<sub>2</sub>R structures, a series of hybrid molecules were designed, synthesised and evaluated. Fragment **14** was attached to a set of pharmacologically and chemically diverse D<sub>2</sub>R structures such as ropinirole (**7**, D<sub>2</sub>R agonist),<sup>17</sup> FAUC73 (**19**, a non-canonical dopamine bioisostere (D<sub>2</sub>R agonist)),<sup>18</sup> 1-(2-methoxyphenyl)piperazine (**20**, a weak D<sub>2</sub>R partial agonist)<sup>11</sup> and 7-cyano-1,2,3,4-tetrahydroisoquinoline (**21**, D<sub>2</sub>R antagonist).<sup>19</sup> Synthesis of the hybrid molecule series proceeded with the formation of *des*-propyl analogues of compounds **7** and **19**. Scheme 2 illustrates the synthesis of these two key intermediates in addition to the *de novo* synthesis of **19**. Synthesis of the intermediate 4-(2-(propylamino)ethyl)indolin-2-one (**28**) was carried out following a procedure by Jorg *et al.*,<sup>20</sup> utilising prepared 4-(2-hydroxyethyl)indolin-2-one as the starting material. The alcohol (**26**) was activated via tosylation

then reacted with *n*-propylamine at reflux to furnish **28** in 54% yield. Following the synthetic route described by Hiller *et al.*,<sup>21</sup> compound **19** and its *des*-propyl analogue (**34**) were prepared from the initial Grignard reaction of 1,4-cyclohexane-dione monoethylene acetal (**29**) and ethynylmagnesium bromide which furnished the corresponding tertiary alcohol (**30**). Hydrolysis of the acetal protecting group (**31**) and subsequent reductive amination of the resulting ketone using the required amine in the presence of sodium triacetoxyborohydride (Na(OAc)<sub>3</sub>BH) produced the corresponding amino alcohols (**32**, **33**). The amino alcohols were then dehydrated using a mixture of triphenylphosphine (PPh<sub>3</sub>), I<sub>2</sub> and imidazole to give the products (**19**, **34**) in good yields. Formation of the final hybrid molecules (**21-25**) (Scheme 3) were conducted via a series of nucleophilic substitution reactions in the presence of 7-(4-bromobutoxy)-1,2,3,4-tetrahydroquinolin-2-one (sourced from AK Scientific, USA) and the corresponding secondary amine.

**Scheme 2.** Reaction schemes of key intermediates for hybrid synthesis and **19**<sup>a</sup>



<sup>a</sup>Reagents and conditions: *p*-toluenesulfonyl chloride, DCM, pyridine, 5–10 °C, 55%; (b) *n*-propylamine, reflux, 2 h, 54%; (c) ethynylmagnesium bromide, THF, 0 °C–rt, 24 h, 82%; (d) 80% (v/v) HCOOH, CuSO<sub>4</sub> (0.5 mol%), rt, 18 h, 78%; (e) NaBH(OAc)<sub>3</sub>, AcOH, DCM, 0 °C–rt, 18 h, (i) *n*-propylamine (87%), (ii) dipropylamine (55%); (f) PPh<sub>3</sub>, I<sub>2</sub>, imidazole, DCM, rt, 16 h, 3–41%.

**Scheme 3.** Synthesis of the 1,2,3,4-tetrahydroquinolin-2-one- containing hybrid molecules<sup>a</sup>

<sup>a</sup>Reagents and conditions: (a) 7-(4-bromobutoxy)-1,2,3,4-tetrahydroquinolin-2-one, K<sub>2</sub>CO<sub>3</sub>, MeCN, 18 h-6 d, 32-73%.

### 2.1.3 Pharmacological Characterisation

Compounds of interest were initially tested for their ability to bind the long or SNAP-tagged short isoforms of the D<sub>2</sub>R (D<sub>2L</sub>R and SNAP-D<sub>2S</sub>R, respectively) expressed in FlpIn CHO cells (Figure 5, Tables 1 and 3). Competition binding assays were carried out using either [<sup>3</sup>H]spiperone or [<sup>3</sup>H]raclopride (D<sub>2</sub>R antagonists) as the radioligand and a value of affinity (*K<sub>i</sub>*) was derived for competitive ligands. In order to measure the activity of compounds, we tested their ability to stimulate the inhibition of FSK-induced cAMP production through activation of the D<sub>2L</sub>R or SNAP-D<sub>2S</sub>R. From this assay, we were able to determine initial values of potency (*EC*<sub>50</sub>) and efficacy (*E*<sub>max</sub>) for each compound. Whilst informative, measures of *EC*<sub>50</sub> and *E*<sub>max</sub> can be of limited use since receptor expression levels, and the efficiency with which the pathway is coupled to the receptor, may influence the maximum effect and potency of a compound.<sup>22</sup> To mitigate this system dependence, partial agonists were subsequently fit to an operational model of partial agonism in order to obtain values of functional affinity (*K<sub>A</sub>*) and intrinsic efficacy (*τ*) (Tables 2 and 5). To quantify these values in compounds displaying full agonism, however, a series of cAMP inhibition assays were conducted in cells which were pre-treated with phenoxybenzamine (an alkylating agent which is used to inhibit high affinity orthosteric interactions at the D<sub>2</sub>R).<sup>23</sup> The data for compounds evaluated in the presence of the alkylating agent were then fit to an operational model of receptor depletion in order to determine values of *K<sub>A</sub>* and *τ* (Figure 5, Tables 3 and 5).

The ability of the fragment compounds **9-18** to competitively displace [<sup>3</sup>H]spiperone at the wild-type D<sub>2L</sub>R (Table 1) was evaluated. Compounds containing the orthosterically-binding DCPD motif demonstrated significant increases in affinity compared to **9** as they were progressively elongated towards the THQ moiety. Compounds **10-12** were observed to have an approximate 10-fold increase in affinity ( $K_i = 42.9 - 64.1$  nM) compared to the parent DCPD fragment (**9**,  $K_i = 501$  nM) upon introduction of the alkyl or alkoxy spacers. Incorporation of both the alkoxy spacer and the THQ moiety (to yield **3**) enhanced the binding affinity by 400-fold ( $K_i = 1.25$  nM) compared to **9**, suggesting that the THQ moiety is able to provide additional binding interactions within the D<sub>2</sub>R. Conversely, the THQ-containing fragments were only able to displace the radioligand upon inclusion of an ionisable nitrogen within its structure. Compounds lacking this key feature (i.e. **13** and **14**), appeared to be non-competitive and were unable to displace the radioligand.

**Table 1.** Binding affinities of the DCPD and THQ-containing aripiprazole fragments (**9-18**) and aripiprazole.<sup>a</sup>

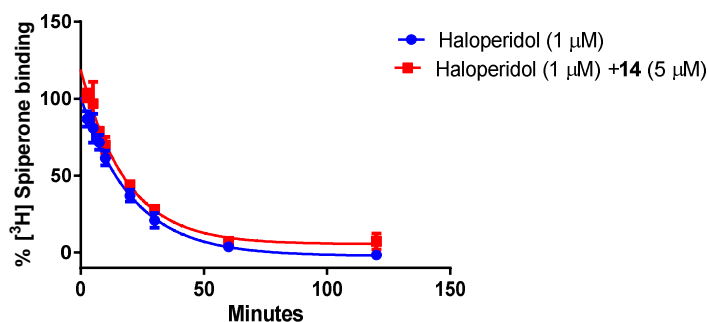
Compound	Fragment Class	p <i>K</i> <sub>i</sub> ± SEM ( <i>K</i> <sub>i</sub> , nM)
<b>9</b>	DCPD	6.30 ± 0.27 (501)****
<b>10</b>		7.34 ± 0.16 (45.9)***
<b>11</b>		7.19 ± 0.17 (64.1)***
<b>12</b>		7.34 ± 0.11 (42.9)***
<b>13</b>	THQ	-
<b>14</b>		-
<b>15</b>		<5 (>10000)
<b>16</b>		<5 (>10000)
<b>17</b>		<5 (>10000)
<b>18</b>		5.11 ± 0.30 (7831)*
<b>Aripiprazole (3)</b>	-	8.91 ± 0.14 (1.25)

<sup>a</sup>Determined by competition binding experiments using radiolabelled antagonist [<sup>3</sup>H]spiperone at D<sub>2L</sub>R expressed in FlpIn CHO cell membranes. Data represents the mean ± SEM of three separate experiments performed in duplicate. Values significantly different from the reference ligand (aripiprazole) as determined by one-way ANOVA (Dunnett's post-hoc test) are indicated by asterisk(s) (\*) (where \* =  $p < 0.05$ , \*\* =  $p < 0.01$ , \*\*\* =  $p < 0.001$ , \*\*\*\* =  $p < 0.0001$ ).

Similar fragment-based SAR investigations of McN-A-343 (a muscarinic receptor partial agonist)<sup>24</sup> and TBPB (a selective M<sub>1</sub> muscarinic acetylcholine receptor agonist)<sup>25</sup> revealed that they bound their target receptors in a bitopic manner, concomitantly engaging an orthosteric and an allosteric site within the receptor.<sup>26</sup> Given the significant enhancement in binding affinity observed upon elongation of the DCPD fragments towards the THQ moiety, we questioned whether **3** may bind to the D<sub>2</sub>R in a bitopic fashion whereby the THQ tail moiety engages with an allosteric binding site within the receptor. In order to probe this, fragment **14** was evaluated in

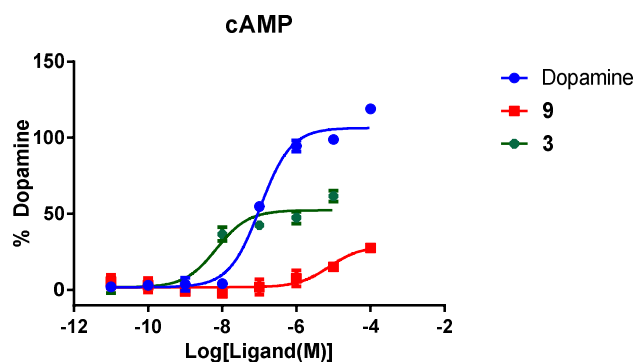
kinetic binding dissociation studies (Figure 4A). The rate of [<sup>3</sup>H]spiperone (1 μM) dissociation was not modulated in the presence of **14** (5 μM), thus, we could not provide clear evidence of the ability of fragment **14** to adopt an allosteric pose or that **3** might adopt a bitopic pose at the D<sub>2</sub>R. We next evaluated the ability of our compounds to activate the D<sub>2</sub>R and cause inhibition of forskolin-stimulated cAMP production. Specifically, we were interested in evaluating agonist efficacy at the D<sub>2</sub>R. An increase in functional affinity (777-fold) and efficacy (approximately 3-fold) was observed in the cAMP inhibition assay when fragments **9** and **14** are combined to yield **3** (Figure 4B, 4C and Table 2). These results demonstrate that the THQ moiety within **3** is important for the partial agonist efficacy of **3** at the D<sub>2</sub>R. Additionally, although the pharmacology of **3** is not the sum of an orthosteric and an allosteric fragment (as was shown to be the case for the partial agonists McN-A-343 and TBPB at the M<sub>2</sub> and M<sub>1</sub> muscarinic receptors, respectively),<sup>24,25</sup> it is interesting to note that our observations differ from those made by Newman *et al.*<sup>11</sup> where it was observed that incorporation of an indole-2-carboxamide containing tail to **9** (to yield R-22) caused a decrease in both affinity and efficacy at the D<sub>2</sub>R.

A



Compound	$t_{1/2}$ (min)	$k_{off} \pm SEM$ (min <sup>-1</sup> )
Haloperidol	14.4	$0.048 \pm 0.01$
Haloperidol + 14	12.7	$0.055 \pm 0.01$

B



C

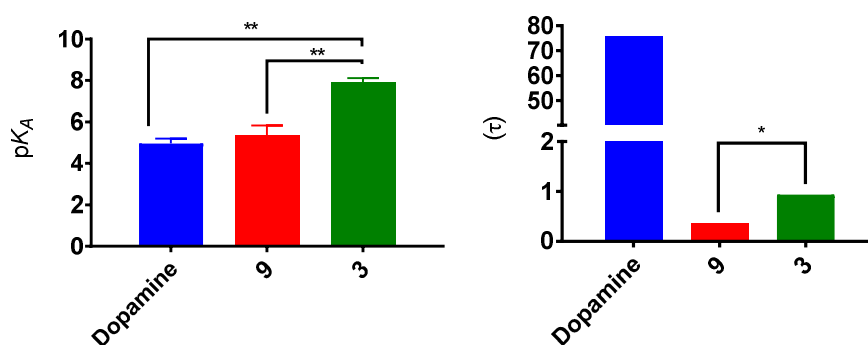


**Figure 4.** Kinetic binding dissociation curve of haloperidol and haloperidol in the presence of **14** showed no significant effect on radioligand dissociation (A). However, FSK-stimulated cAMP inhibition assays show a significant increase in functional affinity and efficacy when **9** and **14** are chemically combined to yield aripiprazole (B,C). Values significantly different as determined by unpaired t-test or one-way ANOVA (Tukey's multiple comparisons test) are indicated by asterisk(s) (\*) (where \* =  $p < 0.05$ , \*\* =  $p < 0.01$ ).

**Table 2.** Potency, functional affinity and intrinsic efficacy values for compound **9** and aripiprazole clearly demonstrate enhancements in affinity and efficacy upon incorporation of the THQ moiety to **9**.

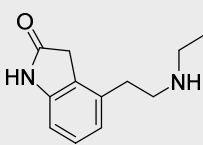
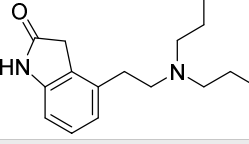
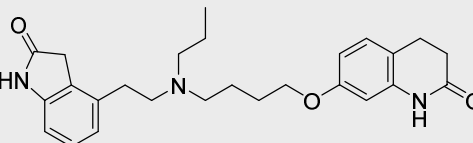
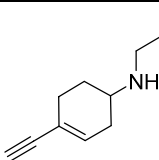
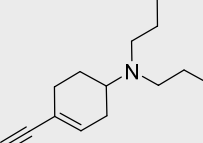
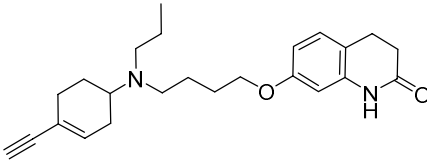
Compound	pEC <sub>50</sub> (EC <sub>50</sub> , nM)	pK <sub>A</sub> ± SEM (K <sub>A</sub> , nM)	Logτ ± SEM (τ)
Dopamine <sup>a</sup>	7.04 ± 0.06 (90.8)	4.97 ± 0.23 (10850)	1.90 ± 0.25 (75.7)
<b>9<sup>b</sup></b>	5.05 ± 0.37 (8917)	5.00 ± 0.44 (9941)	-0.44 ± 0.16 (0.365)
<b>3<sup>b</sup></b>	8.17 ± 0.21 (6.73)	7.90 ± 0.22 (12.8)	-0.03 ± 0.05 (0.940)

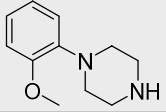
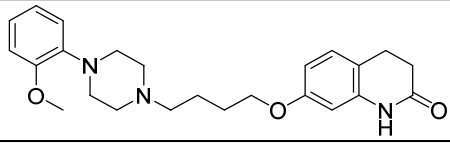
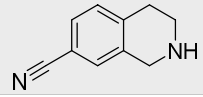
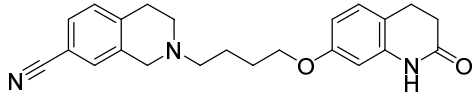
Determined by inhibition of FSK- stimulated cAMP assays in FlpIn CHO cells stably expressing both wild type D<sub>2</sub>L<sub>R</sub> and the CAMYEL biosensor. Data represents the mean ± SEM of three separate experiments performed in duplicate and was fit to an operational model of agonism (<sup>a</sup>) or partial agonism (<sup>b</sup>).

Pharmacological evaluation of the D<sub>2</sub>R orthosteric structures, key intermediates and hybrids **22-25** revealed improvements in both binding and functional affinity (to varying degrees) upon incorporation of fragment **14** with the D<sub>2</sub>R orthosteric structures (**7**, **19-21**) (Table 3 and Figure 5). Hybrid molecules containing D<sub>2</sub>R agonist orthosteric structures, **22** (K<sub>i</sub> = 138 nM) and **23** (K<sub>i</sub> = 41.5 nM), were observed to gain moderate improvements in binding affinity compared to their key intermediates (**28**, K<sub>i</sub> = 2845 nM (21-fold); **34**, K<sub>i</sub> = 7421 nM (179-fold), respectively) and maintained full agonism in cAMP assays relative to dopamine (Table 3). In order to determine whether the hybridisation of **7** and **19** with fragment **14** impacted upon the intrinsic efficacies (τ) of these structures, cAMP assays were carried out in cells pretreated with phenoxybenzamine; an alkylating agent which is used to inhibit high affinity interactions at the D<sub>2</sub>R.<sup>23</sup> Surprisingly, incorporation of the THQ tail fragment (**14**) with key intermediates **28** and **34** demonstrated a trend towards increased efficacy of the hybrid ligands at the D<sub>2</sub>R compared to their parent structures (Table 3, Figures 5A and 5B). Compound **22** demonstrated a 3-fold improvement in efficacy compared to **7** and **28**. Compound **23**, however, displayed a 5-fold and 2-fold enhancement in efficacy compared to **34** and **19**, respectively. In contrast, hybrid molecules containing the partial agonist (**24**, K<sub>i</sub> = 0.651 nM) and antagonist (**25**, K<sub>i</sub> = 17.1 nM) D<sub>2</sub>R orthosteric scaffolds, displayed marked improvements in binding affinity compared to their orthosteric cores (Table 3, Figures 5C and 5D). Incorporation of fragment **14** to these core structures enhanced affinity almost 5000-fold for **24**, and almost 2000-fold for **25**. Although an improvement in efficacy was observed for compound **24**, it could not be quantified due to the poor efficacy of **20**. Whilst changes in efficacy could not be determined for compound **25** since the competitive antagonist pharmacology of its orthosteric parent (**21**) was maintained. Taken together, these results suggest that attachment of fragment **14** was able to provide significant enhancements

in affinity and efficacy to other orthosterically-binding D<sub>2</sub>R scaffolds as observed with **3** (Table 3 and Figure 5).

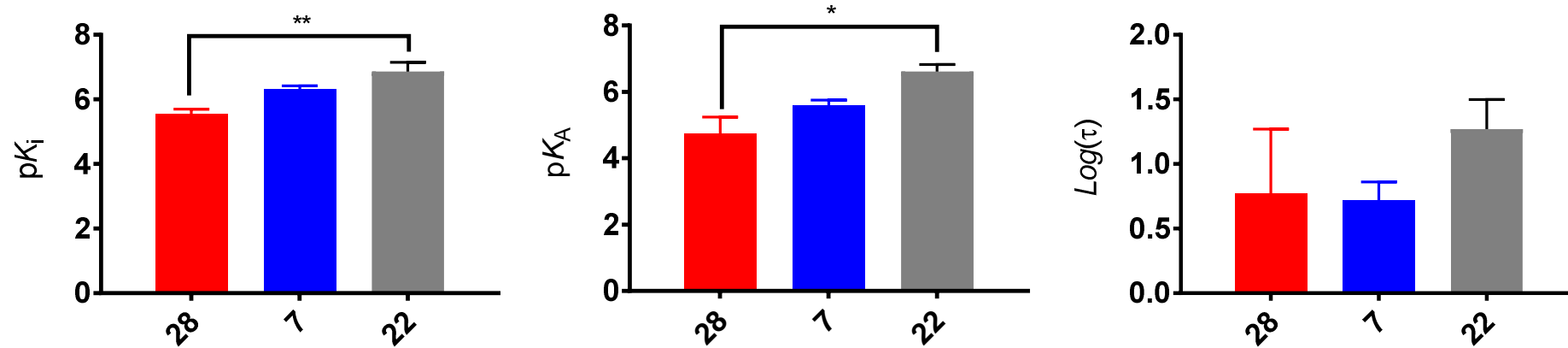
**Table 3.** Radioligand binding affinities<sup>a</sup>, functional affinities<sup>b</sup> and efficacy<sup>c</sup> values of the 7-butoxy-1,2,3,4-tetrahydroquinolin-2-one- containing hybrid ligands, their orthosteric cores and key synthetic intermediates

Compound	Structure	pK <sub>i</sub> ± SEM (K <sub>i</sub> , nM) <sup>a</sup>	Fold Increase in Affinity	pEC <sub>50</sub> ± SEM (EC <sub>50</sub> , nM) [E <sub>max</sub> , %] <sup>b</sup>	pK <sub>A</sub> ± SEM (K <sub>A</sub> , nM) <sup>c</sup>	Logτ ± SEM (τ) <sup>c</sup>
28		5.55 ± 0.15 (2845)	1	5.47 ± 0.12 (3378) [102]	4.73 ± 0.51 (18620)	0.77 ± 0.50 (5.9)
7		6.31 ± 0.11 (492)	5.78	6.82 ± 0.13 (150) [84.5]	5.58 ± 0.18 (1413)	0.72 ± 0.14 (5.3)
22		6.86 ± 0.29 (138)	20.6	8.19 ± 0.10 (6.54) [106]	6.61 ± 0.21 (245)	1.27 ± 0.23 (18.8)
34		5.14 ± 0.12 (7421)	1	5.26 ± 0.22 (5501) [88.6]	5.73 ± 0.20 (1860)	0.50 ± 0.20 (3.16)
19		5.17 ± 0.15 (6761)	1.10	6.32 ± 0.13 (479) [97.5]	5.46 ± 0.29 (3480)	0.85 ± 0.25 (7.07)
23		7.38 ± 0.21 (41.5)	179	8.55 ± 0.15 (2.85) [106]	7.04 ± 0.25 (90.0)	1.18 ± 0.27 (15.0)

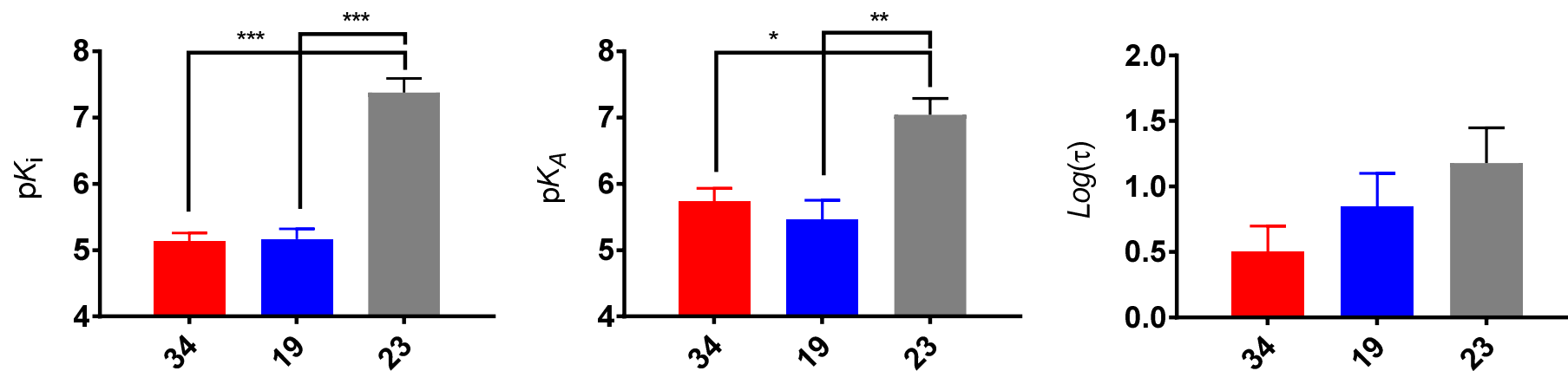
20		$5.52 \pm 0.07$ (3057)	1	<5 (>10000)	ND	ND
24		$9.19 \pm 0.10$ (0.651)	4696	$9.43 \pm 0.18$ (0.373) [47.0]	ND	ND
21		$4.56 \pm 0.13$ (27420)	1	-	ND	ND
25		$7.77 \pm 0.15$ (17.1)	1604	-	ND	ND
<b>Dopamine</b>	-	ND	ND	$7.12 \pm 0.10$ (75.7) (100)	$4.97 \pm 0.22$ (10720)	$1.88 \pm 0.25$ (75.5)

<sup>a</sup>Determined by competition binding experiments using radiolabelled antagonist [<sup>3</sup>H]spiperone at wild type D<sub>2L</sub>R expressed in FlpIn CHO cell membranes. Data represents the mean  $\pm$  SEM of three separate experiments performed in duplicate. <sup>b</sup> Determined by inhibition of FSK- stimulated cAMP assays in cells stably expressing both wild type D<sub>2L</sub>R and the CAMYEL biosensor expressed in FlpIn CHO cells. Data represents the mean  $\pm$  SEM of three separate experiments performed in duplicate and was fit to an operational model of agonism. <sup>c</sup> Determined by inhibition of FSK-stimulated cAMP assays in phenoxybenzamine-pretreated (30 min) cells stably expressing both the wild type D<sub>2L</sub>R and the CAMYEL biosensor expressed in FlpIn CHO cells. Data represents the mean  $\pm$  SEM of three separate experiments performed in duplicate and was fit to an operational model of receptor depletion. ND: Not determined.

A



B



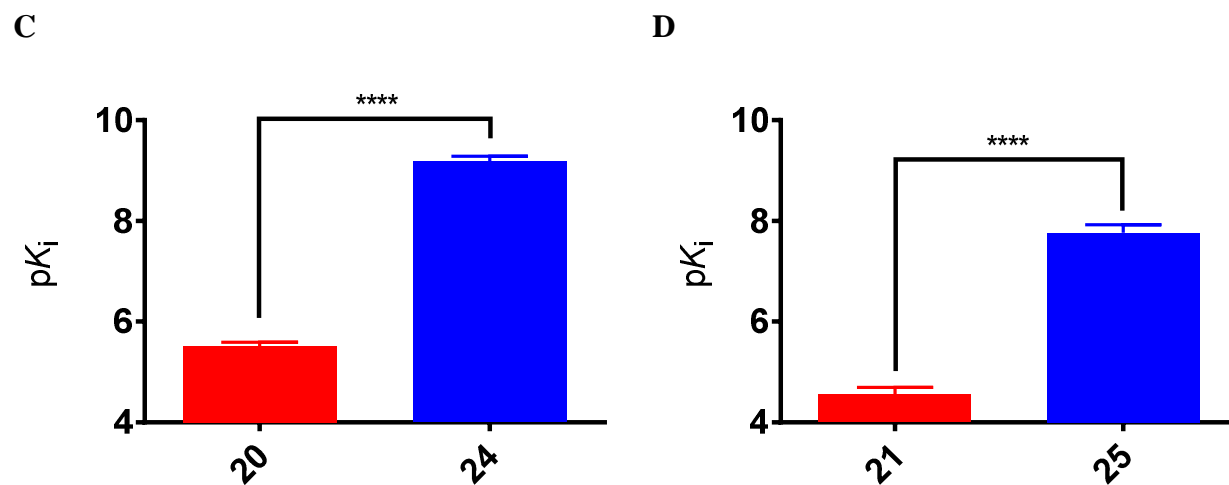


**Figure 5.** Both hybrid molecules with agonist pharmacology demonstrated a small but significant increase in binding affinity, enhancements in functional affinity and a trend towards improved efficacy (A and B). Hybrids with partial agonist and antagonist pharmacology, respectively, were observed to have markedly improved binding affinity compared to their orthosteric D<sub>2</sub>R structures (C and D). Values significantly different as determined by unpaired t-test or one-way ANOVA (Tukey's multiple comparisons test) are indicated by asterisk(s) (\*) (where \* =  $p < 0.05$ , \*\* =  $p < 0.01$ , \*\*\* =  $p < 0.001$ , \*\*\*\* =  $p < 0.0001$ ).

Orthosteric ligand-receptor interactions at the D<sub>2</sub>R have been thoroughly investigated through mutagenesis, affinity labelling, molecular modelling and insights gained from the highly homologous D<sub>3</sub>R crystal structure.<sup>8,9</sup> The structural determinants of agonist efficacy at the D<sub>2</sub>R, however, have been largely unexplored and remain an ongoing challenge in the field of G-protein-coupled receptors (GPCRs). Chien *et al.* observed a secondary binding pocket in the crystal structure of the D<sub>3</sub>R that was distal to the orthosteric binding site and extended out towards the extracellular regions of transmembrane helices (TMs) 1, 2 and 7.<sup>9</sup> Subsequently, Newman and colleagues observed that interaction of their substituted-4-phenylpiperazine compounds within this secondary pocket caused a reorientation of the orthosteric moiety which led to a modulation of efficacy.<sup>11</sup> Unpublished work from our group also revealed that mutations of this secondary binding pocket at the D<sub>2</sub>R were able to modulate the affinity and efficacy of aripiprazole. Mutation of L41<sup>1.39</sup> (superscript numbers refer to Ballesteros-Weinstein nomenclature which allows us to indicate the location of a specific amino acid residue relative to the most conserved residue within a specific TM helix across all class A GPCRs)<sup>27</sup> caused a 5-fold increase in the affinity of aripiprazole but attenuated any functional activity of this molecule in cAMP signalling assays, suggesting that this residue must be a major determinant of aripiprazole's efficacy.<sup>28</sup> Additionally mutations of V91<sup>2.61</sup> and E95<sup>2.65</sup> (located at the top of TM 2) appeared to significantly reduce aripiprazole's binding affinity (8- and 3-fold, respectively),<sup>28</sup> which are also residues which implicated in the binding of other extended ligands such as SB269652 and R-22.<sup>19</sup> It is also interesting to note that whilst these mutations affect the affinity and/or the efficacy of extended structures and some smaller partial agonists (e.g. ropinirole and pardoprunox, respectively) at the D<sub>2</sub>R, they do not appear to affect the affinity or efficacy of dopamine.<sup>28</sup> Thus, in order to gain further insight into the ligand-receptor interactions at TMs 1 and 2 that are important for affinity and efficacy at the D<sub>2</sub>R we chose to evaluate our series of hybrid molecules (**22-25**) in a series of assays using L41<sup>1.39</sup>A, V91<sup>2.61</sup>A and E95<sup>2.65</sup>A SNAP-D<sub>2</sub>R mutant receptors (Figure 6).

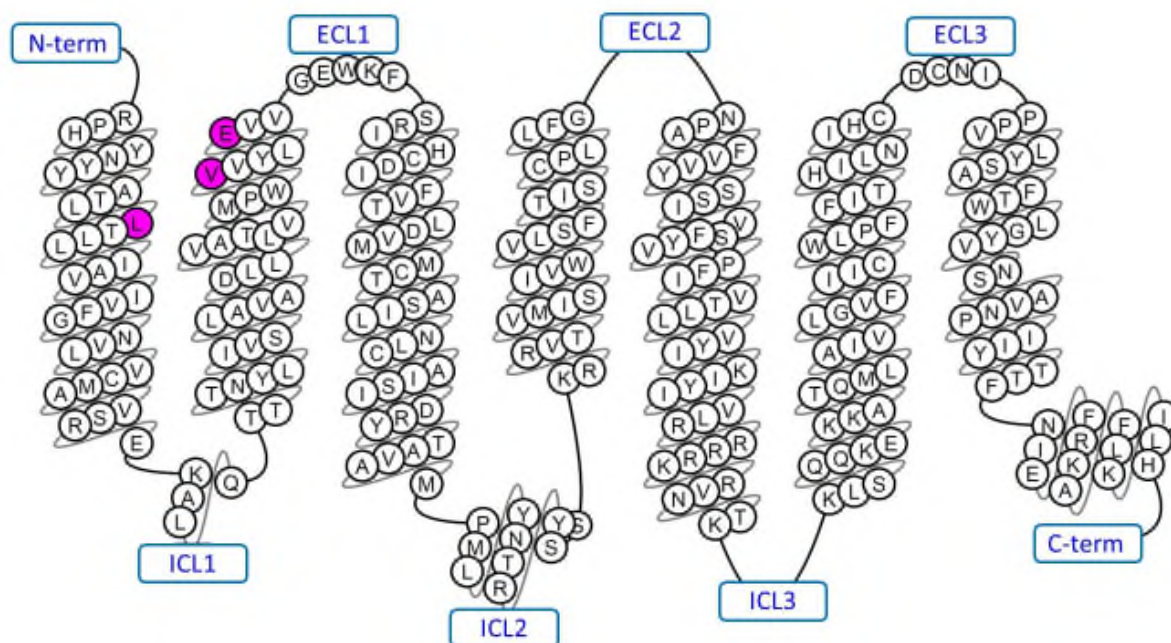


**Figure 6.** A diagram of the human D<sub>2</sub>R highlighting (in purple) residues thought to play a role in agonist efficacy (Diagram generated using [http://gpcrdb.org/protein/drd2\\_human](http://gpcrdb.org/protein/drd2_human)).

All receptor mutants were expressed to the same level as reported by Klein-Herenbrink *et al.*<sup>28</sup> Radioligand binding assays were conducted using the antagonist [<sup>3</sup>H]spiperone with the exception of experiments at the V91<sup>2.61</sup>A mutant at which the affinity of this radioligand was markedly reduced. In this case [<sup>3</sup>H]raclopride was used (Table 4). Of the compounds containing substituted phenylpiperazine scaffolds, both parent scaffolds **9** and **20** demonstrated improvement in affinity upon mutation of the L41<sup>1.39</sup> residue (3- and 5-fold, respectively), whilst compound **20** also showed a 4-fold improvement compared to the wild-type receptor upon mutation of the E95<sup>2.65</sup> residue (Table 4). Both their respective hybrid compounds, **3** and **24**, were observed to have marked improvements in affinity at the L41A<sup>1.39</sup> mutant compared to the wild-type receptor (27- and 14-fold, respectively). Additionally, it is interesting to note that **24** but not **3** demonstrated sensitivity to all the mutations including the V91<sup>2.61</sup> residue, where a 74-fold loss in affinity was observed compared to wild-type despite their relative structural similarity (Table 4). The orthosteric D<sub>2</sub>R antagonist, **21**, and its respective hybrid, **25**, showed no significant changes in affinity at the L41A<sup>1.39</sup> and E95A<sup>2.65</sup> mutant receptors but a significant 10-fold loss in affinity at the V91A<sup>2.61</sup> mutant compared to wild-type. The affinity of the D<sub>2</sub>R agonist-based compounds were also influenced by the mutation of these residues. Ropinirole (**7**) and its key synthetic intermediate, **28**, displayed significantly improved affinity at the E95A<sup>2.65</sup> mutant compared to the wild-type (6- and 15-fold, respectively) receptor. In contrast, only FAUC73 (**19**) demonstrated significant enhancement in affinity at the L41A<sup>1.39</sup> (7-fold) and E95A<sup>2.65</sup> (10-fold) mutants

compared to the wild-type receptor. It is interesting to note that the affinities of both agonist-based hybrid molecules (**22** and **23**) were not significantly affected by mutations at TMs 1 and 2 (Table 4) even though their parent scaffolds were. Taken together, these results demonstrate that interactions within the extracellular regions of TMs 1 and 2 play a role in dictating the affinity of some but not all hybrid compounds at the D<sub>2</sub>R in a manner dependent upon the orthosteric scaffold. Furthermore, it is interesting to note that despite the relative distance of these mutations from the orthosteric binding site, the affinity of the orthosterically-binding D<sub>2</sub>R scaffolds and their key synthetic intermediates are influenced by these mutations. This in turn may suggest that global conformational changes of the D<sub>2</sub>R elicited by residues within the extracellular regions of TMs 1 and 2 are implicated in the differing pharmacological profiles of these molecules.

Hybrid compounds displaying partial agonism (**3** and **24**), and their orthosteric structures (**9** and **20**) were also tested in a standard FSK-stimulated cAMP inhibition assays, whilst the agonist hybrids compounds (**22** and **23**), their key intermediates (**28** and **34**) and orthosteric scaffolds (**7** and **19**) were tested in cAMP inhibition assays following phenoxybenzamine pre-treatment (Table 5, Appendix A1.1). In accordance with findings from radioligand binding assays, changes in functional affinity and efficacy were noted upon mutation of the L41<sup>1.39</sup>, V91<sup>2.61</sup> and E95<sup>2.65</sup> residues of the D<sub>2</sub>R. The agonist-based compounds (**7**, **19**, **22**, **23** and **28**) retained relatively similar functional affinities and efficacies at the L41A<sup>1.39</sup> mutant compared to the wild-type. It was noted, however, that whilst the functional affinity of compound **34** was maintained at the L41A<sup>1.39</sup> mutant, a significant loss in efficacy (2-fold) was noted compared to wild-type. In contrast, the functional affinity and efficacy of the phenylpiperazine-containing extended structures (**3** and **24**) were abrogated upon evaluation at the L41A<sup>1.39</sup> mutant (Table 5, Appendix A1.1). These results suggest that L41<sup>1.39</sup> makes a key interaction that is necessary for the efficacy of the phenylpiperazine-containing structures at the D<sub>2</sub>R despite its distance from the orthosteric binding site. Additionally, the inability of this mutant to drastically alter the functional affinity and efficacy of the agonist-based compounds suggests that there may be alternate ligand-receptor interactions that may be able to compensate for the loss of efficacy caused by the mutation at L41<sup>1.39</sup>. Surprisingly, unlike the agonist-based compounds which did were not influenced by the L41A<sup>1.39</sup> mutation, a 12-fold loss in dopamine's functional affinity was observed despite its distance from the orthosteric binding site. This demonstrates that, as for the extended structures, the secondary binding pocket is also important for the action of smaller endogenous ligands. Indicating that this secondary pocket may play an important role in the D<sub>2</sub>R activation process.

Mutations of the V91<sup>2.61</sup> and E95<sup>2.65</sup> residues residing in TM2 of the D<sub>2</sub>R also resulted in a number of interesting effects compared to wild-type (Table 5). Of the phenylpiperazine-

containing compounds, **3** showed a loss of functional affinity at both mutants but increased efficacy at the E95A<sup>2.65</sup> mutant compared to wild-type, whilst **9** gained functional affinity and efficacy at both mutants. Interestingly, despite structural similarity to **9**, **20** demonstrated no efficacy at the V91A<sup>2.61</sup> and the E95A<sup>2.65</sup> mutants. Additionally in contrast to **3**, **24** demonstrated agonist-like efficacy relative to dopamine at the TM2 mutations and consequently, was unable to fit to the operational model of partial agonism (Appendix A1.1). Of the agonist-based compounds, **7**, **19**, **22**, **28** and **34** were not significantly affected by either mutation compared to wild-type (Table 5). Compound **23**, however, displayed a significant 4-fold loss of functional affinity and a 3-fold gain in efficacy at the E95A<sup>2.65</sup> mutant compared to wild-type. Changes in functional affinity and efficacy at the V91A<sup>2.61</sup> mutant could not be determined for the ropinirole- and FAUC73-based compounds since its sensitivity towards phenoxybenzamine alkylation was markedly reduced.

From these results it is clear to see that mutations of TMs 1 and 2 have an effect on the affinity and efficacy of orthosterically-binding D<sub>2</sub>R ligands and their extended hybrids. The L41A<sup>1.39</sup> mutation caused an abrogation of efficacy for the phenylpiperazine-based compounds and a decrease in dopamine's functional affinity, but showed no significant effect on the functional affinity or efficacy of the agonist-based ligands. In contrast, the V91A<sup>2.61</sup> and E95A<sup>2.65</sup> mutations decreased the functional affinity of the phenylpiperazine-containing structures but enhanced their efficacy. Of the agonist-based compounds, the extended hybrid **23** demonstrated a loss in functional affinity at the E95A<sup>2.65</sup> mutation whilst the remaining agonist-based structures were unaffected. In terms of efficacy, however, key intermediates and extended agonist-based hybrids were observed to improve upon mutation of the E95<sup>2.65</sup> residue whilst their parent scaffolds remained relatively unaffected. Ultimately, these results show that residues at a secondary binding site within the extracellular domains of TMs 1 and 2 are able to influence the affinity and efficacy of not only extended D<sub>2</sub>R scaffolds, but also those of small orthosterically-binding scaffolds.

**Table 4.** Radioligand binding affinities of the 7-butoxy-1,2,3,4-tetrahydroquinolin-2-one-containing hybrid ligands, their orthosteric cores and key synthetic intermediates at the wild-type D<sub>2L</sub>R and wild type or mutant SNAP-D<sub>2S</sub>R proposed to be implicated in agonist efficacy<sup>a</sup>

Compound	pK <sub>i</sub> ± SEM (K <sub>i</sub> , nM)				
	D <sub>2L</sub> R WT [ <sup>3</sup> H]spiperone	D <sub>2S</sub> R L41A [ <sup>3</sup> H]spiperone	D <sub>2S</sub> R E95A [ <sup>3</sup> H]spiperone	D <sub>2S</sub> R WT [ <sup>3</sup> H]raclopride	D <sub>2S</sub> R V91A <sup>b</sup> [ <sup>3</sup> H]raclopride
9	6.30 ± 0.27 (501)	6.80 ± 0.16 (157)	6.29 ± 0.16 (509)	7.45 ± 0.31 (33.3)	7.59 ± 0.17 (25.5)
3	8.91 ± 0.14 (1.25)	10.3 ± 0.12 (0.046)***	9.24 ± 0.08 (0.578)	9.70 ± 0.22 (0.200)	9.47 ± 0.26 (0.341)
28	5.55 ± 0.15 (2845)	5.83 ± 0.11 (1477)	6.72 ± 0.18 (190)**	7.08 ± 0.35 (84.2)	7.62 ± 0.30 (23.9)
7	6.31 ± 0.11 (492)	6.45 ± 0.08 (358)	7.14 ± 0.15 (72.5)**	7.49 ± 0.44 (32.1)	8.25 ± 0.40 (5.68)
22	6.86 ± 0.29 (138)	7.25 ± 0.07 (56.9)	7.54 ± 0.13 (29.0)	8.24 ± 0.35 (5.79)	8.56 ± 0.38 (2.78)
34	5.14 ± 0.12 (7421)	5.59 ± 0.09 (2593)	5.21 ± 0.19 (6140)	6.68 ± 0.39 (207)	6.32 ± 0.24 (484)
19	5.17 ± 0.15 (6761)	6.02 ± 0.09 (951)**	6.18 ± 0.12 (657)**	7.23 ± 0.29 (58.5)	7.13 ± 0.18 (74.0)
23	7.38 ± 0.21 (41.5)	7.37 ± 0.08 (42.4)	7.21 ± 0.27 (62.1)	8.61 ± 0.24 (2.45)	8.00 ± 0.17 (10.1)
20	5.52 ± 0.07 (3057)	6.23 ± 0.15 (595)*	6.12 ± 0.13 (767)*	6.49 ± 0.19 (325)	6.43 ± 0.24 (370)
24	9.19 ± 0.10 (0.651)	10.4 ± 0.09 (0.048)***	9.34 ± 0.16 (0.462)	10.3 ± 0.22 (0.052)	8.41 ± 0.26 (3.86)
21	4.56 ± 0.13 (27420)	4.98 ± 0.08 (10560)	4.87 ± 0.21 (13620)	5.62 ± 0.32 (2406)	5.86 ± 0.21 (1398)
25	7.77 ± 0.15 (17.1)	8.17 ± 0.14 (6.76)	7.54 ± 0.19 (28.9)	8.22 ± 0.27 (6.07)	7.21 ± 0.14 (61.8)

<sup>a</sup>Determined by competition binding experiments using radiolabelled antagonist [<sup>3</sup>H]spiperone or [<sup>3</sup>H]raclopride at wild type D<sub>2L</sub>R, wild type SNAP-D<sub>2S</sub>R or mutant SNAP-D<sub>2S</sub>R expressed in FlpIn CHO cell membranes. Data represents the mean ± SEM of three separate experiments. <sup>b</sup>A final protein concentration of 12.5 µg/mL was used to obtain these data. Values for D<sub>2L</sub>R WT, D<sub>2S</sub>R L41A and D<sub>2S</sub>R E95A significantly different as determined by one-way ANOVA (Tukey's multiple comparisons test) and are indicated by the following notation; significance compared to D<sub>2L</sub>R WT is denoted by (\*) (where \* = *p* < 0.05, \*\* = *p* < 0.01, and \*\*\* = *p* < 0.001).

**Table 5.** Functional affinities and efficacies of the 7-butoxy-1,2,3,4-tetrahydroquinolin-2-one- containing hybrid ligands, their orthosteric cores and key synthetic intermediates at the wild-type and mutant SNAP-D<sub>2S</sub>R proposed to be implicated in agonist efficacy.<sup>a,b</sup>

Compound	pEC <sub>50</sub> ± SEM (EC <sub>50</sub> , nM) <sup>a</sup>				pK <sub>A</sub> ± SEM (K <sub>A</sub> , nM) <sup>b</sup>				Log $\tau$ ± SEM ( $\tau$ ) <sup>b</sup>			
	WT	L41A	V91A	E95A	WT	L41A	V91A	E95A	WT	L41A	V91A	E95A
<b>9</b>	-	-	5.94 ± 0.29 (1138)	5.86 ± 0.30 (1380)	-	-	5.69 ± 0.43 <sup>c</sup> (2054)	5.79 ± 0.35 <sup>c</sup> (1617)	-	-	-0.436 ± 0.11 <sup>c</sup> (0.151)	-0.427 ± 0.11 <sup>c</sup> (0.374)
<b>3</b>	8.49 ± 0.37 (3.24)	-	7.33 ± 0.50 (47.1)	7.98 ± 0.22 (10.4)	8.41 ± 0.25 <sup>c</sup> (3.91)	-	7.05 ± 0.36 <sup>c</sup> (88.3)	7.78 ± 0.19 <sup>c</sup> (16.5)	-0.328 ± 0.07 <sup>c</sup> (0.470)	-	-0.262 ± 0.11 <sup>c</sup> (0.547)	0.108 ± 0.05 <sup>c</sup> (1.28)
<b>28</b>	ND	ND	ND	ND	5.35 ± 0.08 (4452)	5.44 ± 0.08 (3594)	-	5.23 ± 0.17 (5878)	0.573 ± 0.06 (3.74)	0.307 ± 0.05 (2.03)	-	1.01 ± 0.16 (10.1)
<b>7</b>	ND	ND	ND	ND	6.18 ± 0.17 (666)	6.10 ± 0.07 (791)	-	6.26 ± 0.10 (548)	0.927 ± 0.23 (8.44)	0.652 ± 0.05 (4.48)	-	1.05 ± 0.09 (11.1)
<b>22</b>	ND	ND	ND	ND	7.48 ± 0.07 (33.5)	7.14 ± 0.07 (72.6)	-	7.42 ± 0.08 (38.0)	0.551 ± 0.04 (3.55)	0.612 ± 0.05 (4.09)	-	0.783 ± 0.07 (6.06)
<b>34</b>	ND	ND	ND	ND	5.21 ± 0.13 (6171)	4.98 ± 0.16 (10480)	-	4.92 ± 0.09 (12000)	0.296 ± 0.07 (1.98)	-0.860 ± 0.07 (0.820)****	-	0.616 ± 0.07 (4.13)
<b>19</b>	ND	ND	ND	ND	5.72 ± 0.16 (1895)	5.68 ± 0.07 (2098)	-	5.54 ± 0.10 (2869)	0.587 ± 0.24 (3.87)	0.585 ± 0.05 (3.84)	-	0.940 ± 0.10 (8.71)
<b>23</b>	ND	ND	ND	ND	7.40 ± 0.07 (39.9)	7.22 ± 0.06 (59.9)	-	6.79 ± 0.10 (162)**	0.659 ± 0.05 (4.56)	0.650 ± 0.05 (4.47)	-	1.11 ± 0.10 (13.0)**
<b>20</b>	-	-	-	-	-	-	-	-	-	-	-	-
<b>24</b>	9.37 ± 0.26 (0.427)	-	9.08 ± 0.53 (0.835)	9.03 ± 0.19 (0.932)	9.15 ± 0.28 <sup>c</sup> (0.701)	-	-	-	-0.457 ± 0.08 <sup>c</sup> (0.350)	-	-	-
<b>Dopamine</b>	7.55 ± 0.08 (28.1)	6.49 ± 0.11 (324)	8.01 ± 0.07 (9.74)	7.89 ± 0.04 (12.9)	6.47 ± 0.12 (337)	5.40 ± 0.20 (3954)	-	7.12 ± 0.28 (75.3)	0.897 ± 0.16 (7.88)	1.03 ± 0.25 (10.8)	-	0.661 ± 0.35 (4.58)

<sup>a</sup>Determined by inhibition of FSK-stimulated cAMP assays in FlpIN CHO cells stably expressing wild type or mutant SNAP-D<sub>2S</sub>R and transiently expressing the CAMYEL biosensor. Data represents the mean ± SEM of three separate experiments performed in duplicate. <sup>b</sup>Determined by inhibition of FSK-stimulated cAMP assays in phenoxybenzamine-pretreated (30 min) using FlpIN CHO cells stably expressing wild type or mutant SNAP-D<sub>2S</sub>R and transiently expressing the CAMYEL biosensor. Data represents the mean ± SEM of three separate experiments performed in duplicate. <sup>c</sup>Log $\tau$  and pK<sub>a</sub> values were derived for partial agonists which were able to be fit to an operational model of partial agonism. Values significantly different as determined by one-way ANOVA (Tukey's multiple comparisons test) and are indicated by the following notation; significance compared to WT is denoted by (\*) (where \*\* =  $p < 0.01$ , and \*\*\*\* =  $p < 0.0001$ ). ND: Not determined.

#### 2.1.4 Conclusions

In this study we explored the chemical and structural determinants of efficacy at the D<sub>2</sub>R. Using fragment-based SAR, we determined that the THQ moiety (**14**) was a key determinant of affinity and efficacy for **3** using functional and binding assays. Furthermore, we were able to attach the THQ moiety to a chemically and pharmacologically diverse series of orthosterically-binding D<sub>2</sub>R structures (**7**, **19-21**) and evaluate the effects of its addition on the affinity and efficacy of hybrid compounds. Hybrid compounds based on the structures of ropinirole and FAUC73 (**22** and **23**, respectively) maintained the pharmacological profile of their parent scaffolds with improved affinity and a trend towards increased efficacy. Phenylpiperazine-containing scaffolds (**3** and **24**) were observed to gain efficacy in addition to affinity, whilst the antagonist scaffold (**21**) did not gain any efficacy upon hybridisation. Aside from revealing an unappreciated mechanism behind the efficacy of **3**, mutagenesis studies have revealed that extension of structures into a secondary binding pocket is a determinant of agonist efficacy at the D<sub>2</sub>R. Additionally, in comparison to the work conducted by Newman *et al.* surrounding R-22,<sup>11</sup> our work reveals that the nature of the interaction with a secondary binding pocket within TMs 1 and 2 of the D<sub>2</sub>R can modulate the efficacy of extended ligands in different directions. This work, therefore, provides a rational approach for the design of high affinity agonists with desired efficacies (ranging from low to high).

## **Chapter 2.2**

### **Efforts towards the Investigation of Modulating Efficacy at the Dopamine D<sub>2</sub> Receptor using Extended Structures**

### 2.2.1 Rationale

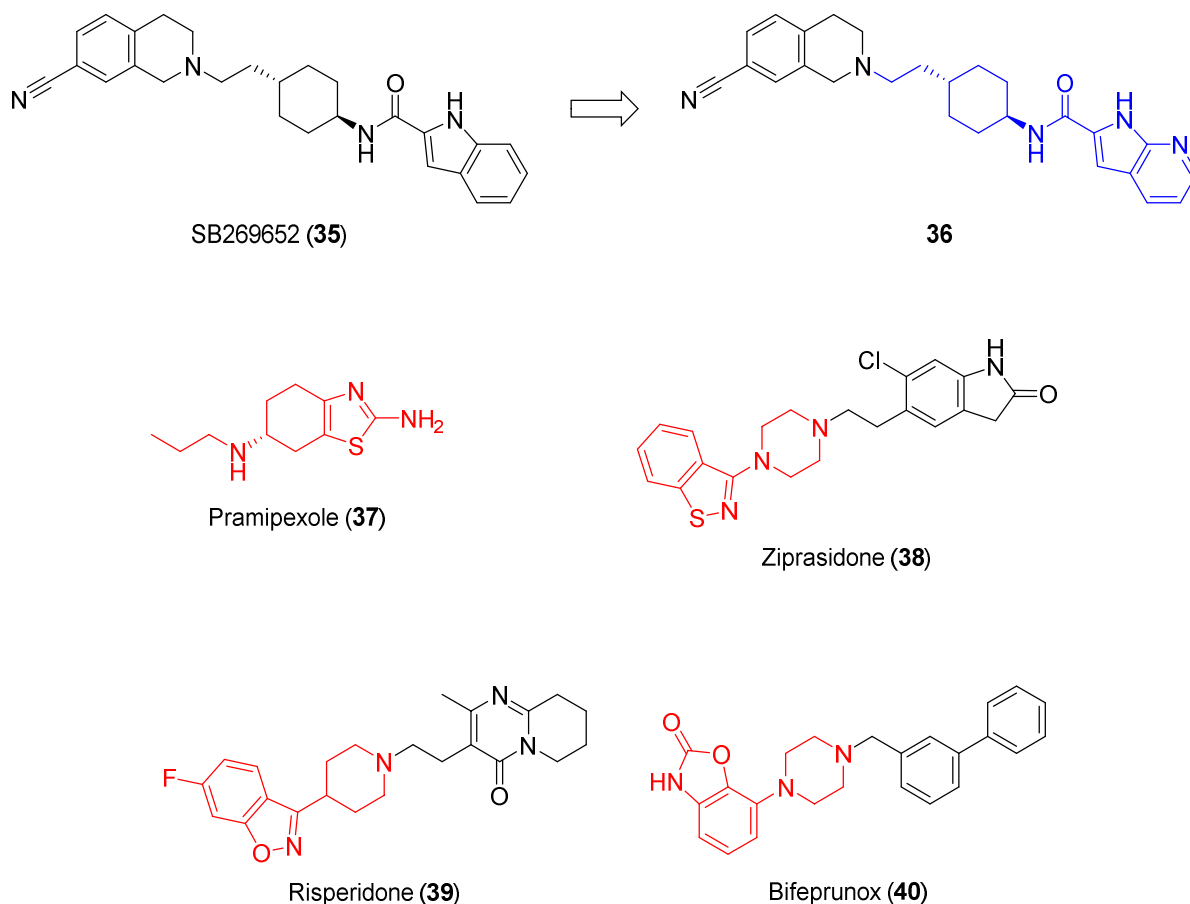
Based on the results obtained in Chapter 2.1, we then questioned whether structurally and pharmacologically differing tail appendages would be able to influence the pharmacological profile of orthosterically-binding cores in a similar manner to **14**. To investigate this further we devised a second series of hybrid molecules that would comprise of a pharmacologically diverse set of orthosteric scaffolds to which we would incorporate the tail moiety of an analogue of SB269652 (**35**), an allosteric modulator of the D<sub>2</sub>R with a bitopic mode of binding.

SB269652 (**35**) was the first drug-like negative allosteric modulator (NAM) described for the D<sub>2</sub>R in 2010 by Silvano *et al.*<sup>29,30</sup> SAR analysis of this molecule within our group has revealed that the cyclohexylene spacer in conjunction with its indole-2-carboxamide tail is a key chemical feature of its affinity and modulatory activity.<sup>31</sup> This work subsequently led to the development of **36**, a 7-azaindole-2-carboxamide derivative with improved affinity and negative cooperativity at the D<sub>2</sub>R. Since we had observed that the THQ moiety of **3** was able to influence the efficacy of orthosterically-binding D<sub>2</sub>R structures, and that the indole moiety of R-22 has previously been shown to decrease efficacy at the D<sub>2</sub>R,<sup>11</sup> we extended our studies to explore the effect of incorporating the 7-azaindole-2-carboxamidoalkyl appendage of **36** (highlighted in blue, Figure 4) with D<sub>2</sub>R-binding core structures. We anticipated that the cyclohexylene linker (which differs to that of R-22) and azaindole moiety may also be able to direct the efficacy of various orthosterically-binding scaffolds. Consequently, the 7-azaindole-2-carboxamidoalkyl moiety of **36** was attached to six structurally and pharmacologically diverse orthosteric D<sub>2</sub>R pharmacophores (i.e. Ropinirole; **7**, FAUC-73; **19**, Pramipexole; **37**, Ziprasidone; **38**, Ripseridone; **39** and Bifeprunox; **40**) and assessed them in a cAMP assay to determine whether the 7-azaindole-2-carboxamide tail may be able to influence affinity or efficacy at the D<sub>2</sub>R.

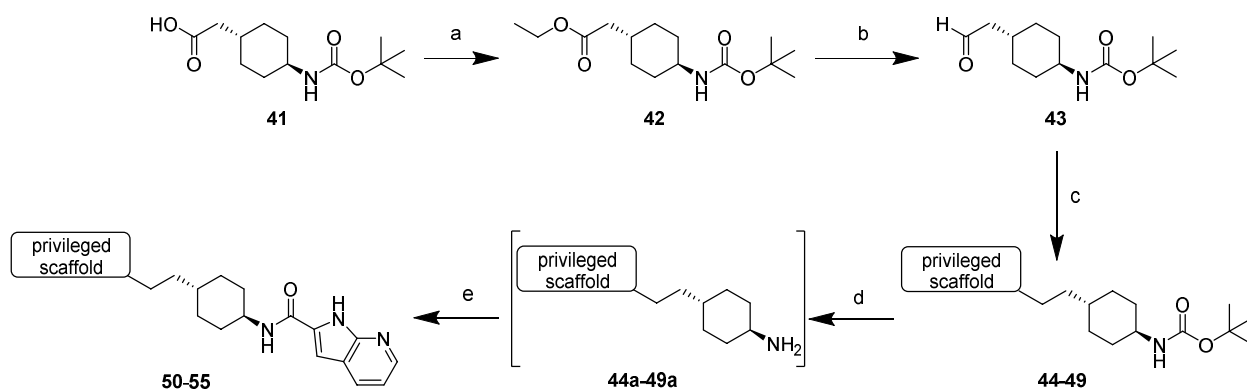
### 2.2.2 Synthesis

Following a synthetic procedure outlined by Shonberg *et al.*,<sup>31</sup> synthesis of these hybrid molecules (Scheme 4) began with the esterification of **41** to yield **42** using ethyl iodide (EtI) and acetonitrile (MeCN) in the presence of potassium carbonate (K<sub>2</sub>CO<sub>3</sub>) which proceeded in quantitative yield. Reduction of **42** in the presence of 1 M diisobutylaluminium hydride (DIBAL-H) in toluene at -78 °C quantitatively yielded the corresponding aldehyde (**41**). Next, reductive alkylation of **41** with the necessary secondary amine derivative of the orthosteric D<sub>2</sub>R pharmacophore (**28**, **34** and Figure 7 (structures highlighted in red)) in the presence of Na(OAc)<sub>3</sub>BH and 1,2-dichloroethane (1,2-DCE) produced compounds **44-49** in 18-75% yield. Finally, de-protection of the boc group

was conducted in the presence of excess trifluoroacetic acid (TFA) in DCM and converted to the free base form using K<sub>2</sub>CO<sub>3</sub> or NaOH. Deprotection was confirmed via TLC or LCMS and the resulting product was carried through to (1-[bis(dimethylamino)methylene]-1*H*-1,2,3-triazolo[4,5-*b*]pyridinium 3-oxid hexafluorophosphate) (HATU)-mediated amide coupling in dry DMF in the presence of base which furnished the final hybrid molecules (**50-55**, Figure 8) in yields of 2-41%.



**Figure 7.** Structures of D<sub>2</sub>R negative allosteric modulators (**35**, **36**), agonist (**37**), inverse agonists (**38**, **39**) and partial agonist (**40**). Structures highlighted in red are the D<sub>2</sub>R orthosteric cores to which the 7-azaindole-2-carboxamidoalkyl appendage (highlighted in blue) was attached.

**Scheme 4.** Synthesis of 7-azaindole-2-carboxamide-containing hybrid molecules<sup>a</sup>

<sup>a</sup>Reagents and conditions: (a) EtI, K<sub>2</sub>CO<sub>3</sub>, MeCN, 50 °C, overnight, quantitative; (b) 1M DIBALH in toluene, toluene, -78 °C, 1 h, quantitative; (c) privileged scaffolds (2° amines), NaBH(OAc)<sub>3</sub>, 1,2-DCE, rt, 16–24 h, 18–75%; (d) TFA, DCM, followed by base, 81%-quantitative; (e) 1*H*-pyrrolo[2,3-*b*]pyridine-2-carboxylic acid, HATU, DMF, DIPEA, rt, 3–24 h, 2–41%.

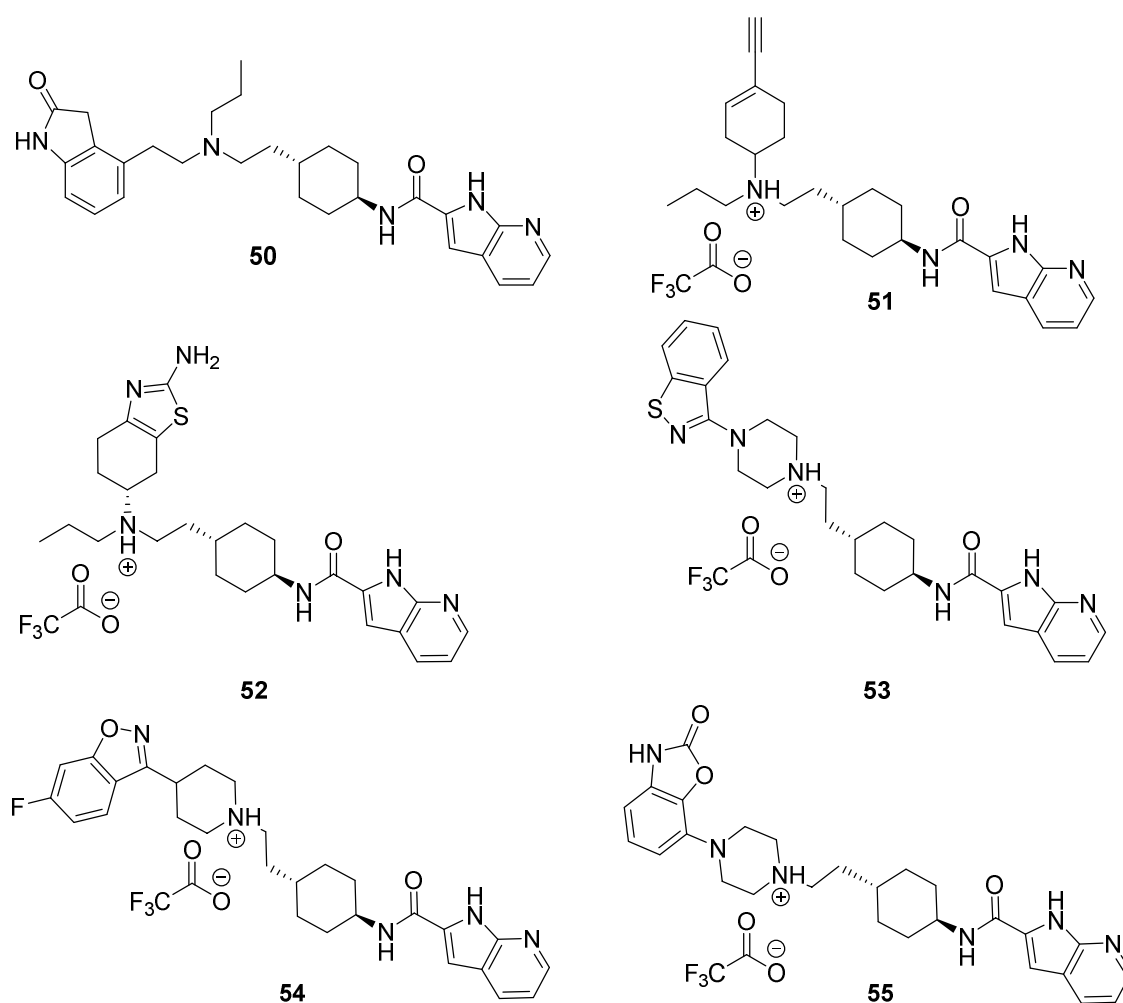
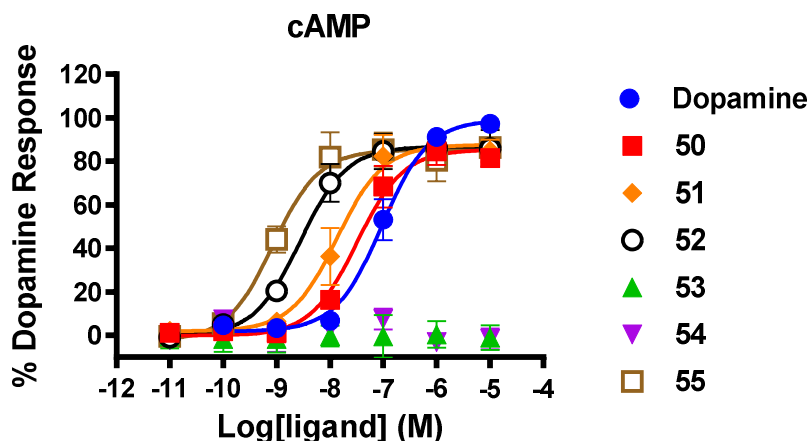


**Figure 8.** The final structures of the synthesised 7-azaindole-2-carboxamide-containing hybrid molecules.

### 2.2.3 Pharmacological evaluation

In order to preliminarily measure the activity of the compounds, we tested their ability to stimulate the inhibition of forskolin (FSK)-induced cyclic adenosine monophosphate (cAMP) production through activation of the D<sub>2L</sub>R expressed in FlpIn CHO cells. From this assay, we were able to determine initial values of potency (EC<sub>50</sub>) and efficacy (E<sub>max</sub>) for each compound as a result of fitting the data to an operational model of agonism.

Incorporation of the 7-azaindole-2-carboxamide tail with the D<sub>2</sub>R orthosteric scaffolds, appeared to improve potency of compounds **50-54** compared to their parent scaffolds. Interestingly, this enhancement was not to the same extent as the incorporation of the 1,2,3,4-tetrahydroquinolin-2-one (THQ) tail utilised in Sub-chapter 2.1. We were also intrigued to note that efficacy appeared unaffected. Compounds **50-54** retained the pharmacological profiles of their parent orthosteric cores, whilst compound **55** could not be fitted to an operational model of partial agonism and acted as a full agonist relative to dopamine in the cAMP inhibition assay. The ropinirole-containing hybrid, **50** (EC<sub>50</sub> = 32.0 nM), was observed to have an improved potency compared to **28** (EC<sub>50</sub> = 3378 nM, 106-fold) and **7** (EC<sub>50</sub> = 150 nM, 5-fold) but did not achieve the same enhancement as **22** (EC<sub>50</sub> = 6.54 nM). A similar scenario was also observed for **51** (EC<sub>50</sub> = 13.7 nM), where improvements in potency compared to its key synthetic intermediate **34** (EC<sub>50</sub> = 5501 nM, 402-fold) and parent D<sub>2</sub>R orthosteric scaffold FAUC73 (**19**, EC<sub>50</sub> = 479 nM, 35-fold) were evident but not to the same extent as the THQ moiety-containing hybrid (**23**, EC<sub>50</sub> = 2.85 nM). The pramipexole-containing hybrid compound, **52** (EC<sub>50</sub> = 2.79 nM), was observed to have an approximate 2-fold improvement in potency compared to its parent structure (**37**, EC<sub>50</sub> = 5 nM).<sup>32</sup> Compounds **53** and **54** which contained the D<sub>2</sub>R antagonist cores of ziprasidone and risperidone (**38** and **39**), respectively, were unable activate the D<sub>2</sub>R. In contrast, the potency of **55** appeared relatively unchanged compared to its parent D<sub>2</sub>R orthosteric scaffold, **40**.<sup>28</sup> These results suggest that the extent to which the spacer and tail moieties of an extended ligand is able to enhance affinity and efficacy may be dictated by the rigidity of their structure and how well they are able to make secondary binding interactions. The cyclohexylene spacer of **36** is conformationally more rigid than the butoxy spacer of **3**, therefore, **50-55** may be unable to make the same secondary binding interactions as a consequence of the positioning of the spacer and tail moieties relative to their orthosterically-binding scaffolds. These observations are similar to those made previously within our group in relation to extended biased agonist structures, where the nature of the orthosteric core, composition of the tail (including the length, orientation and flexibility of the spacer) were influencing factors in their pharmacological profiles.<sup>12</sup>



Compound	pEC <sub>50</sub> ± SEM (EC <sub>50</sub> , nM)	E <sub>max</sub> (% Dopamine) ± SEM
<b>Dopamine</b>	7.03 ± 0.09 (94.1)	97
<b>50</b>	7.49 ± 0.12 (32.0)	86
<b>51</b>	7.86 ± 0.14 (13.7)	86
<b>52</b>	8.56 ± 0.13 (2.79)	87
<b>53</b>	-	-
<b>54</b>	-	-
<b>55</b>	9.07 ± 0.16 (0.857)	88

**Figure 9.** Inhibition of FSK-induced cAMP production. Data represents the mean ± SEM of three separate experiments performed in duplicate.

## 2.2.4 Conclusions

Drawing on the observations that we made in Sub-chapter 2.1, we conducted a preliminary investigation into whether agonism at the D<sub>2</sub>R may be modulated in differing directions by extended structures with differing tail appendages. Using the 7-azaindole-2-carboxamidoalkyl appendage of our highest affinity SB269652 analogue (**36**), we synthesised a second series of extended hybrids (**50-55**). Upon preliminary pharmacological characterisation, we observed that the hybrid analogues retained the pharmacological profiles of their orthosteric parent scaffolds. An increase in potency was also observed for the agonist structures, whilst no change in potency was observed for the bifeprunox-containing structure (**55**). It is interesting to note that the enhancements in potency for this second series of hybrid molecules were not as drastic as those observed for the hybrids containing the THQ tail, nor did we observe a distinct change in efficacy. From these results, it is apparent that the nature and composition of the tail moiety of extended structures play a large role in influencing the potency of these extended structures. We also cannot discount the possibility that compounds **50-55** may have some modulatory properties in the

presence of dopamine since the tail moiety of **35** (and **36**) is thought to be a key structural determinant of its activity as a NAM.<sup>19,31</sup>

## 2.3 Experimental

**Chemistry.** All solvents and chemicals were purchased from standard suppliers and were used without any further purification. <sup>1</sup>H NMR and <sup>13</sup>C NMR spectra were acquired at 400.13 (<sup>1</sup>H spectra) and 100.62 (<sup>13</sup>C spectra) MHz, respectively, on a Bruker Avance III Nanobay 400 MHz NMR spectrometer coupled to the BACS 60 automatic sample changer and equipped with a 5 mm PABBO BB-1H/ D Z-GRD probe. All spectra obtained was processed using MestReNova software (v.6.0). Chemical shifts (δ) for all <sup>1</sup>H spectra are reported in parts per million (ppm) using tetramethylsilane (TMS, 0 ppm) as the reference. The data for all spectra are reported in the following format: chemical shift (δ), (multiplicity, coupling constants *J* (Hz), integral), where the multiplicity is defined as s = singlet, d = doublet, t = triplet, q = quartet, p = pentet, and m = multiplet. <sup>13</sup>C NMR were routinely carried out as *J*-modulated spin-echo experiments (JMOD), all <sup>13</sup>C δ are reported in ppm and assignment of carbon signals were abbreviated as: C = quaternary carbon, CH = methine carbon, CH<sub>2</sub> = methylene carbon, and CH<sub>3</sub> = methyl carbon. Thin layer chromatography (TLC) was carried out routinely on silica gel 60F254 precoated plates (0.25 mm, Merck). Flash column chromatography was carried out using Davisil LC60A silica gel, 40-63 μm.

Liquid chromatography mass spectrometry (LCMS) was detected on one of two instruments; either an Agilent 6100 Series Single Quad LC/MS or an Agilent 1200 Series HPLC (equipped with a 1200 Series G1311A Quaternary Pump, G1329A Thermostatted Autosampler, and a G1314B Variable Wavelength Detector) and the data was processed using LC/MSD Chemstation Rev.B.04.01 SP1 coupled with Easy Access Software. Both systems were equipped with a Reverse Phase Luna C<sub>8</sub>(2) (5 μm, 50 × 4.6 mm, 100 Å) column maintained at 30 °C. An MeCN gradient (5-100%) was used to obtain optimal separation, where 4 min were required for the gradient to reach 100% MeCN and maintained for a further 3 min before requiring 3 min to return to the initial gradient of 5% MeCN (total run time = 10 min). Solvent A = 0.1% aqueous formic acid; Solvent B = MeCN/ 0.1% formic acid.

The purity and retention time of final products were determined using analytical HPLC and high resolution mass spectrometry (HRMS). Analytical HPLC was carried out using an Agilent 1260 Infinity Analytical HPLC fitted with a Zorbax Eclipse Plus C18 Rapid Resolution column (100 mm × 4.60 mm, 3.5 μm) using a binary solvent system: solvent A of 0.1% aqueous TFA; solvent B of 0.1% TFA in MeCN. Gradient elution was achieved over 10 min using 95% A + 5% B to 100% B over 9 min, and 100% B maintained for 1 min at a flow rate of 1 mL/min monitored at both 214 and 254 nm. HRMS were conducted on an Agilent 6224 TOP LC/MS Mass Spectrometer coupled to an Agilent 1290 Infinity. All data was acquired and reference mass corrected via dual-spray electrospray ionisation (ESI) source. Each scan or data point on the total

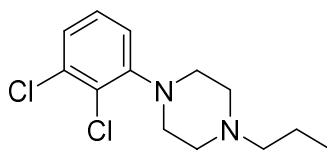
ion chromatogram (TIC) is average of 13700 transients, producing one spectrum per second. Mass spectra were created by averaging the scans across each peak and background subtracted against the first 10 seconds of the TIC. Data acquisition was carried out using the Agilent Mass Hunter Data Acquisition software version B.05.00 Build 5.0.5042 and analysis was performed using Mass Hunter Qualitative Analysis version B.05.00 Build 5.0.519.13.

### **General Procedure A (Reductive Alkylation)**

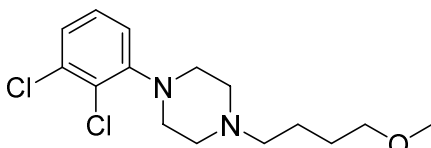
The amine (1 eq.) and aldehyde (1 eq.) were dissolved in dry 1,2-DCE (15 mL). NaBH(OAc)<sub>3</sub> (1.5 eq.) was added and stirred under an atmosphere of N<sub>2</sub> for 24 h. LCMS was used to confirm completion of the reaction. The mixture was then diluted in DCM (20 mL), and washed with 1 M K<sub>2</sub>CO<sub>3</sub> (3 × 20 mL) and brine, then dried over anhydrous Na<sub>2</sub>SO<sub>4</sub> and evaporated to dryness. The crude material was then purified using flash chromatography (3:97 MeOH: DCM) unless otherwise stated.

### **General procedure B (Deprotection of *tert*-butyl carbamate and HATU Amide Coupling)**

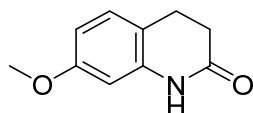
To a stirring solution of protected amine (1 eq.) and DCM (5 mL) at rt was added an excess of TFA (2 mL). The solution was stirred overnight and then diluted with DCM (20 mL). 1 M K<sub>2</sub>CO<sub>3</sub> or 1 M NaOH was added to bring the mixture to pH 12. The product was then extracted using DCM (2 × 20 mL). The combined organic extracts were washed with brine, dried over anhydrous Na<sub>2</sub>SO<sub>4</sub> then concentrated *in vacuo* to yield the free amine. Following confirmation of product formation via TLC or LCMS, the resulting amine (1 eq.), carboxylic acid (1.2 eq.) and the coupling reagent (HATU) (1.2-2 eq.) were stirred in a minimal volume of anhydrous DMF (3 mL). To this, an excess of DIPEA (2 eq.) was added and the reaction was left to stir between 2 and 24 hours. The reaction was ceased upon confirmation of complete consumption of the amine via LCMS. The mixture was then diluted with 1:1 mixture of a sat. NaHCO<sub>3</sub> solution and H<sub>2</sub>O (30 mL) and left to stir for 30 min. The resulting precipitate was filtered and washed. If precipitation had not occurred the product was extracted using EtOAc (3 × 20 mL) and concentrated under vacuum. Any further purification was as specified.

**1-(2,3-Dichlorophenyl)-4-propylpiperazine (10).**<sup>11</sup>

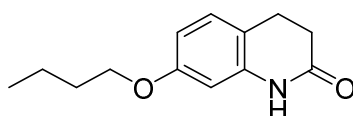
1-(2,3-Dichlorophenyl)piperazine hydrochloride (803 mg, 3.00 mmol), 1-bromopropane (273- $\mu$ L, 3.00 mmol) and K<sub>2</sub>CO<sub>3</sub> (1.24 g, 9.00 mmol) were stirred in acetone under reflux for 16 hours. The resultant mixture was then concentrated *in vacuo* and the resultant residue was diluted with EtOAc, washed with H<sub>2</sub>O (2  $\times$  50 mL) and brine (50 mL), and dried over anhydrous Na<sub>2</sub>SO<sub>4</sub>. The solution was then reduced under pressure and purified via column chromatography (1:9 MeOH: CHCl<sub>3</sub>) to afford 1-(2,3-dichlorophenyl)-4-propylpiperazine as a colourless oil (444 mg, 54%). <sup>1</sup>H NMR (CDCl<sub>3</sub>)  $\delta$  7.14 (m, 2H), 6.96 (m, 1H), 3.07 (br s, 4H), 2.67 (br s, 4H), 2.38 (m, 2H), 1.55 (m, 2H), 0.93 (t, *J* = 7.4 Hz, 3H). <sup>13</sup>C NMR (CDCl<sub>3</sub>)  $\delta$  151.5 (C), 134.1 (C), 127.6 (C), 127.5 (CH), 124.6 (CH), 118.71 (CH), 60.8 (CH<sub>2</sub>), 53.5 (CH<sub>2</sub>), 51.5 (CH<sub>2</sub>), 20.2 (CH<sub>2</sub>), 12.1 (CH<sub>3</sub>). HPLC: *t*<sub>R</sub> 5.93 min, >95% purity. HRMS (*m/z*): [M+H]<sup>+</sup> calcd for C<sub>13</sub>H<sub>19</sub>Cl<sub>2</sub>N<sub>2</sub> requires 273.0920; found 273.0923.

**1-(2,3-Dichlorophenyl)-4-(4-methoxybutyl)piperazine (12).**

1-(2,3-Dichlorophenyl)piperazine hydrochloride (500 mg, 1.87 mmol), 1-bromo-4-methoxybutane (244  $\mu$ L, 1.87 mmol) and K<sub>2</sub>CO<sub>3</sub> (1.24 g, 9.00 mmol) were stirred in acetone at reflux for 16 h. The mixture was then concentrated *in vacuo* and the resultant residue was diluted with EtOAc, washed with H<sub>2</sub>O (2  $\times$  50 mL) and brine (50 mL), and dried over anhydrous Na<sub>2</sub>SO<sub>4</sub>. The solution was then reduced under pressure and purified via column chromatography (3:2 EtOAc: Hexane) to obtain 1-(2,3-dichlorophenyl)-4-(4-methoxybutyl)piperazine as a yellow oil (240 mg, 40%). <sup>1</sup>H NMR (CDCl<sub>3</sub>)  $\delta$  7.15 (m, 2H), 6.96 (m, 1H), 3.41 (app t, *J* = 6.1 Hz, 2H), 3.34 (s, 3H), 3.07 (br s, 4H), 2.64 (br s, 4H), 2.38 (app t, *J* = 7.3 Hz, 2H), 1.65 (m, 4H). <sup>13</sup>C NMR (CDCl<sub>3</sub>)  $\delta$  151.3 (C), 134.0 (C), 127.5 (C), 127.4 (CH), 124.5 (CH), 118.6 (CH), 72.7 (CH<sub>2</sub>), 58.6 (CH<sub>3</sub>), 58.4 (CH<sub>2</sub>), 53.3 (CH<sub>2</sub>), 51.3 (CH<sub>2</sub>), 27.7 (CH<sub>2</sub>), 23.6 (CH<sub>2</sub>). HPLC: *t*<sub>R</sub> 5.85 min, >95% purity. HRMS (*m/z*): [M+H]<sup>+</sup> calcd for C<sub>15</sub>H<sub>23</sub>Cl<sub>2</sub>N<sub>2</sub>O requires 317.1182; found 317.1182.

**7-Methoxy-1,2,3,4-tetrahydroquinolin-2-one (13).**<sup>33</sup>

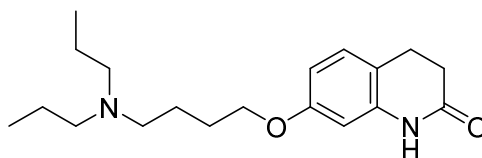
To an rbf containing 7-hydroxy-1,2,3,4-tetrahydroquinolin-2-one (200 mg, 1.23 mmol) and K<sub>2</sub>CO<sub>3</sub> (186 mg, 1.35 mmol), DMF (10 mL) was added and left to stir until completely dissolved. Methyl iodide (76.3  $\mu$ L, 1.23 mmol) was then added to the mixture and the reaction was stirred at room temperature for 16 h. The mixture was then poured into water (100 mL) and neutralised with 1 M HCl. The compound was extracted with EtOAc (6  $\times$  20 mL) and the combined organic phases were washed with water (2  $\times$  100 mL) and brine (100 mL). After the organic phase was dried over anhydrous Na<sub>2</sub>SO<sub>4</sub> and concentrated *in vacuo*. The crude product was purified via column chromatography (1:1 EtOAc: Pet. Spirits) to yield 7-methoxy-1,2,3,4-tetrahydroquinolin-2-one as an opaque, white solid (471 mg, 72%). <sup>1</sup>H NMR (CDCl<sub>3</sub>)  $\delta$  7.55 (br s, 1H), 7.06 (d, *J* = 8.3 Hz, 1H), 6.54 (dd, *J* = 8.3 Hz, 2.5 Hz, 1H), 6.29 (d, *J* = 2.5 Hz, 1H), 3.78 (s, 3H), 2.97 – 2.81 (m, 2H), 2.62 (m, 2H). <sup>13</sup>C NMR (101 MHz, CDCl<sub>3</sub>)  $\delta$  171.79 (C), 159.23 (C), 138.15 (C), 128.71 (CH), 115.82 (C), 108.14 (CH), 101.59 (CH), 55.46 (CH<sub>3</sub>), 31.09 (CH<sub>2</sub>), 24.58 (CH<sub>2</sub>). HPLC: *t*<sub>R</sub> 5.16 min, >95% purity. HRMS (*m/z*): [M+H]<sup>+</sup> calcd for C<sub>10</sub>H<sub>12</sub>NO<sub>2</sub> requires 177.0863; found 177.0863.

**7-butoxy-1,2,3,4-tetrahydroquinolin-2-one (14).**

The phenol (200 mg, 1.23 mmol) was taken up in acetone (15 mL) and added to the solution was potassium carbonate (339 mg, 2.45 mmol) and 1-bromobutane (248  $\mu$ L, 2.45 mmol), and the reaction mixture heated at reflux for 16 h. After this time, the solvents were removed *in vacuo*, then the mixture taken up in 1 M sodium hydroxide solution (15 mL) and the product extracted into chloroform (2  $\times$  20 mL). The combined organic layers were washed with brine (10 mL) then dried over anhydrous sodium sulfate, and evaporated to dryness to reveal a yellow waxy solid. The crude material was then purified by gradient flash column chromatography (1:4 – 1:1 EtOAc: Pet. Spirits) to give the title compound as a colourless oil (65 mg, 24%). <sup>1</sup>H NMR (CDCl<sub>3</sub>)  $\delta$  8.92 (br s, 1H, NH), 7.03 (d, *J* = 8.3 Hz, 1H), 6.52 (dd, *J* = 8.3, 2.4 Hz, 1H), 6.39 (d, *J* = 2.4 Hz, 1H), 3.93 (t, *J* = 6.5 Hz, 2H), 2.94 – 2.84 (m, 2H), 2.62 (dd, *J* = 8.3, 6.7 Hz, 2H), 1.79 – 1.69 (m, 2H), 1.55 – 1.38 (m, 2H), 0.97 (t, *J* = 7.4 Hz, 3H). <sup>13</sup>C NMR (CDCl<sub>3</sub>)  $\delta$  172.4 (C), 159.0 (C), 138.3 (C),

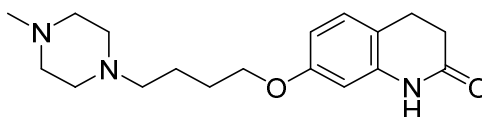
128.7 (CH), 115.7 (C), 108.9 (CH), 102.4 (CH), 68.0 (CH<sub>2</sub>), 31.4 (CH<sub>2</sub>), 31.3 (CH<sub>2</sub>), 24.7 (CH<sub>2</sub>), 19.3 (CH<sub>2</sub>), 14.0 (CH<sub>3</sub>). HPLC:  $t_R$  = 10.0 min, >95% purity.

#### 7-(4-(dipropylamino)butoxy)-1,2,3,4-tetrahydroquinolin-2-one (15).



The alkyl halide (300 mg, 1.01 mmol, Sigma Aldrich, USA) was taken up in acetone (30 mL), then potassium carbonate (278 mg, 2.01 mmol), sodium iodide (533 mg, 3.56 mmol) and di-*n*-propylamine (550  $\mu$ L, 4.02 mmol) were added to the stirred mixture. The reaction mixture was heated at reflux for 2 d, after which point complete consumption of starting material was evident by LCMS. The mixture was evaporated to dryness and taken up in water (20 mL) and ethyl acetate (2  $\times$  20 mL). The organic phase was then washed with 1 M potassium carbonate solution (15 mL), then the product was extracted into 1 M hydrogen chloride solution (2  $\times$  15 mL). The acidic aqueous phase was then neutralised with ammonium hydroxide solution to pH = 10, and then the product extracted back into ethyl acetate (2  $\times$  25 mL). The final organic phases were combined, washed with brine (10 mL), then dried over anhydrous sodium sulfate and evaporated to dryness to give the product as a colourless oil (310 mg, 97%). <sup>1</sup>H NMR (CDCl<sub>3</sub>)  $\delta$  9.14 (s, 1H), 7.02 (d,  $J$  = 8.3 Hz, 1H), 6.51 (dd,  $J$  = 8.3, 2.4 Hz, 1H), 6.41 (d,  $J$  = 2.4 Hz, 1H), 3.93 (t,  $J$  = 6.4 Hz, 2H), 2.89 (t,  $J$  = 7.5 Hz, 2H), 2.67 – 2.56 (m, 2H), 2.51 – 2.42 (m, 2H), 2.40 – 2.32 (m, 4H), 1.83 – 1.70 (m, 2H), 1.64 – 1.52 (m, 2H), 1.51 – 1.38 (m, 4H), 0.93 – 0.81 (m, 6H). <sup>13</sup>C NMR (CDCl<sub>3</sub>)  $\delta$  172.0 (C), 158.3 (C), 138.5 (C), 128.7 (CH), 116.2 (C), 108.8 (CH), 102.5 (CH), 67.2 (CH<sub>2</sub>), 54.4 (CH<sub>2</sub>), 52.6 (CH<sub>2</sub>), 50.8 (CH<sub>2</sub>), 31.2 (CH<sub>2</sub>), 26.6 (CH<sub>2</sub>), 24.7 (CH<sub>2</sub>), 20.8 (CH<sub>2</sub>), 17.3 (CH<sub>2</sub>), 11.4 (CH<sub>3</sub>). HPLC ( $\lambda$  = 254 nm)  $t_R$  = 7.85 min, >95% purity. LCMS ( $m/z$ ): [M+H]<sup>+</sup> 319.2.

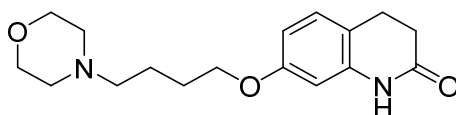
#### 7-(4-(4-methylpiperazin-1-yl)butoxy)-1,2,3,4-tetrahydroquinolin-2-one (16).



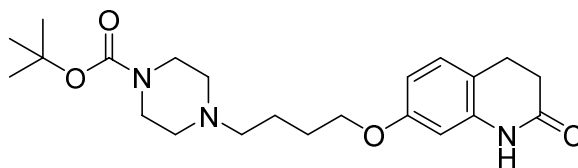
The alkyl halide (160 mg, 539  $\mu$ mol) was taken up in acetone (15 mL), and added to the solution was potassium carbonate (124 mg, 899  $\mu$ mol), sodium iodide (135 mg, 899  $\mu$ mol) and 1-methylpiperazine (49.8  $\mu$ L, 449  $\mu$ mol). The mixture was heated at reflux for 16 h, after which

point LCMS confirmed the complete consumption of all piperazine starting material. The mixture was evaporated of solvents *in vacuo*, and then taken up in chloroform (20 mL) and washed with 1 M potassium carbonate solution (2 × 15 mL). The organic extract was then washed with brine (15 mL), dried over anhydrous sodium sulfate, and evaporated to dryness to give a yellow oil. The product was then purified by column chromatography (1:4 MeOH: CHCl<sub>3</sub>) to give the title compound as a colourless oil (74 mg, 52%). <sup>1</sup>H NMR (CDCl<sub>3</sub>) δ 9.12 (s, 1H), 7.03 (d, *J* = 8.3 Hz, 1H), 6.51 (dd, *J* = 8.3, 2.4 Hz, 1H), 6.39 (d, *J* = 2.4 Hz, 1H), 3.94 (t, *J* = 6.3 Hz, 2H), 2.89 (t, *J* = 7.5 Hz, 2H), 2.61 (dd, *J* = 8.4, 6.7 Hz, 2H), 2.58 – 2.42 (m, 8H), 2.40 (d, *J* = 7.6 Hz, 2H), 2.30 (s, 3H), 1.84 – 1.72 (m, 2H), 1.72 – 1.59 (m, 2H). <sup>13</sup>C NMR (CDCl<sub>3</sub>) δ 172.4 (C), 158.7 (C), 138.3 (C), 128.6 (CH), 115.7 (C), 108.8 (CH), 102.3 (CH), 67.9 (CH<sub>2</sub>), 58.2 (CH<sub>2</sub>), 55.2 (CH<sub>2</sub>), 53.2 (CH<sub>2</sub>), 46.1 (CH<sub>3</sub>), 31.2 (CH<sub>2</sub>), 27.3 (CH<sub>2</sub>), 24.6 (CH<sub>2</sub>), 23.5 (CH<sub>2</sub>). HPLC (λ = 254 nm) *t*<sub>R</sub> = 5.65 min, >95% purity. LCMS (*m/z*): [M+H]<sup>+</sup> 318.2.

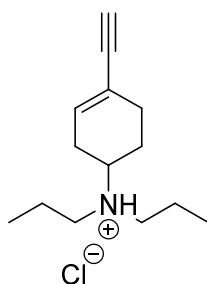
#### 7-(4-Morpholinobutoxy)-1,2,3,4-tetrahydroquinolin-2-one (17).<sup>34</sup>



A suspension of morpholine (201 μL, 2.30mmol), 7-(4-bromobutoxy)-1,2,3,4-tetrahydroquinolin-2-one (570 mg, 1.91 mmol) and potassium carbonate (789 mg, 5.73 mmol) in acetone was left to stir under reflux overnight. The resultant mixture was then concentrated *in vacuo* to yield a white precipitate. The solid product was taken up in 1 M HCl (30 mL) and EtOAc (30 mL) and the aqueous layer was collected. Sat. Na<sub>2</sub>CO<sub>3</sub> was used to basify the solution to pH 13 and the product was extracted using EtOAc (4 × 20 mL). The combined organic fractions were then washed with water (2 × 50 mL) brine (50 mL) and dried over anhydrous Na<sub>2</sub>SO<sub>4</sub>. The product was concentrated *in vacuo* to yield 7-(4-morpholinobutoxy)-1,2,3,4-tetrahydroquinolin-2-one as a yellow oil (422 mg, 72%). <sup>1</sup>H NMR (CDCl<sub>3</sub>) δ 7.90 (br s, 1H), 7.04 (d, *J* = 8.0 Hz, 1H), 6.52 (dd, *J* = 8.0 Hz, 4.0 Hz, 1H), 6.30 (d, *J* = 2.0 Hz, 1H), 3.95 (t, *J* = 6.3 Hz, 2H), 3.72 (app t, *J* = 4.0 Hz, 4H), 2.90 (app t, *J* = 6.0 Hz, 2H), 2.62 (m, 2H), 2.41 (m, 6H), 1.79 (m, 2H), 1.67 (m, 2H). <sup>13</sup>C NMR (CDCl<sub>3</sub>) δ 171.6 (C), 158.7 (C), 138.1 (C), 128.7 (CH), 115.8 (C), 108.6 (CH), 102.1 (CH), 67.9 (CH<sub>2</sub>), 67.0 (CH<sub>2</sub>), 58.6 (CH<sub>2</sub>), 53.7 (CH<sub>2</sub>), 31.0 (CH<sub>2</sub>), 27.2 (CH<sub>2</sub>), 24.6 (CH<sub>2</sub>), 23.1 (CH<sub>2</sub>). HPLC: *t*<sub>R</sub> 4.36 min, >95% purity. HRMS (*m/z*): [M+H]<sup>+</sup> calcd for C<sub>17</sub>H<sub>25</sub>N<sub>2</sub>O<sub>3</sub> requires 305.1860; found 305.1862.

***tert*-Butyl 4-(4-((2-oxo-1,2,3,4-tetrahydroquinolin-7-yl)oxy)butyl)piperazine-1-carboxylate (18).**

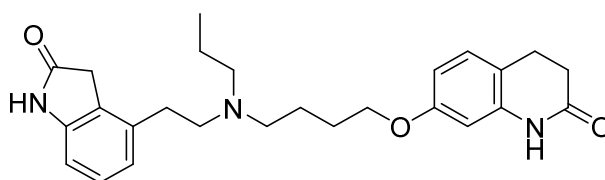
A suspension of *tert*-butyl piperazine-1-carboxylate (300 mg, 1.61 mmol), 7-(4-bromobutoxy)-1,2,3,4-tetrahydroquinolin-2-one (320 mg, 1.07 mmol) and potassium carbonate (594 mg, 4.30 mmol) in acetone (20 mL) was heated and stirred at reflux overnight. The resultant mixture was taken up in 20 mL EtOAc and washed with water (2 × 30 mL) and brine. The organic mixture was then dried over anhydrous Na<sub>2</sub>SO<sub>4</sub> and concentrated *in vacuo*. Column chromatography (1:19 MeOH: DCM) was then used to yield *tert*-butyl 4-(4-((2-oxo-1,2,3,4-tetrahydroquinolin-7-yl)oxy)butyl)piperazine-1-carboxylate as a yellow oil (196 mg, 45%). <sup>1</sup>H NMR (CDCl<sub>3</sub>) δ 8.20 (br s, 1H), 7.04 (d, *J* = 8.0 Hz, 1H), 6.52 (dd, *J* = 8.3, 2.4 Hz, 1H), 6.33 (d, *J* = 2.4 Hz, 1H), 3.94 (t, *J* = 6.2 Hz, 2H), 3.43 (app t, *J* = 6.0 Hz, 4H), 2.90 (app t, *J* = 6.0 Hz, 2H), 2.63 (app dd, *J* = 8.3, 6.7 Hz, 2H), 2.41 (m, 6H), 1.80 (m, 2H), 1.67 (m, 2H), 1.46 (s, 9H). <sup>13</sup>C NMR (CDCl<sub>3</sub>) δ 171.8 (C), 158.6 (C), 154.8 (C), 138.1 (C), 128.7 (CH), 115.7 (C), 108.7 (CH), 102.2 (CH), 79.6 (CH<sub>2</sub>), 67.8 (CH<sub>2</sub>), 58.2 (CH<sub>2</sub>), 53.0 (CH<sub>2</sub>), 31.1 (CH<sub>2</sub>), 28.4 (CH<sub>3</sub>), 27.2 (CH<sub>2</sub>), 24.6 (CH<sub>2</sub>), 23.3 (CH<sub>2</sub>). HPLC: *t*<sub>R</sub> 5.46 min, > 95% purity. HRMS (*m/z*): [M+H]<sup>+</sup> calcd for C<sub>22</sub>H<sub>34</sub>N<sub>3</sub>O<sub>4</sub> requires 404.2544; found 404.2550.

**4-Ethynyl-*N,N*-dipropylcyclohex-3-en-1-amine hydrochloride (19).<sup>18</sup>**

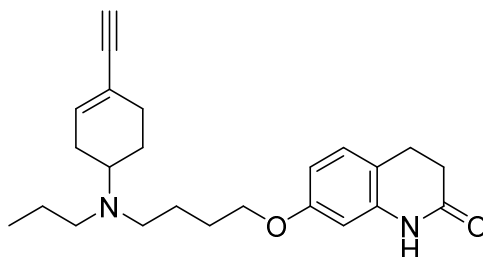
A suspension of imidazole (522 mg, 7.66 mmol), 4-(dipropylamino)-1-ethynylcyclohexan-1-ol (856 mg, 3.83 mmol), and PPh<sub>3</sub> (3.02 g, 11.5 mmol) in DCM (40 mL) was gently warmed (50 °C) until completely dissolved. A solution of iodine (1.95 g, 7.66 mmol) in DCM (21 mL) was added dropwise to this mixture at rt, causing it to go from a transparent yellow to opaque yellow. This mixture was left to stir for 72 h at rt. The reaction was quenched upon addition of saturated

NaHCO<sub>3</sub> and basified using 6 M NaOH. The product was extracted from the aqueous layer using DCM, and the combined layers were then dried over anhydrous Na<sub>2</sub>SO<sub>4</sub> and concentrated under pressure. The resultant pale yellow solid was initially purified by flash chromatography using a MeOH: DCM: NH<sub>3</sub> (30% (v/v)) (3:97:1) system but yielded impure product. The crude was then loaded onto a second silica column and flushed with DCM until triphenylphosphine oxide could no longer be visualised by TLC and then the initially stated column conditions were then used to obtain the product as a yellow oil (23.7 mg, 3%). The resultant oil was then taken up in DCM and converted to the HCl salt using an excess of 1 M HCl in Et<sub>2</sub>O. The solution was concentrated *in vacuo* to quantitatively yield the product salt as a yellow solid. <sup>1</sup>H NMR (CDCl<sub>3</sub>) δ 6.19 – 6.12 (m, 1H), 2.81 – 2.72 (m, 2H), 2.46 – 2.32 (m, 4H), 2.30 – 2.05 (m, 4H), 1.89 – 1.78 (m, 1H), 1.53 – 1.35 (m, 5H), 0.86 (t, *J* = 7.4 Hz, 6H). <sup>13</sup>C NMR (CDCl<sub>3</sub>) δ 135.9 (CH), 119.6 (C), 85.1 (C), 74.7 (CH), 55.5 (CH), 52.6 (CH<sub>2</sub>), 30.2 (CH<sub>2</sub>), 28.5 (CH<sub>2</sub>), 25.1 (CH<sub>2</sub>), 22.1 (CH<sub>2</sub>), 11.9 (CH<sub>3</sub>). HPLC: *t*<sub>R</sub> (λ 214 nm) 4.78 min, > 95% purity. HRMS (*m/z*): [M+H]<sup>+</sup> calcd for C<sub>14</sub>H<sub>24</sub>N requires 206.1903; found 206.1905.

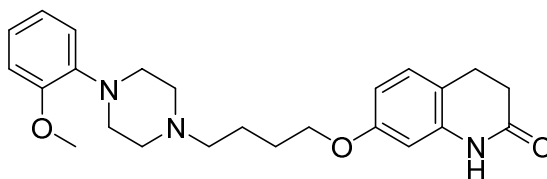
**7-(4-((2-(2-Oxoindolin-4-yl)ethyl)(propyl)amino)butoxy)-1,2,3,4-tetrahydroquinolin-2-one (22).**



4-(2-(Propylamino)ethyl)indolin-2-one (171 mg, 670 μmol), 7-(4-bromobutoxy)-1,2,3,4-tetrahydroquinolin-2-one (200 mg, 670 μmol) and K<sub>2</sub>CO<sub>3</sub> (185 mg, 1.34 mmol) were stirred in MeCN (20 mL) at reflux for 24 h. The resultant mixture was concentrated *in vacuo* and purified using column chromatography (1:9 MeOH: DCM) to afford the product as a purple oil (92.2 mg, 32%). <sup>1</sup>H NMR (CDCl<sub>3</sub>) δ 9.59 (s, 1H), 9.32 (s, 1H), 7.10 (app t, *J* = 7.8 Hz, 1H), 7.00 (d, *J* = 8.3 Hz, 1H), 6.82 (d, *J* = 7.7 Hz, 1H), 6.74 (d, *J* = 7.7 Hz, 1H), 6.52 – 6.37 (m, 2H), 3.86 (t, *J* = 6.0 Hz, 2H), 3.49 (br s, 2H), 2.92 – 2.45 (m, 12H), 1.77 – 1.42 (m, 6H), 0.89 (t, *J* = 7.3 Hz, 3H). <sup>13</sup>C NMR (CDCl<sub>3</sub>) δ 178.0 (C), 172.5 (C), 158.6 (C), 142.7 (C), 138.3 (C), 136.6 (C), 128.5 (CH), 128.1 (CH), 124.1 (C), 122.8 (CH), 115.7 (C), 108.5 (CH), 107.9 (CH), 102.5 (CH), 67.7 (CH<sub>2</sub>), 56.1 (CH<sub>2</sub>), 53.9 (CH<sub>2</sub>), 53.4 (CH<sub>2</sub>), 35.2 (CH<sub>2</sub>), 31.0 (CH<sub>2</sub>), 30.5 (CH<sub>2</sub>), 27.0 (CH<sub>2</sub>), 24.5 (CH<sub>2</sub>), 23.4 (CH<sub>2</sub>), 20.0 (CH<sub>2</sub>), 11.9 (CH<sub>3</sub>). HPLC: *t*<sub>R</sub> 5.45 min, >95% purity. HRMS (*m/z*): [M+H]<sup>+</sup> calcd for C<sub>26</sub>H<sub>34</sub>N<sub>3</sub>O<sub>3</sub> requires 436.2595; found 436.2603.

**7-(4-((4-Ethynylcyclohex-3-en-1-yl)(propyl)amino)butoxy)-1,2,3,4-tetrahydroquinolin-2-one (23).**

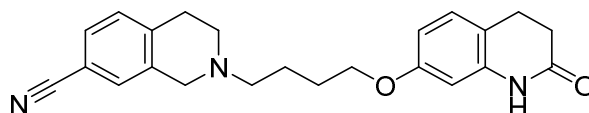
7-(4-Bromobutoxy)-1,2,3,4-tetrahydroquinolin-2-one (148 mg, 494  $\mu$ mol), 4-ethynyl-*N*-propylcyclohex-3-en-1-amine (73.8 mg, 452  $\mu$ mol), and K<sub>2</sub>CO<sub>3</sub> (192 mg, 1.4 mmol) in MeCN were heated in an rbf at reflux for 6 d. The reaction was terminated upon LCMS confirmation that the amino starting material had been consumed. The mixture was evaporated *in vacuo* and initially purified using flash chromatography (3:97 MeOH: DCM). The persistence of impurities led to further purification via flash chromatography (1:9 MeOH: DCM) which was unsuccessful in purifying the compound to a satisfactory standard. Ultimately, a solvent system of 100% EtOAc yielded the pure compound as a yellow oil using flash chromatography methods in good yield (77.3 mg, 45%). <sup>1</sup>H NMR (CDCl<sub>3</sub>)  $\delta$  8.36 (s, 1H), 7.03 (d, *J* = 8.3 Hz, 1H), 6.51 (dd, *J* = 8.3, 2.4 Hz, 1H), 6.34 (d, *J* = 2.4 Hz, 1H), 6.16 – 6.10 (m, 1H), 3.93 (t, *J* = 6.4 Hz, 2H), 2.93 – 2.84 (m, 2H), 2.83 – 2.71 (m, 2H), 2.65 – 2.58 (m, 2H), 2.52 – 2.34 (m, 4H), 2.31 – 2.14 (m, 3H), 2.13 – 2.01 (m, 1H), 1.89 – 1.81 (m, 1H), 1.81 – 1.69 (m, 2H), 1.62 – 1.36 (m, 5H), 0.86 (t, *J* = 7.3 Hz, 3H). <sup>13</sup>C NMR (CDCl<sub>3</sub>)  $\delta$  171.9 (C), 158.7 (C), 138.1 (C), 135.8 (CH), 128.6 (CH), 119.6 (C), 115.7 (C), 108.7 (CH), 102.2 (CH), 85.1 (C), 74.9 (CH), 68.1 (CH<sub>2</sub>), 55.2 (CH), 52.4 (CH<sub>2</sub>), 50.1 (CH<sub>2</sub>), 31.1 (CH<sub>2</sub>), 30.2 (CH<sub>2</sub>), 28.4 (CH<sub>2</sub>), 27.1 (CH<sub>2</sub>), 25.4 (CH<sub>2</sub>), 25.0 (CH<sub>2</sub>), 24.6 (CH<sub>2</sub>), 22.1 (CH<sub>2</sub>), 11.9 (CH<sub>3</sub>). HPLC: *t*<sub>R</sub> 5.66 min, >95% purity. HRMS (*m/z*): [M+H]<sup>+</sup> calcd for C<sub>24</sub>H<sub>33</sub>N<sub>2</sub>O<sub>2</sub> requires 381.2537; found 381.2546.

**7-(4-(4-(2-Methoxyphenyl)piperazin-1-yl)butoxy)-1,2,3,4-tetrahydroquinolin-2-one (24).**

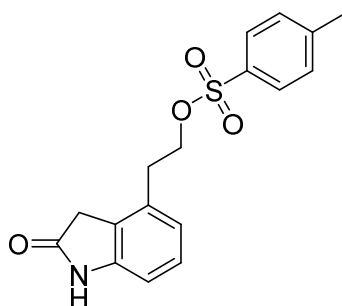
An rbf containing 1-(2-methoxyphenyl)piperazine hydrochloride (320 mg, 1.40 mmol), 7-(4-bromobutoxy)-1,2,3,4-tetrahydroquinolin-2-one (500 mg, 1.68 mmol) and K<sub>2</sub>CO<sub>3</sub> (193 mg, 1.40 mmol) in MeCN (30 mL) was stirred at reflux for 72 h. The resultant mixture was

concentrated *in vacuo* and purified using column chromatography (1:9 MeOH: DCM). The product obtained was a yellow oil (389 mg, 68%). <sup>1</sup>H NMR (CDCl<sub>3</sub>) δ 9.33 (s, 1H), 7.03 – 6.82 (m, 5H), 6.50 (dd, *J* = 8.3, 2.4 Hz, 1H), 6.40 (d, *J* = 2.4 Hz, 1H), 3.94 (t, *J* = 6.1 Hz, 2H), 3.84 (s, 3H), 3.10 (br s, 4H), 2.87 (t, *J* = 7.5 Hz, 2H), 2.62 (m, 6H), 2.47 (t, *J* = 7.5 Hz, 2H), 1.86 – 1.65 (m, 4H). <sup>13</sup>C NMR (CDCl<sub>3</sub>) δ 172.5 (C), 158.7 (C), 152.3 (C), 141.4 (C), 138.3 (C), 128.5 (CH), 122.9 (CH), 121.0 (CH), 118.2 (CH), 115.6 (C), 111.2 (CH), 108.8 (CH), 102.3 (CH), 67.9 (CH<sub>2</sub>), 58.3 (CH<sub>2</sub>), 55.4 (CH<sub>3</sub>), 53.5 (CH<sub>2</sub>), 50.7 (CH<sub>2</sub>), 31.1 (CH<sub>2</sub>), 27.3 (CH<sub>2</sub>), 24.6 (CH<sub>2</sub>), 23.4 (CH<sub>2</sub>). HPLC: *t*<sub>R</sub> 5.50 min, >95% purity. HRMS (*m/z*): [M+H]<sup>+</sup> calcd for C<sub>24</sub>H<sub>32</sub>N<sub>3</sub>O<sub>3</sub> requires 410.2438; found 410.2443.

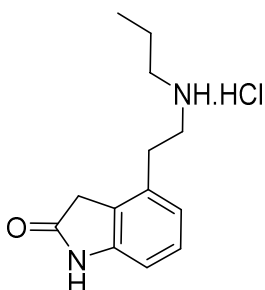
**2-(4-((2-Oxo-1,2,3,4-tetrahydroquinolin-7-yl)oxy)butyl)-1,2,3,4-tetrahydroisoquinoline-7-carbonitrile (25).**



1,2,3,4-Tetrahydroisoquinoline-7-carbonitrile (117 mg, 738 μmol), 7-(4-bromobutoxy)-1,2,3,4-tetrahydroquinolin-2-one (200 mg, 671 μmol) and K<sub>2</sub>CO<sub>3</sub> (92.7 mg, 671 μmol) in MeCN (20 mL) were added to an rbf and stirred at reflux for 72 h. The resultant mixture was concentrated *in vacuo* and purified using column chromatography (1:1 MeOH: DCM). The product obtained was a yellow oil (185 mg, 73%). <sup>1</sup>H NMR (CDCl<sub>3</sub>) δ 9.04 (s, 1H), 7.39 (d, *J* = 7.9 Hz, 1H), 7.31 (s, 1H), 7.18 (d, *J* = 7.9 Hz, 1H), 7.03 (d, *J* = 8.3 Hz, 1H), 6.51 (dd, *J* = 8.3, 2.4 Hz, 1H), 6.39 (d, *J* = 2.4 Hz, 1H), 3.97 (t, *J* = 6.0 Hz, 2H), 3.63 (s, 2H), 2.92 (m, 4H), 2.75 (t, *J* = 5.9 Hz, 2H), 2.60 (m, 4H), 1.79 (m, 4H). <sup>13</sup>C NMR (CDCl<sub>3</sub>) δ 172.3 (C), 158.7 (C), 140.4 (C), 138.3 (C), 136.3 (C), 130.4 (CH), 129.6 (CH), 129.5 (CH), 128.6 (CH), 119.1 (C), 115.7 (C), 109.4 (C), 109.0 (CH), 102.3 (CH), 67.8 (CH<sub>2</sub>), 57.8 (CH<sub>2</sub>), 55.5 (CH<sub>2</sub>), 50.2 (CH<sub>2</sub>), 31.1 (CH<sub>2</sub>), 29.5 (CH<sub>2</sub>), 27.2 (CH<sub>2</sub>), 24.6 (CH<sub>2</sub>), 23.6 (CH<sub>2</sub>). HPLC: *t*<sub>R</sub> 5.45 min, >95 % purity. HRMS (*m/z*): [M+H]<sup>+</sup> calcd for C<sub>23</sub>H<sub>26</sub>N<sub>3</sub>O<sub>2</sub> requires 376.2020; found 376.2025.

**2-(2-Oxindolin-4-yl)ethyl 4-methylbenzenesulfonate (27).**<sup>20</sup>

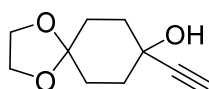
Using a procedure outlined in Jörg *et al.*,<sup>20</sup> a suspension of 4-(2-hydroxyethyl)indolin-2-one (6.30 g, 35.6 mmol) and pyridine (14.1 g, 178 mmol) were stirred in an rbf at 5–10 °C. A solution of *p*-toluenesulfonyl chloride (8.13 g, 42.7 mmol) in DCM (32 mL) was then added to the reaction dropwise over 30 min. The reaction mixture was maintained at 5–10 °C and left to stir for 4 h. 6 M HCl (35 mL) was then added in order to maintain the mixture at temperatures below 15 °C, and the aqueous was extracted with DCM. The combined organic layers were washed with H<sub>2</sub>O, dried over anhydrous Na<sub>2</sub>SO<sub>4</sub> and concentrated *in vacuo*. The organic layer was concentrated until a residual volume of 50 mL was observed and a further 50 mL of Pet. Spirits were added to induce product crystallisation. The suspension was then filtered and the precipitant washed with a mixture of Pet. Spirits: DCM (1:1), dried overnight under vacuum to yield the title compound as a white solid (6.53 g, 55%). <sup>1</sup>H NMR (CDCl<sub>3</sub>) δ 8.38 (br s, 1H), 7.67 – 7.63 (m, 2H), 7.27 (d, *J* = 7.9 Hz, 2H), 7.13 (app t, *J* = 7.8 Hz, 1H), 6.76 (t, *J* = 8.2 Hz, 2H), 4.23 (t, *J* = 6.7 Hz, 2H), 3.32 (s, 2H), 2.89 (t, *J* = 6.7 Hz, 2H), 2.43 (s, 3H). <sup>13</sup>C NMR (CDCl<sub>3</sub>) δ 176.7 (C), 145.2 (C), 142.4 (C), 132.9 (C), 132.8 (C), 129.8 (CH), 128.4 (CH), 127.8 (CH), 124.5 (C), 122.9 (CH), 108.3 (CH), 69.2 (CH<sub>2</sub>), 34.8 (CH<sub>2</sub>), 32.4 (CH<sub>2</sub>), 21.62 (CH<sub>3</sub>). LCMS (m/z): [M+H]<sup>+</sup> 332.2.

**4-(2-(Propylamino)ethyl)indolin-2-one hydrochloride (28).**<sup>20</sup>

Following a method described by Jörg *et al.*,<sup>20</sup> 2-(2-oxindolin-4-yl)ethyl 4-methylbenzenesulfonate (2.00 g, 6.04 mmol) was dissolved in propylamine (2.46 mL, 24.1 mmol). The mixture was stirred at reflux for 1.5 h then partitioned between EtOAc and 1 M aq. K<sub>2</sub>CO<sub>3</sub>.

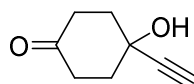
The aqueous layer was extracted with 1 M aq. HCl (3 × 50 mL) then reduced *in vacuo*. The resultant residue was re-suspended in MeOH, filtered and then washed with additional MeOH to yield the title compound as a yellow solid (1.62 g, 54%) in accordance with the literature. <sup>1</sup>H NMR (D<sub>2</sub>O) δ 6.93 (t, *J* = 7.8 Hz, 1H), 6.64 (d, *J* = 7.8 Hz, 1H), 6.53 (d, *J* = 7.8 Hz, 1H), 3.10 – 2.93 (m, 2H), 2.78 – 2.65 (m, 2H), 2.65 – 2.51 (m, 2H), 1.49 – 1.23 (sext, *J* = 7.5 Hz, 2H), 0.64 (t, *J* = 7.5 Hz, 3H). <sup>13</sup>C NMR (D<sub>2</sub>O) δ 179.9 (C), 142.3 (C), 132.2 (C), 128.3 (CH), 124.6 (C), 122.6 (CH), 109.0 (CH), 49.0 (CH<sub>2</sub>), 46.5 (CH<sub>2</sub>), 28.7 (CH<sub>2</sub>), 18.9 (CH<sub>2</sub>), 9.9 (CH<sub>3</sub>).

### 8-Ethynyl-1,4-dioxaspiro[4.5]decan-8-ol (30).<sup>21</sup>



Following an amended procedure initially described by Hiller *et al.*<sup>21</sup>, 0.5 M ethynylmagnesium bromide in THF (76.8 mL, 38.4 mmol) was diluted in THF (50 mL) and cooled to 0 °C. To this mixture, was added a solution of 1,4-dioxaspiro[4.5]decan-8-one (4.00 g, 25.6 mmol) dissolved in THF (20 mL) dropwise. The reaction mixture was left to stir and warm to rt overnight. Completion of the reaction was tracked by TLC and visualised using potassium permanganate (KMnO<sub>4</sub>). Sat. NH<sub>4</sub>Cl was added to the reaction mixture and stirred briefly and diethyl ether (Et<sub>2</sub>O) (3 × 100 mL) was used to extract the product from the aqueous phase. The combined organic phases were dried over anhydrous Na<sub>2</sub>SO<sub>4</sub>, filtered and evaporated to dryness. The resultant yellow oil was purified using vacuum distillation (124 °C, 6 mmHg) to furnish the product as a pale yellow oil (3.85 g, 82%). <sup>1</sup>H NMR (CDCl<sub>3</sub>) δ 3.88 (s, 4H), 2.96 (s, 1H), 2.44 (s, 1H), 1.98 – 1.60 (m, 8H). <sup>13</sup>C NMR (CDCl<sub>3</sub>) δ 108.0 (C), 87.1 (C), 72.1 (CH), 64.2 (CH<sub>2</sub>), 36.9 (CH<sub>2</sub>), 30.3 (CH<sub>2</sub>).

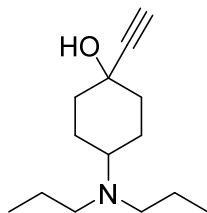
### 4-Ethynyl-4-hydroxycyclohexan-1-one (31).<sup>21</sup>



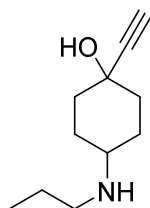
Following a procedure described by Hiller *et al.*<sup>21</sup>, a catalytic amount (0.5 mol%) of copper (II) sulfate (26.5 mg) was added to a solution of 8-ethynyl-1,4-dioxaspiro[4.5]decan-8-ol (3.85 g, 21.1 mmol) in 80 % (v/v) formic acid (14 mL) and left to stir overnight at rt. Consumption of the starting material was tracked by TLC and visualised using KMnO<sub>4</sub>. Upon completion of the reaction, the mixture was diluted with H<sub>2</sub>O, basified to a pH of 12 with 6 M sodium hydroxide

(NaOH) and the product was extracted from the aqueous layer using Et<sub>2</sub>O (10 × 50 mL). The combined organic phases were dried over anhydrous Na<sub>2</sub>SO<sub>4</sub>, filtered and concentrated *in vacuo* to give a waxy white solid (2.29 g, 78%). <sup>1</sup>H NMR (CDCl<sub>3</sub>) δ 2.67 – 2.37 (m, 5H), 2.31 – 2.07 (m, 5H). <sup>13</sup>C NMR (CDCl<sub>3</sub>) δ 209.7 (C), 85.8 (C), 73.1 (CH), 66.3 (C), 38.7 (CH<sub>2</sub>), 37.3 (CH<sub>2</sub>).

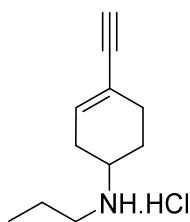
#### 4-(Dipropylamino)-1-ethynylcyclohexan-1-ol (32).



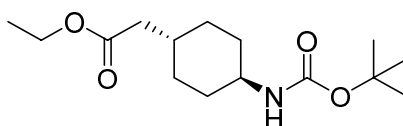
Using the method prescribed by Hiller *et al.*<sup>21</sup>, a suspension containing sodium triacetoxyborohydride (3.83 g, 18.1 mmol) in DCM (27 mL) was cooled on ice. To this, a solution of 4-ethynyl-4-hydroxycyclohexan-1-one (1.00 g, 7.24 mmol) in DCM (13 mL) was added dropwise over 30 min, followed by *N,N*-dipropylamine (3.97 mL, 29.0 mmol) and glacial acetic acid (455 μL, 8.00 mmol). The reaction mixture was then allowed to warm to rt and left to stir overnight. The reaction was quenched with saturated NaHCO<sub>3</sub> and basified to pH 12 using 6 M NaOH. The product was extracted from the aqueous layer using DCM, and the combined organic layers were dried over anhydrous Na<sub>2</sub>SO<sub>4</sub> and concentrated *in vacuo*. The resultant residue was purified using flash chromatography using a mixture of MeOH and DCM (1:19) supplemented with 1% (v/v) ammonia solution (NH<sub>3</sub> (30% (v/v))), which yielded the product as a waxy white residue (893 mg, 55%) in accordance to the literature. <sup>1</sup>H NMR (CDCl<sub>3</sub>) δ 2.60 – 2.44 (m, 2H), 2.42 – 2.26 (m, 4H), 2.03 (dd, *J* = 10.3, 2.4 Hz, 2H), 1.83 – 1.48 (m, 7H), 1.47 – 1.35 (m, 4H), 0.85 (td, *J* = 7.3, 2.6 Hz, 6H). <sup>13</sup>C NMR (CDCl<sub>3</sub>) δ 73.1 (C), 70.4 (CH), 69.3 (C), 58.8 (CH), 53.0 (CH<sub>2</sub>), 52.8 (CH<sub>2</sub>), 39.4 (CH<sub>2</sub>), 38.4 (CH<sub>2</sub>), 25.6 (CH<sub>2</sub>), 23.3 (CH<sub>2</sub>), 22.3 (CH<sub>2</sub>), 11.9 (CH<sub>3</sub>).

**1-Ethynyl-4-(propylamino)cyclohexan-1-ol (33).**<sup>21</sup>

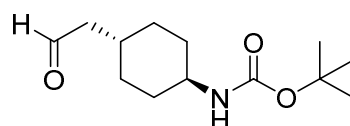
Using *n*-propylamine as the secondary amine, the procedure outlined for **32** was used to yield the product as a waxy white residue (1.75 g, 69%). <sup>1</sup>H NMR (CDCl<sub>3</sub>) δ 2.62 – 2.39 (m, 4H), 2.08 – 1.86 (m, 3H), 1.76 (m, 2H), 1.66 – 1.38 (m, 7H), 0.96 – 0.86 (m, 3H). <sup>13</sup>C NMR (CDCl<sub>3</sub>) δ 87.2 (C), 73.5 (CH), 71.2 (C), 56.1 (CH), 49.46 (CH<sub>2</sub>), 38.8 (CH<sub>2</sub>), 37.2 (CH<sub>2</sub>), 30.7 (CH<sub>2</sub>), 28.3 (CH<sub>2</sub>), 23.9 (CH<sub>2</sub>), 11.88 (CH<sub>3</sub>).

**4-Ethynyl-*N*-propylcyclohex-3-en-1-aminium chloride (34).**<sup>21</sup>

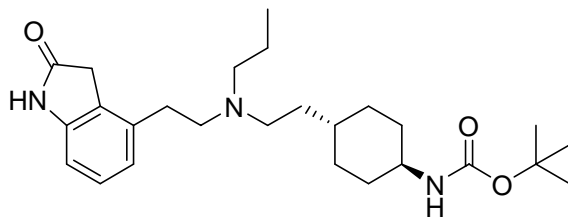
Using 1-ethynyl-4-(propylamino)cyclohexan-1-ol as the required reactant, the synthetic procedure outlined for **19** was followed. The resultant pale yellow solid was purified by flash chromatography. The crude was loaded onto the column and flushed with DCM until triphenylphosphine oxide was no longer visualised by TLC. Purification of the product was undertaken in a solvent mixture of MeOH: DCM: NH<sub>3</sub> (30% (v/v)) (3:97:1) to obtain the title compound as a yellow oil (997 mg, 41%). The resultant oil was then taken up in DCM and converted to the HCl salt using an excess of 1 M HCl in diethyl ether. The solution was concentrated *in vacuo* to quantitatively yield the product salt as a yellow solid. <sup>1</sup>H NMR (CDCl<sub>3</sub>) δ 6.05 (d, *J* = 1.6 Hz, 1H), 2.76 (s, 1H), 2.72 – 2.62 (m, 1H), 2.61 – 2.47 (m, 2H), 2.40 – 2.05 (m, 3H), 1.95 – 1.79 (m, 2H), 1.69 (s, 1H), 1.53 – 1.31 (m, 3H), 0.91 – 0.78 (m, 3H). <sup>13</sup>C NMR (CDCl<sub>3</sub>) δ 134.2 (CH), 119.6 (C), 84.9 (C), 75.0 (CH), 52.1 (CH), 48.9 (CH<sub>2</sub>), 32.8 (CH<sub>2</sub>), 28.6 (CH<sub>2</sub>), 28.3 (CH<sub>2</sub>), 23.4 (CH<sub>2</sub>), 11.8 (CH<sub>3</sub>). HPLC: *t*<sub>R</sub> (λ 214 nm) 4.03 min, > 95% purity. HRMS (*m/z*): [M+H]<sup>+</sup> calcd for C<sub>11</sub>H<sub>18</sub>N requires 164.1466; found 164.1469.

**Ethyl 2-((*trans*)-4-((*tert*-butoxycarbonyl)amino)cyclohexyl)acetate (42).<sup>31</sup>**

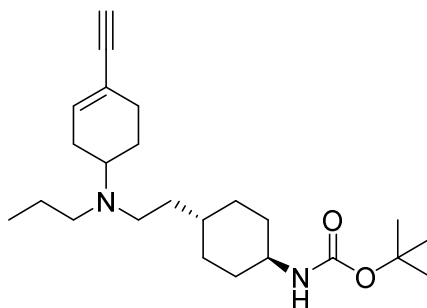
Following a procedure outlined by Shonberg *et al.*,<sup>31</sup> 2-((*trans*)-4-((*tert*-butoxycarbonyl)amino)cyclohexyl)acetic acid (500 mg, 1.94 mmol) and K<sub>2</sub>CO<sub>3</sub> (403 mg, 2.91 mmol) were suspended in 30 mL of MeCN. To this suspension was added EtI (173  $\mu$ L, 2.16 mmol) and the reaction was heated at 50 °C overnight. Once the mixture had cooled, it was then concentrated *in vacuo* to remove both the MeCN and EtI. The resultant residue was taken up in EtOAc and washed with H<sub>2</sub>O (30 mL), sat. NaHCO<sub>3</sub> (2  $\times$  30 mL) and brine (30 mL). After evaporation, the product was obtained as a wax-like, opaque white solid (551 mg, quantitative yield). <sup>1</sup>H NMR (CDCl<sub>3</sub>)  $\delta$  4.39 (br s, 1H), 4.11 (q, *J* = 7.1 Hz, 2H), 3.37 (br s, 1H), 2.17 (app d, *J* = 6.8 Hz, 2H), 2.10 – 1.93 (m, 2H), 1.83 – 1.65 (m, 3H), 1.44 (s, 9H), 1.26 (t, *J* = 7.1 Hz, 3H), 1.19 – 1.01 (m, 4H); <sup>13</sup>C NMR (CDCl<sub>3</sub>)  $\delta$  172.9 (C), 155.2 (C), 79.1 (C), 60.2 (CH<sub>2</sub>), 49.5 (CH), 41.5 (CH<sub>2</sub>), 34.0 (CH), 33.2 (CH<sub>2</sub>), 31.6 (CH<sub>2</sub>), 28.4 (CH<sub>3</sub>), 14.3 (CH<sub>3</sub>).

***tert*-Butyl ((*trans*)-4-(2-oxoethyl)cyclohexyl)carbamate (43).<sup>31</sup>**

Using a method previously described by Shonberg *et al.*,<sup>31</sup> ethyl 2-((*trans*)-4-((*tert*-butoxycarbonyl)amino)cyclohexyl)acetate (551 mg, 1.93 mmol) was dissolved in dry toluene (10 mL). The mixture was then degassed with nitrogen for 15 min before cooling to -78 °C in a bath of dry ice and MeCN. To the stirred solution was added 1 M DIBAL-H in toluene (3.90 mL, ~2 eq.) and the temperature was maintained (-78 °C) for 3 h. The reaction was then quenched with the drop-wise addition of MeOH (4 mL) and warmed to rt. After a further 15 min of stirring, sat. potassium sodium tartrate solution (Rochelle's salt) was added (20 mL) and left to stir for another 30 min. The reaction mixture was then extracted with Et<sub>2</sub>O (4  $\times$  25 mL), and the combined organic extracts were dried over anhydrous Na<sub>2</sub>SO<sub>4</sub> concentrated *in vacuo* to yield the product as a white solid (434 mg, 93%). <sup>1</sup>H NMR (CDCl<sub>3</sub>)  $\delta$  9.76 (t, *J* = 4.0 Hz, 1H), 4.39 (br s, 1H), 3.38 (br s, 1H), 2.33 (dd, *J* = 4.0 Hz, 2.0 Hz, 2H), 2.10 – 2.00 (m, 2H), 1.90 – 1.70 (m, 3H), 1.44 (s, 9H), 1.22 – 1.05 (m, 4H). <sup>13</sup>C NMR (CDCl<sub>3</sub>)  $\delta$  202.1 (CH), 155.2 (C), 78.8 (C), 50.6 (CH<sub>2</sub>), 49.3 (CH), 33.0 (CH<sub>2</sub>), 31.7 (CH<sub>2</sub>), 31.6 (CH), 28.3 (CH<sub>3</sub>).

***tert*-Butyl ((*trans*)-4-(2-((2-(2-oxoindolin-4-yl)ethyl)(propyl)amino)ethyl)cyclohexyl)carbamate (44).**

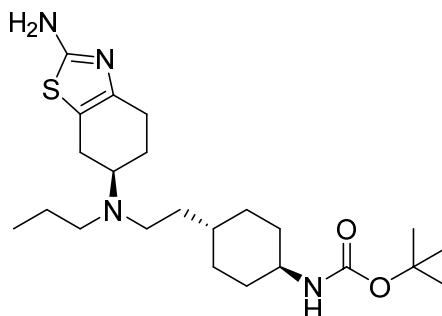
Using 4-(2-(propylamino)ethyl)indolin-2-one as the amine and *tert*-butyl ((*trans*)-4-(2-oxoethyl)cyclohexyl)carbamate as the aldehyde, general procedure A was followed. Flash chromatography yielded the title compound as an oil (49.8 mg, 18%). <sup>1</sup>H NMR (CDCl<sub>3</sub>) δ 8.92 (br s, 1H), 7.13 (app t, *J* = 7.8 Hz, 1H), 6.82 (d, *J* = 7.8 Hz, 1H), 6.74 (d, *J* = 7.7 Hz, 1H), 4.43 (d, *J* = 6.5 Hz, 1H), 3.47 (s, 2H), 3.35 (m, 1H), 2.71 (s, 4H), 2.60 – 2.40 (m, 4H), 1.96 (m, 2H), 1.70 (m, 2H), 1.58 – 1.30 (m, 13H), 1.24 – 0.93 (m, 5H), 0.88 (t, *J* = 7.3 Hz, 3H). <sup>13</sup>C NMR (CDCl<sub>3</sub>) δ 177.5 (C), 155.3 (C), 142.6 (C), 136.2 (C), 128.1 (CH), 124.1 (C), 122.7 (CH), 107.8 (CH), 79.1 (C), 55.7 (CH<sub>2</sub>), 53.9 (CH<sub>2</sub>), 51.6 (CH<sub>2</sub>), 49.8 (CH), 43.5 (CH<sub>2</sub>), 35.1 (CH<sub>2</sub>), 35.0 (CH), 33.4 (CH<sub>2</sub>), 31.9 (CH<sub>2</sub>), 30.3 (CH<sub>2</sub>), 28.4 (CH<sub>3</sub>), 19.7 (CH<sub>2</sub>), 11.9 (CH<sub>3</sub>). LCMS (*m/z*): [M+H]<sup>+</sup> 444.3.

***tert*-Butyl ((*trans*)-4-(2-((4-ethynylcyclohex-3-en-1-yl)(propyl)amino)ethyl)cyclohexyl)carbamate (45).**

Using 4-ethynyl-*N*-propylcyclohex-3-en-1-amine as the amine and *tert*-butyl ((*trans*)-4-(2-oxoethyl)cyclohexyl)carbamate as the aldehyde, general procedure A was followed. Flash chromatography afforded the product as a yellow oil (289 mg, 73%). <sup>1</sup>H NMR (401 MHz, CDCl<sub>3</sub>) δ 6.15 (s, 1H), 4.35 (s, 1H), 3.35 (s, 1H), 2.80 (s, 1H), 2.52 – 2.33 (m, 3H), 2.32 – 1.95 (m, 6H), 1.90 – 1.51 (m, 6H), 1.44 (s, 9H), 1.28 (m, 4H), 1.13 – 0.92 (m, 5H), 0.86 (t, *J* = 7.3 Hz, 3H). <sup>13</sup>C NMR (CDCl<sub>3</sub>) δ 119.8 (C), 85.0 (C), 75.0 (CH), 61.0 (CH), 55.7 (CH), 52.6 (CH<sub>2</sub>), 48.5 (CH<sub>2</sub>), 35.4 (CH), 33.6 (CH<sub>2</sub>), 32.1 (CH<sub>2</sub>), 32.0 (CH<sub>2</sub>), 30.3 (CH<sub>2</sub>), 28.5 (CH<sub>3</sub>), 25.2 (CH<sub>2</sub>), 22.1 (CH<sub>2</sub>),

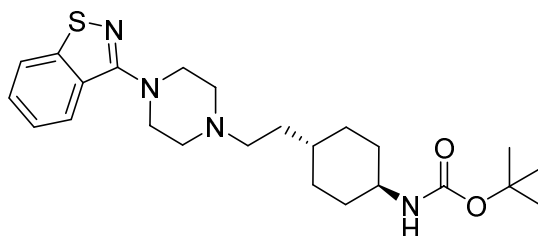
12.0 (CH<sub>3</sub>). NOTE: Two quaternary and one methylene signal could not be observed in the carbon spectrum due to signal broadening. LCMS (*m/z*): [M+H]<sup>+</sup> 389.3.

***tert*-Butyl ((*trans*)-4-(2-(((*S*)-2-amino-4,5,6,7-tetrahydrobenzo[*d*]thiazol-6-yl)(propyl)amino)ethyl)cyclohexyl)carbamate (46).**



Using (*S*)-*N*<sup>6</sup>-propyl-4,5,6,7-tetrahydrobenzo[*d*]thiazole-2,6-diamine as the amine and *tert*-butyl ((*trans*)-4-(2-oxoethyl)cyclohexyl)carbamate as the aldehyde, general procedure A was followed. The resultant product was purified via flash chromatography (1:19 MeOH: DCM) to yield a yellow foam (94.8 mg, 31%). <sup>1</sup>H NMR (CDCl<sub>3</sub>) δ 5.61 (br s, 2H), 4.45 (d, *J* = 7.9 Hz, 1H), 3.35 (br s, 1H), 3.08 – 2.97 (m, 1H), 2.75 – 2.32 (m, 7H), 1.99 (m, 4H), 1.82 – 1.54 (m, 3H), 1.50 – 1.41 (m, 10H), 1.30 (m, 4H), 1.15 – 0.92 (m, 4H), 0.87 (t, *J* = 7.3 Hz, 3H). <sup>13</sup>C NMR (CDCl<sub>3</sub>) δ 166.6 (C), 155.2 (C), 144.2 (C), 116.5 (C), 79.1 (C), 57.4 (CH), 52.5 (CH<sub>2</sub>), 49.9 (CH), 48.6 (CH<sub>2</sub>), 35.7 (CH<sub>2</sub>), 35.2 (CH), 33.4 (CH<sub>2</sub>), 32.0 (CH<sub>2</sub>), 28.4 (CH<sub>3</sub>), 26.2 (CH<sub>2</sub>), 25.6 (CH<sub>2</sub>), 24.8 (CH<sub>2</sub>), 22.0 (CH<sub>2</sub>), 11.8 (CH<sub>3</sub>). LCMS (*m/z*): [M+H]<sup>+</sup> 437.4.

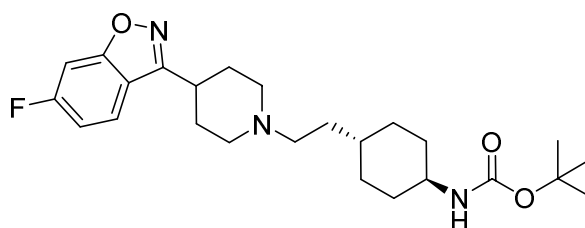
***tert*-Butyl ((*trans*)-4-(2-(4-(benzo[*d*]isothiazol-3-yl)piperazin-1-yl)ethyl)cyclohexyl)carbamate (47).**



Using 3-(piperazin-1-yl)benzo[*d*]isothiazole as the amine and *tert*-butyl ((*trans*)-4-(2-oxoethyl)cyclohexyl)carbamate as the aldehyde, general procedure A was followed. Upon purification the title compound was garnered as an oil (227 mg, 75%). <sup>1</sup>H NMR (CDCl<sub>3</sub>) δ 7.89 (d, *J* = 8.2 Hz, 1H), 7.78 (d, *J* = 8.1 Hz, 1H), 7.55 – 7.42 (m, 1H), 7.33 (ddd, *J* = 8.0, 7.0, 0.9 Hz,

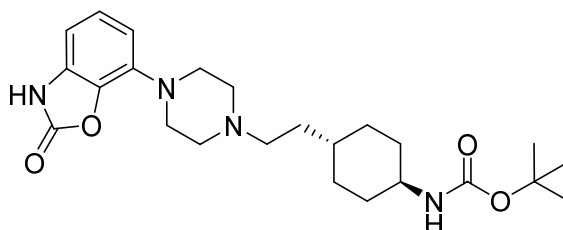
1H), 4.54 (br s, 1H), 3.59 – 3.48 (m, 4H), 3.37 (br s, 1H), 2.73 – 2.56 (m, 4H), 2.43 (m, 2H), 2.07 – 1.91 (m, 2H), 1.82 – 1.66 (m, 2H), 1.43 (m, 10H), 1.30 – 1.13 (m, 1H), 1.13 – 0.89 (m, 5H). <sup>13</sup>C NMR (CDCl<sub>3</sub>) δ 163.9 (C), 155.3 (C), 152.7 (C), 128.0 (C), 127.5 (CH), 123.9 (CH), 120.6 (CH), 79.0 (C), 56.6 (CH<sub>2</sub>), 53.0 (CH<sub>2</sub>), 50.0 (CH<sub>2</sub>), 49.9 (CH), 39.7 (CH<sub>2</sub>), 35.4 (CH), 33.7 (CH<sub>2</sub>), 33.4 (CH<sub>2</sub>), 32.0 (CH<sub>2</sub>), 31.9 (CH<sub>2</sub>), 28.5 (CH<sub>3</sub>). LCMS (*m/z*): [M+H]<sup>+</sup> 445.2.

***tert*-Butyl ((*trans*)-4-(2-(4-(6-fluorobenzo[*d*]isoxazol-3-yl)piperidin-1-yl)ethyl)cyclohexyl)carbamate (48).**



Using 6-fluoro-3-(piperidin-4-yl)benzo[*d*]isoxazole as the amine and *tert*-butyl ((*trans*)-4-(2-oxoethyl)cyclohexyl)carbamate as the aldehyde, general procedure A was followed. Flash chromatography afforded the product as an oil (198 mg, 66%). <sup>1</sup>H NMR (CDCl<sub>3</sub>) δ 7.71 (dd, *J* = 8.7, 5.1 Hz, 1H), 7.23 (dd, *J* = 8.5, 1.9 Hz, 1H), 7.05 (td, *J* = 8.9, 2.1 Hz, 1H), 4.46 (d, *J* = 6.0 Hz, 1H), 3.38 (s, 1H), 3.18 – 2.96 (m, 3H), 2.47 – 2.37 (m, 2H), 2.20 – 2.04 (m, 6H), 2.03 – 1.72 (m, 5H), 1.44 (s, 9H), 1.33 – 1.17 (m, 1H), 1.15 – 0.96 (m, 5H). <sup>13</sup>C NMR (CDCl<sub>3</sub>) δ 164.1 (d, <sup>1</sup>*J*<sub>CF</sub> = 250.6 Hz, C), 163.9 (d, <sup>3</sup>*J*<sub>CF</sub> = 13.6 Hz, C), 161.2 (C), 155.3 (C), 122.7 (d, <sup>3</sup>*J*<sub>CF</sub> = 11.1 Hz, CH), 117.3 (C), 112.4 (d, <sup>2</sup>*J*<sub>CF</sub> = 25.3 Hz, CH), 97.5 (d, <sup>2</sup>*J*<sub>CF</sub> = 26.7 Hz, CH), 79.1 (C), 57.0 (CH<sub>2</sub>), 53.8 (CH<sub>2</sub>), 49.9 (CH), 35.6 (CH), 34.7 (CH), 34.0 (CH<sub>2</sub>), 33.5 (CH<sub>2</sub>), 32.0 (CH<sub>2</sub>), 30.5 (CH<sub>2</sub>), 28.5 (CH<sub>3</sub>). LCMS (*m/z*): [M+H]<sup>+</sup> 446.2.

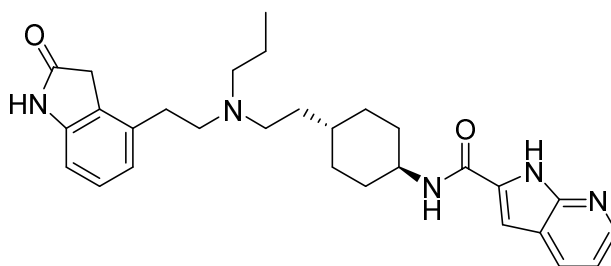
***tert*-Butyl ((*trans*)-4-(2-(4-(2-oxo-2,3-dihydrobenzo[*d*]oxazol-7-yl)piperazin-1-yl)ethyl)cyclohexyl)carbamate (49).**



Using 7-(piperazin-1-yl)benzo[*d*]oxazol-2(3*H*)-one as the amine and *tert*-butyl ((*trans*)-4-(2-oxoethyl)cyclohexyl)carbamate as the aldehyde, general procedure A was followed. The resultant

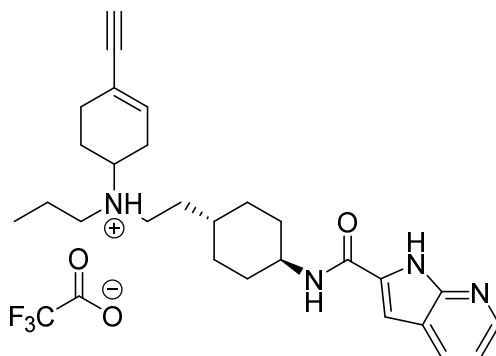
product was purified via flash chromatography (3:97 MeOH: DCM) to yield a colourless oil (117 mg, 38%). <sup>1</sup>H NMR (401 MHz, CDCl<sub>3</sub>) δ 7.03 (t, *J* = 8.1 Hz, 1H), 6.69 – 6.48 (m, 2H), 4.53 (d, *J* = 8.1 Hz, 1H), 3.46 – 3.17 (m, 5H), 2.64 (s, 4H), 2.50 – 2.35 (m, 2H), 1.99 (d, *J* = 8.6 Hz, 2H), 1.87 – 1.71 (m, 2H), 1.56 – 1.34 (m, 12H), 1.33 – 1.15 (m, 1H), 1.20 – 0.94 (m, 4H). <sup>13</sup>C NMR (CDCl<sub>3</sub>) δ 155.3 (C), 135.8 (C), 134.1 (C), 130.7 (C), 124.5 (CH), 110.2 (CH), 102.5 (CH), 79.1 (C), 56.67 (CH<sub>2</sub>), 53.1 (CH<sub>2</sub>), 49.7 (CH), 48.9 (CH<sub>2</sub>), 35.5 (CH), 33.5 (CH<sub>2</sub>), 33.3 (CH<sub>2</sub>), 31.9 (CH<sub>2</sub>), 28.4 (CH<sub>3</sub>). LCMS (*m/z*): [M+H]<sup>+</sup> 445.3.

***N*-((*trans*)-4-(2-((2-(2-Oxoindolin-4-yl)ethyl)(propyl)amino)ethyl)cyclohexyl)-1*H*-pyrrolo[2,3-*b*]pyridine-2-carboxamide (50).**



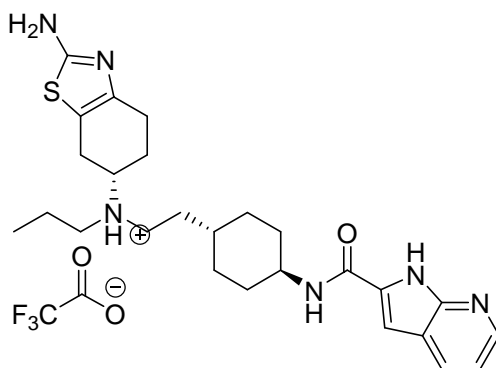
Using *tert*-butyl ((*trans*)-4-(2-((2-(2-oxoindolin-4-yl)ethyl)(propyl)amino)ethyl)cyclohexyl)carbamate as the protected amine, general procedure B was followed. Upon confirmation of *tert*-butyl carbamate deprotection via TLC, the amide coupling procedure was carried out. The resultant precipitate was purified using flash chromatography (1:4 MeOH: DCM) to yield the product as an off-white solid (18.7 mg, 34%). <sup>1</sup>H NMR (*d*<sub>6</sub>-DMSO) δ 12.04 (s, 1H), 10.34 (s, 1H), 8.32 (dd, *J* = 4.6, 1.5 Hz, 1H), 8.23 (d, *J* = 7.9 Hz, 1H), 8.05 (dd, *J* = 7.9, 1.4 Hz, 1H), 7.14 – 7.04 (m, 3H), 6.79 (d, *J* = 7.7 Hz, 1H), 6.65 (d, *J* = 7.6 Hz, 1H), 3.74 (m, 1H), 3.45 (d, *J* = 8.9 Hz, 1H), 2.62 (s, 4H), 2.43 (s, 3H), 1.88 (m, 2H), 1.75 (m, 2H), 1.50 – 1.15 (m, 8H), 1.01 (m, 2H), 0.85 (t, *J* = 7.3 Hz, 3H). <sup>13</sup>C NMR (*d*<sub>6</sub>-DMSO) δ 176.3 (C), 159.6 (C), 148.3 (C), 148.1 (C), 145.1 (CH), 143.5 (C), 132.4 (C), 129.9 (CH), 127.5 (CH), 124.5 (C), 121.9 (CH), 119.3 (C), 116.3 (CH), 106.9 (CH), 101.8 (CH), 55.2 (CH<sub>2</sub>), 53.6 (CH<sub>2</sub>), 50.9 (CH<sub>2</sub>), 48.4 (CH), 34.6 (CH<sub>2</sub>), 34.5 (CH), 32.3 (CH<sub>2</sub>), 32.2 (CH<sub>2</sub>), 31.7 (CH<sub>2</sub>), 11.8 (CH<sub>3</sub>). HPLC: *t*<sub>R</sub> 5.62 min, >95% purity. HRMS (*m/z*): [M+H]<sup>+</sup> calcd for C<sub>29</sub>H<sub>38</sub>N<sub>5</sub>O<sub>2</sub> requires 488.3020; found 488.3032.

***N*-((*trans*)-4-(1*H*-Pyrrolo[2,3-*b*]pyridine-2-carboxamido)cyclohexyl)ethyl)-4-ethynyl-*N*-propylcyclohex-3-en-1-aminium 2,2,2-trifluoroacetate (51).**



Using *tert*-butyl ((*trans*)-4-(2-((4-ethynylcyclohex-3-en-1-yl)(propyl)amino)ethyl)cyclohexyl)carbamate as the protected amine, general procedure B was followed. Upon confirmation of complete deprotection via LCMS, the amide coupling procedure was carried out. The resultant precipitate was purified using gradient flash chromatography (5–10% MeOH in DCM) followed by preparative HPLC to furnish the TFA salt as a yellow solid (7.70 mg, 2%). <sup>1</sup>H NMR (MeOD) δ 8.38 (d, *J* = 7.0 Hz, 1H), 7.40 (br s, 1H), 7.30 (s, 1H), 6.09 (d, *J* = 4.6 Hz, 1H), 3.89 (m, 1H), 3.61 (m, 1H), 3.34 – 3.31 (m, 1H), 3.29 – 3.03 (m, 5H), 2.61 – 2.33 (m, 4H), 2.21 – 2.01 (m, 3H), 1.96 – 1.58 (m, 7H), 1.46 (m, 3H), 1.25 (m, 2H), 1.04 (t, *J* = 7.4 Hz, 3H). HPLC: *t*<sub>R</sub> 5.07 min, >95% purity. HRMS (*m/z*): [M+H]<sup>+</sup> calcd for C<sub>27</sub>H<sub>37</sub>N<sub>4</sub>O requires 433.2962; found 433.2977.

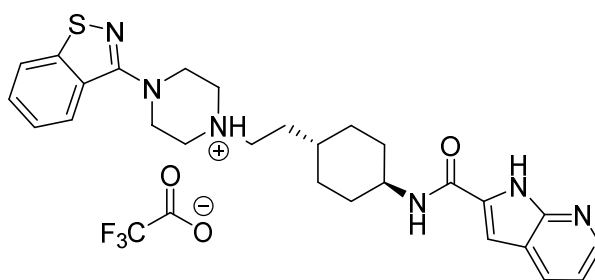
**2-((1*R*,4*S*)-4-(1*H*-Pyrrolo[2,3-*b*]pyridine-2-carboxamido)cyclohexyl)-1-((*S*)-((*S*)-2-amino-4,5,6,7-tetrahydrobenzo[*d*]thiazol-6-yl)(propyl)-1*H*-azaneyl)ethan-1-ylum 2,2,2-trifluoroacetate (52).**



Using *tert*-butyl ((*trans*)-4-(2-(((*S*)-2-amino-4,5,6,7-tetrahydrobenzo[*d*]thiazol-6-yl)(propyl)amino)ethyl)cyclohexyl)carbamate as the protected amine, general procedure B was followed. Upon confirmation of complete deprotection via LCMS, the amide coupling procedure

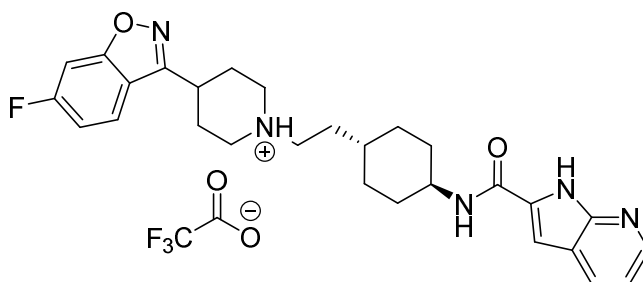
was carried out. The resultant precipitate was purified using preparative HPLC to yield the product salt as an off-white solid (32.3 mg, 31%). <sup>1</sup>H NMR (MeOD) δ 8.60 – 8.29 (m, 2H), 7.37 (s, 1H), 7.28 (s, 1H), 4.00 – 3.80 (m, 2H), 3.40 – 3.11 (m, 4H), 3.12 – 2.64 (m, 4H), 2.36 (d, *J* = 10.7 Hz, 1H), 2.19 – 2.00 (m, 3H), 2.00 – 1.59 (m, 6H), 1.58 – 1.35 (m, 3H), 1.33 – 1.14 (m, 2H), 1.05 (t, *J* = 7.3 Hz, 3H). <sup>13</sup>C NMR (101 MHz, DMSO) δ 168.5 (C), 159.6 (C), 148.2 (C), 145.0 (CH), 137.0 (C), 132.5 (C), 129.9 (CH), 119.3 (C), 116.4 (CH), 111.0 (C), 101.8 (CH), 58.5 (CH), 52.1 (CH<sub>2</sub>), 49.2 (CH<sub>2</sub>), 48.1 (CH), 34.5 (CH), 32.0 (CH<sub>2</sub>), 30.9 (CH<sub>2</sub>), 22.8 (CH<sub>2</sub>), 22.2 (CH<sub>2</sub>), 17.8 (CH<sub>2</sub>), 10.9 (CH<sub>3</sub>). HPLC: *t*<sub>R</sub> 3.89 min, >95% purity. HRMS (*m/z*): [M+H]<sup>+</sup> calcd for C<sub>26</sub>H<sub>37</sub>N<sub>6</sub>OS requires 481.2744; found 481.2758.

**1-(2-((*trans*)-4-(1*H*-Pyrrolo[2,3-*b*]pyridine-2-carboxamido)cyclohexyl)ethyl)-4-(benzo[*d*]isothiazol-3-yl)piperazin-1-ium 2,2,2-trifluoroacetate (53).**



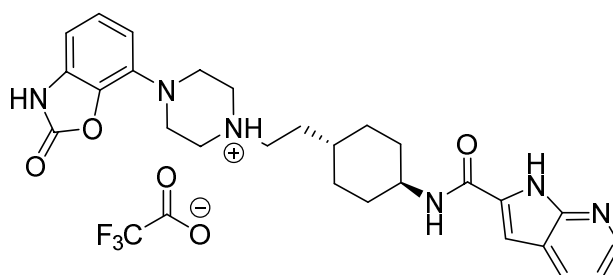
Using *tert*-butyl ((*trans*)-4-(2-(4-(benzo[*d*]isothiazol-3-yl)piperazin-1-yl)ethyl)cyclohexyl)carbamate as the protected amine, general procedure B was followed. Upon confirmation of complete deprotection via LCMS, the amide coupling procedure was carried out. The resultant precipitate was purified using preparative HPLC which yielded the product as an off-white solid (113 mg, 41%). <sup>1</sup>H NMR (*d*<sub>6</sub>-DMSO) δ 12.01 (s, 1H), 8.31 (dd, *J* = 4.5, 1.3 Hz, 1H), 8.23 (d, *J* = 7.9 Hz, 1H), 8.05 (d, *J* = 7.9 Hz, 3H), 7.56 (app t, *J* = 7.4 Hz, 1H), 7.44 (app t, *J* = 7.6 Hz, 1H), 7.10 (dd, *J* = 7.9, 4.6 Hz, 2H), 3.84 – 3.66 (m, 1H), 3.45 (s, 4H), 2.59 (s, 4H), 2.46 – 2.32 (m, 2H), 1.94 – 1.78 (m, 4H), 1.50 – 0.90 (m, 8H). <sup>13</sup>C NMR (*d*<sub>6</sub>-DMSO) δ 164.1 (C), 160.1 (C), 152.5 (C), 148.8 (C), 144.9 (CH), 133.0 (C), 130.3 (CH), 128.3 (CH), 127.8 (C), 124.9 (CH), 124.6 (CH), 121.6 (CH), 119.7 (C), 116.7 (CH), 102.2 (CH), 56.3 (CH<sub>2</sub>), 53.1 (CH<sub>2</sub>), 50.2 (CH<sub>2</sub>), 48.8 (CH), 35.3 (CH), 34.0 (CH<sub>2</sub>), 32.7 (CH<sub>2</sub>), 32.2 (CH<sub>2</sub>). HPLC: *t*<sub>R</sub> 5.27 min, >95% purity. HRMS (*m/z*): [M+H]<sup>+</sup> calcd for C<sub>27</sub>H<sub>33</sub>N<sub>6</sub>OS requires 489.2431; found 489.2424.

**1-(2-((*trans*)-4-(1*H*-Pyrrolo[2,3-*b*]pyridine-2-carboxamido)cyclohexyl)ethyl)-4-(6-fluorobenzo[*d*]isoxazol-3-yl)piperidin-1-ium 2,2,2-trifluoroacetate (54).**



Using *tert*-butyl ((*trans*)-4-(2-(4-(6-fluorobenzo[*d*]isoxazol-3-yl)piperidin-1-yl)ethyl)cyclohexyl)carbamate as the protected amine, general procedure B was followed. Upon confirmation of complete deprotection via LCMS, the amide coupling procedure was carried out. The resultant precipitate was purified using preparative HPLC to afford the product as an off-white solid (34.1 mg, 12%). <sup>1</sup>H NMR (*d*<sub>6</sub>-DMSO) δ 12.05 (s, 1H), 9.60 (s, 1H), 8.43 – 8.24 (m, 2H), 8.15 – 7.95 (m, 2H), 7.74 (d, *J* = 7.3 Hz, 1H), 7.36 (t, *J* = 8.1 Hz, 1H), 7.14 (s, 2H), 3.73 (m, 3H), 3.27 – 3.03 (m, 4H), 2.31 (m, 2H), 2.11 (m, 2H), 1.88 (m, 4H), 1.70 – 1.54 (m, 2H), 1.37 (m, 3H), 1.23 – 1.02 (m, 2H). <sup>13</sup>C NMR (*d*<sub>6</sub>-DMSO) δ 164.6 (d, <sup>1</sup>*J*<sub>CF</sub> = 177.6 Hz, C), 163.6 (C), 163.0 (C), 160.5 (C), 160.1 (C), 148.6 (C), 145.5 (CH), 133.0 (C), 130.5 (CH), 124.08 (d, <sup>3</sup>*J*<sub>CF</sub> = 11.0 Hz, CH), 117.3 (C), 116.4 (CH), 113.3 (d, <sup>2</sup>*J*<sub>CF</sub> = 25.4 Hz, CH), 102.4 (CH), 98.0 (d, <sup>2</sup>*J*<sub>CF</sub> = 27.5 Hz, CH), 54.9 (CH<sub>2</sub>), 51.9 (CH<sub>2</sub>), 48.6 (CH), 34.8 (CH), 32.4 (CH<sub>2</sub>), 31.6 (CH<sub>2</sub>), 31.5 (CH), 30.6 (CH<sub>2</sub>), 27.7 (CH<sub>2</sub>). HPLC: *t*<sub>R</sub> 5.18 min, >95% purity. HRMS (*m/z*): [M+H]<sup>+</sup> calcd for C<sub>28</sub>H<sub>33</sub>FN<sub>5</sub>O<sub>2</sub> requires 490.2613; found 490.2610.

**1-(2-((1*r*,4*r*)-4-(1*H*-pyrrolo[2,3-*b*]pyridine-2-carboxamido)cyclohexyl)ethyl)-4-(2-oxo-2,3-dihydrobenzo[*d*]oxazol-7-yl)piperazin-1-ium 2,2,2-trifluoroacetate (55)**



Using *tert*-butyl ((*trans*)-4-(2-(4-(2-oxo-2,3-dihydrobenzo[*d*]oxazol-7-yl)piperazin-1-yl)ethyl)cyclohexyl)carbamate as the protected amine, general procedure B was followed. Upon confirmation of complete deprotection via LCMS, the amide coupling procedure was carried out. The resultant precipitate was purified using preparative HPLC which yielded the product as an

off-white solid (5.47 mg, 4%). <sup>1</sup>H NMR (MeOD) δ 8.34 (br s, 1H), 8.13 (d, *J* = 7.9 Hz, 1H), 7.14 (m, 3H), 6.83 – 6.64 (m, 2H), 4.04 – 3.83 (m, 3H), 3.81 – 3.55 (m, 3H), 3.30 – 3.06 (m, 4H), 2.07 (m, 2H), 1.92 (m, 2H), 1.79 – 1.66 (m, 2H), 1.46 (m, 3H), 1.32 – 1.09 (m, 3H). <sup>13</sup>C NMR (101 MHz, MeOD) δ 162.5 (C), 156.5 (C), 148.2 (C), 135.0 (C), 133.5 (C), 132.7 (C), 132.5 (CH), 132.3 (CH), 125.96 (CH), 112.7 (C), 111.9 (CH), 110.9 (C), 105.2 (CH), 103.6 (CH), 56.6 (CH<sub>2</sub>), 53.1 (CH<sub>2</sub>), 50.3 (CH), 47.9 (CH<sub>2</sub>), 36.0 (CH), 33.2 (CH<sub>2</sub>), 32.7 (CH<sub>2</sub>), 31.8 (CH<sub>2</sub>). NOTE: One methine signal could not be observed in the carbon spectrum due to signal broadening. HPLC: *t<sub>R</sub>* 4.31 min, >95% purity. HRMS (*m/z*): [M+H]<sup>+</sup> calcd for C<sub>27</sub>H<sub>33</sub>N<sub>6</sub>O<sub>3</sub> requires 489.2609; found 489.2606.

## Pharmacology

**Cell Lines and Transfection.** FlpIn CHO cells stably expressing the wild-type D<sub>2L</sub>R were transfected and maintained in the conditions stated by Szabo *et al.*<sup>13</sup>

For FlpIn CHO cells stably expressing both the wild-type D<sub>2L</sub>R and the YFP-Epac-RLuc biosensor (CAMYEL), FlpIn CHO cells were both transfected with pGO44 (Invitrogen Life Technology) and the D<sub>2L</sub>R gene cloned in pEF5/FRT/v-dest plasmid (Invitrogen Life Technology) and selected with 700 μg/ mL Hygromycin B Gold (Invivogen). The cells stably expressing the D<sub>2L</sub>R were then transfected with the CAMYEL construct<sup>35</sup> and selected as a monoclonal cell line using both Hygromycin B Gold and G418 (Gibco Life Technology) at a concentration of 700 μg/ mL.

FlpIn CHO cells stably expressing the wild-type or mutant SNAP-D<sub>2S</sub>R were grown in DMEM supplemented with 10% foetal bovine serum and maintained at 37 °C in a humidified incubator containing 5% CO<sub>2</sub>. The FlpIn CHO cells were transfected with the pOG44 vector encoding Flp recombinase and the pDEST vecotor encoding the wild-type or mutant SNAP-D<sub>2S</sub>R at a ratio of 9:1 using polyethylenimine as the transfection agent.<sup>36</sup> 24 hours post-transfection, the cells were subcultured in media that was supplemented with 700 μg/mL hygromycin B as a selection agent to obtain cells stably expressing the SNAP-D<sub>2S</sub>R.

**Membrane Preparation.** FlpIn CHO cells stably expressing the wild-type D<sub>2L</sub>R, wild-type SNAP-D<sub>2S</sub>R or mutant SNAP-D<sub>2S</sub>R were grown to confluency using 500 cm<sup>2</sup> cell culture plates. The cells were harvested in PBS containing 2 mM EDTA and centrifuged at 300g for 3 min at 4 °C. The resulting pellet was resuspended in ice cold assay buffer (20 mM HEPES, 100 mM

NaCl, 6 mM MgCl<sub>2</sub>, 1 mM EGTA and 1 mM EDTA, pH 7.4) and the centrifugation was repeated. The intact cell pellet was then resuspended in assay buffer and homogenised using a Polytron homogeniser. After centrifugation (300g, 5 min, 4 °C), the supernatant was centrifuged at 30,000g for 1 h at 4 °C using a Sorval Evolution RC ultracentrifuge (Thermo Scientific). The resulting pellet was resuspended in the assay buffer and stored in 250 µL aliquots at -80 °C. Membrane protein concentration was determined using the Bradford method.

**[<sup>3</sup>H]Spiperone and [<sup>3</sup>H]Raclopride Competitive Binding Assays.** All radioligand binding experiments were conducted in a 1 mL reaction volume in assay buffer (20 mM HEPES, 100 mM NaCl, 6 mM MgCl<sub>2</sub>, 1 mM EGTA and 1 mM EDTA, pH 7.4). In all cases non-specific binding was determined in the presence of 1 µM haloperidol. To obtain affinity estimates of unlabelled agonists, partial agonists and antagonists, competition binding experiments were performed at equilibrium to measure the ability of increasing concentrations of the test ligands to compete 0.1 nM [<sup>3</sup>H]spiperone or 1 nM [<sup>3</sup>H]raclopride for binding at either the D<sub>2L</sub>R (wild-type), or the SNAP-D<sub>2S</sub>R (wild-type or mutant). The membranes (5 µg, unless otherwise stated) were incubated with the drugs for 3 h at 37 °C ([<sup>3</sup>H]spiperone) or 25 °C ([<sup>3</sup>H]raclopride). Following incubation, bound and free radioligand were separated by fast-flow filtration through GF/B filters using a Brandel harvester followed by three washes with ice cold NaCl (0.9% (m/v)). Filter-bound radioactivity was measured by scintillation spectrometry after the addition of 3.5 mL of Ultima Gold (PerkinElmer) using a Tri-Carb 2900TR liquid scintillation counter (PerkinElmer).

**[<sup>3</sup>H]Spiperone Binding Dissociation Assays.** All binding dissociation experiments were conducted in a 1 mL reaction volume in assay buffer (20 mM HEPES, 100 mM NaCl, 6 mM MgCl<sub>2</sub>, 1 mM EGTA and 1 mM EDTA, pH 7.4). In all cases non-specific binding was determined in the presence of 0.5 µM haloperidol. D<sub>2L</sub>R (wild-type) membranes (5 µg, unless otherwise stated) were equilibrated with [<sup>3</sup>H]spiperone (0.1 nM) in assay buffer for 2.5 h at 37 °C. Upon equilibration, haloperidol (0.5 µM final concentration) or haloperidol and the test ligand (0.5 and 5 µM final concentrations, respectively) were added to the corresponding test tubes at the appropriate time points and thoroughly mixed whilst being maintained at 37 °C. To quench the experiment, bound and free radioligand were separated by fast-flow filtration and filter-bound radioactivity was measured using the same procedure as outlined for competitive binding assays.

**Bioluminescence Resonance Energy Transfer (BRET) cAMP assay.** Flp-In-CHO cells stably expressing wild-type D<sub>2L</sub>R and the CAMYEL biosensor were plated at a density of 50,000 cells per well into 96-well CulturPlates (PerkinElmer) and grown overnight. Alternately, for experiments utilising the wild-type or mutant SNAP-D<sub>2S</sub>R, cells were seeded at a density of 1,000,000 cells per 10 cm dish and were transfected the following day with 4 µg CAMYEL to allow the detection of cAMP levels within the cells. 24 h post-transfection, the cells were plated into 96-well CulturPlates and grown overnight. The cells were equilibrated in Hank's balanced salt solution (HBSS) at 37 °C before commencing the experiment. The cells were co-stimulated with the ligands and 10 µM (final concentration) forskolin for the indicated times prior to BRET measurement. Coelenterazine (Promega) was added at a final concentration of 5 µM at least 5 min prior to measurement. The signals were detected at 445–505 and 505–565 nm using a LUMIstar Omega instrument (BMG LabTech, Offenburg, Germany).

Phenoxybenzamine-treated experiments were carried out in Flp-In-CHO cells stably expressing the wild-type or mutant SNAP-D<sub>2S</sub>R which The cells were then treated with 0.1, 0.3 or 1 µM of Phenoxybenzamine (Sigma Aldrich) and equilibrated at 37 °C for 30 min prior to the commencement of the assay.

**Data Analysis.** The results obtained were analysed using Prism 6.01 (GraphPad Software Inc., San Diego, CA). For the displacement of [<sup>3</sup>H]spiperone or [<sup>3</sup>H]raclopride data were fit to a one-site model with a variable Hill slope:

$$Y = \frac{(top-bottom)x^{n_H}}{x^{n_H} + IC_{50}^{n_H}} \quad (1)$$

where Y denotes the percent specific binding; top and bottom denote the maximal and minimal asymptotes, respectively; x denotes the inhibitor potency (mid-point location) parameter; n<sub>H</sub> denotes the Hill slope factor. With the assumption of simple competition, IC<sub>50</sub> values were converted to K<sub>i</sub> values via the Cheng-Prusoff equation.<sup>37</sup> [<sup>3</sup>H]spiperone binding dissociation data were fit to a one phase exponential decay model:

$$Y = (Y(0) - NS)e^{-KX} + NS \quad (2)$$

where  $Y$  denotes the percent specific binding;  $Y(0)$  denotes percent binding at time zero;  $NS$  denotes percent non-specific binding at infinite times;  $-K$  is the inverse rate constant in minutes;  $X$  denotes time in minutes. In the functional cAMP assay, agonist concentration-response curves were fitted to the following three parameter equation by use of Prism 6:

$$response = bottom + \frac{top - bottom}{1 + 10^{(\log EC_{50} - \log[A])}} \quad (3)$$

where top and bottom represent the maximal and minimal asymptote of the dose-response curve;  $[A]$  is the molar concentration of the agonist;  $EC_{50}$  is the molar concentration of agonist required to give a response midway between the bottom and top. Dose-response data were also fitted to the following form of the operational model of agonism<sup>38</sup>:

$$Y = basal + \frac{E_m - basal}{1 + \left(\frac{K_A + [A]}{\tau \times [A]}\right)^n} \quad (4)$$

where  $E_m$  is the maximal response of the system;  $K_A$  denotes the functional equilibrium dissociation constant of the agonist  $[A]$ ;  $\tau$  is an index of the coupling efficiency (efficacy) of the agonist and is defined as  $R_T/K_E$  (where  $R_T$  is the total concentration of receptors and  $K_E$  is the concentration of agonist-receptor complex that yield half the  $E_m$ ; and  $n$  is the slope of the transducer function that links occupancy to response. For partial agonists, the  $K_A$  value was estimated directly from the functional data via (4). The determination of  $K_A$  values for compounds determined through receptor depletion by phenoxybenzamine alkylation were determined as follows; given the proportional relationship of  $R_T$  to measured  $\tau$ ,  $K_A$  is invariant with receptor depletion. Thus, unique estimates of  $K_A$  could be obtained by direct operational model fitting of the family of concentration-response curves for each agonist.<sup>39, 40</sup>

## 2.4 References

1. Strange, P. G. Antipsychotic drug action: antagonism, inverse agonism or partial agonism. *Trends Pharmacol. Sci.* **2008**, 29, 314-321.
2. Strange, P. G. Inverse agonism of the antipsychotic drugs at the D<sub>2</sub> dopamine receptor. *Int. Congr. Ser.* **2003**, 1249, 153-162.
3. Zhang, B.; Albaker, A.; Plouffe, B.; Lefebvre, C.; Tiberi, M. Chapter Seven - Constitutive Activities and Inverse Agonism in Dopamine Receptors. In *Advances in Pharmacology*, Ya-Xiong, T., Ed. Academic Press: 2014; Vol. Volume 70, pp 175-214.
4. Kehne, J. H.; Andree, T. H.; Heinrich, J. N. D<sub>2</sub> receptor partial agonists: treatment of CNS disorders of dopamine function. *Curr. Top. Med. Chem.* **2008**, 8, 1068-1088.
5. Tamminga, C. A. Partial dopamine agonists in the treatment of psychosis. *J. Neural Transm.* **2002**, 109, 411-420.
6. Stahl, S. M. Mechanism of action of cariprazine. *CNS Spectr.* **2016**, 21, 123-127.
7. Garnock-Jones, K. P. Brexpiprazole: A Review in Schizophrenia. *CNS drugs* **2016**, 30, 335-342.
8. Shi, L.; Javitch, J. A. The binding site of aminergic G protein-coupled receptors: the transmembrane segments and second extracellular loop. *Annu. Rev. Pharmacol. Toxicol.* **2002**, 42, 437-467.
9. Chien, E. Y.; Liu, W.; Zhao, Q.; Katritch, V.; Han, G. W.; Hanson, M. A.; Shi, L.; Newman, A. H.; Javitch, J. A.; Cherezov, V.; Stevens, R. C. Structure of the human dopamine D<sub>3</sub> receptor in complex with a D<sub>2</sub>/D<sub>3</sub> selective antagonist. *Science* **2010**, 330, 1091-1095.
10. Weichert, D.; Kruse, A. C.; Manglik, A.; Hiller, C.; Zhang, C.; Hübner, H.; Kobilka, B. K.; Gmeiner, P. Covalent agonists for studying G protein-coupled receptor activation. *PNAS* **2014**, 111, 10744-10748.
11. Newman, A. H. B., T.; Banala, A. K.; Donthamsetti, P.; Pongetti, K.; LaBounty, A.; Levy, B.; Cao, J.; Michino, M.; Luedtke, R. R.; Javitch, J. A.; Shi, L. Molecular Determinants of Selectivity and Efficacy at the Dopamine D<sub>3</sub> Receptor. *J. Med. Chem.* **2012**, 55, 6689-6699.
12. Shonberg, J.; Herenbrink, C. K.; Lopez, L.; Christopoulos, A.; Scammells, P. J.; Capuano, B.; Lane, J. R. A structure-activity analysis of biased agonism at the dopamine D<sub>2</sub> receptor. *J. Med. Chem.* **2013**, 56, 9199-9221.

13. Szabo, M.; Klein Herenbrink, C.; Christopoulos, A.; Lane, J. R.; Capuano, B. Structure–Activity Relationships of Privileged Structures Lead to the Discovery of Novel Biased Ligands at the Dopamine D<sub>2</sub> Receptor. *J. Med. Chem.* **2014**, *57*, 4924-4939.
14. Allen, J. A. Y., J. M.; Setola, V.; Chen, X.; Sassano, M. F.; Chen, M.; Peterson, S.; Yadav, P. N.; Huang, X.; Feng, B.; Jensen, N. H.; Che, X.; Bai, X.; Frye, S. V.; Wetsel, W. C.; Caron, M. G.; Javitch, J. A.; Roth, B. L.; Jin, J. Discovery of  $\beta$ -Arrestin–Biased Dopamine D<sub>2</sub> Ligands for Probing Signal Transduction Pathways Essential for Antipsychotic Efficacy. *PNAS* **2011**, *45*, 18488-18493.
15. Moller, D.; Kling, R. C.; Skultety, M.; Leuner, K.; Hubner, H.; Gmeiner, P. Functionally selective dopamine D(2), D(3) receptor partial agonists. *J. Med. Chem.* **2014**, *57*, 4861-75.
16. Weichert, D.; Banerjee, A.; Hiller, C.; Kling, R. C.; Hübner, H.; Gmeiner, P. Molecular Determinants of Biased Agonism at the Dopamine D<sub>2</sub> Receptor. *J. Med. Chem.* **2015**, *58*, 2703-2717.
17. Gallagher, G.; Lavanchy, P. G.; Wilson, J. W.; Hieble, J. P.; DeMarinis, R. M. 4-[2-(Di-*n*-propylamino)ethyl]-2(3*H*)-indolone: a prejunctional dopamine receptor agonist. *J. Med. Chem.* **1985**, *28*, 1533-1536.
18. Hübner, H.; Haubmann, C.; Utz, W.; Gmeiner, P. Conjugated Enynes as Nonaromatic Catechol Bioisosteres: Synthesis, Binding Experiments, and Computational Studies of Novel Dopamine Receptor Agonists Recognizing Preferentially the D<sub>3</sub> Subtype. *J. Med. Chem.* **2000**, *43*, 756-762.
19. Lane, J. R.; Donthamsetti, P.; Shonberg, J.; Draper-Joyce, C. J.; Dentry, S.; Michino, M.; Shi, L.; Lopez, L.; Scammells, P. J.; Capuano, B.; Sexton, P. M.; Javitch, J. A.; Christopoulos, A. A new mechanism of allostery in a G protein-coupled receptor dimer. *Nat. Chem. Biol.* **2014**, *10*, 745-752.
20. Jörg, M.; Kaczor, A. A.; Mak, F. S.; Lee, K. C. K.; Poso, A.; Miller, N. D.; Scammells, P. J.; Capuano, B. Investigation of novel ropinirole analogues: synthesis, pharmacological evaluation and computational analysis of dopamine D<sub>2</sub> receptor functionalized congeners and homobivalent ligands. *MedChemComm.* **2014**, *5*, 891.
21. Hiller, C.; Kling, R. C.; Heinemann, F. W.; Meyer, K.; Hübner, H.; Gmeiner, P. Functionally Selective Dopamine D<sub>2</sub>/D<sub>3</sub> Receptor Agonists Comprising an Enyne Moiety. *J. Med. Chem.* **2013**, *56*, 5130-5141.
22. Shonberg, J.; Lopez, L.; Scammells, P. J.; Christopoulos, A.; Capuano, B.; Lane, J. R. Biased Agonism at G Protein-Coupled Receptors: The Promise and the Challenges-A Medicinal Chemistry Perspective. *Med. Res. Rev.* **2014**.

23. Sibley, D. R.; Creese, I. Regulation of ligand binding to pituitary D-2 dopaminergic receptors. Effects of divalent cations and functional group modification. *J. Biol. Chem.* **1983**, 258, 4957-4965.
24. Valant, C.; Gregory, K. J.; Hall, N. E.; Scammells, P. J.; Lew, M. J.; Sexton, P. M.; Christopoulos, A. A novel mechanism of G protein-coupled receptor functional selectivity. Muscarinic partial agonist McN-A-343 as a bitopic orthosteric/allosteric ligand. *J. Biol. Chem.* **2008**, 283, 29312-29321.
25. Keov, P.; Valant, C.; Devine, S. M.; Lane, J. R.; Scammells, P. J.; Sexton, P. M.; Christopoulos, A. Reverse Engineering of the Selective Agonist TBPB Unveils Both Orthosteric and Allosteric Modes of Action at the M<sub>1</sub> Muscarinic Acetylcholine Receptor. *Mol. Pharmacol.* **2013**, 84, 425-437.
26. Christopoulos, A.; Changeux, J.-P.; Catterall, W. A.; Fabbro, D.; Burris, T. P.; Cidlowski, J. A.; Olsen, R. W.; Peters, J. A.; Neubig, R. R.; Pin, J.-P.; Sexton, P. M.; Kenakin, T. P.; Ehlert, F. J.; Spedding, M.; Langmead, C. J. International Union of Basic and Clinical Pharmacology. XC. Multisite Pharmacology: Recommendations for the Nomenclature of Receptor Allosterism and Allosteric Ligands. *Pharmacol. Rev.* **2014**, 66, 918-947.
27. Ballesteros, J. A.; Weinstein, H. [19] Integrated methods for the construction of three-dimensional models and computational probing of structure-function relations in G protein-coupled receptors. In *Methods in Neurosciences*, Stuart, C. S., Ed. Academic Press: 1995; Vol. 25, pp 366-428.
28. Klein Herenbrink, C. Understanding biased agonism at the dopamine D<sub>2</sub> receptor. Monash University, 2016.
29. Silvano, E.; Millan, M. J.; Mannoury la Cour, C.; Han, Y.; Duan, L.; Griffin, S. A.; Luedtke, R. R.; Aloisi, G.; Rossi, M.; Zazzeroni, F.; Javitch, J. A.; Maggio, R. The tetrahydroisoquinoline derivative SB269,652 is an allosteric antagonist at dopamine D<sub>3</sub> and D<sub>2</sub> receptors. *Mol. Pharmacol.* **2010**, 78, 925-934.
30. Kopinathan, A.; Scammells, P. J.; Lane, J. R.; Capuano, B. Multivalent approaches and beyond: novel tools for the investigation of dopamine D<sub>2</sub> receptor pharmacology. *Future Med. Chem.* **2016**, 8, 1349-1372.
31. Shonberg, J.; Draper-Joyce, C.; Mistry, S. N.; Christopoulos, A.; Scammells, P. J.; Lane, J. R.; Capuano, B. Structure-Activity Study of *N*-((*trans*)-4-(2-(7-Cyano-3,4-dihydroisoquinolin-2(1*H*)-yl)ethyl)cyclohexyl)-1*H*-indole-2-carboxamide (SB269652), a Bitopic Ligand That Acts as a Negative Allosteric Modulator of the Dopamine D<sub>2</sub> Receptor. *J. Med. Chem.* **2015**, 58, 5287-5307.

32. Liu, D.; Dijkstra, D.; de Vries, J. B.; Wikström, H. V. A novel synthesis and pharmacological evaluation of a potential dopamine D<sub>1</sub>/D<sub>2</sub> agonist: 1-Propyl-1,2,3,4,4a,5,10,10a-octahydrobenzo[g]quinoline-6,7-diol. *Bioorg. Med. Chem.* **2008**, *16*, 3438-3444.
33. Felpin, F.-X.; Coste, J.; Zakri, C.; Fouquet, E. Preparation of 2-Quinolones by Sequential Heck Reduction–Cyclization (HRC) Reactions by Using a Multitask Palladium Catalyst. *Chem. Eur. J.* **2009**, *15*, 7238-7245.
34. Lan, Y.; Chen, Y.; Xu, X.; Qiu, Y.; Liu, S.; Liu, X.; Liu, B.-F.; Zhang, G. Synthesis and biological evaluation of a novel sigma-1 receptor antagonist based on 3,4-dihydro-2(1*H*)-quinolinone scaffold as a potential analgesic. *Eur. J. Med. Chem.* **2014**, *79*, 216-230.
35. Jiang, L. I.; Collins, J.; Davis, R.; Lin, K.-M.; DeCamp, D.; Roach, T.; Hsueh, R.; Rebres, R. A.; Ross, E. M.; Taussig, R.; Fraser, I.; Sternweis, P. C. Use of a cAMP BRET Sensor to Characterize a Novel Regulation of cAMP by the Sphingosine 1-Phosphate/G<sub>13</sub> Pathway. *J. Biol. Chem.* **2007**, *282*, 10576-10584.
36. Akinc, A.; Thomas, M.; Klibanov, A. M.; Langer, R. Exploring polyethylenimine-mediated DNA transfection and the proton sponge hypothesis. *J. Gene Med.* **2005**, *7*, 657-663.
37. Cheng, Y.; Prusoff, W. H. Relationship between the inhibition constant (K<sub>1</sub>) and the concentration of inhibitor which causes 50 per cent inhibition (I<sub>50</sub>) of an enzymatic reaction. *Biochem. Pharmacol.* **1973**, *22*, 3099-3108.
38. Black, J. W.; Leff, P. Operational Models of Pharmacological Agonism. *Proc. R. Soc. Lond., B, Biol. Sci.* **1983**, *220*, 141-162.
39. Keov, P.; López, L.; Devine, S. M.; Valant, C.; Lane, J. R.; Scammells, P. J.; Sexton, P. M.; Christopoulos, A. Molecular Mechanisms of Bitopic Ligand Engagement with the M<sub>1</sub> Muscarinic Acetylcholine Receptor. *J. Biol. Chem.* **2014**, *289*, 23817-23837.
40. Black, J. W.; Leff, P.; Shankley, N. P.; Wood, J. An operational model of pharmacological agonism: the effect of E/[A] curve shape on agonist dissociation constant estimation. *Br. J. Pharmacol.* **1985**, *84*, 561-571.

---

## **Chapter 3**

# **Probing Allostery at the Dopamine D<sub>2</sub> Receptor**

---

**An SAR Investigation of ‘Next Generation’ Analogues of the Drug-like  
Dopamine D<sub>2</sub> Receptor Negative Allosteric Modulator SB269652**

### 3.1 Introduction

The dopamine D<sub>2</sub> receptor (D<sub>2</sub>R) is a member of the class A G protein-coupled receptor (GPCR) family, and is considered a well-established therapeutic target for the treatment of disorders affecting the central nervous system (CNS) such as schizophrenia (SCZ).<sup>1</sup> To date, drug discovery at this target has primarily focussed on the development of orthosterically-binding ligands with a spectrum of efficacies (e.g. agonists, partial agonists, inverse agonists and antagonists) and are used routinely in clinical settings to treat ailments of the CNS. Although many of these orthosterically-binding D<sub>2</sub>R antipsychotics are effective at treating the positive symptoms of diseases such as SCZ, the therapeutic utility of these drugs is often marred by the significant side-effects with which they are also associated.<sup>2</sup> First generation antipsychotics (e.g. haloperidol and chlorpromazine) which tend to have high D<sub>2</sub>R occupancy often lead to extrapyramidal side-effects (EPS) despite providing efficacy for symptoms of psychoses. In contrast, second generation antipsychotics (exemplified by clozapine) lower the risk of EPS compared to their predecessors, but are known to cause side-effects such as agranulocytosis or hyperprolactinemia, respectively.<sup>3,4</sup>

More recently, research efforts have shifted towards the development of allosteric modulators which interact with a topographically distinct binding site of a receptor, proximal to that of the endogenous ligand. Allosteric modulators provide a number of advantages over their orthosteric counterparts. Aside from improved sub-type selectivity, allosteric modulators allow the endogenous neurotransmitter to bind the receptor and are able to modulate this response without disrupting the spatio-temporal profile of physiological signalling. In addition, allosteric modulators have a saturable effect determined by their cooperativity with the endogenous ligands, thus a negative allosteric modulator (NAM) may act to partially antagonise the D<sub>2</sub>R, relieving the positive symptoms of the disease without causing the complete blockade which is associated with EPS.<sup>2,5</sup>

Efforts towards the development of allosteric modulators for the D<sub>2</sub>R have been bolstered by the discovery of SB269652's (**1**) modulatory properties by Silvano *et al.*<sup>6</sup> Initially synthesised in an effort to develop selective orthosteric D<sub>3</sub>R ligands by SmithKline Beecham, re-assessment of its pharmacological profile by Silvano and colleagues demonstrated that **1** was unable to completely displace high concentrations of radioligand, or entirely block G protein activation in the presence of high concentrations of dopamine.<sup>6,7</sup> Ultimately this led Silvano *et al.* to the conclusion that **1** was a NAM of the D<sub>2</sub>R and D<sub>3</sub>R.<sup>2</sup> This atypical behaviour was subsequently reconciled within our own group where **1** was found to be a bitopic D<sub>2</sub>R ligand through a structure-activity relationship (SAR) study of fragments of **1**.<sup>8</sup> The SAR study determined that the 1,2,3,4-tetrahydroisoquinoline-7-carbonitrile motif (7CN-THIQ) of **1**, which contains a tertiary amine that

is positively charged at physiological pH, was essential for making an orthosteric interaction with the highly conserved aspartate residue (D114<sup>3,32</sup>, where superscript numbering denotes Ballesteros-Weinstein nomenclature).<sup>8,9</sup> The indole-2-carboxamide tail was found to extend into a secondary binding pocket between transmembrane helices (TMs) 2 and 7 of the D<sub>2</sub>R. Furthermore, a hydrogen-bond interaction with the side chain of the E95<sup>2,65</sup> was found to be important for the allosteric behaviour of **1**. Additionally, the competitive pharmacological profile of the *cis*-stereoisomer of **1** added further weight to the idea that **1** must engage both the orthosteric and an allosteric binding site in order to observe negative cooperativity.<sup>8</sup> Our group was then able to reconcile both the bitopic binding mode and pharmacological profile of **1** across a D<sub>2</sub>R dimer. Using functional complementation assays, we were able to demonstrate that **1** behaved as a NAM in a dimeric system where both protomers were wild-type D<sub>2</sub>Rs (i.e. **1** bound to the binding site of one protomer and modulated the functional affinity of dopamine, that had bound the adjacent protomer). However, in a heterodimeric system which consisted of a wild-type receptor and a D114A<sup>3,32</sup> mutant receptor (which could no longer facilitate key orthosteric binding interactions), **1** was observed to have competitive pharmacology.<sup>8</sup> Based on these results, further SAR investigations of **1** within our group were conducted to determine the structural determinants of allostery at the D<sub>2</sub>R. We investigated the modification of the 7CN-THIQ “head”, the cyclohexylene “spacer” or the indole-2-carboxamide “tail” and how this impacted upon negative cooperativity at the D<sub>2</sub>R (Figure 1).<sup>5</sup> The results of this study showed that head groups with small substituents at the 7-position were necessary to maintain the negative cooperativity of **1**, whilst replacement of the cyclohexylene spacer with polymethylene spacers of varying lengths were observed to cause linker length dependent changes to allosteric modulation. Alterations to the indole-2-carboxamide tail, however, proved more critical to the negative cooperativity of **1**. The replacement of the bicyclic indole with smaller aromatic and non-aromatic heterocyclic moieties (i.e. pyrrole, proline) led to the abrogation of weak negative cooperativity, whilst a series of N-methylated derivatives confirmed the importance of the indolic NH as a key hydrogen bond donor which is necessary for NAM activity. This also underlined the requirement of a hydrogen bond interaction between the indolic NH and the E95<sup>2,65</sup> residue of the D<sub>2</sub>R for the allosteric pharmacology of these compounds. Interestingly, substitution of the indole-carboxamide with a 7-azaindole-2-carboxamide (**2**) led to the highest affinity analogue of **1** to date. Whilst compound **1** demonstrated a functional affinity of 776 nM and a negative cooperativity ( $\alpha\beta$ ) of 0.06 which confers a maximal 17-fold decrease in dopamine potency, compound **2** ( $K_B = 23.4$  nM;  $\alpha\beta = 0.04$ ) was observed to have 30-fold greater affinity whilst maintaining similar capabilities in attenuating dopamine potency (25-fold).<sup>5</sup>

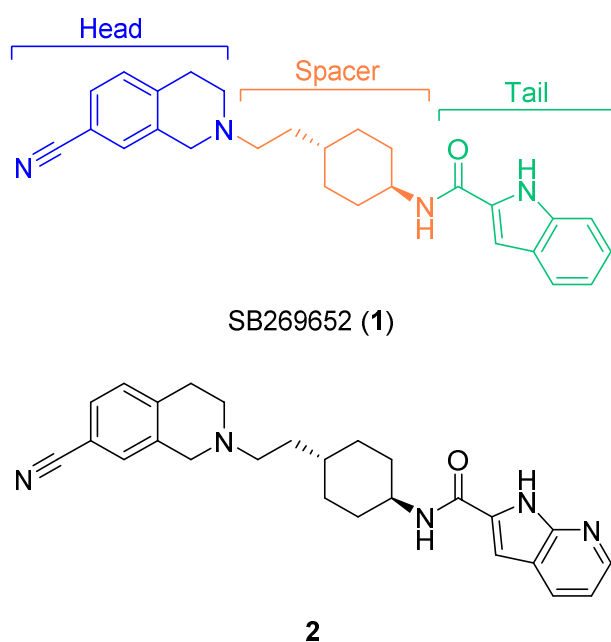


**Figure 1.** The chemical structure of SB269652 (**1**) highlighting its head, spacer and tail sections, and the structure chemical of the highest affinity analogue (**2**) that resulted from our initial SAR investigation.

Given that our initial SAR investigation determined the indole-2-carboxamide moiety to be an integral structural motif in maintaining the NAM properties of **1** and the magnitude of this allosteric effect, a further SAR study focussed primarily on the effects of modifications to the tail of SB269652 was conducted. In making modifications to this specific region of **1**, the aim was to develop a suite of analogues that displayed varying degrees of negative cooperativity in order to further our understanding of allosterism at the D<sub>2</sub>R.

### 3.2 Synthesis

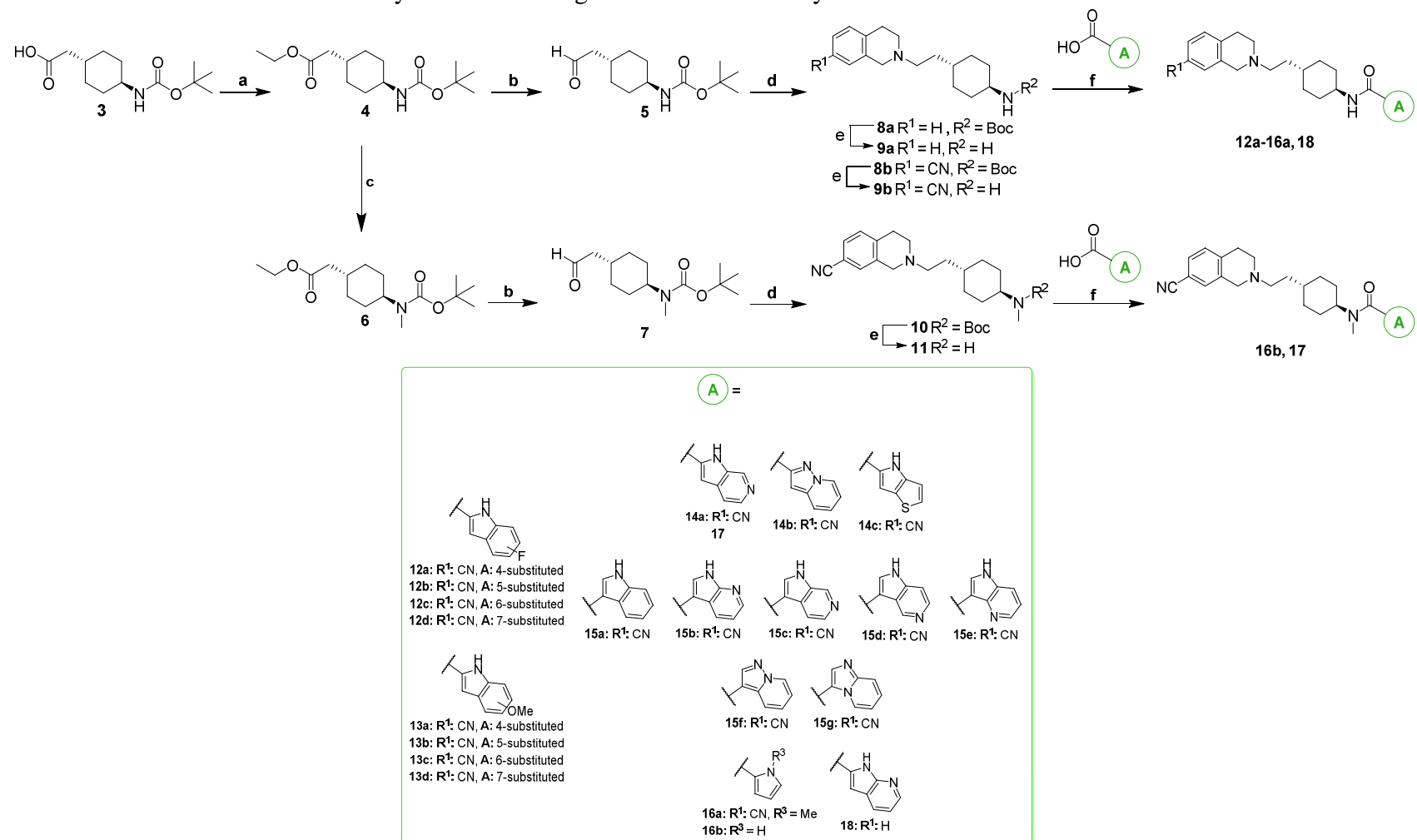
A library of analogues of **1** that primarily focussed on modifications to the indole-2-carboxamide tail was synthesised to build a library of compounds with varying degrees of negative cooperativities. The SAR study began with the synthesis of a series of compounds comprising the best “head”, “spacer” and “tail” moieties of our initial SAR investigation to determine whether a beneficial additive effect on affinity and allosteric pharmacology could be observed. The effects of electron-donating and electron-withdrawing substituents on negative cooperativity through attachment of either a methoxy or fluorine substituent, respectively, at positions 4-7 of the indole ring was also investigated. Then, to explore various azaindole-2-carboxamide tail moieties, a nitrogen walk around the benzo portion of the indole ring of **1** was conducted since **2** showed a 30-fold enhancement in affinity and maintained negative cooperativity at the D<sub>2</sub>R. A thienopyrrole

analogue was also synthesised as an isosteric replacement for the indole ring system of **1**. Finally, based on our initial SAR investigation, N-methylation of the carboxamide of **1** was observed to cause a 4-fold decrease in the attenuation of dopamine's affinity at the D<sub>2</sub>R.<sup>5</sup> As such, the effects of alkylation of the carboxamide and indolic NH moieties were evaluated as a means of tuning potent compounds identified with high negative cooperativity.

Scheme 1 depicts the synthetic route employed to derive the majority of analogues synthesised with varying “tail” moieties, and the synthesis of N-methylated amide derivatives. The synthesis of all compounds generally followed previously described established methods employed for the synthesis of **1** and associated analogues from our initial SAR investigations.<sup>5,8</sup> Following the procedure outlined in Lane *et al.*, compound **3** was quantitatively esterified to the ethyl ester (**4**) in the presence of ethyl iodide (EtI) and potassium carbonate (K<sub>2</sub>CO<sub>3</sub>), and reduced to the corresponding aldehyde (**5**) in the presence of 1 M diisobutylaluminium hydride (DIBAL-H) in anhydrous toluene at -78°C. Reductive amination in the presence of sodium triacetoxyborohydride in 1,2-dichloroethane (1,2-DCE) facilitated the attachment of the required “head” group moiety to furnish compounds **8a** and **8b** in 80% yield. Removal of the boc protecting group was carried out using an excess of trifluoroacetic acid (TFA) in DCM and garnered compounds **9a** and **9b** as the free base following an aqueous base extraction.<sup>8</sup> Three differing amide coupling reagents were used in order to attach the “tail” moieties since some carboxylic acids were unreactive in the presence of certain coupling reagents. 1-[Bis(dimethylamino)methylene]-1*H*-1,2,3-triazolo[4,5-*b*]pyridinium 3-oxid hexafluorophosphate (HATU) in the presence of DIPEA and dry DMF, however, facilitated the majority of amide couplings and yielded compounds **12a-16a**. To evaluate the effects of electron-donating and electron-withdrawing substituents on allosteric pharmacology we synthesised **12a-d** and **13a-d**. The fluorine-substituted analogues (**12a-d**) were synthesised via HATU-mediated coupling in yields of up to 57%, whilst the methoxy-substituted carboxylic acids were coupled using (benzotriazol-1-yloxy)tris(dimethylamino)phosphonium hexafluorophosphate (BOP) in dry DMF and in the presence of excess DIPEA to afford **13a-d** in yields of up to 74%. Given the improved affinity of **2** in our previous SAR investigation, a nitrogen walk comprising of the various azaindole-2-carboxylic acids, and the corresponding pyrazolo- and imidazo-pyridine-2-carboxylic acids was conducted. Upon attempting these couplings, however, we were only able to synthesise compounds **14a-c** successfully. The remaining 2-substituted carboxylic acids generally favoured self-dimerisation over coupling to the primary amine (**9a-b**) (See Appendix A.2.1), and in some cases, coupling was not favoured at all. Therefore, in order to avoid the issue of dimerisation and non-reactivity and to allow a more thorough investigation of the biological impact of isosteric

replacement of the CH for N, the nitrogen scan was conducted using the corresponding 3-carboxylic acid substituted derivatives of indole, azaindoles, pyrazolo-pyridine and imidazopyridine to garner **15a-g** in respectable yields. Compound **18** was synthesised using both *N*-(3-dimethylaminopropyl)-*N'*-ethylcarbodiimide hydrochloride (EDC) and 1*H*-benzo[*d*][1,2,3]triazol-1-ol (HOBt) with DIPEA in DCM to furnish the final product in 20% yield. A series of *N*-methylated amide derivatives were synthesised to investigate the ability of methylation, as a general mechanism, to attenuate the allosteric pharmacology of derivatives. Following an amended procedure which was initially described by Shonberg *et al.*, **4** underwent quantitative *N*-methylation of the amide functionality using an excess of sodium hydride (NaH), methyl iodide (MeI) in dry DMF under inert atmosphere to yield **6**.<sup>5</sup> Compound **6** was then exposed to the chemistry previously outlined for the un-substituted derivatives to obtain compounds **16b** and **17** via HATU-mediated coupling in respectable yields.

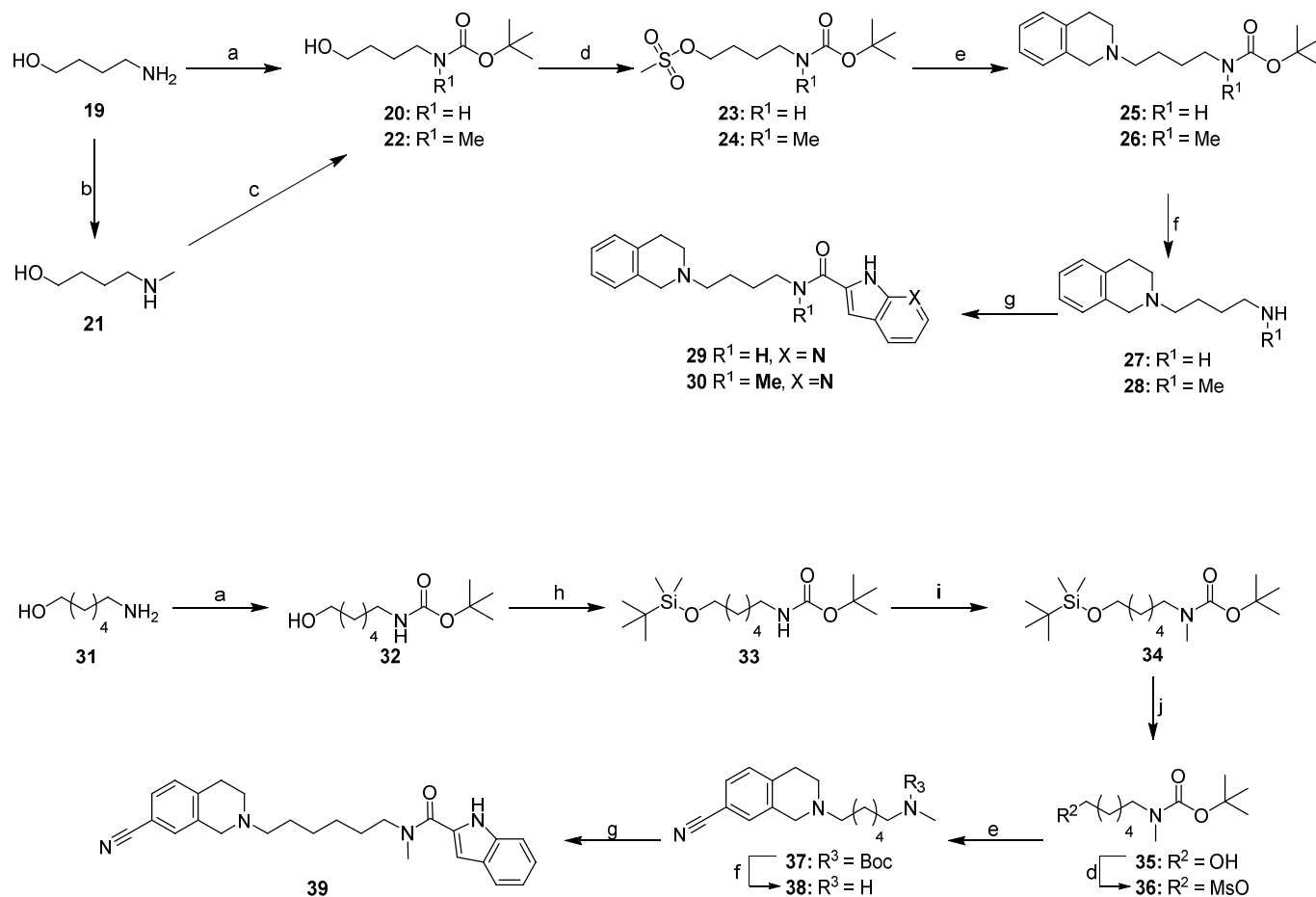
**Scheme 1.** Synthesis of analogues of **1** and N- methylated amide derivatives thereof.<sup>a</sup>



<sup>a</sup>Reagents and conditions: (a) EtI,  $\text{K}_2\text{CO}_3$ , MeCN, overnight 50 °C, quantitative; (b) 1M DIBALH in toluene, -78 °C, 1 h, quantitative; (c) MeI, NaH, dry DMF, 3 d, quantitative; (d) THIQ or 7CN-THIQ,  $\text{NaBH}(\text{OAc})_3$ , 1,2-DCE, rt, 16–24 h, 80%; (e) TFA, DCM, base extraction, 84%-quantitative; (f) EDC and HOBt or HATU or BOP, DCM or dry DMF, DIPEA, rt, 3-24 h, 5-74%. NOTE: Compounds **15c-16a** were isolated as the trifluoroacetate salts and compound **18** was isolated as the hydrochloride salt.

Scheme 2 describes the synthesis of derivatives of **1** comprising of polymethylene spacers and N-methylated amides thereof. To synthesise the derivatives comprising of a butylene spacer **19** was boc-protected to quantitatively yield the primary amine **20** following basic workup. Alternately, the N-alkylation of **19** occurred via formylation and lithium aluminium hydride (LiAlH<sub>4</sub>) reduction to yield **21** in 72% yield. **21** was then boc-protected to furnish **22** in respectable yields. The primary alcohol functionality of the either derivative was then activated using methanesulfonyl chloride (MsCl) to their corresponding mesylated derivatives (**23** and **24**). Given the instability of **23** and **24**, reaction progression was monitored with TLC, and upon complete conversion, were reacted on without further purification with 1,2,3,4-tetrahydroisoquinoline (THIQ) to yield compounds **25** and **26**. Boc de-protection was carried out using an excess of trifluoroacetic acid in DCM and produced compounds **27** and **28** as their respective free base forms upon basic aqueous extraction in quantitative yields. The final compounds (**29** and **30**) were generated using HATU-mediated coupling conditions. To generate the N-methylated hexylene derivative (**39**), **31** was quantitatively boc-protected using standard conditions to furnish **32**. Following a procedure outlined by Thuring *et al.*,<sup>10</sup> the primary alcohol of **32** was protected using *tert*-butyldimethylsilyl chloride (TBS-Cl) to yield **33** in 89% yield. N-methylation of **33** was conducted using sodium hydride and methyl iodide to obtain **34** in 72% yield. The TBDMS protecting group was removed using tetrabutylammonium fluoride (TBAF) to furnish **35**, and the primary alcohol was activated with Ms-Cl. Again, due to instability **36** was carried through without further purification and immediately reacted with 7CN-THIQ to afford **37** in respectable yields. Boc de-protection and HATU-mediated amide coupling were performed as previously stated for the propylene derivatives to produce compound **39** in 21% yield.

**Scheme 2.** Synthesis of polymethylene derivatives and their N-methylated amide variants.<sup>a</sup>



<sup>a</sup>Reagents and conditions: (a)  $Boc_2O$ , DIPEA, DCM, overnight, reflux, quantitative; (b)(i) Ethyl formate, EtOH, reflux, 16 h, quantitative, (ii) 1M  $LiAlH_4$  in THF, anhydrous THF, reflux 3 h, aqueous workup, 72%; (c)  $Boc_2O$ , DIPEA, DCM, rt, 2 d, 59%; (d)  $MsCl$ , DCM, 0 °C, 30 min, 0 °C - rt, overnight, quantitative; (e) THIQ or 7CN-THIQ,  $K_2CO_3$ , reflux or rt, overnight, 14-72%; (f) TFA, DCM, base extraction, quantitative; (g) indole-2-carboxylic acid or 7-azaindole-2-carboxylic acid, HATU, dry DMF, DIPEA, rt, 3-24 h, 9-21%; (h) Imidazole, DCM, 0 °C - rt, 30 min, TBS-Cl, 0 °C - rt, overnight, 89%; (i) NaH, MeI, 0 °C - rt, 22 h, 72%; (j) 1 M TBAF in THF, THF, 0 °C - rt, overnight, 77%. NOTE: Compounds **30** and **39** were isolated as the trifluoroacetate salts.

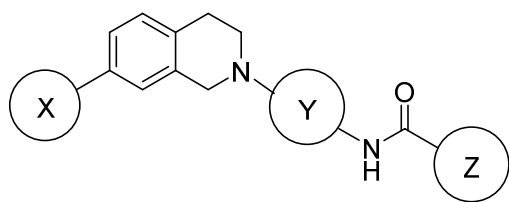
### 3.3 Pharmacological Evaluation

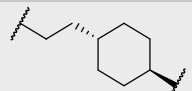
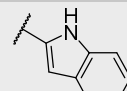
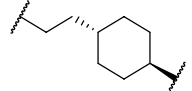
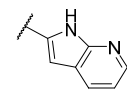
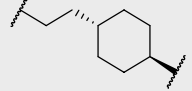
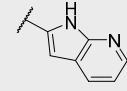
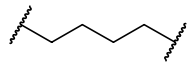
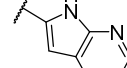
In order to determine the effect of the synthesised compounds upon the neurotransmitter dopamine, all compounds were tested in an assay measuring phosphorylation of extracellular signal-regulated kinases 1/2 (pERK1/2) through activation of the long isoform of the D<sub>2</sub>R (D<sub>2L</sub>R) expressed in FlpIn CHO cells. Compounds were assessed for their ability to antagonise the action of increasing concentrations of dopamine. An example of these data is presented in Figure 2. The data was fitted with a derivation of the operational model of allosterism to derive values of functional affinity ( $K_B$ ) and allosteric cooperativity with dopamine ( $\alpha\beta$ , where  $\alpha$  is negative cooperativity with dopamine binding (signified by a limited concentration-dependent rightward shift in curves), and  $\beta$  is the modulation of dopamine efficacy (signified by a concentration-dependent depression in  $E_{max}$ )).<sup>5,11</sup> The data were also fit to a Gaddum-Schild model of competitive antagonism to derive values of  $K_B$  and a Schild slope. In instances where a Schild slope was not significantly different from unity (i.e. Schild slope = 1), compounds were considered to demonstrate competitive antagonism. The data for each compound were analysed using both models and the best fit was determined by an *F*-test. These data (Tables 1, 2, 3, 4 and Figures 2 and 3) are presented as logarithms to allow for statistical comparison.<sup>12</sup> Values of  $\text{Log } \alpha\beta < 0$  signify negative cooperativity.

The first series of synthesised compounds combined the head, spacer and tail motifs which had a beneficial effect on functional affinity and maintained negative cooperativity from our initial SAR efforts.<sup>5</sup> From this previous work, replacing the head or spacer moieties of **1** with THIQ or butylene, respectively, enhanced functional affinity almost 10-fold whilst maintaining similar negative cooperativity to that of **1**. Similarly, replacement of the indole-2-carboxamide tail with a 7-azaindole-2-carboxamide enhanced functional affinity more than 30-fold and maintained similar negative cooperativity to that of the parent compound. It was anticipated that incorporation of these favourable modifications may have an additive effect on functional affinity as well as negative cooperativity (Table 1). Upon pharmacological evaluation of compounds **18** and **29**, however, we found that the sum of these favourable structural attributes were not additive. Compound **18** ( $K_B = 467$  nM,  $\alpha\beta = 0.14$ ) was observed to have no significant enhancement of functional affinity or negative cooperativity compared to **1** ( $K_B = 776$  nM,  $\alpha\beta = 0.06$ ). In contrast, compound **29** ( $K_B = 44.7$  nM) demonstrated competitive pharmacology upon evaluation in the pERK1/2 assay but was observed to have a functional affinity 17-fold greater than **1**. From this series of compounds, it was evident that incorporation of all the beneficial structural modifications into a single compound did not provide additive improvements in functional affinity and negative cooperativity. It is noteworthy, however, that the rigidity of the cyclohexylene spacer in **18** was

beneficial in maintaining some negative cooperativity whilst the flexible butylene spacer of **29** was beneficial for affinity and appeared to confer a competitive mode of interaction with dopamine (Table 1).

**Table 1.** Functional parameters for analogues containing the most favourable head, tail and spacer moieties determined from our initial SAR



Compound	X	Y	Z	pK <sub>B</sub> ± SEM, (K <sub>B</sub> , nM)	Logαβ ± SEM, (αβ)	Schild Slope ± SEM
<b>1</b>	CN			6.11 ± 0.02 (776)	-1.23 ± 0.14 (0.06)	n/a <sup>a</sup>
<b>2</b>	CN			7.63 ± 0.10 (23.4)*	-1.42 ± 0.09 (0.04)*	n/a <sup>a</sup>
<b>18</b>	H			6.33 ± 0.18 (467)	-0.86 ± 0.09 (0.14)	n/a <sup>a</sup>
<b>29</b>	H			7.35 ± 0.22 (44.7)	n/a <sup>b</sup>	-0.86 ± 0.10

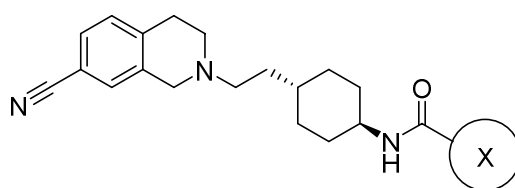
Determined by ERK1/2 phosphorylation studies in the presence of dopamine. Data represents the mean ± SEM of three individual experiments conducted in duplicate; <sup>a</sup>n/a: Compound demonstrated a Schild slope significantly different from unity, therefore, the compound demonstrated negative cooperativity; <sup>b</sup>n/a: Compound displayed competitive antagonism in the presence of dopamine, therefore, no value of cooperativity factor was derived.

Next, we were interested in evaluating the impact of inductive effects on negative cooperativity given that replacement of the indole-2-carboxamide tail of **1** with the electron deficient 7-azaindole-2-carboxamide (**2**) resulted in the most potent analogue in our initial SAR investigation. We synthesised a series of compounds containing fluorine-substituted and methoxy-substituted indole-2-carboxamide tails (**12a-12d** and **13a-13d**, respectively; Table 2) to test the effects of electron-withdrawing and electron-donating moieties on negative cooperativity. Upon pharmacological evaluation, it was clear to see that electron withdrawing functional groups were clearly beneficial to NAM activity at the D<sub>2</sub>R. Compound **12a** (4-F, K<sub>B</sub> = 47 nM, αβ = 0.03) was observed to have virtually identical pharmacological characteristics as **2**, with a 30-fold improvement in functional affinity relative to **1**. Compounds **12b** (5-F, K<sub>B</sub> = 7 nM, αβ = 0.02) and

**12d** (7-F,  $K_B = 4$  nM,  $\alpha\beta = 0.02$ ) were observed to have significant improvements in functional affinity (110- and 194-fold, respectively) and negative cooperativity (3-fold) compared to **1**. In contrast, compound **12c** (6-F,  $K_B = 219$  nM,  $\alpha\beta = 0.06$ ) maintained functional affinity and negative cooperativity similar to that of **1**. This suggests that whilst incorporation of fluorine substituents at the 4, 5 and 7 position of the indole-2-carboxamide tail are well tolerated, fluorine substituents at the 6 position are not as favourable (Table 2). It is also interesting to note, that, with the exception of **12b** and **12c**, these results are in accordance with those of a previous study conducted within our group which yielded a novel class of indole-2-carboxamide small molecule allosteric modulators for the D<sub>2</sub>R.<sup>13</sup> Within this study the *N*-isopropyl-1*H*-indole-2-carboxamide compounds with fluorine substituents at the 4- and 7-positions demonstrated negative cooperativity whilst analogues containing fluorine substituents at the 5- and 6- positions displayed competitive pharmacology. These results suggest that the NAM activity of these compounds does not solely rely on the tail moiety but is also dependent on the nature of the head and spacer moieties and their orientation within the binding site. Consequently, we are able to observe NAM profiles for compounds **12b** and **12c** despite the fact that their small molecule counterparts only displayed competitive pharmacology. In contrast to the fluorinated derivatives, the methoxy derivatives (**13a-d**) clearly demonstrated that ring activating substituents were detrimental to NAM activity (Table 2). Although compounds **13b-d** demonstrated competitive antagonist pharmacology in the pERK1/2 assay, we observed significant improvements in functional affinity (**13b**; 111-fold, **13c**; 31-fold and **13d**; 15-fold). Interestingly, compound **13a** (4-MeO,  $K_B = 617$  nM,  $\alpha\beta = 0.30$ ) appeared to act as a NAM and possessed weak negative cooperativity (5-fold less than **1**) and maintained similar functional affinity to **1**. Based on this result, it may be possible that **13a** may be interacting with a previously unidentified hydrogen-bond donating residue within the allosteric binding site that may elicit NAM activity.

Based on this series of compounds, it is apparent that inductive effects may influence NAM activity at the D<sub>2</sub>R. It was evident to see that the electron-withdrawing fluorine substituent was more favourable for NAM pharmacology whilst the electron-donating methoxy-containing derivatives were not. This series of analogues were also considered to be particularly interesting given that the majority of the analogues were observed to have significant increases in functional affinity and negative cooperativity (where applicable) upon addition of either substituent. This finding is also significant as it suggests that the tail moieties of this series contribute to the affinity of these compounds, which was not the case with **1** (where affinity was driven predominantly by the orthosteric head group as opposed to the allosteric tail).<sup>8,13</sup> It must be acknowledged, however, that these observations are the outcome of a preliminary investigation of substituent effects on

allostery. The use of larger substituents such as chlorine, bromine or iodine may produce very different effects compared to fluorine, as would hydroxyl or methyl substituents compared to methoxy.

**Table 2.** Pharmacological evaluation of the fluoro- or methoxy-indole-2-carboxamide substituted analogues.

Compound	X	$pK_B \pm SEM,$ ( $K_B, nM$ )	$Log\alpha\beta \pm$ $SEM, (\alpha\beta)$	Schild Slope $\pm SEM$
<b>1</b>		$6.11 \pm 0.02$ (776)	$-1.23 \pm 0.14$ (0.06)	n/a <sup>a</sup>
<b>2</b>		$7.63 \pm 0.10$ (23.4)*	$-1.42 \pm 0.09$ (0.04)*	n/a <sup>a</sup>
<b>12a</b>		$7.33 \pm 0.24$ (47)*	$-1.50 \pm 0.19$ (0.03)	n/a <sup>a</sup>
<b>12b</b>		$8.17 \pm 0.29$ (7)*	$-1.80 \pm 0.22$ (0.02)*	n/a <sup>a</sup>
<b>12c</b>		$6.66 \pm 0.39$ (219)	$-1.19 \pm 0.29$ (0.06)	n/a <sup>a</sup>
<b>12d</b>		$8.35 \pm 0.29$ (4)*	$-1.79 \pm 0.18$ (0.02)*	n/a <sup>a</sup>
<b>13a</b>		$6.21 \pm 0.06$ (617)	$-0.52 \pm 0.11$ (0.30)*	n/a <sup>a</sup>
<b>13b</b>		$8.70 \pm 0.32$ (7)*	n/a <sup>b</sup>	$0.54 \pm 0.05$
<b>13c</b>		$7.60 \pm 0.17$ (25)*	n/a <sup>b</sup>	$0.69 \pm 0.04$
<b>13d</b>		$7.29 \pm 0.13$ (51)*	n/a <sup>b</sup>	$1.28 \pm 0.09$

Determined by ERK1/2 phosphorylation studies in the presence of dopamine. Data represents the mean  $\pm$  SEM of three individual experiments conducted in duplicate; <sup>a</sup>n/a: Compound demonstrated a Schild slope significantly different from unity, therefore, the compound demonstrated negative cooperativity; <sup>b</sup>n/a: Compound displayed competitive antagonism in the presence of dopamine, therefore, no value of cooperativity factor was derived. (\*) Statistically different from the corresponding parameters for **1** ( $p < 0.05$ , one-way ANOVA, Dunnett's post-hoc test).

Since a marked improvement in functional affinity was observed for compound **2** (30-fold) compared to **1**, we chose to conduct a nitrogen scaffold hop around the six-membered ring of the indole tail. The scaffold-hopping strategy is a commonly applied medicinal chemistry method for molecular backbone replacements (in our instance, replacing the carbon at various positions of the benzo portion of the indole ring with nitrogen). It is a drug design strategy that is often utilised in the development of novel compounds with increased potency and altered physicochemical characteristics (Table 3).<sup>14</sup> As previously mentioned, due to the synthetic intractability of the imidazopyridine- and a number of the azaindole-2-carboxylic acids, only compounds **14a-c** were able to be synthesised. Nonetheless, we were astonished to observe drastic increases in functional affinity and negative cooperativity upon moving the nitrogen from the 7-position (**2**) to the 6-position (**14a**) of the indole moiety. Compound **14a** ( $K_B = 3$  nM,  $\alpha\beta = 0.0005$ ) was observed to have a functional affinity that was 260- and 8-fold greater functional affinity than **1** and **2**, respectively. More intriguingly, **14a** was able to induce an 1800-fold decrease in dopamine potency compared to **1** (17-fold) and **2** (25-fold), yielding the NAM with the highest negative cooperativity thus far. The pyrazolopyridine-2-carboxamide derivative, **14b** ( $K_B = 165$  nM,  $\alpha\beta = 0.03$ ) displayed a 5-fold improvement in functional affinity compared to **1**, but maintained negative cooperativity similar to that of **2** despite a comparative 16-fold loss in functional affinity. It is also interesting to note that despite lacking the crucial indolic NH which acts as a hydrogen bond donor for the E95<sup>2.65</sup> residue at the extracellular regions of transmembrane helix 2 (TM 2),<sup>5</sup> **14b** was still able to demonstrate NAM activity (Table 3). In contrast to this the thienopyrrole-2-carboxamide derivative, **14c** ( $K_B = 87$  nM) displayed competitive antagonism at the D<sub>2L</sub>R, suggesting that isoteric replacement of the phenyl ring was detrimental to NAM activity (Table 3).

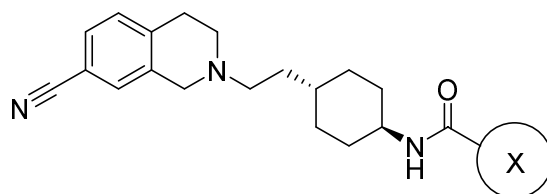
The attachment point to the scaffold was altered from the 2-position to the 3-position to avoid the previously observed self-dimerisation issues associated with some the aryl-2-carboxylic acids. Aside from investigating the biological impact of aryl-3-carboxamide derivatives, we were confident that the change in connection point would solve this dimerization issue. The pyrazolopyridine-, imidazopyridine- and isomeric azaindole-3-carboxamides were successfully synthesised (**15a-g**, Table 3 and Figure 2) and self-dimerisation was not evident during product formation. The indole-3-carboxamide variant of **1**, compound **15a** ( $K_B = 63$  nM), demonstrated competitive antagonist pharmacology at the D<sub>2L</sub>R in the pERK1/2 assays but displayed a 12-fold improvement in functional affinity compared to **1**. The simple change in attachment point of the indole relative to **1** produced a dramatic change in pharmacology. Surprisingly, the 7-azaindole-3-carboxamide derivative, **15b** ( $K_B = 34$  nM,  $\alpha\beta = 0.03$ ), maintained similar values of negative cooperativity and functional affinity as compared to **2**. Compound **15c** ( $K_B = 24$  nM,  $\alpha\beta = 0.003$ )

displayed an 8-fold loss in functional affinity and a 6-fold loss in negative cooperativity compared to its 2-carboxamide derivative, **14a**. The 5-azaindole-3-carboxamide variant, **15d** ( $K_B = 3$  nM), displayed a functional affinity similar to that of our highest affinity analogue (**14a**) but was not observed to have a Schild slope which significantly deviated from unity, and thus, was considered to be a competitive antagonist. Unlike its 2-carboxamide analogue (**14b**), **15f** ( $K_B = 3$  nM), displayed a 4-fold improvement in functional affinity but appeared to behave as a competitive antagonist. The imidazopyridine-3-carboxamide analogue (**15g**;  $K_B = 24$  nM,  $\alpha\beta = 0.005$ ), however, displayed NAM activity similar to **15c** despite lacking the presence of an indolic NH which is able to interact with the side chain of the E95<sup>2.65</sup> residue within TM 2 (Table 3).

Remarkably, the 4-azaindole-3-carboxamide derivative (**15e**) displayed a novel pharmacological profile unlike any previous analogues synthesised to date. Not only was **15e** observed to cause a limited dextral shift in dopamine's potency at the D<sub>2L</sub>R in a similar fashion to our previous analogues, but it was also observed to cause a significant limited depression in dopamine's efficacy ( $E_{max}$ ) (Figure 2). Compound **15e** ( $K_B = 0.15$  nM,  $\alpha = 0.05$ ,  $\beta = 0.16$ ) (Figure 2) is, to our knowledge, the first D<sub>2</sub>R NAM to display sub-nanomolar functional affinity for the D<sub>2L</sub>R and not only acts to modulate both dopamine's potency (21-fold) as observed for **1**, but also exerts an additional effect upon dopamine's efficacy (6-fold). Thus, this expands the behaviour of bitopic SB269652 derivatives at the D<sub>2</sub>R.

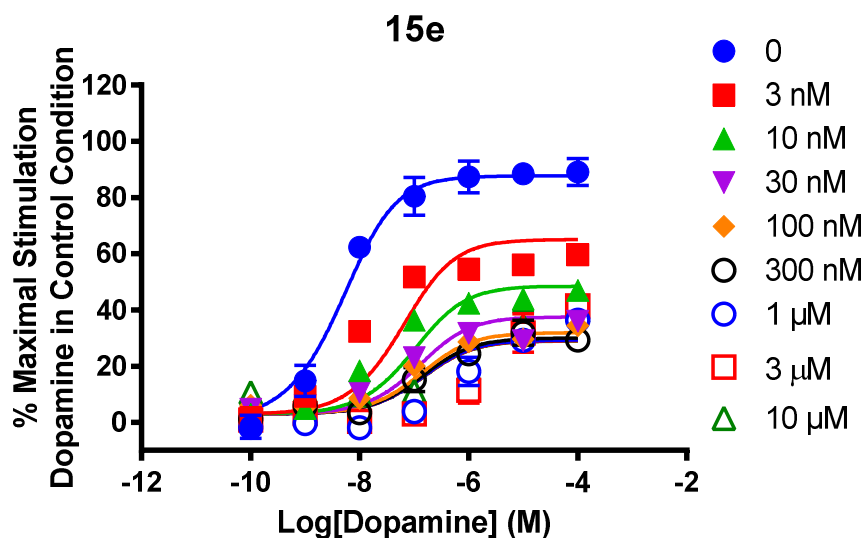
Taken together, these results suggest that subtle changes to the indolic tail of **1** have varying effects on both functional affinity and negative cooperativity at the D<sub>2</sub>R. It is clear that incorporation of a second heteroatom within the tail of **1** was beneficial for functional affinity since all of the analogues synthesised had improved results compared to **1**. The positioning of the second nitrogen atom within the tail as well as the attachment point of the aryl motif to the spacer unit (either 2- or 3-substituted), in particular, influenced the negative cooperativity and the functional affinity drastically and led to the discovery of compounds **14a** and **15e** (Table 3 and Figure 2). It was also interesting to note that **15e** demonstrated a distinctly unique functional profile compared to the other analogues, with the observation of modulatory effects upon both dopamine's affinity and efficacy in functional assays (Figure 2). In addition to this, negative cooperativity was maintained despite some analogues (e.g. **14b** and **15g**) lacking the indolic NH and therefore, the capability to make hydrogen bond interactions to the previously identified E95<sup>2.65</sup> residue at the top of TM 2. This finding is in agreement with our mutagenesis studies that revealed that mutation of E95<sup>2.65</sup> to alanine did not result in a competitive mode of action for **1** but instead modulated the degree of negative cooperativity. Thus a hydrogen bond interaction between the indolic NH of **1** and the side chain of E95<sup>2.65</sup> appears to determine the degree of cooperativity

but not whether **1** and its derivatives display allosteric versus competitive pharmacology. We can also consider the possibility of an additional interaction between the amide NH of **1** and its derivatives and the E95<sup>2,65</sup>. It was also evident that isosteric replacement of the benzo portion of the tail was unfavourable since **14c** demonstrated competitive pharmacology upon evaluation in pERK1/2 assays. This may suggest that interactions with aromatic amino acid residues within the extracellular regions of TM 2 and TM 7 may be important for NAM activity at the D<sub>2</sub>R.

**Table 3.** Pharmacological characterisation for analogues synthesised in the nitrogen scaffold hop of the indole-2-carboxamide tail

Compound	X	$pK_B \pm \text{SEM}$ , ( $K_B$ , nM)	$\text{Log}\alpha\beta \pm \text{SEM}$ , ( $\alpha\beta$ )	Schild Slope $\pm \text{SEM}$
<b>1</b>		$6.11 \pm 0.02$ (776)	$-1.23 \pm 0.14$ (0.06)	n/a <sup>a</sup>
<b>2</b>		$7.63 \pm 0.10$ (23.4)*	$-1.39 \pm 0.16$ (0.04)*	n/a <sup>a</sup>
<b>14a</b>		$8.57 \pm 0.09$ (3)	$-3.26 \pm 0.09$ (0.0005)*	n/a <sup>a</sup>
<b>14b</b>		$6.78 \pm 0.12$ (165)	$-1.52 \pm 0.09$ (0.03)	n/a <sup>a</sup>
<b>14c</b>		$7.06 \pm 0.10$ (87)*	n/a <sup>b</sup>	$1.04 \pm 0.04$
<b>15a</b>		$7.20 \pm 0.15$ (63)*	n/a <sup>b</sup>	$1.01 \pm 0.06$
<b>15b</b>		$7.47 \pm 0.11$ (34)*	$-1.50 \pm 0.09$ (0.03)	n/a <sup>a</sup>
<b>15c</b>		$8.00 \pm 0.11$ (24)	$-2.44 \pm 0.15$ (0.003)	n/a <sup>a</sup>
<b>15d</b>		$8.46 \pm 0.21$ (3)	n/a <sup>b</sup>	$0.90 \pm 0.04$
<b>15f</b>		$7.39 \pm 0.21$ (40)	n/a <sup>b</sup>	$0.71 \pm 0.07$
<b>15g</b>		$7.62 \pm 0.12$ (24)	$-2.31 \pm 0.12$ (0.005)	n/a <sup>a</sup>

Determined by ERK1/2 phosphorylation studies in the presence of dopamine. Data represents the mean  $\pm$  SEM of three individual experiments conducted in duplicate; <sup>a</sup>n/a: Compound demonstrated a Schild slope significantly different from unity, therefore, the compound demonstrated negative cooperativity; <sup>b</sup>n/a: Compound displayed competitive antagonism in the presence of dopamine, therefore, no value of cooperativity factor was derived. (\*) Statistically different from the corresponding parameters for **1** ( $p < 0.05$ , one-way ANOVA, Dunnett's post-hoc test).

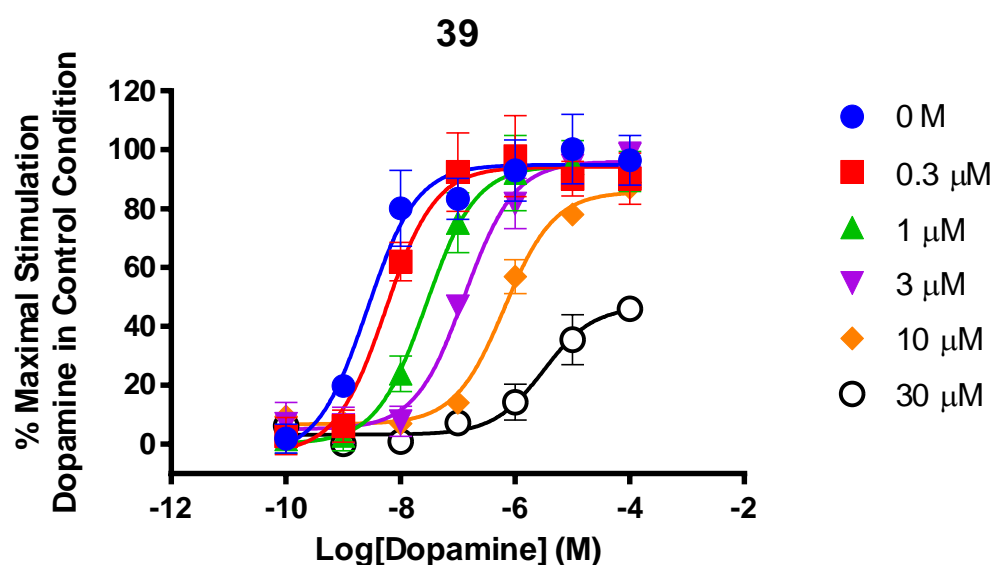


Compound	Structure	$pK_B \pm \text{SEM}$ , ( $K_B$ , nM)	$\text{Log}\alpha \pm \text{SEM}$ , ( $\alpha$ )	$\text{Log}\beta \pm \text{SEM}$ , ( $\beta$ )
15e		$9.83 \pm 0.16$ (0.15 nM)	$-1.32 \pm 0.14$ (0.05)	$-0.80 \pm 0.08$ (0.16)

**Figure 2.** Concentration-response curve of **15e** in the presence of dopamine showing both negative modulation of affinity (limited dextral shift) and efficacy (concentration-dependent depression in  $E_{\text{max}}$ ). Determined by ERK1/2 phosphorylation studies in the presence of dopamine. Data represents the mean  $\pm$  SEM of three individual experiments conducted in duplicate.

Initial synthesis of the polymethylene derivatives in our previous SAR investigation, uncovered a linker length dependency in NAM activity at the D<sub>2</sub>R.<sup>5</sup> Analogues containing polymethylene spacers were observed to demonstrate NAM activity at lengths of 4 ( $K_B = 81$  nM,  $\alpha\beta = 0.05$ ) or 6 units ( $K_B = 30$  nM,  $\alpha\beta = 0.02$ ) (i.e. butylene and hexylene, respectively), whilst the derivative consisting of a 5 unit spacer (i.e. pentylene;  $K_B = 132$  nM) behaved as a competitive antagonist. Since our previous studies illustrated that the interaction with E95<sup>2.65</sup> was a determinant of the magnitude of cooperativity with orthosteric ligands, we hypothesised that a polymethylene spacer which was 4 units (i.e. butylene) in length was able to make the key hydrogen bond interaction with the E95<sup>2.65</sup> residue via the indolic NH of the tail, whilst the hexylene derivative made this interaction via the amide NH.<sup>5</sup> Additionally, within our current investigation, compounds **14b** and **15g** were able to confer NAM activity despite lacking an indolic NH to make this key interaction. To test this hypothesis, we synthesised the N-methylated amide variant of the analogue containing the hexylene spacer (**39**; Figure 3) to determine whether the amide NH was involved in the hydrogen bond with the E95<sup>2.65</sup> residue which is thought to be important for NAM activity. Upon pharmacological evaluation we observed a pharmacological

profile similar to that of **15e**, where, **39** appeared to be modulating both the affinity ( $\alpha = 0.02$ ) and efficacy ( $\beta$  fixed to  $-3$  to represent high negative cooperativity as no limit in this effect was observed) of dopamine in pERK1/2 assays (Figure 3). However, we must also consider the possibility that this result may be a reflection of the transient nature of the signalling assay conducted. This is because it is not possible to achieve equilibrium due to the short time lapse between administration of the agonist and the point at which response measurement takes place (i.e. dopamine is added 5 minutes prior to screening in order to obtain a robust signal). Consequently, these results may be an observation of the actions of a slow-off antagonist in hemi-equilibrium conditions.<sup>15,16</sup> Further experiments are required to explore these two possibilities.

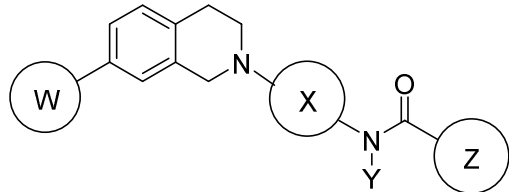


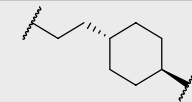
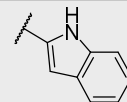
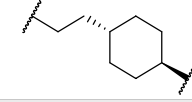
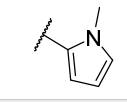
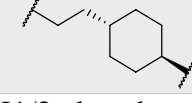
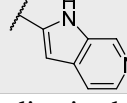
Compound	Structure	$pK_B \pm \text{SEM}$ , ( $K_B$ , nM)	$\text{Log} \alpha \pm \text{SEM}$ , ( $\alpha$ )	$\text{Log} \beta \pm \text{SEM}$ , ( $\beta$ ) <sup>a</sup>
<b>39</b>		$7.04 \pm 0.12$ (91 nM)	$-1.72 \pm 0.08$ (0.02)	$-3$

**Figure 3.** Concentration-response curve of **39** in the presence of dopamine. Determined by ERK1/2 phosphorylation studies in the presence of dopamine. Data represents the mean  $\pm$  SEM of three individual experiments conducted in duplicate. <sup>a</sup>Data was constrained to fit the operational model of allosterism.

Our current experimental approach has allowed the successful determination of both functional affinity and negative cooperativity for ligands that have demonstrated allosteric pharmacology. Despite this, it is equally important to remember that we cannot exclude the possibility that compounds which behave competitively in the presence of dopamine may, in fact, display very high negative cooperativity given that such compounds would be indistinguishable

from competitive antagonists.<sup>5</sup> Our previous studies illustrated that N-methylation of the indolic NH of **1** appeared to confer a competitive mode of interaction whilst N-methylation of the amide NH of analogues led to a dampening of negative cooperativity.<sup>5, 8</sup> With this in mind, we synthesised compounds **16a-b**, **17** and **30** whereby methylation of the indolic or amide NH of compounds that displayed competitive pharmacology or high negative cooperativity was conducted in the hope that we might identify ligands with limited negative cooperativity (Table 4). Due to time constraints, however, pharmacological characterisation could only be obtained for compounds **16a** and **17** prior to the submission of this thesis. Compound **16a** ( $K_B = 10$  nM,  $\alpha\beta = 0.008$ ) demonstrated a 3-fold loss in functional affinity compared to its desmethylated variant from our previous SAR investigation ( $K_B = 3$  nM)<sup>5</sup> but displayed negative cooperativity 7-fold greater than **1**. This result was interesting since the pyrrole derivative displayed pharmacology indistinguishable from a competitive mode of interaction. Given **16a** was methylated at the NH of the pyrrole and not the amide we hypothesise that abrogation of the interaction between the pyrrolic NH and E95<sup>2,65</sup> may act to decrease negative cooperativity (Table 4). Furthermore, compound **16a** also lacked the benzo ring which we have previously proposed to be important for NAM activity. In contrast, the N-methylated amide variant of **14a**, compound **17** ( $K_B = 23$  nM), was observed to be a competitive antagonist with an 8-fold loss in functional affinity compared to its desmethylated counterpart (Table 4).

**Table 4.** Pharmacological characterisation of the N-methylated amide or indolic NH derivatives


Compound	W	X	Y	Z	pK <sub>B</sub> ± SEM, (K <sub>B</sub> , nM)	Log αβ ± SEM, (αβ)	Schild Slope ± SEM
<b>1</b>	CN		H		6.11 ± 0.02 (776)	-1.23 ± 0.14 (0.06)	n/a <sup>a</sup>
<b>16a</b>	CN		H		8.00 ± 0.11 (10)	-2.08 ± 0.10 (0.008)	n/a <sup>a</sup>
<b>17</b>	CN		Me		7.64 ± 0.23 (23)	n/a <sup>b</sup>	0.98 ± 0.08

Determined by ERK1/2 phosphorylation studies in the presence of dopamine. Data represents the mean ± SEM of three individual experiments conducted in duplicate; <sup>a</sup>n/a: Compound demonstrated a Schild slope significantly different from unity, therefore, the compound demonstrated negative cooperativity; <sup>b</sup>n/a: Compound displayed competitive antagonism in the presence of dopamine, therefore, no value of cooperativity factor was derived.

Taken together, this investigation further highlights the role of the tail moiety in determining the degree of negative cooperativity of **1** and its derivatives. It illustrates that hydrogen bonding involving both the indolic and amide NH may determine the level of cooperativity and that SAR is not an additive phenomenon. This work also suggests that it is most likely that a number of receptor-ligand interactions, and not only hydrogen bonding with the E95<sup>2,65</sup>, that determines the degree of negative cooperativity. Furthermore, we cannot discount the possibility that N-methylation may alter the orientation of the tail moiety within the secondary pocket as it adds steric bulk to these compounds.

### 3.4 Conclusions

Based on our previous SAR investigation of **1**, we determined that the indole-2-carboxamide tail to be a key structural determinant of NAM activity at the D<sub>2</sub>R. Using this knowledge, analogues of **1** were designed, synthesised and pharmacologically characterised with varying tail moieties in order to probe their effects on negative cooperativity at the D<sub>2</sub>R. Since incorporation of a second nitrogen atom within the indole-2-carboxamide tail of **1** in our initial SAR investigation led to the discovery of our highest affinity analogue (**2**), the influence of electronic effects upon allostery at

the D<sub>2</sub>R were evaluated. A series of derivatives substituted with either a fluorine or methoxy substituent at the various positions around the benzo portion of the indole tail were synthesised. It was evident that the electron-withdrawing fluorine was favourable for allostery at the D<sub>2</sub>R. The fluoro-substituted derivatives (**12a-d**) demonstrated significant increases in affinity and modulated cooperativity based on the positioning of the fluorine. Electron-donating methoxy-substituted derivatives, in contrast, proved to be detrimental to allostery at the D<sub>2</sub>R with the exception of compound **13a** which displayed similar functional affinity and reduced negative cooperativity (5-fold) compared to **1**. It was also noted that the affinity of the fluoro- and methoxy-substituted derivatives were driven primarily by their tail moieties; this was considered particularly unusual since the affinity of **1** is believed to be driven by its 7CN-THIQ head. The effects of incorporating a second nitrogen atom via a scaffold hop analysis of indole tail were also studied. In general, the nitrogen scaffold hop was observed to be beneficial to the functional affinity of all the synthesised compounds within the series. It was particularly interesting to note that allostery was modulated by the position of the nitrogen within the 6-membered ring of the indole tail in a similar fashion to the fluorine substituted analogues. Incredibly, shifting the nitrogen from the 7- to the 6-position of the benzo ring (**14a**) caused a drastic increase in negative cooperativity (70-fold greater) compared to our best analogue to date (**2**), which equated to an 1800-fold decrease in dopamine's affinity at the D<sub>2</sub>R. The subtle repositioning of the attachment point of the indole-carboxamide tail from the 2- position to the 3-position led to some unanticipated pharmacological results. Synthesis of the indole-3-carboxamide analogues yielded compound **15e**, which was observed to be a sub-nanomolar affinity NAM which could modulate both the affinity and efficacy of dopamine. Compound **15e** is the first derivative of **1** to show modulation of both pharmacological parameters (i.e. affinity and efficacy) and subnanomolar functional affinity for the D<sub>2</sub>R. Finally, the N-methylated analogues and analogues comprising the best head, spacer and tail moieties from our initial SAR investigation illustrate that our SAR was not additive and highlight the complex nature of SAR for a bitopic allosteric modulator. Nonetheless, we were able to show how allostery of **1** and its analogues are strongly influenced by the nature of the tail moiety. This investigation also enabled the generation of analogues with varying NAM activities and provided further insight into the structural determinants of negative cooperativity at the D<sub>2</sub>R.

### 3.5 Experimental

**Chemistry.** All solvents and chemicals were purchased from standard suppliers and were used without any further purification. <sup>1</sup>H NMR and <sup>13</sup>C NMR spectra were acquired at 400.13 (<sup>1</sup>H spectra) and 100.62 (<sup>13</sup>C spectra) MHz, respectively, on a Bruker Avance III Nanobay 400 MHz NMR spectrometer coupled to the BACS 60 automatic sample changer and equipped with a 5 mm PABBO BB-1H/ D Z-GRD probe. All spectra obtained was processed using MestReNova software (v.6.0). Chemical shifts (δ) for all <sup>1</sup>H spectra are reported in parts per million (ppm) using tetramethylsilane (TMS, 0 ppm) as the reference. The data for all spectra are reported in the following format: chemical shift (δ), (multiplicity, coupling constants *J* (Hz), integral), where the multiplicity is defined as s = singlet, d = doublet, t = triplet, q = quartet, p = pentet, and m = multiplet. <sup>13</sup>C NMR were routinely carried out as *J*-modulated spin-echo experiments (JMOD), all <sup>13</sup>C δ are reported in ppm and assignment of carbon signals were abbreviated as: C = quaternary carbon, CH = methine carbon, CH<sub>2</sub> = methylene carbon, and CH<sub>3</sub> = methyl carbon. Thin layer chromatography (TLC) was carried out routinely on silica gel 60F254 precoated plates (0.25 mm, Merck). Flash column chromatography was carried out using Davisil LC60A silica gel, 40-63 μm.

Liquid chromatography mass spectrometry (LCMS) was detected on one of two instruments; either an Agilent 6100 Series Single Quad LC/MS or an Agilent 1200 Series HPLC (equipped with a 1200 Series G1311A Quaternary Pump, G1329A Thermostatted Autosampler, and a G1314B Variable Wavelength Detector) and the data was processed using LC/MSD Chemstation Rev.B.04.01 SP1 coupled with Easy Access Software. Both systems were equipped with a Reverse Phase Luna C<sub>8</sub>(2) (5 μm, 50 × 4.6 mm, 100 Å) column maintained at 30 °C. An MeCN gradient (5-100%) was used to obtain optimal separation, where 4 min were required for the gradient to reach 100% MeCN and maintained for a further 3 min before requiring 3 min to return to the initial gradient of 5% MeCN (total run time = 10 min). Solvent A = 0.1% aqueous formic acid; Solvent B = MeCN/ 0.1% formic acid.

The purity and retention time of final products were determined using analytical HPLC and high resolution mass spectrometry (HRMS). Analytical HPLC was carried out using an Agilent 1260 Infinity Analytical HPLC fitted with a Zorbax Eclipse Plus C18 Rapid Resolution column (100 mm × 4.60 mm, 3.5 μm) using a binary solvent system: solvent A of 0.1% aqueous TFA; solvent B of 0.1% TFA in MeCN. Gradient elution was achieved over 10 min using 95% A + 5% B to 100% B over 9 min, and 100% B maintained for 1 min at a flow rate of 1 mL/min monitored at both 214 and 254 nm. HRMS were conducted on an Agilent 6224 TOP LC/MS Mass Spectrometer coupled to an Agilent 1290 Infinity. All data was acquired and reference mass corrected via dual-spray electrospray ionisation (ESI) source. Each scan or data point on the total

ion chromatogram (TIC) is average of 13700 transients, producing one spectrum per second. Mass spectra were created by averaging the scans across each peak and background subtracted against the first 10 seconds of the TIC. Data acquisition was carried out using the Agilent Mass Hunter Data Acquisition software version B.05.00 Build 5.0.5042 and analysis was performed using Mass Hunter Qualitative Analysis version B.05.00 Build 5.0.519.13.

#### **General Procedure A (Reductive Alkylation)**

The amine (1 eq.) and aldehyde (1 eq.) were dissolved in dry 1,2-DCE (15 mL). NaBH(OAc)<sub>3</sub> (1.5 eq.) was added and stirred under an atmosphere of N<sub>2</sub> for 24 h. LCMS was used to confirm completion of the reaction. The mixture was then diluted in DCM (20 mL), and washed with 1 M K<sub>2</sub>CO<sub>3</sub> (3 × 20 mL) and brine, then dried over anhydrous Na<sub>2</sub>SO<sub>4</sub> and evaporated to dryness. The crude material was then purified using flash chromatography (MeOH:DCM 3:97) unless otherwise stated.

#### **General Procedure B (De-protection of *tert*-Butyl carbamate)**

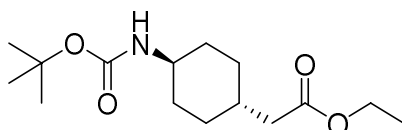
To a stirred solution of protected amine (1 eq.) and DCM (5 mL) at rt was added an excess of TFA (2 mL). The solution was stirred overnight and then diluted with DCM (20 mL). 1 M K<sub>2</sub>CO<sub>3</sub> or 1 M NaOH was added to bring the mixture to pH 12. The product was then extracted using DCM (2 × 20 mL). The combined organic extracts were then washed with brine and dried over anhydrous Na<sub>2</sub>SO<sub>4</sub> before being concentrated *in vacuo* to yield the product as the free amine.

#### **General Procedure C (HATU Amide Coupling)**

The amine (1 eq.), carboxylic acid (1.2 eq.) and the coupling reagent, HATU (1.2 eq.), were stirred in a minimal volume of anhydrous DMF (3-4 mL). To this was added an excess of DIPEA (2 eq.) and the reaction was left to stir between 2 h and overnight and ceased upon complete consumption of the amine which was determined via LCMS. The mixture was then diluted with a sat. NaHCO<sub>3</sub> and H<sub>2</sub>O solution (1:1) which was ten times the volume of DMF added to the reaction and left to stir for 30 min. The resulting precipitate was filtered and washed, or if precipitation had not occurred, the product was extracted from the aqueous using EtOAc (3 × 20 mL). Any further purification was as specified.

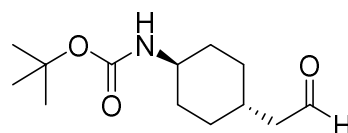
**General Procedure D (Synthesis of Methoxy-Substituted Derivatives):** To a solution of the methoxy-substituted indole-2-carboxylic acid (1 eq.) in DMF (5 mL) was added *N,N*-diisopropylethylamine (1.2 eq.) under N<sub>2</sub> at rt. BOP (1.1 eq.) was then added, and the reaction left to stir for 5-10 min. 2-(2-((*trans*)-4-Aminocyclohexyl)ethyl)-1,2,3,4-tetrahydroisoquinoline-7-carbonitrile (1.2 eq.) was then added slowly, and after 16 h the solvent was removed *in vacuo* and the resulting residue dissolved in DCM (20 mL) and partitioned between NaHCO<sub>3</sub> (30 mL). The aqueous phase was further extracted with 3 × 10 mL portions of DCM. The organic layers were then collected and washed with H<sub>2</sub>O (30 mL), brine (30 mL), dried over anhydrous Na<sub>2</sub>SO<sub>4</sub>, filtered and concentrated to give the crude product. To remove excess HMPA, the crude product was dissolved in EtOAc and washed with 3 × 20 mL portions of 2 M brine. Purification of the product was achieved via column chromatography (2:98 MeOH:CHCl<sub>3</sub>).

**Ethyl 2-((*trans*)-4-((*tert*-butoxycarbonyl)amino)cyclohexyl)acetate (4).<sup>5</sup>**



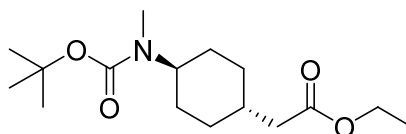
Refer to compound **42** in Chapter 2.

***tert*-Butyl ((*trans*)-4-(2-oxoethyl)cyclohexyl)carbamate (5)<sup>5</sup>**



Refer to compound **43** in Chapter 2.

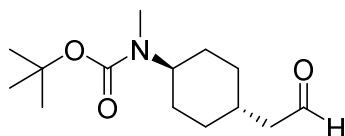
**Ethyl 2-((*trans*)-4-((*tert*-butoxycarbonyl)(methyl)amino)cyclohexyl)acetate (6).<sup>5</sup>**



Following a modified procedure by Shonberg *et al.*,<sup>5</sup> ethyl 2-((*trans*)-4-((*tert*-butoxycarbonyl)amino)cyclohexyl)acetate (635 mg, 2.23 mmol) was taken up in dry DMF (16 mL) and cooled to 0 °C. To the stirred solution was added sodium hydride (60% dispersion in mineral

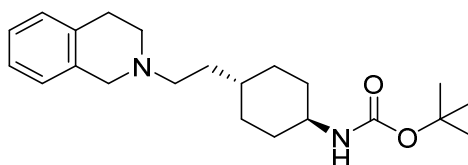
oil) (890 mg, 22.3 mmol). After 30 min stirring, iodomethane (4.16 mL, 66.8 mmol) was slowly added and the mixture was allowed to warm to rt. After 4 d, the reaction appeared yellow in colour and was diluted with H<sub>2</sub>O (60 mL) and the product extracted into EtOAc (2 × 60 mL), the combined organic extracts were washed with brine and dried over anhydrous Na<sub>2</sub>SO<sub>4</sub> and evaporated to dryness. The product was then purified using flash column chromatography (1:99 MeOH:DCM) to give the title compound as a pale yellow oil in quantitative yield (667 mg). <sup>1</sup>H NMR (401 MHz, CDCl<sub>3</sub>) δ 4.12 (q, *J* = 7.1 Hz, 2H), 4.01 – 3.60 (m, 1H), 2.71 (s, 3H), 2.18 (d, *J* = 7.0 Hz, 2H), 1.82 (d, *J* = 13.0 Hz, 2H), 1.76 – 1.64 (m, 3H), 1.49 – 1.40 (m, 9H), 1.31 – 1.20 (m, 4H), 1.11 (d, *J* = 11.3 Hz, 2H). <sup>13</sup>C NMR (101 MHz, CDCl<sub>3</sub>) δ 173.0 (C), 155.8 (C), 79.3 (C), 60.4 (CH<sub>2</sub>), 41.7 (CH<sub>2</sub>), 34.3 (CH), 32.2 (CH<sub>2</sub>), 29.9 (CH<sub>2</sub>), 28.7 (CH<sub>3</sub>), 28.4 (CH<sub>3</sub>), 14.4 (CH<sub>3</sub>). NOTE: One methine signal could not be observed due to signal broadening.

***tert*-Butyl methyl((*trans*)-4-(2-oxoethyl)cyclohexyl)carbamate (7).<sup>5</sup>**



Following the same procedure outlined for *tert*-butyl ((*trans*)-4-(2-oxoethyl)cyclohexyl)carbamate the product was obtained as a pale yellow oil (216 mg, 97%). <sup>1</sup>H NMR (CDCl<sub>3</sub>) δ 9.76 (t, *J* = 2.0 Hz, 1H), 4.07 - 3.58 (m, 1H), 2.72 (s, 3H), 2.38 - 2.23 (m, 2H), 1.81 (m, 2H), 1.74 – 1.56 (m, 3H), 1.54 – 1.38 (m, 12H), 1.21 – 1.06 (m, 2H). <sup>13</sup>C NMR (CDCl<sub>3</sub>) δ 202.2 (CH), 149.4 (C), 79.3 (C), 50.8 (CH<sub>2</sub>), 46.8 (CH), 38.8 (CH), 32.2 (CH<sub>2</sub>), 31.8 (CH<sub>3</sub>), 29.6 (CH<sub>2</sub>), 28.5 (CH<sub>3</sub>).

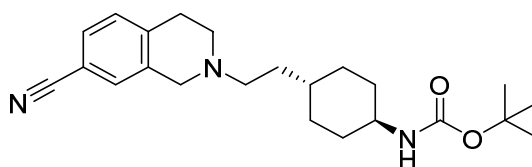
***tert*-Butyl ((*trans*)-4-(2-(3,4-dihydroisoquinolin-2(1*H*)-yl)ethyl)cyclohexyl)carbamate (8a).<sup>5</sup>**



Using 1,2,3,4-tetrahydroisoquinoline as the amine and *tert*-butyl ((*trans*)-4-(2-oxoethyl)cyclohexyl)carbamate as the aldehyde, general procedure A was followed to furnish the product as a pale yellow oil (77.2 mg, 35%). <sup>1</sup>H NMR (CDCl<sub>3</sub>) δ 7.08 – 6.91 (m, 4H), 4.31 (br s, 1H), 3.54 (s, 2H), 3.30 (br s, 1H), 2.83 (t, *J* = 5.9 Hz, 2H), 2.65 (t, *J* = 5.9 Hz, 2H), 2.45 (m, 2H),

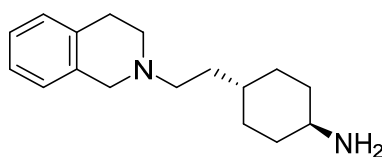
1.96 – 1.68 (m, 4H), 1.49 – 1.26 (m, 11H), 1.20 (m, 1H), 1.08 – 0.86 (m, 4H). <sup>13</sup>C NMR (CDCl<sub>3</sub>) δ 155.3 (C), 134.7 (C), 134.3 (C), 128.6 (CH), 126.6 (CH), 126.1 (CH), 125.6 (CH), 79.0 (C), 56.3 (CH<sub>2</sub>), 56.2 (CH<sub>2</sub>), 51.0 (CH<sub>2</sub>), 49.9 (CH), 35.3 (CH), 34.1 (CH<sub>2</sub>), 33.5 (CH<sub>2</sub>), 32.0 (CH<sub>2</sub>), 29.0 (CH<sub>2</sub>), 28.5 (CH<sub>3</sub>). LCMS (*m/z*): [M+H]<sup>+</sup> 359.3.

***tert*-Butyl ((*trans*)-4-(2-(7-cyano-3,4-dihydroisoquinolin-2(1*H*)-yl)ethyl)cyclohexyl)carbamate (8b).**<sup>5</sup>

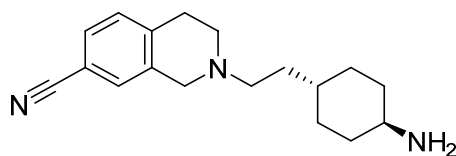


Using 1,2,3,4-tetrahydroisoquinoline-7-carbonitrile as the amine and *tert*-butyl ((*trans*)-4-(2-oxoethyl)cyclohexyl)carbamate as the aldehyde, general procedure A was followed. The resultant product obtained was a pale yellow solid (175 mg, 73%). <sup>1</sup>H NMR (CDCl<sub>3</sub>) δ 7.33 (app dd, *J* = 7.9, 1.5 Hz, 1H), 7.25 (br s, 1H), 7.13 – 7.11 (d, *J* = 8.0, 1H), 4.31 (br s, 1H), 3.55 (s, 2H), 3.31 (br s, 1H), 2.88 (app t, *J* = 5.7 Hz, 2H), 2.67 (app t, *J* = 5.8 Hz, 2H), 2.47 (app t, *J* = 8.0 Hz, 2H), 1.96 – 1.86 (m, 2H), 1.75 – 1.66 (m, 2H), 1.46 – 1.33 (m, 11H), 1.21 – 1.17 (m, 1H), 1.06 – 1.00 (m, 4H); <sup>13</sup>C NMR (CDCl<sub>3</sub>) δ 155.3 (C), 140.3 (C), 136.1 (C), 130.4 (CH), 129.6 (CH), 129.5 (CH), 119.1 (C), 109.4 (C), 79.1 (C), 56.1 (CH<sub>2</sub>), 55.5 (CH<sub>2</sub>), 50.2 (CH<sub>2</sub>), 49.8 (CH), 35.2 (CH), 33.9 (CH<sub>2</sub>), 33.4 (CH<sub>2</sub>), 32.0 (CH<sub>2</sub>), 29.3 (CH<sub>2</sub>), 28.4 (CH<sub>3</sub>). LCMS (*m/z*): [M+H]<sup>+</sup> 384.3.

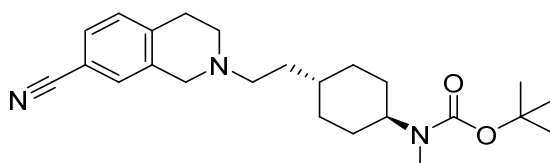
**(*trans*)-4-(2-(3,4-Dihydroisoquinolin-2(1*H*)-yl)ethyl)cyclohexan-1-amine (9a).**<sup>5</sup>



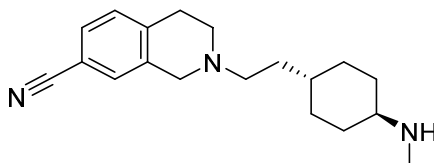
Using *tert*-butyl ((*trans*)-4-(2-(3,4-dihydroisoquinolin-2(1*H*)-yl)ethyl)cyclohexyl)carbamate as the protected amine, general procedure B was followed to furnish an oil in quantitative yields (50.0 mg). <sup>1</sup>H NMR (CDCl<sub>3</sub>) δ 7.13 – 6.98 (m, 4H), 3.61 (s, 2H), 2.90 (t, *J* = 5.9 Hz, 2H), 2.71 (t, *J* = 5.9 Hz, 2H), 2.66 – 2.46 (m, 3H), 1.93 – 1.72 (m, 4H), 1.64 – 1.40 (m, 5H), 1.17 – 0.93 (m, 4H). <sup>13</sup>C NMR (CDCl<sub>3</sub>) δ 134.9 (C), 134.4 (C), 128.6 (CH), 126.6 (CH), 126.1 (CH), 125.6 (CH), 56.5 (CH<sub>2</sub>), 56.3 (CH<sub>2</sub>), 51.1 (CH<sub>2</sub>), 50.8 (CH), 36.7 (CH<sub>2</sub>), 35.5 (CH), 34.3 (CH<sub>2</sub>), 32.2 (CH<sub>2</sub>), 29.1 (CH<sub>2</sub>). LCMS (*m/z*): [M+H]<sup>+</sup> 259.3.

**2-(2-((*trans*)-4-Aminocyclohexyl)ethyl)-1,2,3,4-tetrahydroisoquinoline-7-carbonitrile (9b).**<sup>5</sup>

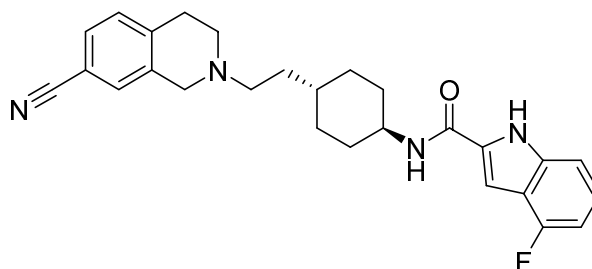
Using *tert*-butyl ((*trans*)-4-(2-(7-cyano-3,4-dihydroisoquinolin-2(1*H*)-yl)ethyl)cyclohexyl)carbamate as the protected amine, general procedure B was followed to garner the product as a yellow oil (135 mg, 94%). <sup>1</sup>H NMR (CDCl<sub>3</sub>) δ 7.41 (dd, *J* = 7.9 Hz, 1.6 Hz, 1H), 7.20 (app d, *J* = 7.9 Hz, 1H), 7.20 (d, *J* = 7.9 Hz, 1H), 3.61 (s, 2H), 3.30 (br s, 2H), 2.95 (t, *J* = 5.8 Hz, 2H), 2.73 (t, *J* = 5.9 Hz, 3H), 2.54 (m, 2H), 1.86 (m, 4H), 1.54 – 1.43 (m, 2H), 1.35 – 0.90 (m, 5H). <sup>13</sup>C NMR (CDCl<sub>3</sub>) δ 140.4 (C), 136.4 (C), 130.4 (CH), 129.6 (CH), 129.5 (CH), 119.2 (C), 109.3 (C), 56.1 (CH<sub>2</sub>), 55.63 (CH<sub>2</sub>), 50.7 (CH), 50.3 (CH<sub>2</sub>), 35.1 (CH), 35.0 (CH<sub>2</sub>), 34.1 (CH<sub>2</sub>), 31.8 (CH<sub>2</sub>), 29.5 (CH<sub>2</sub>). LCMS (*m/z*): [M+H]<sup>+</sup> 284.2.

***tert*-Butyl ((*trans*)-4-(2-(7-cyano-3,4-dihydroisoquinolin-2(1*H*)-yl)ethyl)cyclohexyl)(methyl)carbamate (10).**<sup>5</sup>

Using 1,2,3,4-tetrahydroisoquinoline-7-carbonitrile as the amine and *tert*-butyl methyl((*trans*)-4-(2-oxoethyl)cyclohexyl)carbamate as the aldehyde, general procedure A was followed to give the title compound as a yellow oil (234 mg, 70%). <sup>1</sup>H NMR (CDCl<sub>3</sub>) δ 7.39 (d, *J* = 7.9 Hz, 1H), 7.32 (s, 1H), 7.19 (d, *J* = 7.9 Hz, 1H), 4.08 – 3.74 (m, 1H), 3.61 (s, 2H), 2.94 (t, *J* = 5.8 Hz, 2H), 2.77 – 2.67 (m, 6H), 2.56 – 2.49 (m, 2H), 1.84 (m, 2H), 1.68 (m, 2H), 1.54 – 1.41 (m, 12H), 1.32 – 1.21 (m, 2H), 1.09 (m, 3H). <sup>13</sup>C NMR (101 MHz, CDCl<sub>3</sub>) δ 155.7 (C), 140.4 (C), 136.4 (C), 130.4 (CH), 129.6 (CH), 129.5 (CH), 119.2 (C), 109.4 (C), 79.2 (C), 56.1 (CH<sub>2</sub>), 55.6 (CH<sub>2</sub>), 50.3 (CH<sub>2</sub>), 45.3 (CH), 39.7 (CH<sub>2</sub>), 35.3 (CH<sub>3</sub>), 34.1 (CH<sub>2</sub>), 33.5 (CH), 32.4 (CH<sub>2</sub>), 29.5 (CH<sub>2</sub>), 28.6 (CH<sub>3</sub>). LCMS (*m/z*): [M+H]<sup>+</sup> 398.3.

**2-(2-((*trans*)-4-(Methylamino)cyclohexyl)ethyl)-1,2,3,4-tetrahydroisoquinoline-7-carbonitrile (11).<sup>5</sup>**

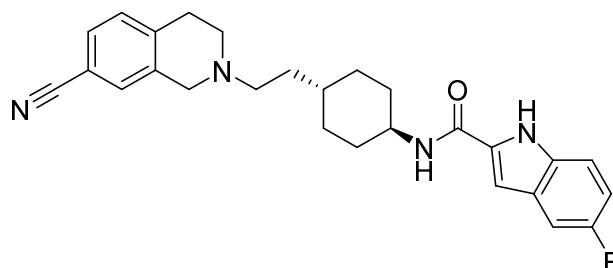
Using *tert*-butyl((*trans*)-4-(2-(7-cyano-3,4-dihydroisoquinolin-2(1*H*)-yl)ethyl)cyclohexyl)(methyl) carbamate as the protected amine, general procedure B was followed to furnish the product as a yellow oil in quantitative yield. <sup>1</sup>H NMR (CDCl<sub>3</sub>) δ 7.37 (dd, *J* = 7.9, 1.5 Hz, 1H), 7.31 (d, *J* = 1.0 Hz, 1H), 7.18 (d, *J* = 7.9 Hz, 1H), 3.60 (s, 2H), 2.97 – 2.89 (m, 2H), 2.72 (t, *J* = 5.9 Hz, 2H), 2.57 – 2.48 (m, 2H), 2.43 (s, 3H), 2.40 – 2.28 (m, 1H), 2.02 – 1.91 (m, 2H), 1.87 – 1.73 (m, 2H), 1.54 – 1.44 (m, 3H), 1.17 – 0.92 (m, 5H). <sup>13</sup>C NMR (101 MHz, CDCl<sub>3</sub>) δ 140.2 (C), 136.3 (C), 130.1 (CH), 129.3 (CH), 129.2 (CH), 118.9 (C), 109.1 (C), 58.4 (CH), 56.0 (CH<sub>2</sub>), 55.4 (CH<sub>2</sub>), 50.3 (CH<sub>2</sub>), 35.3 (CH), 34.0 (CH<sub>2</sub>), 33.1 (CH<sub>3</sub>), 32.3 (CH<sub>2</sub>), 31.6 (CH<sub>2</sub>), 29.2 (CH<sub>2</sub>). LCMS (*m/z*): [M+H]<sup>+</sup> 298.2.

***N*-((*trans*)-4-(2-(7-Cyano-3,4-dihydroisoquinolin-2(1*H*)-yl)ethyl)cyclohexyl)-4-fluoro-1*H*-indole-2-carboxamide (12a).**

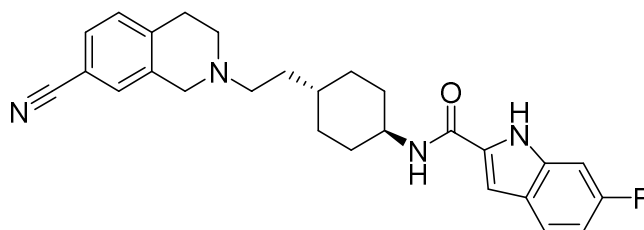
Using 2-(2-((*trans*)-4-aminocyclohexyl)ethyl)-1,2,3,4-tetrahydroisoquinoline-7-carbonitrile (126 mg, 444 μmol) as the amine and 4-fluoro-1*H*-indole-2-carboxylic acid (95.5 mg, 533 μmol) as the acid, general procedure C was followed. The resultant precipitate was then recrystallised via hot filtration in a mixture of MeOH and H<sub>2</sub>O to yield the product (111 mg, 56%). <sup>1</sup>H NMR (CDCl<sub>3</sub>) δ 9.59 (br s, 1H), 7.41 (dd, *J* = 7.9, 1.5 Hz, 1H), 7.33 (s, 1H), 7.23 – 7.16 (m, 3H), 6.89 (d, *J* = 1.7 Hz, 1H), 6.80 (ddd, *J* = 10.2, 6.9, 1.5 Hz, 1H), 6.02 (d, *J* = 8.2 Hz, 1H), 4.01 – 3.88 (m, 1H), 3.63 (s, 2H), 2.96 (t, *J* = 5.7 Hz, 2H), 2.75 (t, *J* = 5.9 Hz, 2H), 2.58 (d, *J* = 9.8 Hz, 2H), 2.13 (d, *J* = 9.8 Hz, 2H), 1.88 (d, *J* = 12.3 Hz, 2H), 1.54 (m, 2H), 1.42 – 1.06 (m, 5H). <sup>13</sup>C NMR (*d*<sub>6</sub>-DMSO) δ 160.1 (C), 156.6 (d, <sup>1</sup>*J*<sub>CF</sub> = 245.5 Hz, C), 141.2 (C), 139.3 (d, <sup>3</sup>*J*<sub>CF</sub> = 10.9 Hz, C), 137.2 (C), 132.9 (C), 130.8 (CH), 130.1 (CH), 129.9 (CH), 124.1 (d, <sup>4</sup>*J*<sub>CF</sub> = 4.1 Hz, CH), 119.6 (C), 116.7 (d, <sup>2</sup>*J*<sub>CF</sub> = 22.0 Hz, C), 109.3 (CH), 108.6 (C), 104.3 (d, <sup>2</sup>*J*<sub>CF</sub> = 18.1 Hz, CH), 98.4 (CH),

55.8 (CH<sub>2</sub>), 55.3 (CH<sub>2</sub>), 50.3 (CH<sub>2</sub>), 48.7 (CH), 35.2 (CH), 34.1 (CH<sub>2</sub>), 32.7 (CH<sub>2</sub>), 32.2 (CH<sub>2</sub>), 29.4 (CH<sub>2</sub>). HPLC:  $t_R$  6.36 min, >95% purity. HRMS ( $m/z$ ): C<sub>27</sub>H<sub>30</sub>FN<sub>4</sub>O requires [M+H]<sup>+</sup> 445.2398; found 445.2404.

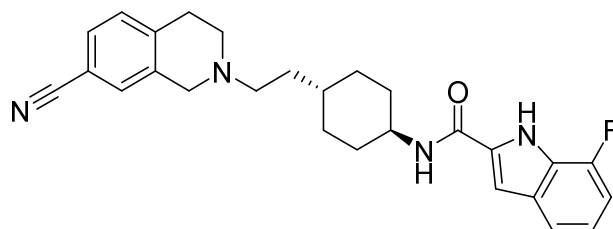
***N*-((*trans*)-4-(2-(7-Cyano-3,4-dihydroisoquinolin-2(1*H*)-yl)ethyl)cyclohexyl)-5-fluoro-1*H*-indole-2-carboxamide (12b).**



Using 2-(2-((*trans*)-4-aminocyclohexyl)ethyl)-1,2,3,4-tetrahydroisoquinoline-7-carbonitrile (126 mg, 444  $\mu$ mol) as the amine and 5-fluoro-1*H*-indole-2-carboxylic acid (95.5 mg, 533  $\mu$ mol) as the acid, general procedure C was followed. The resultant precipitate was then recrystallised via hot filtration in a mixture of MeOH and H<sub>2</sub>O to yield the product (103 mg, 52%). <sup>1</sup>H NMR (*d*<sub>6</sub>-DMSO)  $\delta$  11.62 (s, 1H), 8.25 (d,  $J$  = 8.1 Hz, 1H), 7.62 – 7.52 (m, 2H), 7.43 – 7.34 (m, 2H), 7.31 (d,  $J$  = 8.4 Hz, 1H), 7.13 (d,  $J$  = 1.5 Hz, 1H), 7.02 (td,  $J$  = 9.4, 2.6 Hz, 1H), 3.83 – 3.69 (m, 1H), 3.57 (s, 2H), 2.88 (t,  $J$  = 5.6 Hz, 2H), 2.66 (t,  $J$  = 5.8 Hz, 2H), 2.51 – 2.45 (m, 2H), 1.84 (m, 4H), 1.54 – 1.22 (m, 5H), 1.06 (m, 2H). <sup>13</sup>C NMR (*d*<sub>6</sub>-DMSO)  $\delta$  160.3 (C), 157.6 (d, <sup>1</sup> $J_{CF}$  = 232.3 Hz, C), 141.2 (C), 137.2 (C), 134.2 (C), 133.5 (C), 130.8 (CH), 130.1 (CH), 129.9 (CH), 127.6 (d, <sup>3</sup> $J_{CF}$  = 10.5 Hz, C), 119.6 (C), 113.9 (d, <sup>3</sup> $J_{CF}$  = 9.8 Hz, CH), 112.1 (CH), 108.6 (C), 106.0 (d, <sup>2</sup> $J_{CF}$  = 23.1 Hz, CH), 102.9 (d, <sup>4</sup> $J_{CF}$  = 4.7 Hz, CH), 55.8 (CH<sub>2</sub>), 55.3 (CH<sub>2</sub>), 50.3 (CH<sub>2</sub>), 48.7 (CH), 35.2 (CH), 34.1 (CH<sub>2</sub>), 32.7 (CH<sub>2</sub>), 32.2 (CH<sub>2</sub>), 29.4 (CH<sub>2</sub>). HPLC:  $t_R$  6.36 min, >95% purity. HRMS ( $m/z$ ): C<sub>27</sub>H<sub>30</sub>FN<sub>4</sub>O requires [M+H]<sup>+</sup> 445.2398; found 445.2404.

***N*-((*trans*)-4-(2-(7-Cyano-3,4-dihydroisoquinolin-2(1*H*)-yl)ethyl)cyclohexyl)-6-fluoro-1*H*-indole-2-carboxamide (12c).**

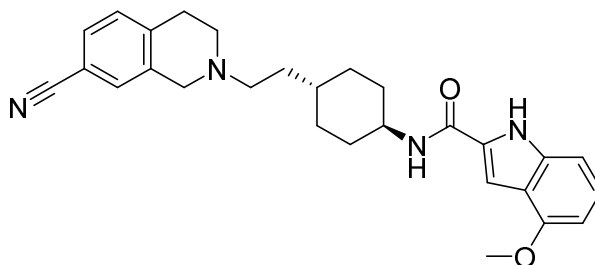
Using 2-(2-((*trans*)-4-aminocyclohexyl)ethyl)-1,2,3,4-tetrahydroisoquinoline-7-carbonitrile (126 mg, 444  $\mu\text{mol}$ ) as the amine and 6-fluoro-1*H*-indole-2-carboxylic acid (95.5 mg, 533  $\mu\text{mol}$ ) as the acid, general procedure C was followed. The resultant precipitate was then recrystallised via hot filtration in a mixture of MeOH and H<sub>2</sub>O to yield the product (58.2 mg, 30%). <sup>1</sup>H NMR (*d*<sub>6</sub>-DMSO)  $\delta$  11.59 (s, 1H), 8.20 (d, *J* = 8.1 Hz, 1H), 7.60 (m, 3H), 7.31 (d, *J* = 8.4 Hz, 1H), 7.22 – 7.06 (m, 2H), 7.06 – 6.83 (m, 1H), 3.88 – 3.68 (m, 1H), 3.57 (s, 2H), 2.88 (t, *J* = 5.6 Hz, 2H), 2.66 (t, *J* = 5.8 Hz, 2H), 2.52 – 2.38 (m, 2H), 1.95 – 1.73 (m, 4H), 1.58 – 1.27 (m, 5H), 1.06 (d, *J* = 12.6 Hz, 2H). <sup>13</sup>C NMR (*d*<sub>6</sub>-DMSO)  $\delta$  160.4 (C), 160.2 (d, <sup>1</sup>*J*<sub>CF</sub> = 237.1 Hz, C), 141.1 (C), 137.2 (C), 136.7 (d, <sup>3</sup>*J*<sub>CF</sub> = 12.9 Hz, C), 133.3 (d, <sup>3</sup>*J*<sub>CF</sub> = 3.6 Hz, C), 130.8 (CH), 130.1 (CH), 129.9 (CH), 124.4 (C), 123.3 (d, <sup>3</sup>*J*<sub>CF</sub> = 10.3 Hz, CH), 119.6 (C), 109.1 (d, <sup>2</sup>*J*<sub>CF</sub> = 24.8 Hz, CH), 108.6 (C), 103.1 (CH), 98.2 (d, <sup>2</sup>*J*<sub>CF</sub> = 25.6 Hz, CH), 55.8 (CH<sub>2</sub>), 55.3 (CH<sub>2</sub>), 50.3 (CH<sub>2</sub>), 48.7 (CH), 35.2 (CH), 34.1 (CH<sub>2</sub>), 32.8 (CH<sub>2</sub>), 32.2 (CH<sub>2</sub>), 29.4 (CH<sub>2</sub>). HPLC: *t*<sub>R</sub> 6.39 min, >95% purity. HRMS (*m/z*): C<sub>27</sub>H<sub>30</sub>FN<sub>4</sub>O requires [M+H]<sup>+</sup> 445.2398; found 445.2405.

***N*-((*trans*)-4-(2-(7-Cyano-3,4-dihydroisoquinolin-2(1*H*)-yl)ethyl)cyclohexyl)-7-fluoro-1*H*-indole-2-carboxamide (12d).**

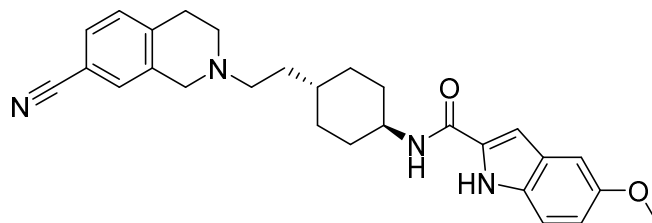
Using 2-(2-((*trans*)-4-aminocyclohexyl)ethyl)-1,2,3,4-tetrahydroisoquinoline-7-carbonitrile (126 mg, 444  $\mu\text{mol}$ ) as the amine and 7-fluoro-1*H*-indole-2-carboxylic acid (95.5 mg, 533  $\mu\text{mol}$ ) as the acid, general procedure C was followed. The resultant solid was then recrystallised via hot filtration in a mixture of MeOH and H<sub>2</sub>O to yield the product (112 mg, 57%). <sup>1</sup>H NMR (*d*<sub>6</sub>-DMSO)  $\delta$  11.95 (s, 1H), 8.22 (d, *J* = 7.9 Hz, 1H), 7.59 – 7.54 (m, 2H), 7.45 – 7.40 (m, 1H), 7.31 (d, *J* =

8.4 Hz, 1H), 7.19 (d,  $J = 2.5$  Hz, 1H), 7.04 – 6.96 (m, 2H), 3.75 (m, 1H), 3.57 (s, 2H), 2.88 (t,  $J = 5.6$  Hz, 2H), 2.66 (t,  $J = 5.8$  Hz, 2H), 2.55 – 2.44 (m, 2H), 1.96 – 1.75 (m, 4H), 1.45 (dd,  $J = 14.5$ , 6.8 Hz, 2H), 1.40 – 1.23 (m, 3H), 1.14 – 0.96 (m, 2H). <sup>13</sup>C NMR (*d*<sub>6</sub>-DMSO)  $\delta$  160.0 (C), 149.7 (d,  $^1J_{CF} = 245.1$  Hz, C), 141.2 (C), 137.2 (C), 134.0 (C), 131.3 (d,  $^3J_{CF} = 5.7$  Hz, C), 130.8 (CH), 130.1 (CH), 129.9 (CH), 125.0 (d,  $^2J_{CF} = 13.4$  Hz, C), 120.4 (d,  $^3J_{CF} = 6.0$  Hz, CH), 119.6 (C), 118.0 (d,  $^3J_{CF} = 3.4$  Hz, CH), 108.6 (C), 108.3 (d,  $^3J_{CF} = 16.2$  Hz, CH), 104.6 (CH), 55.8 (CH<sub>2</sub>), 55.3 (CH<sub>2</sub>), 50.3 (CH<sub>2</sub>), 48.8 (CH), 35.2 (CH), 34.0 (CH<sub>2</sub>), 32.7 (CH<sub>2</sub>), 32.1 (CH<sub>2</sub>), 29.4 (CH<sub>2</sub>). HPLC:  $t_R$  6.36 min, >95% purity. HRMS ( $m/z$ ): C<sub>27</sub>H<sub>30</sub>N<sub>4</sub>O requires [M+H]<sup>+</sup> 445.2398; found 445.2405.

***N*-((*trans*)-4-(2-(7-Cyano-3,4-dihydroisoquinolin-2(1*H*)-yl)ethyl)cyclohexyl)-4-methoxy-1*H*-indole-2-carboxamide (13a).**

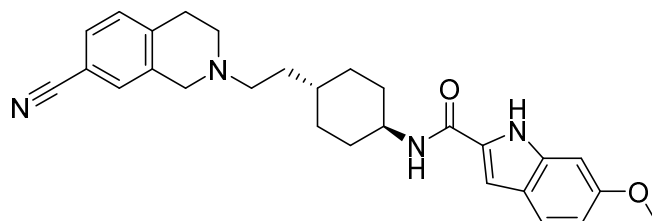


Following general procedure D, using 4-methoxy-1*H*-indole-2-carboxylic acid (35 mg, 0.18 mmol), gave the product as a beige solid (47 mg, 56%). <sup>1</sup>H NMR (*d*<sub>6</sub>-DMSO)  $\delta$  11.50 (d,  $J = 1.7$  Hz, 1H) 8.13 (d,  $J = 8.1$  Hz, 1H), 7.57 – 7.56 (m, 2H), 7.31 (d,  $J = 8.4$  Hz, 1H), 7.24 (m, 1H), 7.09 – 6.99 (m, 2H), 6.49 (d,  $J = 7.4$  Hz, 1H), 3.87 (s, 3H), 3.74 (m, 1H), 3.58 (s, 2H), 2.88 (m, 2H), 2.67 (m, 2H), 2.48 (m, 2H), 1.88 – 1.79 (m, 4H), 1.45 (dd,  $J = 14.4$ , 6.8 Hz, 2H), 1.34 – 1.28 (m, 3H), 1.06 (m, 2H). <sup>13</sup>C NMR (*d*<sub>6</sub>-DMSO)  $\delta$  160.1 (C), 153.6 (C), 140.6 (C), 137.7 (C), 136.7 (C), 130.6 (C), 130.4 (CH), 129.7 (CH), 129.5 (CH), 124.1 (CH), 119.1 (C), 118.1 (C), 108.2 (C), 105.4 (CH), 100.1 (CH), 99.2 (CH), 55.3 (CH<sub>2</sub>), 55.0 (CH<sub>3</sub>), 54.8 (CH<sub>2</sub>), 49.8 (CH<sub>2</sub>), 48.2 (CH), 34.7 (CH), 33.6 (CH<sub>2</sub>), 32.3 (CH<sub>2</sub>), 31.7 (CH<sub>2</sub>), 28.9 (CH<sub>2</sub>). HPLC:  $t_R$  6.32 min, >99% purity. HRMS ( $m/z$ ): C<sub>28</sub>H<sub>33</sub>N<sub>4</sub>O<sub>2</sub> requires [M+H]<sup>+</sup> 457.2604; found 457.2614.

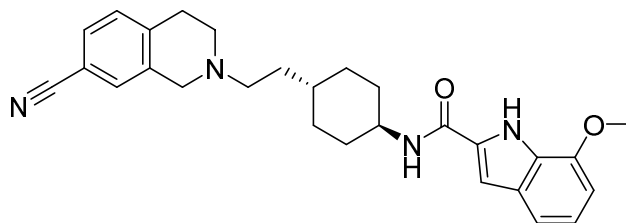
***N*-((*trans*)-4-(2-(7-Cyano-3,4-dihydroisoquinolin-2(1*H*)-yl)ethyl)cyclohexyl)-5-methoxy-1*H*-indole-2-carboxamide (13b).**

Following general procedure D, using 5-methoxy-1*H*-indole-2-carboxylic acid (29 mg, 0.15 mmol) gave the product as a white solid (39 mg, 56%). <sup>1</sup>H NMR (*d*<sub>6</sub>-DMSO) δ 11.35 (d, *J* = 1.7 Hz, 1H), 8.13 (d, *J* = 8.1 Hz, 1H), 7.56 – 7.57 (m, 2H), 7.31 (d, *J* = 9.0 Hz, 2H), 7.06 – 7.04 (m, 2H), 6.82 (dd, *J* = 8.9, 2.5 Hz, 1H), 3.75 (s, 3H), 3.74 (m, 1H), 3.58 (s, 2H), 2.88 (m, 2H), 2.67 (m, 2H), 2.48 (m, 2H), 1.89 – 1.80 (m, 4H), 1.44 (dd, *J* = 14.5, 6.8 Hz, 2H), 1.28 – 1.37 (m, 3H), 1.06 (m, 2H). <sup>13</sup>C NMR (*d*<sub>6</sub>-DMSO) δ 160.2 (C), 153.7 (C), 140.7 (C), 136.7 (C), 132.3 (C), 131.6 (C), 130.4 (CH), 129.7 (CH), 129.4 (CH), 127.4 (C), 119.1 (C), 114.2 (CH), 113.1 (CH), 108.2 (C), 102.2 (CH), 101.9 (CH), 55.4 (CH<sub>2</sub>), 55.3 (CH<sub>3</sub>), 54.8 (CH<sub>2</sub>), 49.8 (CH<sub>2</sub>), 48.2 (CH), 34.8 (CH), 33.6 (CH<sub>2</sub>), 32.3 (CH<sub>2</sub>), 31.7 (CH<sub>2</sub>), 28.9 (CH<sub>2</sub>). HPLC: *t*<sub>R</sub> 5.98 min, >99% purity.

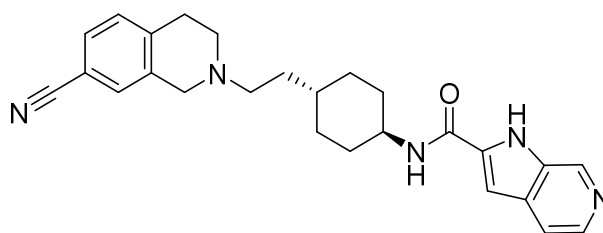
HRMS (*m/z*): C<sub>28</sub>H<sub>33</sub>N<sub>4</sub>O<sub>2</sub> requires [M+H]<sup>+</sup> 457.2604; found 457.2620.

***N*-((*trans*)-4-(2-(7-Cyano-3,4-dihydroisoquinolin-2(1*H*)-yl)ethyl)cyclohexyl)-6-methoxy-1*H*-indole-2-carboxamide (13c).**

Following general procedure D, using 6-methoxy-1*H*-indole-2-carboxylic acid (35 mg, 0.18 mmol) gave the product as a white solid (40 mg, 47%). <sup>1</sup>H NMR (*d*<sub>6</sub>-DMSO) δ 11.32 (d, *J* = 1.6 Hz, 1H), 8.06 (d, *J* = 8.1 Hz, 1H), 7.57 – 7.56 (m, 2H), 7.46 (d, *J* = 8.7 Hz, 1H), 7.31 (d, *J* = 8.4 Hz, 1H), 7.07 (d, *J* = 1.5 Hz, 1H), 6.88 (d, *J* = 2.2 Hz, 1H), 6.68 (dd, *J* = 8.7, 2.3 Hz, 1H), 3.76 (s, 3H), 3.74 (m, 1H), 3.57 (s, 2H), 2.88 (m, 2H), 2.66 (m, 2H), 2.48 (m, 2H), 1.88 – 1.79 (m, 4H), 1.45 (dd, *J* = 14.4, 6.8 Hz, 2H), 1.35 – 1.29 (m, 3H), 1.07 (m, 2H). <sup>13</sup>C NMR (*d*<sub>6</sub>-DMSO) δ 160.3 (C), 156.9 (C), 140.7 (C), 137.3 (C), 136.7 (C), 130.9 (C), 130.4 (CH), 129.7 (CH), 129.4 (CH), 122.2 (CH), 121.3 (C), 119.1 (C), 110.8 (CH), 108.2 (C), 102.7 (CH), 94.2 (CH), 55.4 (CH<sub>2</sub>), 55.1 (CH<sub>3</sub>), 54.8 (CH<sub>2</sub>), 49.8 (CH<sub>2</sub>), 48.1 (CH), 34.8 (CH), 33.6 (CH<sub>2</sub>), 32.4 (CH<sub>2</sub>), 31.8 (CH<sub>2</sub>), 28.9 (CH<sub>2</sub>). HPLC: *t*<sub>R</sub> 6.25 min, 93% purity. HRMS (*m/z*): C<sub>28</sub>H<sub>32</sub>N<sub>4</sub>O<sub>2</sub> requires [M+H]<sup>+</sup> 457.2604; found 457.2606.

***N*-((*trans*)-4-(2-(7-Cyano-3,4-dihydroisoquinolin-2(1*H*)-yl)ethyl)cyclohexyl)-7-methoxy-1*H*-indole-2-carboxamide (13d).**

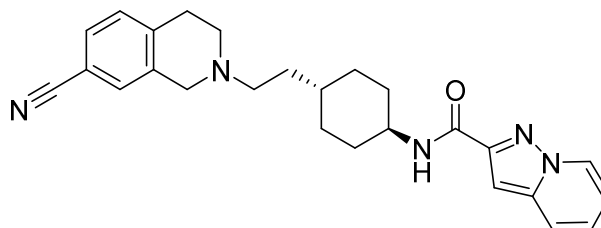
Following general procedure D, using 7-methoxy-1*H*-indole-2-carboxylic acid (30 mg, 0.16 mmol) gave the product as pale yellow solid (53 mg, 74%). <sup>1</sup>H NMR (CDCl<sub>3</sub>) δ 9.34 (s, 1H), 7.43 (dd, *J* = 7.9, 1.6 Hz, 1H), 7.35 (m, 1H), 7.23 (t, *J* = 7.6 Hz, 2H), 7.06 (t, *J* = 7.9 Hz, 1H), 6.81 (d, *J* = 2.3 Hz, 1H), 6.71 (d, *J* = 7.3 Hz, 1H), 6.05 (d, *J* = 8.2 Hz, 1H), 3.96 (m, 1H), 3.97 (s, 3H), 3.69 (s, 2H), 3.00 (m, 2H), 2.81 (m, 2H), 2.61 (m, 2H), 2.13 (m, 2H), 1.87 (m, 2H), 1.57 (dd, *J* = 15.1, 6.8 Hz, 2H), 1.35 (m, 1H), 1.30 – 1.16 (m, 4H). <sup>13</sup>C NMR (CDCl<sub>3</sub>) δ 160.7 (C), 146.7 (C), 140.3 (C), 136.1 (C), 130.8 (C), 130.5 (CH), 129.9 (CH), 129.7 (CH), 128.9 (C), 127.4 (C), 121.2 (C), 119.2 (C), 114.2 (CH), 109.7 (C), 103.6 (CH), 102.3 (CH), 56.03 (CH<sub>2</sub>), 55.5 (CH<sub>3</sub>), 55.4 (CH<sub>2</sub>), 50.2 (CH<sub>2</sub>), 48.9 (CH), 35.3 (CH), 33.8 (CH<sub>2</sub>), 33.2 (CH<sub>2</sub>), 32.0 (CH<sub>2</sub>), 29.2 (CH<sub>2</sub>). HPLC: *t*<sub>R</sub> 6.39 min, 94% purity. HRMS (*m/z*): C<sub>28</sub>H<sub>33</sub>N<sub>4</sub>O requires [M+H]<sup>+</sup> 457.2604; found 457.2602.

***N*-((*trans*)-4-(2-(7-Cyano-3,4-dihydroisoquinolin-2(1*H*)-yl)ethyl)cyclohexyl)-1*H*-pyrrolo[2,3-*c*]pyridine-2-carboxamide (14a).**

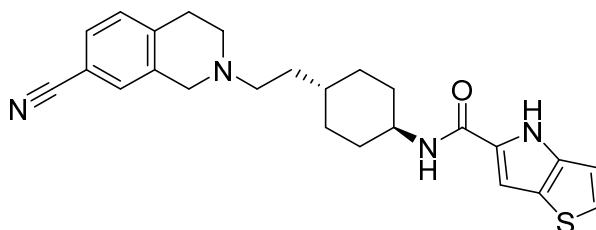
Using 2-(2-((*trans*)-4-aminocyclohexyl)ethyl)-1,2,3,4-tetrahydroisoquinoline-7-carbonitrile (29.2 mg, 103 μmol) as the amine and 1*H*-pyrrolo[2,3-*c*]pyridine-2-carboxylic acid (33.4 mg, 206 μmol) as the acid, general procedure C was followed. Prior to work up and purification, a small amount of precipitate was noted, this was filtered under vacuum and discarded. The filtrate was washed as per general procedure C. The mixture was then extracted using EtOAc, washed with H<sub>2</sub>O (2 × 20 mL) and brine (20 mL) and dried over anhydrous Na<sub>2</sub>SO<sub>4</sub>. The mixture was then evaporated to dryness and purified by flash chromatography (1:9 MeOH:DCM) to produce the title compound as an off-white, oily residue (18 mg, 41%). <sup>1</sup>H NMR (MeOD) δ 8.75 (br s, 1H), 8.08 (br s, 1H), 7.63 (m, 1H), 7.46 (m, 2H), 7.28 (d, *J* = 8.5 Hz, 1H), 7.12 (s, 1H), 3.85 (m, 1H), 3.73 (s, 2H), 2.98 (m, 2H), 2.90 – 2.80 (m, 2H), 2.64 (m, 2H), 2.02 – 1.81 (m, 4H), 1.63 – 1.51

(m, 2H), 1.51 – 1.28 (m, 3H), 1.28 – 1.05 (m, 2H). <sup>13</sup>C NMR (MeOD) δ 210.5 (C), 162.2 (C), 141.3 (C), 138.2 (CH), 137.4 (C), 136.7 (C), 136.0 (CH), 134.2 (C), 131.7 (CH), 131.1 (CH), 130.9 (CH), 119.9 (C), 110.7 (C), 102.9 (CH), 57.0 (CH<sub>2</sub>), 56.0 (CH<sub>2</sub>), 51.3 (CH<sub>2</sub>), 50.6 (CH), 36.6 (CH), 34.4 (CH<sub>2</sub>), 33.4 (CH<sub>2</sub>), 33.1 (CH<sub>2</sub>), 30.7 (CH), 29.5 (CH<sub>2</sub>). HPLC: *t*<sub>R</sub> 4.45 min, >95% purity. HRMS (*m/z*): C<sub>26</sub>H<sub>30</sub>N<sub>5</sub>O requires [M+H]<sup>+</sup> 428.2445; found 428.2457.

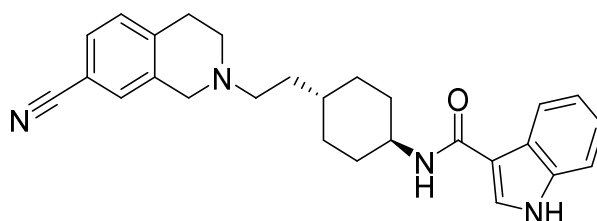
***N*-((*trans*)-4-(2-(7-Cyano-3,4-dihydroisoquinolin-2(1*H*)-yl)ethyl)cyclohexyl)pyrazolo[1,5-*a*]pyridine-2-carboxamide (14b).**



Using 2-(2-((*trans*)-4-aminocyclohexyl)ethyl)-1,2,3,4-tetrahydroisoquinoline-7-carbonitrile (75.0 mg, 265 μmol) as the amine and pyrazolo[1,5-*a*]pyridine-2-carboxylic acid (51.5 mg, 318 μmol) as the acid, general procedure C was followed. The resultant precipitate was recrystallised from a mixture of MeOH and H<sub>2</sub>O to furnish the title compound as an amorphous solid (55.4 mg, 49%). <sup>1</sup>H NMR (CDCl<sub>3</sub>) δ 8.38 (dd, *J* = 7.0, 0.8 Hz, 1H), 7.59 (app d, *J* = 8.9 Hz, 1H), 7.40 (app d, *J* = 7.9 Hz, 1H), 7.33 (app s, 1H), 7.19 (d, *J* = 7.9 Hz, 1H), 7.14 (m, 1H), 7.06 (s, 1H), 6.93 (d, *J* = 8.4 Hz, 1H), 6.85 (td, *J* = 7.0, 1.3 Hz, 1H), 4.07 – 3.85 (m, 1H), 3.62 (s, 2H), 2.95 (t, *J* = 5.8 Hz, 2H), 2.74 (t, *J* = 5.9 Hz, 2H), 2.67 – 2.49 (m, 2H), 2.13 (app d, *J* = 9.7 Hz, 2H), 1.86 (app d, *J* = 12.0 Hz, 2H), 1.53 (m, 2H), 1.42 – 1.04 (m, 5H). <sup>13</sup>C NMR (CDCl<sub>3</sub>) δ 161.3 (C), 148.2 (C), 141.4 (C), 140.4 (C), 136.4 (C), 130.4 (CH), 129.6 (CH), 129.5 (CH), 128.4 (CH), 123.7 (CH), 119.3 (CH), 119.2 (C), 113.6 (CH), 109.4 (C), 98.0 (CH), 56.1 (CH<sub>2</sub>), 55.7 (CH<sub>2</sub>), 50.3 (CH<sub>2</sub>), 48.4 (CH), 35.3 (CH), 34.1 (CH<sub>2</sub>), 33.0 (CH<sub>2</sub>), 31.9 (CH<sub>2</sub>), 29.5 (CH<sub>2</sub>). HPLC: *t*<sub>R</sub> 5.05 min, >95% purity. HRMS (*m/z*): C<sub>26</sub>H<sub>30</sub>N<sub>5</sub>O requires [M+H]<sup>+</sup> 428.2445; found 428.2449.

***N*-((*trans*)-4-(2-(7-Cyano-3,4-dihydroisoquinolin-2(1*H*)-yl)ethyl)cyclohexyl)-4*H*-thieno[3,2-*b*]pyrrole-5-carboxamide (14c).**

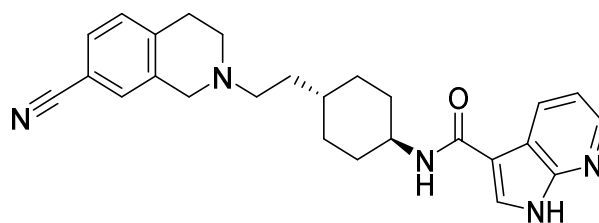
Using 2-(2-((*trans*)-4-aminocyclohexyl)ethyl)-1,2,3,4-tetrahydroisoquinoline-7-carbonitrile (118 mg, 416  $\mu\text{mol}$ ) as the amine and 4*H*-thieno[3,2-*b*]pyrrole-5-carboxylic acid (83.5 mg, 500  $\mu\text{mol}$ ) as the acid, general procedure C was followed. The resultant precipitate was recrystallised from a mixture of MeOH and H<sub>2</sub>O to furnish a solid (11.4 mg, 6%). <sup>1</sup>H NMR (CDCl<sub>3</sub>)  $\delta$  9.39 (s, 1H), 7.43 (dd, *J* = 7.9, 1.6 Hz, 1H), 7.35 (app s, 1H), 7.26 (d, *J* = 5.3 Hz, 1H), 7.22 (d, *J* = 7.9 Hz, 1H), 6.99 (dd, *J* = 5.3, 0.6 Hz, 1H), 6.75 (dd, *J* = 1.9, 0.6 Hz, 1H), 5.76 (d, *J* = 8.1 Hz, 1H), 4.02 – 3.85 (m, 1H), 3.64 (s, 2H), 2.98 (t, *J* = 5.8 Hz, 2H), 2.76 (t, *J* = 5.9 Hz, 2H), 2.61 – 2.55 (m, 2H), 2.12 (m, 2H), 1.90 (m, 2H), 1.55 (m, 2H), 1.31 – 1.10 (m, 5H). <sup>13</sup>C NMR (CDCl<sub>3</sub>)  $\delta$  187.4 (C), 160.5 (C), 140.3 (C), 140.1 (C), 136.3 (C), 130.4 (CH), 129.6 (CH), 129.5 (CH), 127.8 (CH), 124.5 (C), 119.1 (C), 111.3 (CH), 109.4 (C), 100.8 (CH), 56.1 (CH<sub>2</sub>), 55.6 (CH<sub>2</sub>), 50.3 (CH<sub>2</sub>), 48.8 (CH), 35.3 (CH), 34.0 (CH<sub>2</sub>), 33.2 (CH<sub>2</sub>), 31.9 (CH<sub>2</sub>), 29.5 (CH<sub>2</sub>). HPLC: *t*<sub>R</sub> 5.93 min, >95% purity. HRMS (*m/z*): C<sub>25</sub>H<sub>29</sub>N<sub>4</sub>OS requires [M+H]<sup>+</sup> 433.2057; found 433.2062.

***N*-((*trans*)-4-(2-(7-Cyano-3,4-dihydroisoquinolin-2(1*H*)-yl)ethyl)cyclohexyl)-1*H*-indole-3-carboxamide (15a).**

Using 2-(2-((*trans*)-4-aminocyclohexyl)ethyl)-1,2,3,4-tetrahydroisoquinoline-7-carbonitrile (126 mg, 445  $\mu\text{mol}$ ) as the amine and 1*H*-indole-3-carboxylic acid (86.0 mg, 534  $\mu\text{mol}$ ) as the acid, general procedure C was followed. The resultant precipitate was recrystallised via hot filtration from a mixture of MeOH and H<sub>2</sub>O to yield the product (97.0 mg, 51%). <sup>1</sup>H NMR (*d*<sub>6</sub>-DMSO)  $\delta$  11.49 (s, 1H), 8.12 (d, *J* = 7.9 Hz, 1H), 8.01 (d, *J* = 2.6 Hz, 1H), 7.57 (m, 3H), 7.40 (d, *J* = 7.7 Hz, 1H), 7.31 (d, *J* = 8.3 Hz, 1H), 7.10 (m, 2H), 3.82 – 3.64 (m, 1H), 3.57 (s, 2H), 2.87 (t, *J* = 5.3 Hz, 2H), 2.66 (t, *J* = 5.7 Hz, 2H), 2.49 (m, 2H), 1.95 – 1.73 (m, 4H), 1.45 (m, 2H), 1.38 –

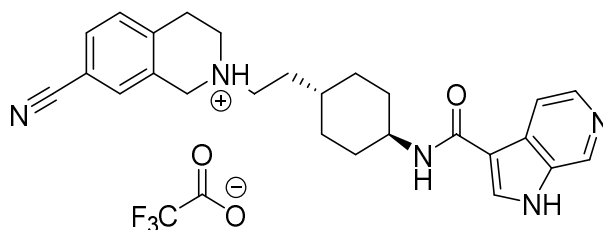
1.18 (m, 3H), 1.05 (m, 2H). <sup>13</sup>C NMR (*d*<sub>6</sub>-DMSO) δ 164.2 (C), 141.2 (C), 137.2 (C), 136.5 (C), 130.8 (CH), 130.1 (CH), 129.9 (CH), 127.8 (CH), 126.8 (C), 122.2 (CH), 121.6 (CH), 120.6 (CH), 119.6 (C), 112.1 (CH), 111.3 (C), 108.6 (C), 55.8 (CH<sub>2</sub>), 55.3 (CH<sub>2</sub>), 50.3 (CH<sub>2</sub>), 48.1 (CH), 35.3 (CH), 34.1 (CH<sub>2</sub>), 33.1 (CH<sub>2</sub>), 32.4 (CH<sub>2</sub>), 29.4 (CH<sub>2</sub>). HPLC: *t*<sub>R</sub> 5.58 min, >95% purity. HRMS (*m/z*): C<sub>27</sub>H<sub>31</sub>N<sub>4</sub>O requires [M+H]<sup>+</sup> 427.2492; found 427.2497.

***N*-((*trans*)-4-(2-(7-Cyano-3,4-dihydroisoquinolin-2(1*H*)-yl)ethyl)cyclohexyl)-1*H*-pyrrolo[2,3-*b*]pyridine-3-carboxamide (15b)**



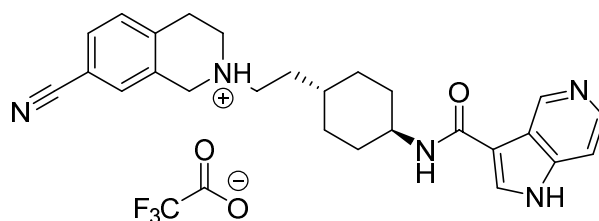
Using 2-(2-((*trans*)-4-aminocyclohexyl)ethyl)-1,2,3,4-tetrahydroisoquinoline-7-carbonitrile (162 mg, 573 μmol) as the amine and 1*H*-pyrrolo[2,3-*b*]pyridine-3-carboxylic acid (112 mg, 688 μmol) as the acid, general procedure C was followed. The resultant precipitate was recrystallised via hot filtration from a mixture of MeOH and H<sub>2</sub>O to furnish an off-white solid (84.5 mg, 35%). <sup>1</sup>H NMR (*d*<sub>6</sub>-DMSO) δ 12.01 (s, 1H), 8.43 (dd, *J* = 7.9, 1.6 Hz, 1H), 8.25 (dd, *J* = 4.6, 1.6 Hz, 1H), 8.16 (s, 1H), 7.73 (d, *J* = 7.9 Hz, 1H), 7.56 (m, 2H), 7.31 (d, *J* = 8.4 Hz, 1H), 7.15 (dd, *J* = 7.9, 4.7 Hz, 1H), 3.82 – 3.66 (m, 1H), 3.57 (s, 2H), 2.88 (t, *J* = 5.6 Hz, 2H), 2.66 (t, *J* = 5.8 Hz, 2H), 2.50 – 2.44 (m, 2H), 1.85 (m, 4H), 1.36 (m, 5H), 1.05 (m, 2H). <sup>13</sup>C NMR (*d*<sub>6</sub>-DMSO) δ 163.6 (C), 148.8 (C), 143.8 (CH), 141.2 (C), 137.2 (C), 130.8 (CH), 130.1 (CH), 129.9 (CH), 129.7 (CH), 128.2 (CH), 119.6 (C), 119.1 (C), 117.2 (CH), 110.1 (C), 108.6 (C), 55.82 (CH<sub>2</sub>), 55.3 (CH<sub>2</sub>), 50.3 (CH<sub>2</sub>), 48.2 (CH), 35.3 (CH), 34.1 (CH<sub>2</sub>), 33.1 (CH<sub>2</sub>), 32.3 (CH<sub>2</sub>), 29.4 (CH<sub>2</sub>). HPLC: *t*<sub>R</sub> 4.88 min, >95% purity. HRMS (*m/z*): C<sub>26</sub>H<sub>30</sub>N<sub>5</sub>O requires [M+H]<sup>+</sup> 428.2445; found 428.2453.

**2-(2-((*trans*)-4-(1*H*-Pyrrolo[2,3-*c*]pyridine-3-carboxamido)cyclohexyl)ethyl)-7-cyano-1,2,3,4-tetrahydroisoquinolin-2-ium 2,2,2-trifluoroacetate (15c).**



Using 2-(2-((*trans*)-4-aminocyclohexyl)ethyl)-1,2,3,4-tetrahydroisoquinoline-7-carbonitrile (184 mg, 649  $\mu\text{mol}$ ) as the amine and 1*H*-pyrrolo[2,3-*c*]pyridine-3-carboxylic acid (126 mg, 778  $\mu\text{mol}$ ), general procedure C was followed. The resultant precipitate purified via preparative HPLC to furnish the product salt as an off-white solid (86.3 mg, 25%). <sup>1</sup>H NMR (MeOD)  $\delta$  9.17 (s, 1H), 8.76 (s, 1H), 8.63 (d,  $J = 6.4$  Hz, 1H), 8.35 (d,  $J = 6.5$  Hz, 1H), 7.67 – 7.59 (m, 2H), 7.49 – 7.41 (m, 1H), 4.75 – 4.32 (m, 3H), 3.98 – 3.85 (m, 1H), 3.76 – 3.50 (m, 2H), 3.43 – 3.34 (m, 2H), 3.33 – 3.20 (m, 1H), 2.15 – 2.02 (m, 2H), 2.00 – 1.89 (m, 2H), 1.89 – 1.75 (m, 2H), 1.55 – 1.40 (m, 3H), 1.33 – 1.12 (m, 2H). <sup>13</sup>C NMR (MeOD)  $\delta$  163.1 (C), 138.9 (CH), 136.9 (C), 136.7 (C), 132.0 (C), 131.3 (CH), 130.6 (CH), 129.7 (CH), 129.6 (C), 129.3 (CH), 128.0 (CH), 117.9 (CH), 117.8 (C), 112.8 (C), 110.7 (C), 54.7 (CH<sub>2</sub>), 52.0 (CH<sub>2</sub>), 49.2 (CH<sub>2</sub>), 48.6 (CH), 34.7 (CH), 31.9 (CH<sub>2</sub>), 31.3 (CH<sub>2</sub>), 30.6 (CH<sub>2</sub>), 25.4 (CH<sub>2</sub>). HPLC:  $t_R$  4.04 min, >95% purity. HRMS ( $m/z$ ): C<sub>26</sub>H<sub>30</sub>N<sub>5</sub>O requires [M+H]<sup>+</sup> 428.2445; found 428.2450.

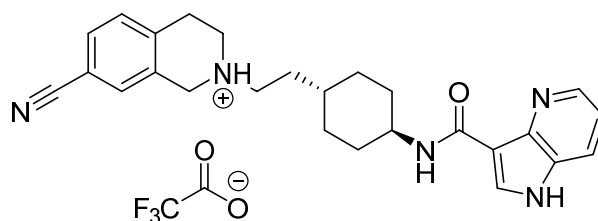
**2-(2-((*trans*)-4-(1*H*-Pyrrolo[3,2-*c*]pyridine-3-carboxamido)cyclohexyl)ethyl)-7-cyano-1,2,3,4-tetrahydroisoquinolin-2-ium 2,2,2-trifluoroacetate (15d).**



Using 2-(2-((*trans*)-4-aminocyclohexyl)ethyl)-1,2,3,4-tetrahydroisoquinoline-7-carbonitrile (114 mg, 402  $\mu\text{mol}$ ) as the amine and 1*H*-pyrrolo[3,2-*c*]pyridine-3-carboxylic acid (78.3 mg, 483  $\mu\text{mol}$ ), general procedure C was followed. The resultant precipitate purified via preparative HPLC to garner the product salt as an off-white solid (26.9 mg, 12%) <sup>1</sup>H NMR (MeOD)  $\delta$  9.51 (s, 1H), 8.47 – 8.40 (m, 2H), 8.03 (d,  $J = 6.6$  Hz, 1H), 7.72 – 7.62 (m, 2H), 7.47 (d,  $J = 8.0$  Hz, 1H), 4.53 (br s, 2H), 3.96 – 3.82 (m, 1H), 3.65 (br s, 2H), 3.40 – 3.32 (m, 3H), 3.30 – 3.26 (m, 1H), 2.01 (m, 4H), 1.85 – 1.74 (m, 2H), 1.45 (m, 3H), 1.25 (m, 2H). <sup>13</sup>C NMR (101 MHz, MeOD)  $\delta$  162.4 (C),

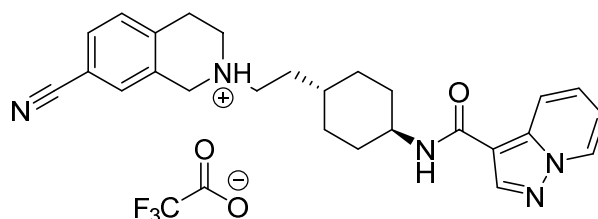
136.8 (C), 135.9 (CH), 135.8 (C), 135.6 (CH), 132.9 (C), 131.3 (CH), 130.5 (CH), 129.7 (CH), 129.6 (C), 128.7 (CH), 117.8 (CH), 117.7 (C), 110.8 (C), 106.9 (C), 54.7 (CH<sub>2</sub>), 52.0 (CH<sub>2</sub>), 49.2 (CH<sub>2</sub>), 48.3 (CH), 34.6 (CH), 32.0 (CH<sub>2</sub>), 31.3 (CH<sub>2</sub>), 30.6 (CH<sub>2</sub>), 25.4 (CH<sub>2</sub>). HPLC: *t*<sub>R</sub> 4.02 min, >95% purity. HRMS (*m/z*): C<sub>26</sub>H<sub>30</sub>N<sub>5</sub>O requires [M+H]<sup>+</sup> 428.2445; found 428.2448.

**2-(2-((*trans*)-4-(1*H*-Pyrrolo[3,2-*b*]pyridine-3-carboxamido)cyclohexyl)ethyl)-7-cyano-1,2,3,4-tetrahydroisoquinolin-2-ium 2,2,2-trifluoroacetate (15e).**



Using 2-(2-((*trans*)-4-aminocyclohexyl)ethyl)-1,2,3,4-tetrahydroisoquinoline-7-carbonitrile (114 mg, 402 μmol) as the amine and 1*H*-pyrrolo[3,2-*b*]pyridine-3-carboxylic acid (78.3 mg, 483 μmol), general procedure C was followed. The resultant precipitate purified via preparative HPLC to yield the product salt as an off-white solid (30.0 mg, 14%). <sup>1</sup>H NMR (MeOD) δ 8.70 – 8.56 (m, 3H), 7.76 (dd, *J* = 8.2, 5.9 Hz, 1H), 7.69 – 7.60 (m, 2H), 7.50 – 7.43 (m, 1H), 4.68 – 4.32 (m, 2H), 3.94 (m, 1H), 3.60 (m, 2H), 3.43 – 3.32 (m, 2H), 3.30 – 3.23 (m, 1H), 2.13 – 2.14 (m, 2H), 1.98 – 1.90 (m, 2H), 1.86 – 1.75 (m, 2H), 1.53 – 1.40 (m, 4H), 1.34 – 1.14 (m, 2H). <sup>13</sup>C NMR (MeOD) δ 162.4 (C), 136.8 (C), 135.9 (CH), 135.8 (C), 135.6 (CH), 132.9 (C), 131.3 (CH), 130.5 (CH), 129.7 (CH), 129.6 (C), 128.7 (CH), 117.8 (CH), 117.7 (C), 110.8 (C), 106.9 (C), 54.7 (CH<sub>2</sub>), 52.0 (CH<sub>2</sub>), 49.2 (CH<sub>2</sub>), 48.3 (CH), 34.6 (CH), 32.0 (CH<sub>2</sub>), 31.3 (CH<sub>2</sub>), 30.6 (CH<sub>2</sub>), 25.4 (CH<sub>2</sub>). HPLC: *t*<sub>R</sub> 4.14 min, >95% purity. HRMS (*m/z*): C<sub>26</sub>H<sub>30</sub>N<sub>5</sub>O requires [M+H]<sup>+</sup> 428.2445; found 428.2449.

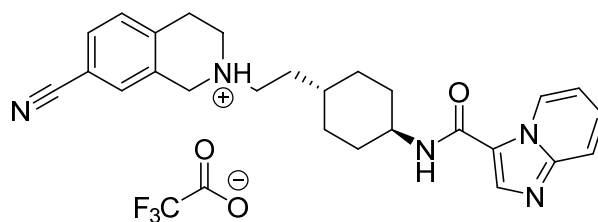
**7-Cyano-2-(2-((*trans*)-4-(pyrazolo[1,5-*a*]pyridine-3-carboxamido)cyclohexyl)ethyl)-1,2,3,4-tetrahydroisoquinolin-2-ium 2,2,2-trifluoroacetate (15f).**



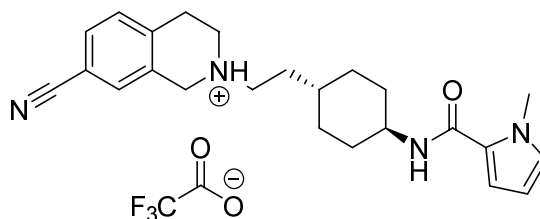
Using 2-(2-((*trans*)-4-aminocyclohexyl)ethyl)-1,2,3,4-tetrahydroisoquinoline-7-carbonitrile (114 mg, 402 μmol) as the amine and pyrazolo[1,5-*a*]pyridine-3-carboxylic acid (78.3 mg,

483  $\mu\text{mol}$ ), general procedure C was followed. The resultant precipitate purified via preparative HPLC to furnish the product salt as an off- white solid (53.5 mg, 25%). <sup>1</sup>H NMR (MeOD)  $\delta$  8.60 (d,  $J = 7.0$  Hz, 1H), 8.45 (s, 1H), 8.23 (d,  $J = 8.9$  Hz, 1H), 7.71 – 7.62 (m, 2H), 7.51 – 7.42 (m, 2H), 7.05 (td,  $J = 6.9, 1.3$  Hz, 1H), 4.77 – 4.27 (m, 2H), 3.99 – 3.32 (m, 6H), 3.30 – 3.23 (m, 1H), 2.10 – 1.88 (m, 4H), 1.85 – 1.72 (m, 2H), 1.53 – 1.38 (m, 3H), 1.32 – 1.13 (m, 2H). <sup>13</sup>C NMR (MeOD)  $\delta$  165.0 (C), 142.3 (CH), 141.9 (C), 138.1 (C), 132.7 (CH), 131.9 (CH), 131.2 (CH), 130.9 (C), 130.1 (CH), 128.1 (CH), 120.2 (CH), 119.1 (C), 115.2 (CH), 112.2 (C), 107.9 (C), 56.2 (CH<sub>2</sub>), 53.4 (CH<sub>2</sub>), 50.7 (CH<sub>2</sub>), 49.7 (CH), 36.1 (CH), 33.4 (CH<sub>2</sub>), 32.8 (CH<sub>2</sub>), 32.0 (CH<sub>2</sub>), 26.8 (CH<sub>2</sub>). HPLC:  $t_R$  4.97 min, >95% purity. HRMS ( $m/z$ ): C<sub>26</sub>H<sub>30</sub>N<sub>5</sub>O requires [M+H]<sup>+</sup> 428.2445; found 428.2448.

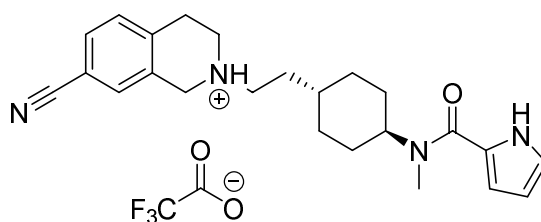
**7-Cyano-2-(2-((*trans*)-4-(imidazo[1,2-*a*]pyridine-3-carboxamido)cyclohexyl)ethyl)-1,2,3,4-tetrahydroisoquinolin-2-ium 2,2,2-trifluoroacetate (15g).**



Using 2-(2-((*trans*)-4-aminocyclohexyl)ethyl)-1,2,3,4-tetrahydroisoquinoline-7-carbonitrile (114 mg, 402  $\mu\text{mol}$ ) as the amine and imidazo[1,2-*a*]pyridine-3-carboxylic acid (78.3 mg, 483  $\mu\text{mol}$ ), general procedure C was followed. The resultant precipitate purified via preparative HPLC to obtain the product salt as an off- white solid (30.0 mg, 14%). <sup>1</sup>H NMR (CDCl<sub>3</sub>)  $\delta$  9.52 (m, 1H), 8.33 (br s, 1H), 7.81 – 7.62 (m, 2H), 7.60 – 7.52 (m, 2H), 7.40 – 7.35 (m, 1H), 7.21 (t,  $J = 6.9$  Hz, 1H), 4.58 – 4.32 (m, 2H), 3.81 (m, 1H), 3.55 (br s, 2H), 3.32 – 3.22 (m, 3H), 3.20 – 3.15 (m, 1H), 2.01 – 1.92 (m, 2H), 1.88 – 1.79 (m, 2H), 1.75 – 1.65 (m, 2H), 1.49 – 1.29 (m, 3H), 1.24 – 1.03 (m, 2H). <sup>13</sup>C NMR (CDCl<sub>3</sub>)  $\delta$  160.9 (C), 145.6 (C), 138.3 (CH), 138.2 (C), 132.7 (CH), 131.9 (CH), 131.8 (CH), 131.2 (CH), 130.9 (C), 119.1 (C), 118.9 (C), 116.9 (CH), 116.2 (CH), 113.8 (CH), 112.2 (C), 56.1 (CH<sub>2</sub>), 53.4 (CH<sub>2</sub>), 50.7 (CH<sub>2</sub>), 49.6 (CH), 36.0 (CH), 33.2 (CH<sub>2</sub>), 32.7 (CH<sub>2</sub>), 32.0 (CH<sub>2</sub>), 26.8 (CH<sub>2</sub>). HPLC:  $t_R$  4.27 min, >95% purity. HRMS ( $m/z$ ): C<sub>26</sub>H<sub>30</sub>N<sub>5</sub>O requires [M+H]<sup>+</sup> 428.2445; found 428.2459.

**7-Cyano-2-(2-((*trans*)-4-(1-methyl-1*H*-pyrrole-2-carboxamido)cyclohexyl)ethyl)-1,2,3,4-tetrahydroisoquinolin-2-ium 2,2,2-trifluoroacetate (16a).**

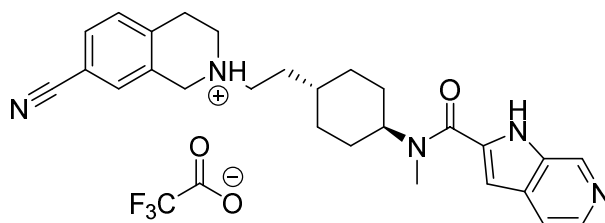
Using 2-(2-((*trans*)-4-aminocyclohexyl)ethyl)-1,2,3,4-tetrahydroisoquinoline-7-carbonitrile (173 mg, 611  $\mu\text{mol}$ ) as the amine and 1-methyl-1*H*-pyrrole-2-carboxylic acid (91.7 mg, 733  $\mu\text{mol}$ ), general procedure C was followed. The resultant precipitate was recrystallised via hot filtration from a mixture of MeOH and H<sub>2</sub>O. The remaining impurities were removed via preparative HPLC to afford the product salt as a white solid (36.9 mg, 12%) <sup>1</sup>H NMR (CDCl<sub>3</sub>)  $\delta$  7.39 (dd,  $J = 7.9, 1.5$  Hz, 1H), 7.32 (s, 1H), 7.19 (d,  $J = 7.9$  Hz, 1H), 6.71 – 6.68 (m, 1H), 6.49 (dd,  $J = 3.9, 1.7$  Hz, 1H), 6.06 (dd,  $J = 3.9, 2.6$  Hz, 1H), 5.72 (d,  $J = 8.1$  Hz, 1H), 3.93 (s, 3H), 3.88 – 3.78 (m, 1H), 3.63 (s, 2H), 2.95 (app t,  $J = 5.8$  Hz, 2H), 2.75 (app t,  $J = 5.9$  Hz, 2H), 2.61 – 2.51 (m, 2H), 2.11 – 1.96 (m, 2H), 1.88 – 1.78 (m, 2H), 1.52 (m, 2H), 1.37 – 1.00 (m, 5H). <sup>13</sup>C NMR (CDCl<sub>3</sub>)  $\delta$  161.3 (C), 140.3 (C), 136.2 (C), 130.4 (CH), 129.6 (CH), 129.5 (CH), 127.7 (CH), 126.1 (C), 119.1 (C), 111.0 (CH), 109.4 (C), 107.0 (CH), 56.0 (CH<sub>2</sub>), 55.5 (CH<sub>2</sub>), 50.2 (CH<sub>2</sub>), 48.4 (CH), 36.6 (CH<sub>3</sub>), 35.3 (CH), 34.0 (CH<sub>2</sub>), 33.2 (CH<sub>2</sub>), 32.0 (CH<sub>2</sub>), 29.3 (CH<sub>2</sub>). HPLC:  $t_R$  5.31 min, >95% purity. HRMS ( $m/z$ ): C<sub>24</sub>H<sub>31</sub>N<sub>4</sub>O requires [M+H]<sup>+</sup> 391.2492; found 391.2494.

**7-Cyano-2-(2-((*trans*)-4-(*N*-methyl-1*H*-pyrrole-2-carboxamido)cyclohexyl)ethyl)-1,2,3,4-tetrahydroisoquinolin-2-ium 2,2,2-trifluoroacetate (16b)**

Using 2-(2-((*trans*)-4-(methylamino)cyclohexyl)ethyl)-1,2,3,4-tetrahydroisoquinoline-7-carbonitrile (138 mg, 464  $\mu\text{mol}$ ) as the amine and 1*H*-pyrrole-2-carboxylic acid (61.85 mg, 557  $\mu\text{mol}$ ), general procedure C was followed. The crude solid was purified via preparative HPLC to afford the product salt (12.8 mg, 5%). <sup>1</sup>H NMR (*d*<sub>6</sub>-DMSO)  $\delta$  11.34 (s, 1H), 10.07 (br s, 1H), 7.81 – 7.68 (m, 2H), 7.48 (d,  $J = 7.9$  Hz, 1H), 6.90 – 6.82 (m, 1H), 6.46 (s, 1H), 6.15 – 6.08 (m, 1H), 4.70 – 4.52 (m, 1H), 4.41 – 4.21 (m, 2H), 3.74 (br s, 1H), 3.29 – 3.11 (m, 4H), 3.04 – 2.88

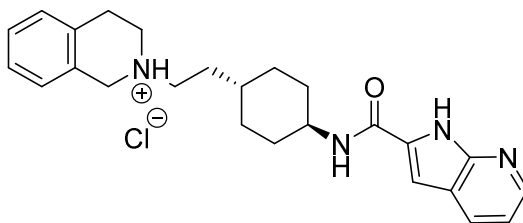
(m, 3H), 1.90 - 1.74 (m, 2H), 1.72 - 1.51 (m, 6H), 1.44 - 1.22 (m, 2H), 1.19 - 1.02 (m, 2H). <sup>13</sup>C NMR (*d*<sub>6</sub>-DMSO) δ 162.3 (C), 138.0 (C), 133.0 (C), 131.6 (CH), 131.2 (CH), 130.4 (CH), 125.5 (C), 121.4 (CH), 119.0 (C), 109.9 (C), 108.9 (CH), 54.0 (CH<sub>2</sub>), 51.7 (CH<sub>2</sub>), 49.2 (CH), 48.8 (CH<sub>2</sub>), 34.4 (CH), 31.8 (CH<sub>2</sub>), 30.7 (CH<sub>2</sub>), 29.5 (CH<sub>2</sub>), 25.9 (CH<sub>3</sub>), 25.7 (CH<sub>2</sub>). Note: One methyl and methylene signal could not be visualised in the carbon spectrum due to signal broadening. HPLC: *t*<sub>R</sub> 5.06 min, >95% purity. HRMS (*m/z*): C<sub>24</sub>H<sub>31</sub>N<sub>4</sub>O requires [M+H]<sup>+</sup> 391.2492; found 391.2504.

**7-Cyano-2-(2-((*trans*)-4-(*N*-methyl-1*H*-pyrrolo[2,3-*c*]pyridine-2-carboxamido)cyclohexyl)ethyl)-1,2,3,4-tetrahydroisoquinolin-2-ium 2,2,2-trifluoroacetate (17).**



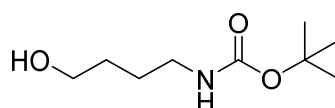
Using 2-(2-((*trans*)-4-(methylamino)cyclohexyl)ethyl)-1,2,3,4-tetrahydroisoquinoline-7-carbonitrile (175 mg, 588 μmol) as the amine and 1*H*-pyrrolo[2,3-*c*]pyridine-2-carboxylic acid (114 mg, 706 μmol), general procedure C was followed. The crude solid was recrystallised in a MeOH/ H<sub>2</sub>O system then purified via preparative HPLC to afford the product salt in good yields (135 mg, 41%). <sup>1</sup>H NMR (CDCl<sub>3</sub>) δ 8.94 (br s, 1H), 8.32 (br s, 1H), 7.59 (s, 1H), 7.42 (d, *J* = 7.9 Hz, 1H), 7.35 (s, 1H), 7.21 (d, *J* = 7.9 Hz, 1H), 6.79 (s, 1H), 4.54 (br s, 1H), 3.64 (s, 2H), 3.21 (br s, 3H), 2.97 (app t, *J* = 5.7 Hz, 3H), 2.77 (app t, *J* = 5.9 Hz, 2H), 2.67 - 2.44 (m, 2H), 2.05 - 1.79 (m, 4H), 1.78 - 1.46 (m, 4H), 1.46 - 1.05 (m, 4H). <sup>13</sup>C NMR (CDCl<sub>3</sub>) δ 162.8 (C), 147.9 (C), 140.4 (C), 138.8 (CH), 136.3 (C), 135.9 (CH), 135.5 (CH), 132.4 (C), 130.6 (CH), 129.8 (CH), 129.7 (CH), 126.8 (C), 119.22 (C), 116.2 (CH), 109.6 (C), 56.1 (CH<sub>2</sub>), 55.7 (CH<sub>2</sub>), 54.1 (CH), 50.4 (CH<sub>2</sub>), 35.3 (CH), 34.0 (CH<sub>2</sub>), 32.2 (CH<sub>2</sub>), 29.5 (CH<sub>2</sub>). Note: One methylene and one methyl signal could not be visualised in the carbon spectrum due to signal broadening. HPLC: *t*<sub>R</sub> 4.29 min, >95% purity. HRMS (*m/z*): C<sub>27</sub>H<sub>32</sub>N<sub>5</sub>O requires [M+H]<sup>+</sup> 442.2601; found 442.2580.

**2-(2-((*trans*)-4-(1*H*-Pyrrolo[2,3-*b*]pyridine-2-carboxamido)cyclohexyl)ethyl)-1,2,3,4-tetrahydroisoquinolin-2-ium chloride (18).**



To an rbf containing 1*H*-pyrrolo[2,3-*b*]pyridine-2-carboxylic acid (14.3 mg, 88.0 μmol), *N*-(3-dimethylaminopropyl)-*N'*-ethylcarbodiimide hydrochloride (EDC) (18.6 mg, 96.8 μmol) and 1*H*-benzo[*d*][1,2,3]triazol-1-ol (HOBt) (13.1 mg, 96.8 μmol) in DCM, DIPEA (133 μL, 185 μmol) was added and left to stir at rt for 1 h until a clear colourless solution was observed. (*trans*)-4-(2-(3,4-dihydroisoquinolin-2(1*H*)-yl)ethyl)cyclohexan-1-amine (25.0 mg, 96.8 μmol) was dissolved in 1 mL of DCM and added to the reaction mixture and left to stir. After 15 min, white precipitate was observed in the rbf and the reaction mixture was left to stir overnight at 40 °C. Upon confirmation of consumption of material by LCMS, the reaction mixture was washed with H<sub>2</sub>O (3 × 10 mL) and upon washing the organic layer with brine (10 mL), a white emulsion formed. The emulsion was concentrated *in vacuo* and was purified using flash chromatography (1:20 MeOH:DCM). The product was further purified by recrystallization (MeOH/ H<sub>2</sub>O) and converted to the corresponding salt using 1 M HCl in ether to form an off-white solid (7.00 mg, 20%). <sup>1</sup>H NMR (*d*<sub>6</sub>-DMSO) δ 12.02 (s, 1H), 8.31 (app d, *J* = 4.6 Hz, 1H), 8.23 (d, *J* = 7.8 Hz, 1H), 8.04 (d, *J* = 7.6 Hz, 1H), 7.20 – 6.94 (m, 6H), 3.75 (m, 1H), 3.53 (s, 2H), 2.80 (t, *J* = 5.4 Hz, 2H), 2.64 (t, *J* = 5.7 Hz, 2H), 2.47 (m, 2H), 2.03 – 1.71 (m, 4H), 1.51 - 1.25 (m, 5H), 1.18 – 0.97 (m, 2H). <sup>13</sup>C NMR (D<sub>2</sub>O) δ 160.6 (C), 140.6 (CH), 138.4 (C), 135.4 (CH), 134.4 (C), 130.7 (C), 128.7 (CH), 128.3 (CH), 127.2 (C), 127.0 (CH), 126.6 (CH), 125.6 (C), 116.5 (CH), 104.3 (CH), 54.3 (CH<sub>2</sub>), 52.8 (CH<sub>2</sub>), 49.8 (CH<sub>2</sub>), 49.6 (CH), 33.9 (CH), 31.3 (CH<sub>2</sub>), 30.7 (CH<sub>2</sub>), 30.3 (CH<sub>2</sub>), 24.7 (CH<sub>2</sub>). HPLC: *t*<sub>R</sub> 4.70 min, >95% purity. HRMS (*m/z*): C<sub>25</sub>H<sub>31</sub>N<sub>4</sub>O requires [M+H]<sup>+</sup> 403.2492; found 403.2503.

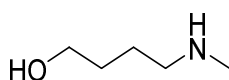
***tert*-Butyl (4-hydroxybutyl)carbamate (20).<sup>17</sup>**



A mixture of 4-aminobutanol (500 mg, 5.61 mmol), di-*tert*-butyl dicarbonate (1.22 g, 5.61 mmol) and DIPEA (860 μL, 6.17 mmol) were stirred in DCM under reflux overnight. The reaction was

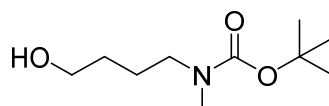
ceased upon confirmation of consumption of the alkanolamine via thin layer chromatography (TLC) (7:3 EtOAc: Pet. Spirits) and visualised using ninhydrin stain. The reaction was concentrated *in vacuo* and, the resultant oil was purified using flash chromatography (7:3 EtOAc: Pet. Spirits) to afford colourless oil in quantitative yields. <sup>1</sup>H NMR (CDCl<sub>3</sub>) δ 5.25 (br s, 1H), 3.99 (br s, 1H), 3.53 (app br s, 2H), 3.04 (app d, *J* = 4.8 Hz, 2H), 1.48 (app br s, 4H), 1.35 (s, 9H). <sup>13</sup>C NMR (CDCl<sub>3</sub>) δ 156.2 (C), 79.2 (C), 62.3 (CH<sub>2</sub>), 40.3 (CH<sub>2</sub>), 29.7 (CH<sub>2</sub>), 28.4 (CH<sub>3</sub>), 26.6 (CH<sub>2</sub>).

#### 4-(Methylamino)butan-1-ol (21).<sup>18</sup>



Following a procedure by Asaki *et. al.*,<sup>18</sup> 4-amino-1-butanol (1.03 mL, 11.2 mmol) was stirred in an rbf with EtOH (10 mL). To this ethyl formate (1.35 mL, 16.8 mmol) was added and the mixture was heated at reflux for 16 h. The volatile reagents were evaporated under vacuum and the resulting crude was carried through without further purification. To 1 M LiAlH<sub>4</sub> in THF (27.7 mL, 27.7 mmol) was added the crude product (1.30 g, 11.1 mmol) in anhydrous THF (20 mL) in a drop-wise fashion. After the mixture was refluxed for 3 h, the reaction was placed on ice and quenched by the drop-wise addition of H<sub>2</sub>O (1 mL) and 15 % (w/v) NaOH solution (1 mL). A further 3 mL of H<sub>2</sub>O was added and the mixture was allowed to reach room temperature over 30 min. The insoluble precipitate was filtered off and rinsed with THF, and the collected filtrate was concentrated *in vacuo*. The residue was washed with DCM to remove any further impurities to furnish the product as a yellow oil (880 mg, 72%). <sup>1</sup>H NMR (CDCl<sub>3</sub>) δ 3.61 – 3.49 (m, 2H), 2.71 – 2.54 (m, 2H), 2.43 (s, 3H), 1.79 – 1.50 (m, 4H). <sup>13</sup>C NMR (CDCl<sub>3</sub>) δ 62.7 (CH<sub>2</sub>), 51.8 (CH<sub>2</sub>), 35.9 (CH<sub>3</sub>), 32.6 (CH<sub>2</sub>), 28.6 (CH<sub>2</sub>).

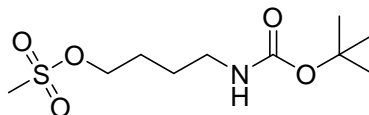
#### *tert*-Butyl (4-hydroxybutyl)(methyl)carbamate (22).<sup>19</sup>



A mixture of 4-(methylamino)butan-1-ol (807 mg, 7.82 mmol), di-*tert*-butyl dicarbonate (1.71 g, 7.82 mmol) and triethylamine (TEA) (1.20 mL, 8.60 mmol) were stirred in DCM at room temperature for 2 d. Upon confirmation of reaction completion (TLC, visualised using ninhydrin), the reaction mixture was concentrated *in vacuo* and purified using flash column chromatography

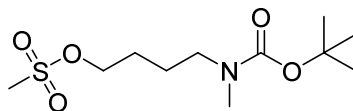
(Pet. Spirits) to furnish the product as a pale yellow oil (934 mg, 59%). <sup>1</sup>H NMR (CDCl<sub>3</sub>) δ 3.75 – 3.56 (m, 2H), 3.34 – 3.15 (m, 2H), 2.84 (s, 3H), 1.65 – 1.51 (m, 4H), 1.45 (s, 9H). <sup>13</sup>C NMR (CDCl<sub>3</sub>) δ 155.9 (C), 79.3 (C), 62.6 (CH<sub>2</sub>), 34.1 (CH<sub>3</sub>), 29.6 (CH<sub>2</sub>), 28.5 (CH<sub>3</sub>), 24.2 (CH<sub>2</sub>).

#### 4-((*tert*-Butoxycarbonyl)amino)butyl methanesulfonate (23).<sup>17</sup>

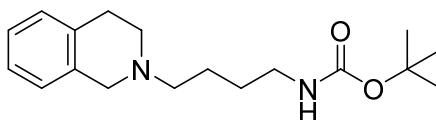


From a procedure by Szabo, *et al.*,<sup>17</sup> *tert*-butyl (4-hydroxybutyl)carbamate (1.03 g, 5.40 mmol) and TEA (2.28 mL, 16.3 mmol) were added to an rbf containing DCM (30 mL) and cooled to 0 °C whilst stirring. MsCl (960 μL, 10.9 mmol) was then added slowly and the reaction was stirred at 0 °C for a further 30 min. The reaction was warmed to rt and stirring continued overnight. The reaction mixture was subsequently diluted with DCM (50 mL), washed with H<sub>2</sub>O (3 × 50 mL) and dried over anhydrous Na<sub>2</sub>SO<sub>4</sub>, filtered and dried *in vacuo* to garner a yellow oil. The product was used in subsequent reactions without any further purification due to instability.

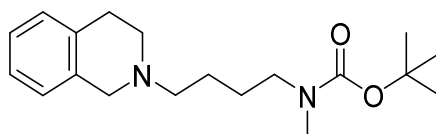
#### 4-((*tert*-Butoxycarbonyl)(methyl)amino)butyl methanesulfonate (24).<sup>20</sup>



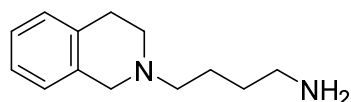
To an rbf of DCM (10 mL) cooled to 0 °C was added *tert*-butyl (4-hydroxybutyl)(methyl)carbamate (932 mg, 4.58 mmol) and TEA (1.90 mL, 13.8 mmol) whilst stirring. MsCl (808 μL, 9.17 mmol) was then added drop-wise and stirring continued at 0 °C for a further 30 min. After this time, the reaction was warmed to room temperature and left to stir overnight. The reaction mixture was then diluted with DCM (30 mL), washed with H<sub>2</sub>O (3 × 30 mL), dried over anhydrous Na<sub>2</sub>SO<sub>4</sub> and concentrated under vacuum to yield the product as yellow oil. The product was immediately carried through to subsequent reactions without any further purification or characterisation due to instability.

***tert*-Butyl (4-(3,4-dihydroisoquinolin-2(1*H*)-yl)butyl)carbamate (25).<sup>17</sup>**

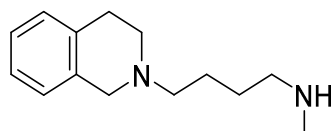
Using a procedure described by Szabo, *et al.*,<sup>17</sup> 4-((*tert*-butoxycarbonyl)amino)butyl methanesulfonate (1.45 g, 5.42 mmol), 1,2,3,4-tetrahydroisoquinoline (1.36 mL, 10.9 mmol) and, K<sub>2</sub>CO<sub>3</sub> (2.25 g, 16.3 mmol) were refluxed overnight in MeCN. The product was then purified using flash chromatography (1:19 MeOH: DCM) and evaporated *in vacuo* to furnish the product (879 mg, 53%). <sup>1</sup>H NMR (CDCl<sub>3</sub>) δ 7.15 – 6.95 (m, 4H), 5.18 (s, 1H), 3.63 (s, 1H), 3.14 (app dd, *J* = 12.0, 6.1 Hz, 2H), 2.91 (t, *J* = 5.9 Hz, 2H), 2.74 (t, *J* = 5.9 Hz, 2H), 2.53 (t, *J* = 7.1 Hz, 2H), 1.68 – 1.32 (m, 13H). <sup>13</sup>C NMR (CDCl<sub>3</sub>) δ 156.1 (C), 134.5 (C), 134.2 (C), 128.6 (CH), 126.6 (CH), 126.2 (CH), 125.6 (CH), 78.9 (C), 57.8 (CH<sub>2</sub>), 55.9 (CH<sub>2</sub>), 50.9 (CH<sub>2</sub>), 40.5 (CH<sub>2</sub>), 28.9 (CH<sub>2</sub>), 28.4 (CH<sub>3</sub>), 28.0 (CH<sub>2</sub>), 24.5 (CH<sub>2</sub>). LCMS (*m/z*): [M+H]<sup>+</sup> 305.3.

***tert*-Butyl (4-(3,4-dihydroisoquinolin-2(1*H*)-yl)butyl)(methyl)carbamate (26).**

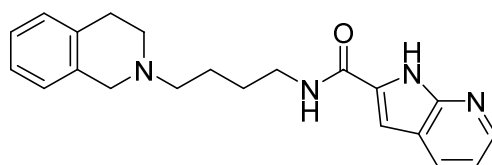
MeCN (40 mL) was added to an rbf containing 4-((*tert*-butoxycarbonyl)(methyl)amino)butyl methanesulfonate (1.29 g, 4.58 mmol), 1,2,3,4-tetrahydroisoquinoline (1.15 mL, 9.17 mmol) and K<sub>2</sub>CO<sub>3</sub> (1.90 g, 13.8 mmol) and left to stir at reflux overnight. The resultant mixture was concentrated under vacuum upon LCMS confirmation of the full consumption of the starting material. The yellow residue was purified using flash column chromatography (3:97 MeOH: DCM) to furnish the product as a yellow oil (1.06 g, 72%). <sup>1</sup>H NMR (CDCl<sub>3</sub>) δ 7.14 – 7.06 (m, 3H), 7.03 – 6.98 (m, 1H), 3.61 (s, 2H), 3.24 (s, 2H), 2.90 (t, *J* = 5.9 Hz, 2H), 2.84 (s, 3H), 2.72 (t, *J* = 5.9 Hz, 2H), 2.61 – 2.47 (m, 2H), 1.62 – 1.52 (m, 4H), 1.45 (s, 9H). <sup>13</sup>C NMR (CDCl<sub>3</sub>) δ 162.2 (C), 134.5 (C), 133.3 (C), 128.8 (CH), 126.7 (CH), 126.2 (CH), 125.7 (CH), 79.3 (C), 58.3 (CH<sub>2</sub>), 56.4 (CH<sub>2</sub>), 51.1 (CH<sub>2</sub>), 34.2 (CH<sub>3</sub>), 29.3 (CH<sub>2</sub>), 28.6 (CH<sub>3</sub>), 24.5 (CH<sub>2</sub>).

**4-(3,4-Dihydroisoquinolin-2(1H)-yl)butan-1-amine (27).<sup>21</sup>**

Using *tert*-butyl (4-(3,4-dihydroisoquinolin-2(1H)-yl)butyl)carbamate as the protected amine, general procedure B was followed. The resultant oil was obtained in quantitative yield (228 mg). <sup>1</sup>H NMR (CDCl<sub>3</sub>) δ 7.18 – 6.98 (m, 4H), 3.64 (s, 2H), 2.92 (t, *J* = 5.8 Hz, 2H), 2.81 – 2.68 (m, 4H), 2.58 – 2.49 (m, 2H), 1.76 – 1.38 (m, 6H). <sup>13</sup>C NMR (CDCl<sub>3</sub>) δ 134.8 (C), 134.3 (C), 128.7 (CH), 126.6 (CH), 126.1 (CH), 125.6 (CH), 58.3 (CH<sub>2</sub>), 56.2 (CH<sub>2</sub>), 51.0 (CH<sub>2</sub>), 42.1 (CH<sub>2</sub>), 31.7 (CH<sub>2</sub>), 29.1 (CH<sub>2</sub>), 24.8 (CH<sub>2</sub>). LCMS (*m/z*): [M+H]<sup>+</sup> 205.2.

***tert*-Butyl (4-(3,4-dihydroisoquinolin-2(1H)-yl)butyl)(methyl)carbamate (28).**

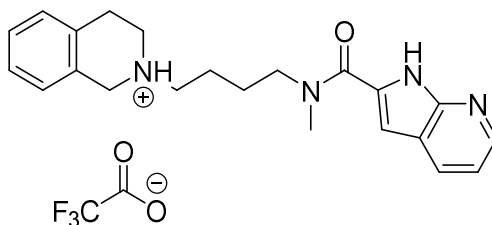
Using *tert*-butyl (4-(3,4-dihydroisoquinolin-2(1H)-yl)butyl)(methyl)carbamate, general procedure B was followed to garner the product as an oil (220 mg, 84%). <sup>1</sup>H NMR (CDCl<sub>3</sub>) δ 7.12 – 7.04 (m, 3H), 7.02 – 6.97 (m, 1H), 3.60 (s, 2H), 3.48 (s, 1H), 2.88 (app t, *J* = 5.9 Hz, 2H), 2.71 (t, *J* = 6.0 Hz, 2H), 2.62 (app t, *J* = 6.5 Hz, 2H), 2.56 – 2.46 (m, 2H), 2.38 (s, 3H), 1.71 – 1.50 (m, 4H). <sup>13</sup>C NMR (CDCl<sub>3</sub>) δ 134.5 (C), 134.0 (C), 128.5 (CH), 126.4 (CH), 126.0 (CH), 125.4 (CH), 58.0 (CH<sub>2</sub>), 55.9 (CH<sub>2</sub>), 51.5 (CH<sub>2</sub>), 50.8 (CH<sub>2</sub>), 35.7 (CH<sub>3</sub>), 28.9 (CH<sub>2</sub>), 27.4 (CH<sub>2</sub>), 24.9 (CH<sub>2</sub>). LCMS (*m/z*): [M+H]<sup>+</sup> 219.2.

***N*-(4-(3,4-Dihydroisoquinolin-2(1H)-yl)butyl)-1H-pyrrolo[2,3-*b*]pyridine-2-carboxamide hydrochloride (29).**

Using 4-(3,4-dihydroisoquinolin-2(1H)-yl)butan-1-amine as the amine (64.4 mg, 315 μmol), and 1H-pyrrolo[2,3-*b*]pyridine-2-carboxylic acid as the acid (61.3 mg, 378 μmol), general procedure C was followed. The resultant precipitate was then recrystallised via hot filtration in a mixture of MeOH and H<sub>2</sub>O to garner the product as a solid (22.0 mg, 20%). <sup>1</sup>H NMR (*d*<sub>6</sub>-DMSO) δ 12.04 (s,

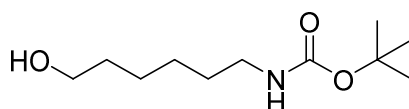
<sup>1</sup>H) 8.50 (t, *J* = 5.5 Hz, 1H), 8.31 (dd, *J* = 4.6, 1.5 Hz, 1H), 8.04 (dd, *J* = 7.9, 1.2 Hz, 1H), 7.27 – 6.95 (m, 6H), 3.54 (s, 2H), 2.80 (t, *J* = 5.7 Hz, 2H), 2.65 (t, *J* = 5.7 Hz, 2H), 2.50 (m, 2H), 1.60 (m, 4H), 1.23 (app s, 2H). <sup>13</sup>C NMR (*d*<sub>6</sub>-DMSO) δ 160.9 (C), 148.7 (C), 145.6 (CH), 135.4 (C), 134.7 (C), 132.9 (C), 130.3 (CH), 128.8 (CH), 126.8 (CH), 126.4 (CH), 125.8 (CH), 119.8 (C), 116.8 (CH), 101.9 (CH), 57.8 (CH<sub>2</sub>), 56.0 (CH<sub>2</sub>), 51.0 (CH<sub>2</sub>), 29.5 (CH<sub>2</sub>), 29.2 (CH<sub>2</sub>), 27.6 (CH<sub>2</sub>), 24.5 (CH<sub>2</sub>). HPLC: *t*<sub>R</sub> 4.68 min, >95% purity. HRMS (*m/z*): C<sub>21</sub>H<sub>25</sub>N<sub>4</sub>O requires [M+H]<sup>+</sup> 349.2023; found 349.2028.

**2-(4-(*N*-Methyl-1*H*-pyrrolo[2,3-*b*]pyridine-2-carboxamido)butyl)-1,2,3,4-tetrahydroisoquinolin-2-ium 2,2,2-trifluoroacetate (30)**



Using 4-(3,4-dihydroisoquinolin-2(1*H*)-yl)-*N*-methylbutan-1-amine (220 mg, 1.01 mmol) as the amine and 1*H*-pyrrolo[2,3-*b*]pyridine-2-carboxylic acid (196 mg, 1.21 mmol), general procedure C was followed. The resultant brown gum was purified via preparative HPLC to obtain the product salt as a tan solid (42.1 mg, 9%). <sup>1</sup>H NMR (MeOD) δ 8.68 – 8.42 (m, 2H), 7.49 (dd, *J* = 7.6, 5.6 Hz, 1H), 7.31 – 7.04 (m, 5H), 4.79 – 4.23 (m, 2H), 3.87 – 3.61 (m, 3H), 3.48 – 3.08 (m, 8H), 1.99 – 1.71 (m, 4H). <sup>13</sup>C NMR (MeOD) δ 162.7 (C), 147.6 (C), 145.1 (CH), 133.4 (CH), 132.5 (C), 132.1 (C), 129.8 (CH), 129.5 (CH), 128.8 (C), 128.3 (CH), 127.8 (CH), 122.4 (C), 117.8 (CH), 105.6 (CH), 57.0 (CH<sub>2</sub>), 54.2 (CH<sub>2</sub>), 51.2 (CH<sub>2</sub>), 49.2 (CH<sub>2</sub>), 48.8 (CH<sub>2</sub>), 37.7 (CH<sub>3</sub>), 26.3 (CH<sub>2</sub>), 22.4 (CH<sub>2</sub>). HPLC: *t*<sub>R</sub> 4.15 min, >95% purity. HRMS (*m/z*): C<sub>22</sub>H<sub>27</sub>N<sub>4</sub>O requires [M+H]<sup>+</sup> 363.2179; found 363.2185.

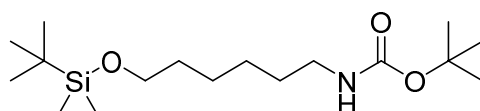
***tert*-Butyl (6-hydroxyhexyl)carbamate (32).<sup>17</sup>**



A mixture of 6-aminohexan-1-ol (2.36 mL, 18.3 mmol), di-*tert*-butyl dicarbonate (4.00 g, 18.3 mmol) and DIPEA (6.38 mL, 36.7 mmol) were stirred in DCM under reflux overnight. The reaction was ceased upon confirmation of consumption of the alkanolamine via thin layer

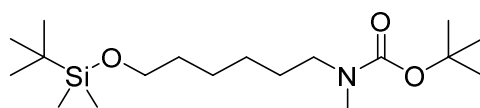
chromatography (TLC) (1:3 EtOAc: Pet. Spirits) and visualised using ninhydrin stain. The reaction was concentrated *in vacuo* and, the resultant oil was purified using flash chromatography (1:3 EtOAc: Pet. Spirits) to afford colourless oil in quantitative yields. <sup>1</sup>H NMR (CDCl<sub>3</sub>) δ 4.53 (s, 1H), 3.64 (t, *J* = 6.5 Hz, 2H), 3.12 (m, 2H), 1.64 – 1.20 (m, 18H). <sup>13</sup>C NMR (CDCl<sub>3</sub>) δ 156.2 (C), 81.2 (C), 62.2 (CH<sub>2</sub>), 39.7 (CH<sub>2</sub>), 32.6 (CH<sub>2</sub>), 30.3 (CH<sub>2</sub>), 28.6 (CH<sub>3</sub>), 26.3 (CH<sub>2</sub>), 25.4 (CH<sub>2</sub>).

***tert*-Butyl (6-((*tert*-butyldimethylsilyl)oxy)hexyl)carbamate (33).<sup>10</sup>**



Following a procedure by Thuring *et al.*,<sup>10</sup> *tert*-Butyl (6-hydroxyhexyl)carbamate (3.98 g, 18.3 mmol) was taken up in DCM (30 mL) and cooled to 0 °C. Imidazole (1.62 g, 23.8 mmol) was then added to the cooled mixture and left to stir at 0 °C until it had completely dissolved. The reaction mixture was left to stir and warm to rt for 25 min before the reaction mixture was again cooled to 0 °C. At this point, TBS-Cl (3.04 g, 20.2 mmol) was taken up in DCM (30 mL) and added dropwise to the reaction over 20 min. The reaction was then left on ice to slowly warm to rt overnight. Once the TLC (1:2 EtOAc: Pet. Spirits) confirmed the consumption of the starting material, the reaction was filtered under vacuum and the filtrate was then washed with 1 M HCl (2 × 25 mL) and brine (30 mL), dried over anhydrous Na<sub>2</sub>SO<sub>4</sub> and concentrated *in vacuo*. This resulted in a yellow oil in good yield (5.42 g, 89%). <sup>1</sup>H NMR (CDCl<sub>3</sub>) δ 4.49 (br s, 1H), 3.59 (t, *J* = 6.5 Hz, 2H), 3.10 (dd, *J* = 13.0, 6.5 Hz, 2H), 1.62 – 1.41 (m, 13H), 1.38 – 1.22 (m, 4H), 0.89 (s, 9H), 0.04 (s, 6H). <sup>13</sup>C NMR (CDCl<sub>3</sub>) δ 156.2 (C), 79.0 (C), 62.6 (CH<sub>2</sub>), 39.8 (CH<sub>2</sub>), 33.0 (CH<sub>2</sub>), 29.8 (CH<sub>2</sub>), 28.4 (CH<sub>3</sub>), 26.4 (CH<sub>2</sub>), 26.0 (CH<sub>3</sub>), 25.5 (CH<sub>2</sub>), 18.4 (C), 5.26 (CH<sub>3</sub>).

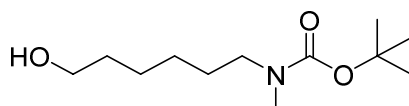
***tert*-Butyl (6-((*tert*-butyldimethylsilyl)oxy)hexyl)(methyl)carbamate (34).<sup>10</sup>**



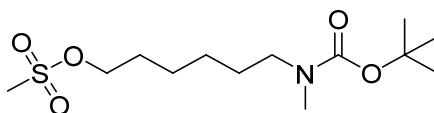
Following the method described by Thuring *et al.*,<sup>10</sup> NaH (60% dispersion in mineral oil) (3.27 g, 81.7 mmol) was added portion-wise to a solution of *tert*-butyl (6-((*tert*-butyldimethylsilyl)oxy)hexyl)carbamate (5.42 g, 16.4 mmol) in anhydrous THF (100 mL) which was cooled to 0 °C and maintained at this temperature as it stirred for 30 min. MeI (3.05 mL, 49.0 mmol) was then added drop-wise at 0 °C and allowed to warm to rt as it stirred for 22 h. Upon

completion of the reaction, sat. NH<sub>4</sub>Cl was added drop-wise to the reaction mixture at 0 °C and stirred for 30 min. The resultant mixture was filtered under vacuum and the filtrate was extracted using *tert*-butyl methyl ether (3 × 50 mL). The combined organic phases were washed with brine, dried over anhydrous Na<sub>2</sub>SO<sub>4</sub>, and concentrated under vacuum. The resultant residue was then purified via flash chromatography (1:9 EtOAc: Pet. Spirits) which yielded the product in respectable yields (4.06 g, 72%). <sup>1</sup>H NMR (CDCl<sub>3</sub>) δ 3.59 (t, *J* = 6.6 Hz, 2H), 3.18 (s, 2H), 2.82 (s, 3H), 1.55 – 1.41 (m, 13H), 1.38 – 1.17 (m, 4H), 0.89 (s, 9H), 0.04 (s, 6H). <sup>13</sup>C NMR (CDCl<sub>3</sub>) δ 78.9 (C), 62.5 (CH<sub>2</sub>), 48.7 (CH<sub>2</sub>), 34.1 (CH<sub>3</sub>), 32.6 (CH<sub>2</sub>), 28.5 (CH<sub>3</sub>), 26.5 (CH<sub>2</sub>), 26.0 (CH<sub>3</sub>), 25.6 (CH<sub>2</sub>), 18.4 (C), 5.30 (CH<sub>3</sub>). NOTE: One quaternary carbon signal could not be visualised due to signal broadening.

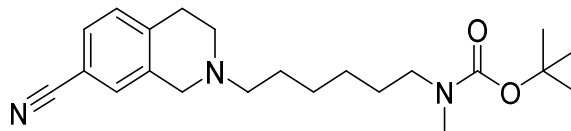
***tert*-Butyl (6-hydroxyhexyl)(methyl)carbamate (35).<sup>10</sup>**



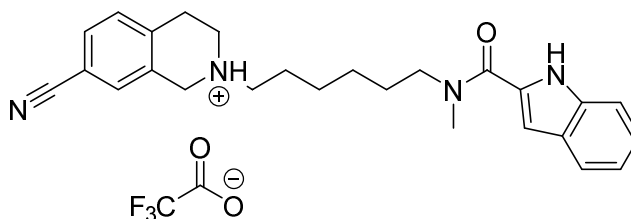
Using a method described by Thuring *et al.*,<sup>10</sup> a solution of 1 M TBAF in THF (36.2 mL, 36.2 mmol) was added in a drop-wise fashion to a solution of *tert*-butyl (6-((*tert*-butyldimethylsilyl)oxy)hexyl)(methyl)carbamate (4.06 g, 11.6 mmol) in THF (80 mL) at 0 °C and the reaction was left to slowly warm to rt whilst stirring overnight. Upon completion of the reaction, the mixture was concentrated *in vacuo* to remove the organic solvent. Ice- water was then added to the residue and the mixture was stirred for 1 h. Cold Pet. Spirits (50 mL, -20 °C) was then added to the reaction mixture and the resultant precipitate was filtered off and discarded. The aqueous layer was separated from the organic layer, and the product was extracted from the aqueous layer with Pet. Spirits (3 × 50 mL). The organic phases were combined, dried over anhydrous Na<sub>2</sub>SO<sub>4</sub> and concentrated *in vacuo*. The resultant product was then purified using flash chromatography (1:1 EtOAc: Pet. Spirits) to garner the product as an oil (2.06 g, 77%). <sup>1</sup>H NMR (CDCl<sub>3</sub>) δ 3.64 (s, 2H), 3.20 (s, 2H), 2.83 (s, 3H), 1.63 – 1.14 (m, 18H). <sup>13</sup>C NMR (CDCl<sub>3</sub>) δ 156.1 (C), 79.3 (C), 62.79\* (CH<sub>2</sub>), 48.5\* (CH<sub>2</sub>), 34.2 (CH<sub>3</sub>), 32.8 (CH<sub>2</sub>), 28.6 (CH<sub>3</sub>), 27.8\* (CH<sub>2</sub>), 26.4\* (CH<sub>2</sub>), 25.4\* (CH<sub>2</sub>). Note: (\*) denotes rotameric signals present in the <sup>13</sup>C NMR spectrum of this compound.

**6-((*tert*-Butoxycarbonyl)(methyl)amino)hexyl methanesulfonate (36).**

*tert*-Butyl (6-hydroxyhexyl)(methyl)carbamate (469 mg, 2.03 mmol) and trimethylamine (TEA) (849  $\mu$ L, 6.08 mmol) was added to an rbf containing DCM (30 mL) and cooled to 0 °C whilst stirring. MsCl (179  $\mu$ L, 2.03 mmol) was then added slowly and the reaction was stirred at 0 °C for 30 min. The reaction was then warmed to rt and left to stir overnight. The reaction mixture was subsequently diluted with DCM (50 mL), washed with H<sub>2</sub>O (3  $\times$  50 mL) and dried over anhydrous Na<sub>2</sub>SO<sub>4</sub>, filtered and dried *in vacuo* to yield yellow oil. The product was used in subsequent reactions without any further purification or characterisation due to instability.

***tert*-Butyl (6-(7-cyano-3,4-dihydroisoquinolin-2(1*H*)-yl)hexyl)(methyl)carbamate (37).**

To an rbf containing 6-((*tert*-butoxycarbonyl)(methyl)amino)hexyl methanesulfonate (627 mg, 2.03 mmol), 1,2,3,4-tetrahydroisoquinoline-7-carbonitrile (481 mg, 3.04 mmol), K<sub>2</sub>CO<sub>3</sub> (841 mg, 6.0 mmol) and MeCN (30 mL) were added. The reaction mixture was stirred at rt overnight. The mixture was concentrated *in vacuo* and purified using flash chromatography (3:97 MeOH: DCM) to obtain the title compound in low yields (103 mg, 14%). <sup>1</sup>H NMR (298 K, *d*<sub>6</sub>-DMSO)  $\delta$  7.60 – 7.45 (m, 2H), 7.34 – 7.19 (m, 1H), 3.54 (s, 2H), 3.12 (t, *J* = 7.1 Hz, 2H), 2.85 (t, *J* = 5.7 Hz, 2H), 2.73 (s, *J* = 9.4 Hz, 3H), 2.62 (t, *J* = 5.9 Hz, 2H), 2.49 (m, 2H), 2.45 – 2.39 (m, 2H), 1.46 – 1.21 (m, 15H). <sup>13</sup>C NMR (CDCl<sub>3</sub>)  $\delta$  155.8 (C), 140.4 (C), 136.4 (C), 130.4 (CH), 129.6 (CH), 129.5 (CH), 119.1 (C), 109.3 (C), 79.1 (C), 58.2 (CH<sub>2</sub>), 55.6 (CH<sub>2</sub>), 50.3 (CH<sub>2</sub>), 34.1 (CH<sub>3</sub>), 29.4 (CH<sub>2</sub>), 28.5 (CH<sub>3</sub>), 27.2 (CH<sub>2</sub>), 26.6 (CH<sub>2</sub>).

**7-Cyano-2-(6-(*N*-methyl-1*H*-indole-2-carboxamido)hexyl)-1,2,3,4-tetrahydroisoquinolin-2-ium 2,2,2-trifluoroacetate (39).**

Using *tert*-butyl (6-(7-cyano-3,4-dihydroisoquinolin-2(1*H*)-yl)hexyl)(methyl)carbamate as the protected amine, general procedure B was followed to yield the title compound in quantitative yields (99.2 mg). The corresponding mass was observed via LCMS and was carried through to the subsequent reaction without further purification or characterisation. LCMS ( $m/z$ ):  $[M+H]^+$  found 272.2. Next, using the synthesised amine and 1*H*-indole-2-carboxylic acid (58.9 mg, 365  $\mu$ mol), general procedure C was followed. The resultant solid was then purified via preparative HPLC. This afforded the product as the TFA salt in respectable yields (31.9 mg, 21%). <sup>1</sup>H NMR (CDCl<sub>3</sub>)  $\delta$  9.45 (s, 1H), 7.64 (dd,  $J = 8.0, 0.7$  Hz, 1H), 7.39 (ddd,  $J = 19.9, 8.1, 1.1$  Hz, 2H), 7.30 – 7.26 (m, 2H), 7.17 – 7.08 (m, 2H), 6.81 (s, 1H), 3.67 (s, 2H), 3.58 (s, 2H), 3.31 (s, 3H), 2.91 (t,  $J = 5.8$  Hz, 2H), 2.70 (t,  $J = 5.9$  Hz, 2H), 2.54 – 2.44 (m, 2H), 1.80 – 1.52 (m, 4H), 1.51 – 1.38 (m, 4H). <sup>13</sup>C NMR (CDCl<sub>3</sub>)  $\delta$  160.4 (C), 140.4 (C), 136.4 (C), 135.5 (C), 135.4 (C), 130.4 (CH), 129.6 (CH), 129.5 (CH), 127.9 (C), 124.4 (CH), 122.0 (CH), 120.4 (CH), 119.2 (C), 111.8 (CH), 109.3 (C), 58.1 (CH<sub>2</sub>), 55.6 (CH<sub>2</sub>), 50.2 (CH<sub>2</sub>), 31.9 (CH<sub>2</sub>), 29.7 (CH<sub>2</sub>), 29.5 (CH<sub>2</sub>), 27.3 (CH<sub>2</sub>), 27.1 (CH<sub>2</sub>), 26.8 (CH<sub>2</sub>). Note: One methylene and one methine signal could not be observed in the carbon spectrum due to signal broadening. HPLC:  $t_R$  5.00 min, >95% purity. HRMS ( $m/z$ ): C<sub>26</sub>H<sub>31</sub>N<sub>4</sub>O requires  $[M+H]^+$  415.2492; found 415.2495.

**Pharmacology.**

**Cell Lines and Transfection.** FlpIn CHO cells stably expressing the wild-type D<sub>2</sub>L<sub>R</sub> were transfected and maintained in the conditions stated by Shonberg *et al.*<sup>5</sup>

**ERK1/2 Phosphorylation Assay.** This assay was performed following the protocol as described by Shonberg *et al.*<sup>5</sup>

**Data Analysis.** A logistic equation of competitive agonist-antagonist interaction was fitted globally to data from functional experiments measuring the interaction between dopamine and all analogues of **1**:

$$response = bottom + \frac{(E_{max} - bottom)}{1 + \left( \frac{10^{-pEC_{50}} \left[ 1 + \left( \frac{[B]}{10^{-pA_2}} \right)^s \right]}{[A]} \right)^{nH}} \quad (1)$$

where  $s$  represents the Schild slope for the antagonist and  $pA_2$  represents the negative logarithm of the molar concentration of the antagonist at which double the concentration of the agonist is needed to elicit the original submaximal response obtained in the absence of the antagonist.

Functional data describing the interaction between all analogues of **1** (with the exception of **15e** and **39**) and dopamine are analysed according to a derivation of the allosteric ternary complex model (2):

$$E = \frac{E_m [A]^{nH}}{[A]^{nH} + [EC_{50}]^{nH} \left( \frac{1 + \frac{[B]}{K_B}}{1 + \frac{\alpha\beta[B]}{K_B}} \right)} \quad (2)$$

where  $E_m$  is the maximal cellular response possible,  $[A]$  and  $[B]$  are the concentrations of orthosteric and allosteric ligands, respectively,  $K_B$  is the equilibrium dissociation constant of the orthosteric and allosteric ligands,  $\alpha\beta$  is the composite cooperativity parameter between orthosteric and allosteric ligands that includes effects upon the affinity and efficacy of the orthosteric ligand,

and nH is the Hill slope of the orthosteric agonist concentration-response curves. Values of  $\alpha$  and/or  $\beta$  greater than 1 denote allosteric potentiation, whereas values less than 1 (but greater than 0) denote allosteric inhibition.

Functional data describing the interaction between **15e** and **39** and dopamine at the D<sub>2</sub>R in a pERK1/2 assay were analyzed using a complete operational model of allostery and agonism according to equation 3:<sup>11</sup>

$$E = \frac{E_m (\tau_A [A] (K_B + \alpha \beta [B]) + \tau_B [B] K_A)^{nH}}{([A] K_B + K_A K_B + K_A [B] + \alpha [A] [B])^{nH} + (\tau_A [A] (K_B + \alpha \beta [B]) + \tau_B [B] K_A)^{nH}} \quad (3)$$

where  $E_m$  is the maximum possible cellular response,  $[A]$  and  $[B]$  are the concentrations of orthosteric and allosteric ligands, respectively,  $K_A$  and  $K_B$  are the equilibrium dissociation constant of the orthosteric and allosteric ligands, respectively, and  $\tau_B$  (constrained to -100) are operational measures of orthosteric and allosteric ligand efficacy (which incorporate both signal efficiency and receptor density), respectively,  $\alpha$  is the binding cooperativity parameter between the orthosteric and allosteric ligand, and  $\beta$  denotes the magnitude of the allosteric effect of the modulator on the efficacy of the orthosteric agonist.  $K_A$  was constrained to 11 nM and represents a value of functional affinity determined by an operational model of partial agonism to dose-response data of dopamine (a partial agonist) and apomorphine (a full agonist) in an pERK1/2 assay).  $\text{Log}\tau_A$  was determined as  $0.74 \pm 0.07$ .

### 3.6 References

1. Kopinathan, A.; Scammells, P. J.; Lane, J. R.; Capuano, B. Multivalent approaches and beyond: novel tools for the investigation of dopamine D<sub>2</sub> receptor pharmacology. *Future Med. Chem.* **2016**, *8*, 1349-1372.
2. Rossi, M.; Fasciani, I.; Marampon, F.; Maggio, R.; Scarselli, M. The First Negative Allosteric Modulator for Dopamine D<sub>2</sub> and D<sub>3</sub> Receptors SB269652 May Lead to a New Generation of Antipsychotic Drugs. *Mol. Pharmacol.* **2017**, *91*, 586-594.
3. Seeman, P. Targeting the dopamine D<sub>2</sub> receptor in schizophrenia. *Expert Opin. Ther. Targets* **2006**, *10*, 515-531.
4. De Hert, M.; Detraux, J.; van Winkel, R.; Yu, W.; Correll, C. U. Metabolic and cardiovascular adverse effects associated with antipsychotic drugs. *Nat. Rev. Endocrinol.* **2012**, *8*, 114-126.
5. Shonberg, J.; Draper-Joyce, C.; Mistry, S. N.; Christopoulos, A.; Scammells, P. J.; Lane, J. R.; Capuano, B. Structure–Activity Study of *N*-((*trans*)-4-(2-(7-Cyano-3,4-dihydroisoquinolin-2(1*H*)-yl)ethyl)cyclohexyl)-1*H*-indole-2-carboxamide (SB269652), a Bitopic Ligand That Acts as a Negative Allosteric Modulator of the Dopamine D<sub>2</sub> Receptor. *J. Med. Chem.* **2015**, *58*, 5287-5307.
6. Silvano, E.; Millan, M. J.; Mannoury la Cour, C.; Han, Y.; Duan, L.; Griffin, S. A.; Luedtke, R. R.; Aloisi, G.; Rossi, M.; Zazzeroni, F.; Javitch, J. A.; Maggio, R. The tetrahydroisoquinoline derivative SB269,652 is an allosteric antagonist at dopamine D<sub>3</sub> and D<sub>2</sub> receptors. *Mol. Pharmacol.* **2010**, *78*, 925-934.
7. Stemp, G.; Ashmeade, T.; Branch, C. L.; Hadley, M. S.; Hunter, A. J.; Johnson, C. N.; Nash, D. J.; Thewlis, K. M.; Vong, A. K. K.; Austin, N. E.; Jeffrey, P.; Avenell, K. Y.; Boyfield, I.; Hagan, J. J.; Middlemiss, D. N.; Reavill, C.; Riley, G. J.; Routledge, C.; Wood, M. Design and synthesis of *trans-N*-[4-[2-(6-cyano-1,2,3,4-tetrahydroisoquinolin-2-yl)ethyl]cyclohexyl]-4-quinolinecarboxamide (SB-277011): A potent and selective dopamine D-3 receptor antagonist with high oral bioavailability and CNS penetration in the rat. *J. Med. Chem.* **2000**, *43*, 1878-1885.
8. Lane, J. R.; Donthamsetti, P.; Shonberg, J.; Draper-Joyce, C. J.; Dentry, S.; Michino, M.; Shi, L.; Lopez, L.; Scammells, P. J.; Capuano, B.; Sexton, P. M.; Javitch, J. A.; Christopoulos, A. A new mechanism of allostery in a G protein-coupled receptor dimer. *Nat. Chem. Biol.* **2014**, *10*, 745-752.
9. Ballesteros, J. A.; Weinstein, H. [19] Integrated methods for the construction of three-dimensional models and computational probing of structure-function relations in G

- protein-coupled receptors. In *Methods in Neurosciences*, Stuart, C. S., Ed. Academic Press: 1995; Vol. Volume 25, pp 366-428.
10. Thuring, J. W. J.; Bonfanti, J. F. Macrocyclic integrase inhibitors. US20130035341 A1, 2013.
  11. Leach, K.; Sexton, P. M.; Christopoulos, A. Allosteric GPCR modulators: taking advantage of permissive receptor pharmacology. *Trends Pharmacol. Sci.* **2007**, 28, 382-389.
  12. Christopoulos, A. Assessing the distribution of parameters in models of ligand-receptor interaction: to log or not to log. *Trends Pharmacol. Sci.* **1998**, 19, 351-357.
  13. Mistry, S. N.; Shonberg, J.; Draper-Joyce, C. J.; Klein Herenbrink, C.; Michino, M.; Shi, L.; Christopoulos, A.; Capuano, B.; Scammells, P. J.; Lane, J. R. Discovery of a Novel Class of Negative Allosteric Modulator of the Dopamine D<sub>2</sub> Receptor Through Fragmentation of a Bitopic Ligand. *J. Med. Chem.* **2015**, 58, 6819-6843.
  14. Tung, Y. S.; Coumar, M. S.; Wu, Y. S.; Shiao, H. Y.; Chang, J. Y.; Liou, J. P.; Shukla, P.; Chang, C. W.; Chang, C. Y.; Kuo, C. C.; Yeh, T. K.; Lin, C. Y.; Wu, J. S.; Wu, S. Y.; Liao, C. C.; Hsieh, H. P. Scaffold-hopping strategy: synthesis and biological evaluation of 5,6-fused bicyclic heteroaromatics to identify orally bioavailable anticancer agents. *J. Med. Chem.* **2011**, 54, 3076-3080.
  15. Charlton, S. J.; Vauquelin, G. Elusive equilibrium: the challenge of interpreting receptor pharmacology using calcium assays. *Br. J. Pharmacol.* **2010**, 161, 1250-1265.
  16. Mould, R.; Brown, J.; Marshall, F. H.; Langmead, C. J. Binding kinetics differentiates functional antagonism of orexin-2 receptor ligands. *Br. J. Pharmacol.* **2014**, 171, 351-363.
  17. Szabo, M.; Klein Herenbrink, C.; Christopoulos, A.; Lane, J. R.; Capuano, B. Structure–Activity Relationships of Privileged Structures Lead to the Discovery of Novel Biased Ligands at the Dopamine D<sub>2</sub> Receptor. *J. Med. Chem.* **2014**, 57, 4924-4939.
  18. Asaki, T.; Hamamoto, T.; Sugiyama, Y.; Kuwano, K.; Kuwabara, K. Structure-activity studies on diphenylpyrazine derivatives: a novel class of prostacyclin receptor agonists. *Bioorg. Med. Chem.* **2007**, 15, 6692-6704.
  19. Das, B.; Reddy, K. R.; Thirupathi, P. A simple, efficient and highly selective deprotection of t-butyldimethylsilyl (TBDMS) ethers using silica supported sodium hydrogen sulfate as a heterogeneous catalyst. *Tetrahedron Lett.* **2006**, 47, 5855-5857.
  20. Muth, A.; Kamel, J.; Kaur, N.; Shicora, A. C.; Ayene, I. S.; Gilmour, S. K.; Phanstiel, O. T. Development of polyamine transport ligands with improved metabolic stability and selectivity against specific human cancers. *J. Med. Chem.* **2013**, 56, 5819-5828.

21. Mokrosz, J. L.; Dereń-Wesołek, A.; Tatarczyńska, E.; Duszyńska, B.; Bojarski, A. J.; Mokrosz, M. J.; Chojnacka-Wójcik, E. 8-[4-[2-(1,2,3,4-Tetrahydroisoquinolinyl)]butyl]-8-azaspiro[4.5]decane-7,9-dione: A New 5-HT<sub>1A</sub> Receptor Ligand with the Same Activity Profile as Buspirone. *J. Med. Chem.* **1996**, 39, 1125-1129.

---

---

## **Chapter 4**

# **Probing Receptor-Ligand Interactions at the Dopamine D<sub>2</sub> Receptor**

---

---

**The Development of a Photoactivatable Bitopic Negative Allosteric  
Modulator for the Dopamine D<sub>2</sub> Receptor**

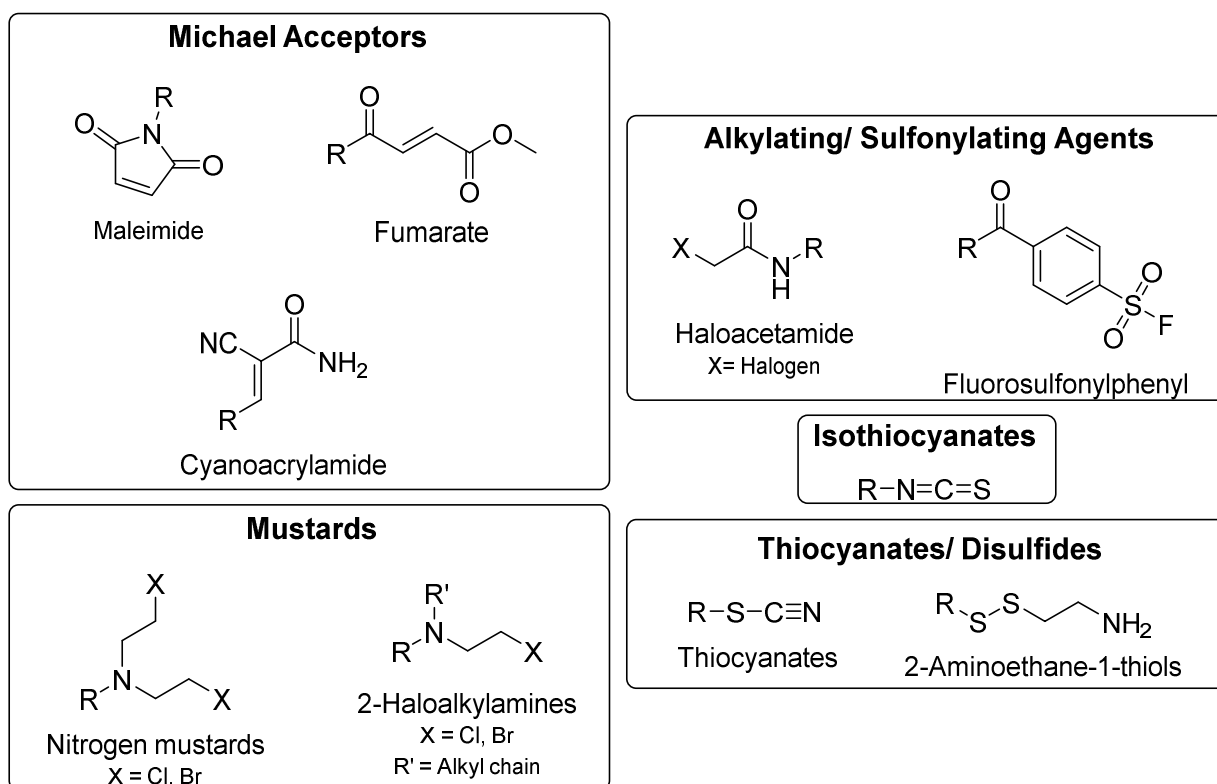
## 4.1 Introduction

G protein-coupled receptors (GPCRs) are the largest family of cell-surface signalling molecules found within the human genome and are involved in a plethora of physiological processes.<sup>1</sup> Despite recent advancements in our knowledge and understanding of GPCRs, the development of novel, high affinity GPCR-targeting molecules is often hampered by the lack of structural and functional information. Consequently, there is still a need for pharmacological tools to probe poorly understood, existing and novel, receptor targets.<sup>2</sup> Ligand-bound X-ray structures often provide invaluable insight into the binding site of a ligand, and thus, provide a strong platform from which bioactive molecules may be rationally designed. However, the X-ray structures of ligand-bound GPCRs are limited due to their low receptor expression levels in native tissue, their inherent flexibility and instability upon their extraction from the membrane, and the low affinity of their endogenous ligands.<sup>2-4</sup>

Irreversible (also known as covalent or affinity) probes are useful tools for the study of receptor-ligand interactions and pharmacology. They are generally molecules which bind a specific target and have the ability to form a covalent bond at, or near, the binding site. The inability of these ligands to dissociate from the targeted binding site provides insight into the structure and function of GPCRs using a variety of techniques. From a drug discovery perspective, this makes the development of irreversible probes a particularly attractive prospect which may aid rational drug design.<sup>2</sup> Whilst from a pharmacological perspective, irreversible probes also provide an opportunity to gain insights into key receptor-ligand interactions which may elicit specific pharmacological functions. There are two common classes of irreversible probes; chemoreactive or photoactivatable.

Chemoreactive probes possess a reactive electrophilic moiety which is able to react covalently with a nucleophilic amino acid residue, but are stable enough to avoid reactivity with water or other nucleophilic moieties within solution.<sup>4</sup> Common chemoreactive moieties include Michael acceptors,<sup>5,6</sup> alkylating and sulfonylating agents,<sup>7,8</sup> mustards,<sup>9</sup> isothiocyanates,<sup>10</sup> disulfides and thiocyanates (Figure 1).<sup>11,12</sup> Chemoreactive probes are often seen to be advantageous as tools for both *in vitro* and *in vivo* applications, since their reactive groups are able to form a covalent bond with a nucleophilic amino acid residue without the need for irradiation. The synthesis of these probes, however, can be complex since synthetic procedures must be devised in a manner such that the reactive functional group is installed in the final synthetic steps to avoid cross-reactivity. It is also worth noting that some chemoreactive groups may form reversible covalent bonds under specific conditions that may not be predicted until after the chemoreactive probes are evaluated in a biological setting.<sup>13</sup> Nonetheless,

chemoreactive probes have been utilised in the structural and functional investigations of a variety of GPCRs including the dopamine D<sub>2</sub> receptor (D<sub>2</sub>R), a validated target for the treatment of CNS disorders such as schizophrenia and Parkinson's disease. For example, the development of fluphenazine-*N*-mustard enabled the study of the functional and behavioural effects of D<sub>2</sub>R blockade and its effects on calmodulin activity.<sup>14,15</sup> Similarly, *N*-(*p*-isothiocyanatophenethyl)piperone (NIPS), phenoxybenzamine and *N*-ethoxycarbonyl-2-ethoxy-1,2-dihydroquinoline (EEDQ) have been widely used for the investigation of D<sub>2</sub>R function in both *in vitro* and *in vivo* settings.<sup>16-19</sup> More recently, chemoreactive probes have also been developed to study GPCR receptor activation containing a disulfide moiety which may cross-link with a mutated cysteine residue in close proximity and have facilitated the crystallisation of the first agonist-bound crystal structure of a GPCR.<sup>20</sup> This strategy has enabled the development of slow dissociating covalent neurotransmitter analogues that may act as tools to facilitate crystallisation of other GPCRs such as the D<sub>2</sub>R.<sup>4,20</sup>

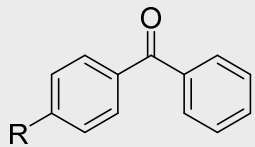
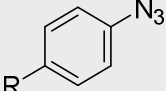


**Figure 1.** Common chemoreactive functional groups.

In contrast, photoactivatable (or, photoaffinity) probes contain a photoreactive functional group that is capable of forming a reactive species (e.g. carbene, nitrene or diradical) upon electronic excitation at a specific wavelength of ultraviolet (UV) light. The reactive species is

then able to rapidly react with a neighbouring residue in close proximity.<sup>21</sup> Unlike their chemoreactive counterparts, photoactivatable probes offer temporal control over reactivity. For example, the receptor may be pre-treated with the “ground-state” ligand and, upon equilibration, irradiated in order to enhance the probability of capturing the receptor-ligand complex of interest. However, like their chemoreactive counterparts, in order to ensure that the binding site of interest is selectively “captured”, photoactivatable probes require a similar affinity and pharmacological profile to that of their parent scaffolds.<sup>22</sup> Since their ability to form an irreversible covalent bond is dependent upon UV irradiation, photoactivatable probes have greater synthetic tractability compared to chemoreactive probes. Common photoreactive moieties which are often employed in the development of photoactivatable probes include; benzophenones, diazirines, and aryl azides (Table 1).<sup>23,24</sup> Of these functionalities, the benzophenones are the most chemically stable and undergo photoactivation at a wavelength of 350–360 nm. Although benzophenones have a high cross-linking efficiency, their bulk may result in less accurate indication of the parent ligand-receptor interaction. Alternatively, if steric clashes are likely to result within the binding pocket, diazirines or aryl azides might be considered an attractive prospect due to their size. Diazirines, which photoactivate at 350–380 nm, are particularly beneficial in instances where a high probability of non-specific reactivity is anticipated due to its low cross-linking efficiency. The difficulty and time-consuming nature of their synthesis, however, poses a major drawback for their use. In contrast, aryl azides are more accessible synthetically, but require irradiation at wavelengths of 250–350 nm which may cause non-specific damage to the biological system being tested.<sup>21,25</sup> However, for the purposes of preliminary evaluations (e.g. in an *in vitro* setting where low wavelength irradiation would be considered less of a concern), the aryl azides provide an ideal starting point for the development of irreversible ligands.

**Table 1.** Common photoactivatable functional groups, required photoactivation wavelengths and advantages or disadvantages of their use.

Functional Group	Photoactivation ( $\lambda$ , nm)	Advantages/Disadvantages
 Benzophenone	350–360	<ul style="list-style-type: none"> <li>➤ Chemically stable</li> <li>➤ High cross-linking efficiency</li> <li>➤ Bulky</li> </ul>
 Diazirine	350–380	<ul style="list-style-type: none"> <li>➤ Small functional group</li> <li>➤ Low cross-linking efficiency</li> <li>➤ Synthetically complicated</li> </ul>
 Aryl azide	250–350	<ul style="list-style-type: none"> <li>➤ Small functional group</li> <li>➤ Synthetically accessible</li> <li>➤ Non-specific tissue damage</li> </ul>

To date, photoactivatable probes have assisted in the identification and characterisation of ligand binding sites,<sup>26,27</sup> provided preliminary evidence of receptor dimerisation,<sup>28</sup> and even facilitated receptor purification, which, in turn, aided GPCR crystallisation.<sup>29</sup> Given that the D<sub>2</sub>R is strongly implicated in CNS disorders such as schizophrenia and Parkinson's disease, the development of D<sub>2</sub>R photoactivatable probes has enabled us to further our knowledge of this receptor in a variety of tissue.<sup>30-32</sup> Dopamine was found to be a native photoactivatable ligand by Nishikori and colleagues in the 1980s.<sup>33</sup> They observed that UV illumination of mammalian nervous tissue in the presence of dopamine led to the covalent attachment of dopamine to specific cellular proteins. Although dopamine does not contain a traditional photoactivatable moiety, Nishikori *et al.* proposed that covalent bond formation occurred via radical formation of an oxygen in the catechol moiety of dopamine which could then cross-link with an amino acid residue within close proximity.<sup>33</sup> Using this discovery, Nishikori and colleagues applied [<sup>3</sup>H]dopamine to mammalian nervous tissue and discovered that not only were they able to observe that D<sub>1</sub> and D<sub>2</sub>-type receptors were co-expressed, but they were also able to quantitate the amount of each receptor subtype present. Photoactivatable ligands for the investigation of D<sub>2</sub>Rs have generally incorporated an azide moiety within the structure of the parent molecule (Figure 2). The first selective photoactivatable ligand for the D<sub>2</sub>R, an azido derivative of the

orthosteric antagonist clebropride, was developed by Niznik *et al.* and was shown to inhibit [<sup>3</sup>H]spiperone binding in human striatal membranes.<sup>30, 31</sup> Subsequent, replacement of the 5-chloro substituent of **1** with radioactive <sup>125</sup>I (**2**) also led to a D<sub>2</sub>R-selective photoactivatable ligand with high specific radioactivity.<sup>34, 35</sup> Other orthosterically-binding azide photoactivatable ligands developed used for the investigation of the D<sub>2</sub>R include azidohaloperidol (**3**),<sup>36</sup> azidosulpride (**4**)<sup>37</sup> and azidomethylspiperone (**5**) (Figure 2).<sup>38</sup> Besides the highly conserved orthosteric binding site which has been thoroughly investigated, there is evidence to suggest that the D<sub>2</sub>R also possesses a topographically distinct allosteric binding site.<sup>39-45</sup> Although a number of extended D<sub>2</sub>R structures have been hypothesised to interact with this secondary binding site, our knowledge about the precise location and structure of this site, and the interactions made within it upon binding, is still in its infancy. Thus, the development of photoactivatable ligands with the ability to probe this putative allosteric site at the D<sub>2</sub>R may be able to significantly enhance our current understanding.

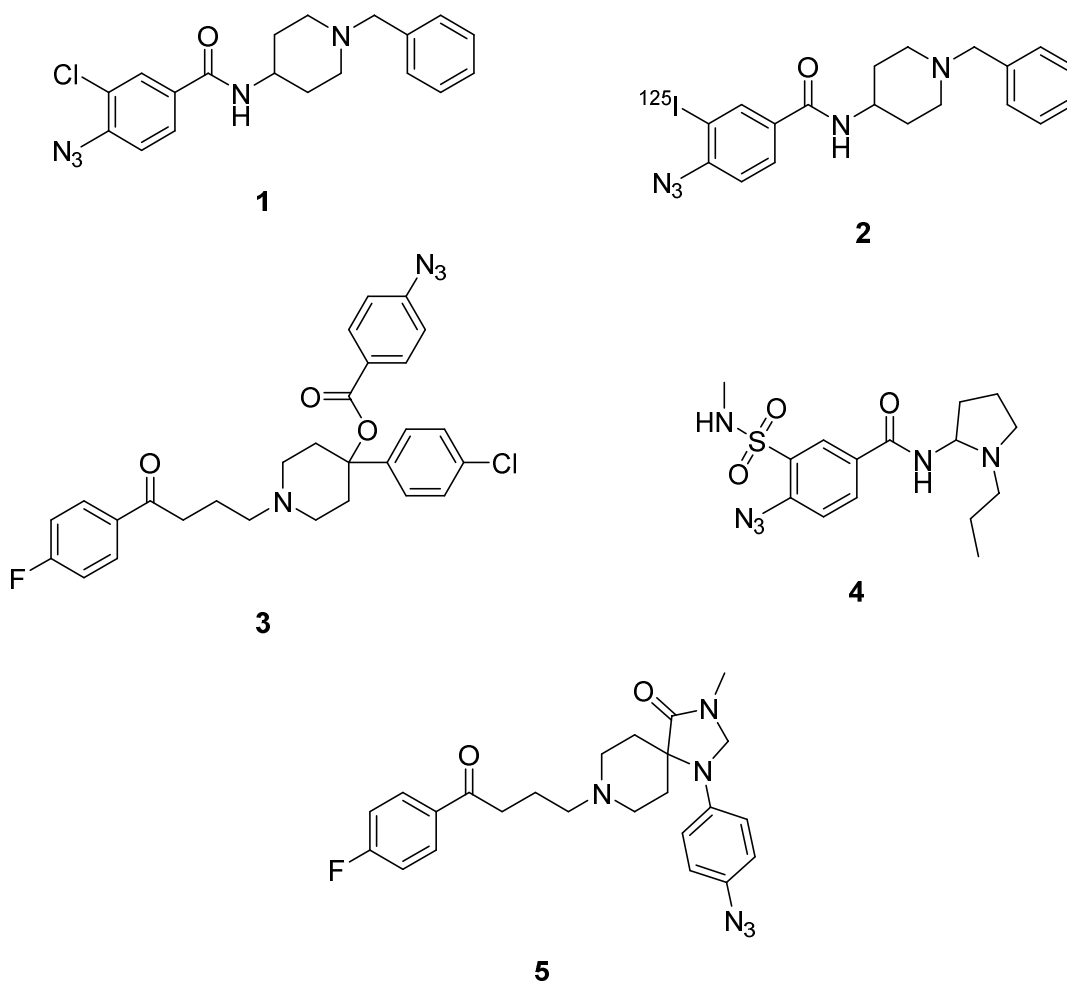


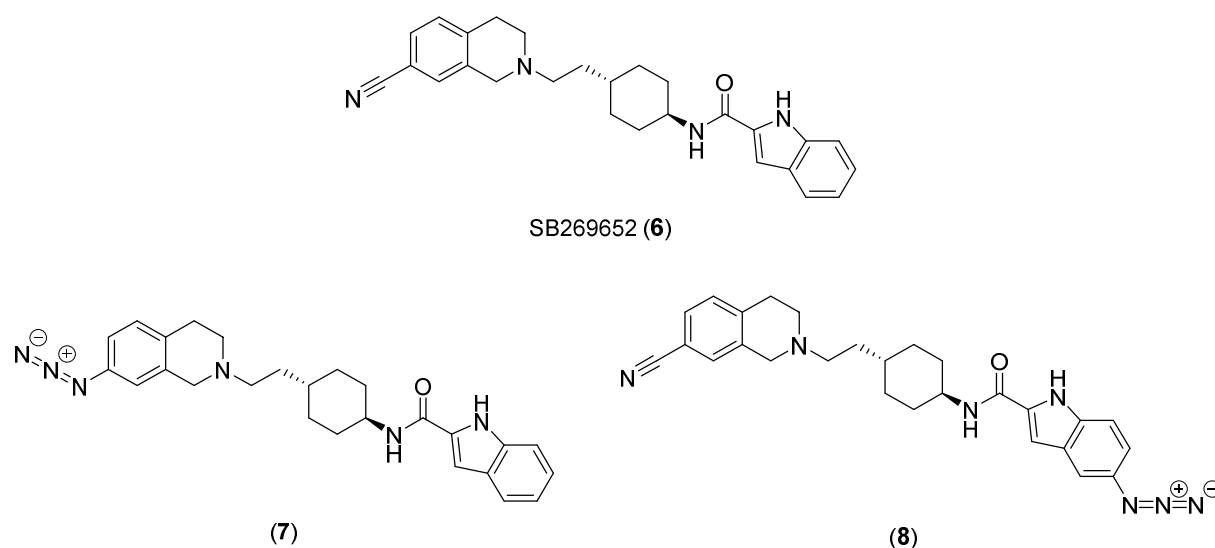
**Figure 2.** Photoactivatable probes developed for the investigation of the D<sub>2</sub>R.

To further our understanding of secondary binding interactions at the D<sub>2</sub>R, we chose to develop a small series of photoactivatable ligands based on the first drug-like allosteric modulator to be described in the literature, namely, SB269652 (**6**) (Figure 3). Aside from being an allosteric modulator, Lane *et al.* discovered that **6** bound the D<sub>2</sub>R in a bitopic fashion (i.e. concomitantly engaging both an orthosteric and allosteric binding site) and was able to modulate the potency of dopamine across a D<sub>2</sub>R homodimer.<sup>45</sup> In addition to this, mutagenesis and molecular modelling studies revealed that the indole-2-carboxamide tail of **6** projected out towards a secondary binding pocket within the extracellular regions of transmembrane helices (TMs) 2 and 7 of the D<sub>2</sub>R. It was also discovered that a key hydrogen bond interaction was being made between E95<sup>2.65</sup> (where superscript numbers refer to Ballesteros-Weinstein nomenclature<sup>46</sup>) and the indolic NH of **6** which was crucial for its modulatory properties.<sup>45</sup> In developing photoactivatable ligands of **6**, we hypothesised that we may be able to synthesise a set of tool compounds that can potentially enhance our understanding of the structure and function of the allosteric binding site of the D<sub>2</sub>R. Additionally, given that **6** is able to engage both the orthosteric

and allosteric binding sites of the D<sub>2</sub>R, it may be envisaged that these tools could have the potential to stabilise a receptor conformation which could, in turn, facilitate its crystallisation.

## 4.2 Synthesis

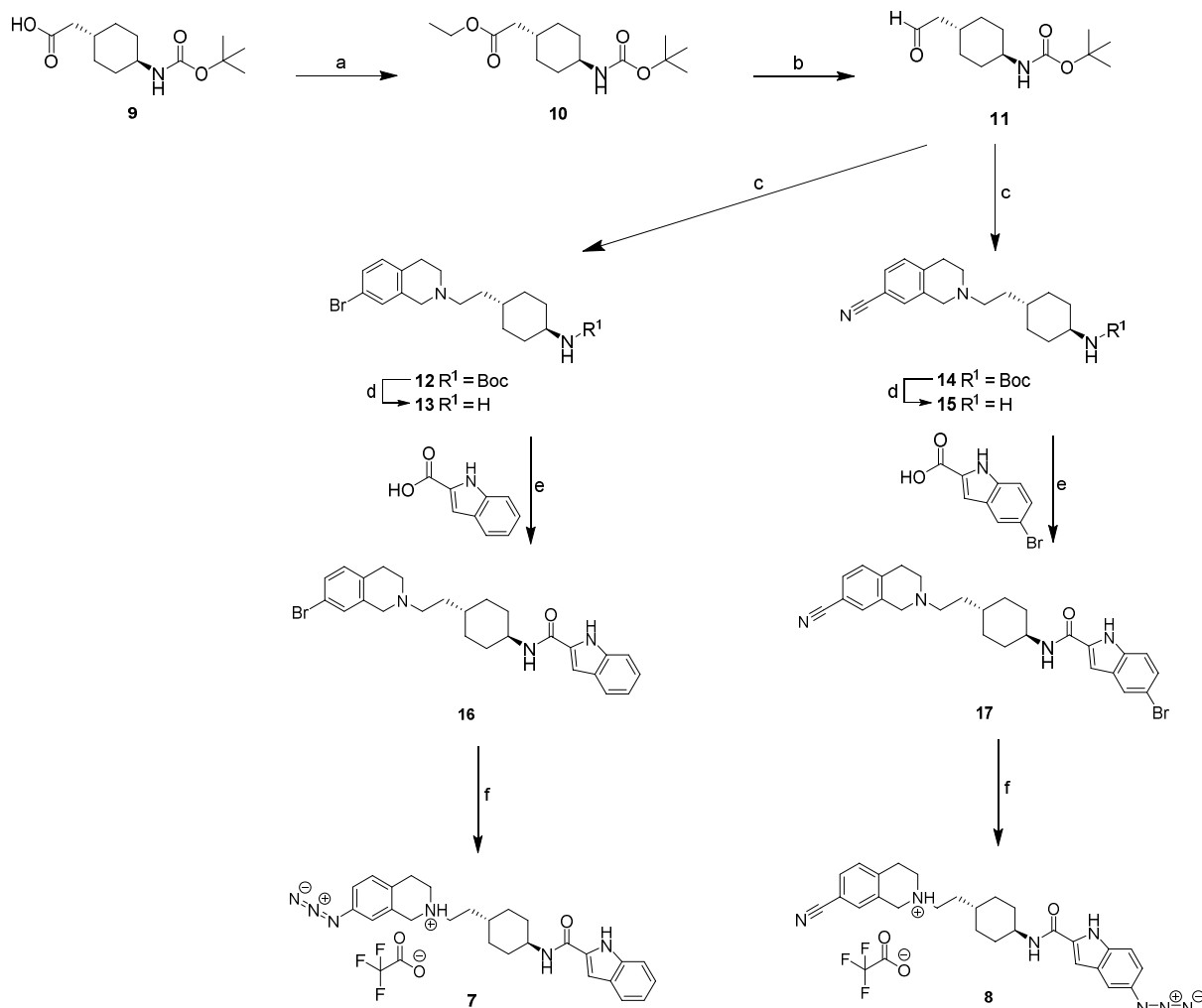
The extensive structure-activity relationship (SAR) analysis of **6** conducted within our group and described in Chapter 3 of this thesis, guided our choice of the azide functionality as our photoactivatable moiety. Two photoactivatable probes consisting of the photoactivatable azide moiety at either the orthosteric head (**7**) or at the allosteric tail (**8**) were designed in order to gain insight into binding interactions at both the orthosteric and allosteric binding sites of the D<sub>2</sub>R (Figure 3). Since small substituents were tolerated at the 7-position of the tetrahydroisoquinoline (THIQ) orthosteric head, the carbonitrile moiety was substituted with that of the azide functionality.<sup>47</sup> Similarly, Chapter 3 demonstrated that electron-withdrawing substituents at the 5-position of the indole ring were well tolerated in terms of maintaining both functional affinity and cooperativity. Hence, the azide was substituted at the 5-position of the indole carboxamide given that it is considered a pseudohalide which has an overall ring deactivating effect despite containing both positive mesomeric and negative inductive effects.<sup>48</sup>



**Figure 3.** The structures of SB269652 (**6**), and the synthesised photoactivatable ligands (**7** and **8**).

The synthesis of **7** and **8** (Scheme 1) followed the synthetic procedures previously outlined in the literature and Chapter 3 to furnish the necessary brominated compounds **16** and **17**.<sup>45, 47</sup> Following the procedure outlined in Lane *et al.*, compound **9** was quantitatively esterified to the ethyl ester (**10**) in the presence of ethyl iodide (EtI) and potassium carbonate

(K<sub>2</sub>CO<sub>3</sub>), and reduced to the corresponding aldehyde (**11**) in the presence of 1 M diisobutylaluminium hydride (DIBAL-H) in anhydrous toluene at -78°C. Reductive amination in the presence of sodium triacetoxyborohydride (NaBH(OAc)<sub>3</sub>) in 1,2-dichloroethane (1,2-DCE) facilitated the attachment of the required 7-substituted tetrahydroisoquinoline to furnish compounds **12** and **14** in 80% yield. Removal of the boc protecting group was carried out using an excess of trifluoroacetic acid (TFA) in DCM and garnered compounds **13** and **15** as the free base following an aqueous base extraction.<sup>45</sup> 1-[Bis(dimethylamino)methylene]-1*H*-1,2,3-triazolo[4,5-*b*]pyridinium 3-oxid hexafluorophosphate (HATU) in the presence of excess base and dry DMF facilitated the amide coupling of the necessary indole-2-carboxamides to **13** and **15** which yielded compounds **16** and **17**, respectively. To install the photoactivatable azide moiety, an azidation procedure described by Andersen *et al.* was employed which converted the aryl bromide compounds (**16** and **17**) into their respective aryl azide derivatives (**7** and **8**) under mild conditions.<sup>49</sup> Although formation of both **7** and **8** progressed in a quantitative fashion, upon reaching approximately 75% conversion, rapid degradation of the product and starting materials was observed. This caused difficulties in the purification of the final aryl azides, and consequently, resulted in the low yields obtained.

**Scheme 1.** Synthesis of phototactivatable ligands **7** and **8**<sup>a</sup>

<sup>a</sup>Reagents and conditions: (a) EtI, K<sub>2</sub>CO<sub>3</sub>, MeCN, overnight 50 °C, quantitative; (b) 1 M DIBALH in toluene, toluene, -78 °C, 1 h, quantitative; (c) 7-bromo-1,2,3,4-tetrahydroisoquinoline or 1,2,3,4-tetrahydroisoquinoline-7-carbonitrile, NaBH(OAc)<sub>3</sub>, 1,2-DCE, rt, 16–24 h, 80%; (d) TFA, DCM, base extraction, quantitative; (e) HATU, dry DMF, DIPEA or 2,6-lutidine, rt, 3–24 h, 31–41%; (f) NaN<sub>3</sub>, CuI, *N*<sup>1</sup>,*N*<sup>2</sup>-dimethylethane-1,2-diamine, EtOH: H<sub>2</sub>O (7:3), reflux, 7–9%.

### 4.3 Pharmacological Characterisation

Pharmacological characterisation of compounds **7** and **8** was carried out in order to determine whether a pharmacological profile similar to that of compound **6** was maintained upon incorporation of the azide functionality. Compounds **7** and **8** were initially tested for their ability to bind the long isoform of the D<sub>2</sub>R (D<sub>2L</sub>R) expressed in FlpIn CHO cells (Figure 5). Competition binding assays were carried out using [<sup>3</sup>H]spiperone as the radioligand to derive a value of affinity (*K*<sub>i</sub>) for haloperidol. In instances where the ligands were unable to completely displace the radioligand even at saturating concentrations (which is consistent with an allosteric mode of interaction), the data were fit using an allosteric ternary complex to derive values of

affinity ( $K_B$ ) and cooperativity with [<sup>3</sup>H]spiperone ( $\alpha$ ). Since competitive binding assays do not provide information regarding the effect of these compounds on the endogenous neurotransmitter dopamine, compounds **7** and **8** were then assessed in an assay which measures the ability of ligands to stimulate the inhibition of forskolin-induced cAMP production through activation of the D<sub>2L</sub>R. More specifically, we assessed the ability of **7** and **8** to antagonise the actions of increasing concentrations of dopamine (Table 2). The data were fitted with a derivation of the operational model of allosterism to derive values of functional affinity ( $K_B$ ) and allosteric cooperativity with dopamine ( $\alpha\beta$ , where  $\alpha$  is negative cooperativity with dopamine binding (signified by a limited concentration-dependent rightward shift in curves), and  $\beta$  is the modulation of dopamine efficacy (signified by a concentration-dependent depression in  $E_{max}$ )).<sup>47</sup>  
<sup>50</sup> The data were also fit to a Gaddum-Schild model of competitive antagonism to derive values of  $K_B$  and a Schild slope. In instances where a Schild slope was not significantly different from unity (i.e. Schild slope = 1), compounds were considered to demonstrate competitive antagonism. The data for each compound were analysed using both models and the best fit was determined by an *F*-test. These data are reported in Table 2 and are presented as logarithms to allow for statistical comparison.<sup>51</sup> Values of  $\text{Log } \alpha\beta < 0$  signify negative cooperativity. Finally, we performed a competitive radioligand binding assay using cell lysates to ascertain whether compounds **7** and **8** were capable of binding irreversibly to the D<sub>2</sub>R. The samples were pre-incubated for 1 h and then exposed to 254 nm UV light for 30 min at 4 °C to ensure photolysis, nitrene formation and covalent cross-linking by the azide moiety (Figure 4 and 6). Given that compounds **7** and **8** presumably occupy both the orthosteric and allosteric sites of the D<sub>2</sub>R, a series of wash steps were carried out to ensure that any unbound ligand would be removed. The cells were then lysed using ultrasonication, and specific binding was measured using [<sup>3</sup>H]spiperone in the presence or absence of haloperidol for each test condition.

To ensure that we were able to selectively “capture” the binding site of interest, we characterised both compounds **7** and **8** in both competitive radioligand binding and cAMP inhibition assays to determine whether they maintained an allosteric profile similar to that of compound **6** (Figure 5 and Table 2). From the competitive binding assay (Figure 5) we observed that, like **6**, compound **7** ( $K_B = 309$  nM) demonstrated incomplete displacement of [<sup>3</sup>H]spiperone and had an affinity that was similar to that of **6** ( $K_B = 534$  nM). Compound **8** ( $K_B = 112$  nM), however, demonstrated almost complete displacement of [<sup>3</sup>H]spiperone and an affinity that was 5-fold greater than **6**. Although complete displacement of the radioligand would suggest that **8** was an orthosterically binding competitive antagonist with no allosteric properties, we have previously noted in Chapter 3 that it may also suggest that the ligand is demonstrating a high

level of negative cooperativity. As such, we could not determine whether **8** was truly allosteric until we examined its function in the presence of dopamine in the cAMP inhibition assays. Consequently, functional assays (Table 2) revealed that in the presence of dopamine, both **7** ( $K_B = 124$  nM;  $\alpha\beta = 0.32$ ) and **8** ( $K_B = 184$  nM;  $\alpha\beta = 0.03$ ) acted as negative allosteric modulators and demonstrated a 6- and 4-fold increase in functional affinity compared to **6** ( $K_B = 747$  nM;  $\alpha\beta = 0.07$ ), respectively. Furthermore, compound **8** was also determined to have modulatory properties which were two-fold greater than that of **6**, suggesting that its observed competitive radioligand binding results were commensurate with an allosteric modulator which shows a high degree of negative cooperativity. Interestingly, despite showing 2-fold greater binding affinity and 6-fold greater functional affinity for the D<sub>2</sub>R compared to compound **6**, compound **7** was observed to have a lower degree of negative cooperativity (5-fold) than compound **6**. Nonetheless, from this characterisation of compounds **7** and **8** in their “ground state”, we were confident that we would be able to “capture” the binding site of interest upon irradiation of the photoactivatable probes.

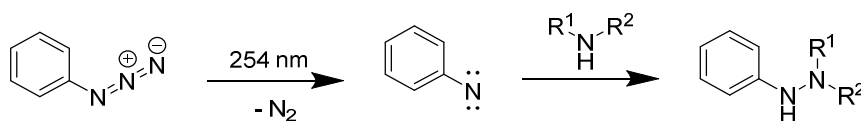
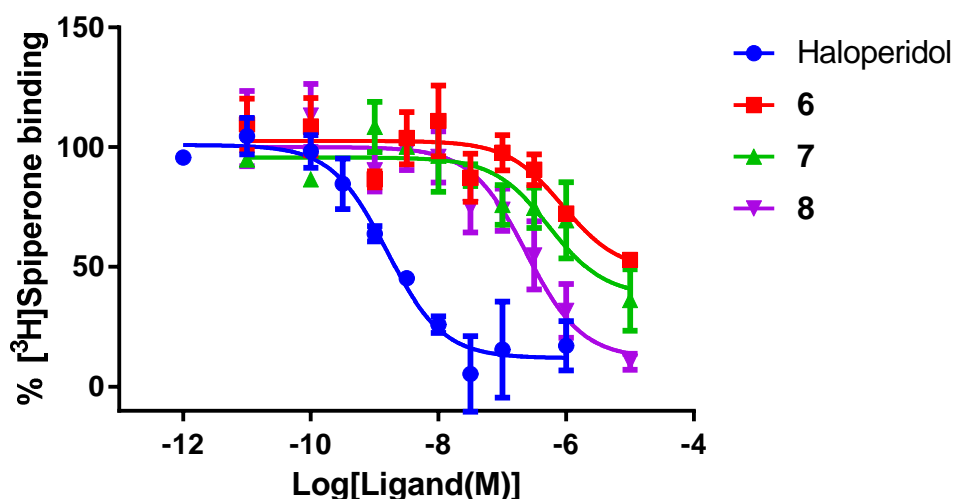


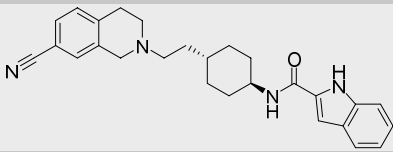
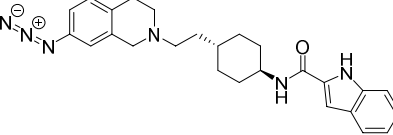
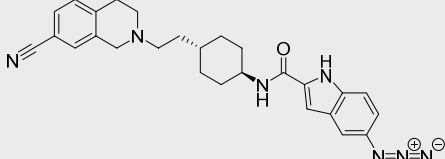
**Figure 4.** The photochemistry of an azide functionality.



Compounds	$pK_i \pm \text{SEM}$ ( $K_i$ , nM)	$pK_B \pm \text{SEM}$ ( $K_B$ , nM)	$\text{Log}\alpha \pm \text{SEM}$ ( $\alpha$ )
Haloperidol	$9.05 \pm 0.16$ (0.884)	-	-
<b>6</b>	-	$6.27 \pm 0.33$ (534)	$-0.55 \pm 0.14$ (0.282)
<b>7</b>	-	$6.51 \pm 0.27$ (309)	$-0.65 \pm 0.17$ (0.224)
<b>8</b>	-	$6.95 \pm 0.19$ (112)	ND

**Figure 5.** Binding curves of **6** and its photoactivatable derivatives, **7** and **8**. Determined by competition binding experiments using radiolabelled antagonist [<sup>3</sup>H]spiperone at D<sub>2</sub>L<sub>R</sub> expressed in FlpIn CHO cell membranes. Data represents the mean  $\pm$  SEM of three separate experiments performed in duplicate. For compounds **6** and **7** data was fit to a ternary complex model of allosterism to determine a value of affinity ( $K_B$ ) and cooperativity with [<sup>3</sup>H]spiperone ( $\text{Log}\alpha$ ). ND, the complete displacement of [<sup>3</sup>H]spiperone caused by **8** meant that we could not determine a value of cooperativity with the radioligand.

**Table 2.** Determination of functional affinities ( $K_B$ ) and negative cooperativities ( $\alpha\beta$ ) of **6** and its photoactivatable probe derivatives.<sup>a</sup>

Compounds	Structure	$pK_B \pm \text{SEM}$ ( $K_B$ , nM)	$\text{Log}\alpha\beta \pm \text{SEM}$ ( $\alpha\beta$ )	Fold-shift loss in dopamine affinity
<b>6</b>		$6.13 \pm 0.14$ (747)	$-1.16 \pm 0.10$ (0.07)	14.5
<b>7</b>		$6.91 \pm 0.24$ (124)	$-0.50 \pm 0.07$ (0.32)	3.2
<b>8</b>		$6.73 \pm 0.12$ (186)	$-1.48 \pm 0.09$ (0.03)	30.2

<sup>a</sup>Determined via the modulation of dopamine's inhibitory effect on forskolin-stimulated cAMP production in FlpIn CHO cells stably expressing both wild type D<sub>2L</sub>R and the CAMYEL biosensor. Data represents the mean  $\pm$  SEM of three separate experiments performed in duplicate and was fit to an operational model of allosterism.

We then assessed whether compounds **7** and **8** were able to bind the D<sub>2</sub>R irreversibly (Figure 6). A significant reduction in specific binding was observed for compound **7** following pre-incubation, irradiation and washings compared to vehicle (Specific binding (% Vehicle) = 58.8%). Additionally, no change in specific binding was observed compared to vehicle following pre-incubation with **7** when UV exposure was omitted (Specific binding (% Vehicle) = 107.6%). These results are indicative of a reduction of [<sup>3</sup>H]spiperone binding and, as a result, indicated the irreversible occupation of the D<sub>2</sub>R by **7**. In contrast, both compounds **6** and **8** demonstrated reductions in specific binding compared to vehicle both in the presence (Specific binding (% Vehicle) = 64.8%; 19.4%, respectively) and absence (Specific binding (% Vehicle) = 75.0%; 17.1%, respectively) of UV exposure. Given that compound **6** has no photoactivatable moiety which may be photo-activated to result in covalent tethering, it is possible that these results are the consequence of slow dissociation of the ligand from the D<sub>2</sub>R. Furthermore, we cannot ascertain whether compound **8** is able to bind irreversibly to the D<sub>2</sub>R since specific binding was significantly reduced with or without UV irradiation. However, it can be postulated that compound **8** in its “ground state”, like compound **6**, may have a slow rate of dissociation. This is because both structures retain the 1,2,3,4-tetrahydroisoquinoline-7-carbonitrile (7CN-THIQ) moiety, which is a crucial element of compound **6**'s ability to bind the orthosteric binding site of the D<sub>2</sub>R.<sup>47</sup> Additionally, we may rationalise that our observation of compound **7**'s irreversibility

may be the result of replacing the carbonitrile substituent with the azide moiety. Since the azide functionality is slightly larger in size than the carbonitrile functionality, it may not sit favourably within the orthosteric binding site and as a consequence, hasten the rate of dissociation. Upon UV irradiation, however, the resulting nitrene which is smaller than the carbonitrile functionality may have the necessary space to enable covalent bond formation within the orthosteric binding site of the D<sub>2</sub>R.

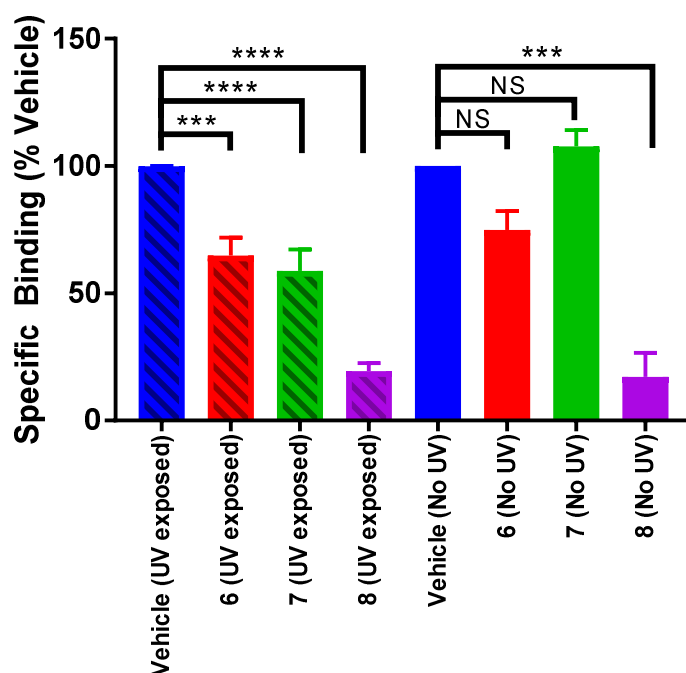


**Figure 6.** Specific binding (% Vehicle) bar graphs where values significantly different from vehicle as determined by one-way ANOVA (Tukey's post-hoc test) are indicated by asterisk(s) (\*) (where \*\*\* =  $p < 0.001$ , \*\*\*\* =  $p < 0.0001$ , and NS = not significant). Values represent the mean  $\pm$  SEM from three experiments conducted in triplicate.

#### 4.4 Conclusions

Herein we report the design, synthesis and preliminary evaluation of a small series of bitopic photoactivatable ligands for the D<sub>2</sub>R. Compounds **7** and **8** were both synthesised in appreciable quantities for preliminary pharmacological characterisation using previously established methods (Scheme 1). *In vitro* pharmacological evaluation of both compounds using [<sup>3</sup>H]spiperone competition binding and cAMP inhibition functional assays confirmed that like their parent molecule, SB269652 (**6**), both **7** and **8** act as bitopic D<sub>2</sub>R negative allosteric modulators (Figure 5, Table 2). Furthermore, we were able to demonstrate that compound **7** is capable of binding to the D<sub>2</sub>R in an irreversible manner upon photo-activation with 254 nm UV

light (Figure 6). However, the nature of compound **8**'s binding could not be ascertained due to slow dissociation from the D<sub>2</sub>R (Figure 6). Despite this, we have developed an irreversible bitopic probe (**7**) for the D<sub>2</sub>R which may be a useful pharmacological tool for probing structural and functional interactions at the putative allosteric site or bitopic interactions at the D<sub>2</sub>R.

## 4.5 Experimental

**Chemistry.** All solvents and chemicals were purchased from standard suppliers and were used without any further purification. <sup>1</sup>H NMR and <sup>13</sup>C NMR spectra were acquired at 400.13 (<sup>1</sup>H spectra) and 100.62 (<sup>13</sup>C spectra) MHz, respectively, on a Bruker Avance III Nanobay 400 MHz NMR spectrometer coupled to the BACS 60 automatic sample changer and equipped with a 5 mm PABBO BB-1H/ D Z-GRD probe. All spectra obtained was processed using MestReNova software (v.6.0). Chemical shifts ( $\delta$ ) for all <sup>1</sup>H spectra are reported in parts per million (ppm) using tetramethylsilane (TMS, 0 ppm) as the reference. The data for all spectra are reported in the following format: chemical shift ( $\delta$ ), (multiplicity, coupling constants *J* (Hz), integral), where the multiplicity is defined as s = singlet, d = doublet, t = triplet, q = quartet, p = pentet, and m = multiplet. <sup>13</sup>C NMR were routinely carried out as *J*-modulated spin-echo experiments (JMOD), all <sup>13</sup>C  $\delta$  are reported in ppm and assignment of carbon signals were abbreviated as: C = quaternary carbon, CH = methine carbon, CH<sub>2</sub> = methylene carbon, and CH<sub>3</sub> = methyl carbon. Thin layer chromatography (TLC) was carried out routinely on silica gel 60F254 precoated plates (0.25 mm, Merck). Flash column chromatography was carried out using Davisil LC60A silica gel, 40-63  $\mu$ m.

Liquid chromatography mass spectrometry (LCMS) was detected on one of two instruments; either an Agilent 6100 Series Single Quad LC/MS or an Agilent 1200 Series HPLC (equipped with a 1200 Series G13111A Quaternary Pump, G1329A Thermostatted Autosampler, and a G1314B Variable Wavelength Detector) and the data was processed using LC/MSD Chemstation Rev.B.04.01 SP1 coupled with Easy Access Software. Both systems were equipped with a Reverse Phase Luna C<sub>8</sub>(2) (5  $\mu$ m, 50  $\times$  4.6 mm, 100  $\text{\AA}$ ) column maintained at 30  $^{\circ}$ C. An MeCN gradient (5-100%) was used to obtain optimal separation, where 4 min were required for the gradient to reach 100% MeCN and maintained for a further 3 min before requiring 3 min to return to the initial gradient of 5% MeCN (total run time = 10 min). Solvent A = 0.1% aqueous formic acid; Solvent B = MeCN/ 0.1% formic acid.

The purity and retention time of final products were determined using analytical HPLC and high resolution mass spectrometry (HRMS). Analytical HPLC was carried out using an Agilent 1260 Infinity Analytical HPLC fitted with a Zorbax Eclipse Plus C18 Rapid Resolution column (100 mm  $\times$  4.60 mm, 3.5  $\mu$ m) using a binary solvent system: solvent A of 0.1% aqueous TFA; solvent B of 0.1% TFA in MeCN. Gradient elution was achieved over 10 min using 95% A + 5% B to 100% B over 9 min, and 100% B maintained for 1 min at a flow rate of 1 mL/min monitored at both 214 and 254 nm. HRMS were conducted on an Agilent 6224 TOP LC/MS Mass Spectrometer coupled to an Agilent 1290 Infinity. All data was acquired and reference mas

corrected via dual-spray electrospray ionisation (ESI) source. Each scan or data point on the total ion chromatogram (TIC) is average of 13700 transients, producing one spectrum per second. Mass spectra were created by averaging the scans across each peak and background subtracted against the first 10 seconds of the TIC. Data acquisition was carried out using the Agilent Mass Hunter Data Acquisition software version B.05.00 Build 5.0.5042 and analysis was performed using Mass Hunter Qualitative Analysis version B.05.00 Build 5.0.519.13.

#### **General Procedure A (Reductive Alkylation)**

The amine (1 eq.) and aldehyde (1 eq.) were dissolved in dry 1,2-DCE (15 mL). NaBH(OAc)<sub>3</sub> (1.5 eq.) was added and stirred under an atmosphere of N<sub>2</sub> for 24 h. LCMS was used to confirm completion of the reaction. The mixture was then diluted in DCM (20 mL), and washed with 1 M K<sub>2</sub>CO<sub>3</sub> (3 × 20 mL) and brine, then dried over anhydrous Na<sub>2</sub>SO<sub>4</sub> and evaporated to dryness. The crude material was then purified using flash chromatography (MeOH: DCM 3:97) unless otherwise stated.

#### **General Procedure B (HATU Amide Coupling)**

The amine (1 eq.), carboxylic acid (1.2 eq.) and the coupling reagent, HATU (1.2-2 eq.). were stirred in a minimal volume of anhydrous DMF (3-4 mL). To this, an excess of DIPEA was added and the reaction was left to stir overnight. The reaction was ceased upon confirmation of complete consumption of the amine via LCMS. The mixture was then diluted with a sat. NaHCO<sub>3</sub> and H<sub>2</sub>O solution (1:1) which was ten times the volume of DMF added to the reaction and left to stir for 30 min. The resulting precipitate was filtered and washed, or if precipitation had not occurred, the product was extracted from the aqueous using EtOAc. Any further purification was as specified.

#### **General Procedure C (De-protection of *tert*-Butyl carbamate and HATU Amide Coupling)**

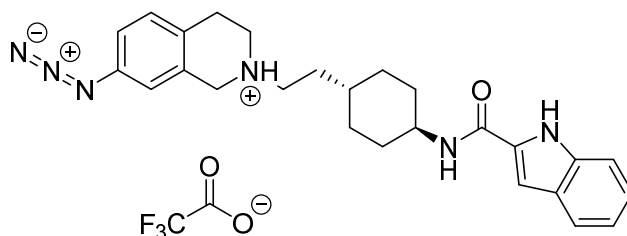
To a stirring solution of protected amine (1 eq.) and DCM (5 mL), an excess of TFA was added at rt. The solution was stirred for 2 h or overnight and then diluted with DCM (20 mL). 1 M K<sub>2</sub>CO<sub>3</sub> or 1 M NaOH was added to bring the mixture to pH 12. The product was then extracted using DCM (2 × 20 mL). The combined organic extracts were then washed with brine and dried over anhydrous Na<sub>2</sub>SO<sub>4</sub> before being concentrated *in vacuo* to yield the free amine. Following

confirmation of product formation via TLC or LCMS, the resulting amine (1 eq.), carboxylic acid (1.2 eq.) and the coupling reagent, 1-[bis(dimethylamino)methylene]-1*H*-1,2,3-triazolo[4,5-*b*]pyridinium 3-oxid hexafluorophosphate (HATU) (1.2-2 eq.) were stirred in a minimal volume of anhydrous DMF (3 mL). To this, an excess of 2,6-lutidine (2 eq.) was added and the reaction was left to stir overnight. The reaction was ceased upon confirmation of complete consumption of the amine via LCMS. The mixture was then diluted with a sat. NaHCO<sub>3</sub> and H<sub>2</sub>O solution (1:1, 30 mL) and left to stir for 30 min. The resulting precipitate was filtered and washed or the product was extracted from the aqueous using EtOAc (3 × 30 mL) if precipitation had not occurred, purification was as specified.

#### General Procedure D (Azidation of an Aryl Bromide)

Following a method described by Andersen *et al.*,<sup>49</sup> the aryl bromide (1 eq.), NaN<sub>3</sub> (2 eq.), sodium ascorbate (0.05 eq.), CuI (0.1 eq.), *N*<sup>1</sup>,*N*<sup>2</sup>-dimethylethane-1,2-diamine (0.15 eq.) and 4 mL EtOH: H<sub>2</sub>O (7:3) were introduced into a two-necked rbf equipped with a condenser and a magnetic stirrer. After the mixture was degassed and under an atmosphere of N<sub>2</sub>, the reaction was stirred at reflux and progress was monitored via HPLC. Additional equivalents of NaN<sub>3</sub> and *N*<sup>1</sup>,*N*<sup>2</sup>-dimethylethane-1,2-diamine were added until cessation of product formation was observed by HPLC, the mixture was cooled to rt and partitioned between EtOAc (10 mL) and brine (10 mL). The product was extracted from the brine using EtOAc (4 × 10 mL). The combined organic washes were dried over anhydrous Na<sub>2</sub>SO<sub>4</sub>, concentrated *in vacuo* and purified by preparative HPLC to yield the respective product as the TFA salt.

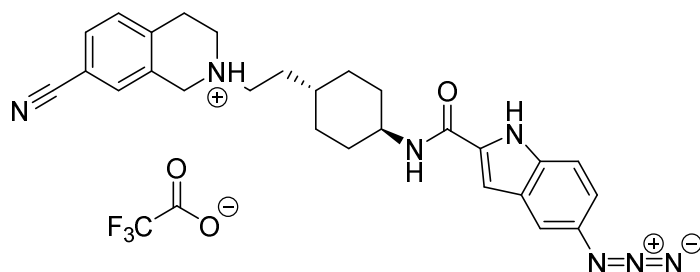
#### 2-(2-((*trans*)-4-(1*H*-Indole-2-carboxamido)cyclohexyl)ethyl)-7-azido-1,2,3,4-tetrahydroisoquinolin-2-ium 2,2,2-trifluoroacetate (7)



Using *N*-((*trans*)-4-(2-(7-Bromo-3,4-dihydroisoquinolin-2(1*H*)-yl)ethyl)cyclohexyl)-1*H*-indole-2-carboxamide as the aryl bromide, general procedure D was followed to yield the product salt as a yellow solid (3.70 mg, 9%). <sup>1</sup>H NMR (*d*<sub>6</sub>-DMSO) δ 11.51 (s, 1H), 10.15 (br s, 1H), 8.23

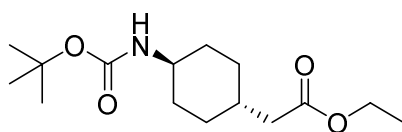
(d, J = 6.7 Hz, 1H), 7.89 – 6.76 (m, 8H), 4.73 – 4.49 (m, 1H), 4.38 – 4.13 (m, 1H), 3.86 – 3.65 (m, 2H), 3.42 – 2.89 (m, 5H), 2.00 – 1.59 (m, 6H), 1.46 – 1.24 (m, 3H), 1.19 – 1.01 (m, 2H). <sup>13</sup>CNMR (*d*<sub>6</sub>-DMSO) δ 160.2 (C), 137.9 (C), 136.3 (C), 133.5 (C), 132.0 (C), 128.3 (C), 127.2 (CH), 127.0 (C), 123.2 (CH), 121.4 (CH), 119.6 (CH), 118.8 (CH), 117.0 (CH), 112.3 (CH), 102.5 (CH), 53.5 (CH<sub>2</sub>), 51.5 (CH<sub>2</sub>), 49.0 (CH<sub>2</sub>), 48.0 (CH), 34.2 (CH), 32.0 (CH<sub>2</sub>), 31.3 (CH<sub>2</sub>), 30.3 (CH<sub>2</sub>), 24.4 (CH<sub>2</sub>). HPLC: *t*<sub>R</sub> 5.99 min, >95% purity. HRMS (*m/z*): C<sub>26</sub>H<sub>31</sub>N<sub>6</sub>O requires [M+H]<sup>+</sup> 443.2554; found 443.2564.

**2-(2-((*trans*)-4-(5-Azido-1*H*-indole-2-carboxamido)cyclohexyl)ethyl)-7-cyano-1,2,3,4-tetrahydroisoquinolin-2-ium 2,2,2-trifluoroacetate (8)**

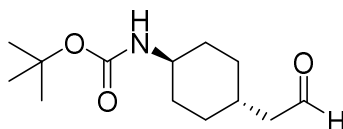


Using 5-bromo-*N*-((*trans*)-4-(2-(7-cyano-3,4-dihydroisoquinolin-2(1*H*)-yl)ethyl)cyclohexyl)-1*H*-indole-2-carboxamide as the aryl bromide, general procedure D was followed to yield the product salt as a brown solid (2.96 mg, 7%). <sup>1</sup>H NMR (*d*<sub>6</sub>-DMSO) δ 11.68 (s, 1H), 11.19 – 10.08 (m, 2H), 8.38 – 8.21 (m, 1H), 7.74 (s, 2H), 7.49 – 7.42 (m, 2H), 7.35 (s, 1H), 7.11 (s, 1H), 6.93 (dd, J = 8.7, 1.8 Hz, 1H), 4.66 – 4.21 (m, 2H), 3.85 – 3.56 (m, 3H), 3.27 – 3.03 (m, 3H), 1.97 – 1.53 (m, 6H), 1.44 – 1.03 (m, 5H). <sup>13</sup>C NMR (*d*<sub>6</sub>-DMSO) δ 159.9 (C), 136.8 (C), 134.2 (C), 133.5 (C), 131.2 (C), 131.0 (CH), 130.7 (CH), 129.9 (CH), 127.8 (C), 123.6 (CH), 118.5 (C), 115.5 (CH), 113.8 (CH), 110.7 (CH), 109.4 (C), 53.7 (CH<sub>2</sub>), 51.0 (CH<sub>2</sub>), 48.3 (CH<sub>2</sub>), 48.0 (CH), 34.3 (CH), 32.0 (CH<sub>2</sub>), 31.3 (CH<sub>2</sub>), 24.9 (CH<sub>2</sub>). NOTE: One quaternary and one methylene resonance could not be observed due to signal broadening. HPLC: *t*<sub>R</sub> 4.29 min, >95% purity. HRMS (*m/z*): C<sub>27</sub>H<sub>30</sub>N<sub>7</sub>O requires [M+H]<sup>+</sup> 468.2506; found 468.2502.

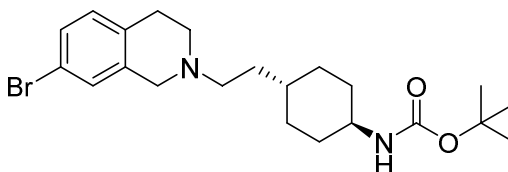
**Ethyl 2-((*trans*)-4-((*tert*-butoxycarbonyl)amino)cyclohexyl)acetate (10)<sup>47</sup>**



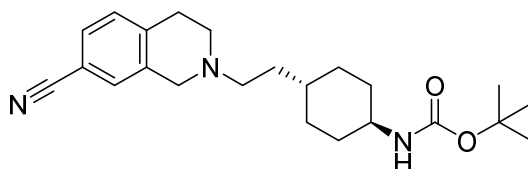
Refer to compound **42** in Chapter 2.

**tert-Butyl ((trans)-4-(2-oxoethyl)cyclohexyl)carbamate (11)**<sup>47</sup>

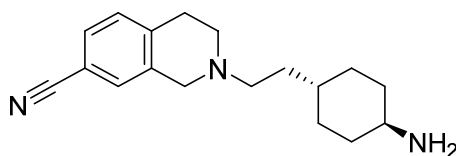
Refer to compound **43** in Chapter 2.

**tert-Butyl ((trans)-4-(2-(7-bromo-3,4-dihydroisoquinolin-2(1H)-yl)ethyl)cyclohexyl)carbamate (12)**<sup>47</sup>

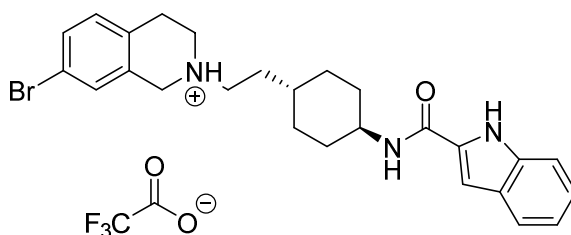
Using 7-bromo-1,2,3,4-tetrahydroisoquinoline as the amine and tert-butyl ((trans)-4-(2-oxoethyl)cyclohexyl)carbamate as the aldehyde, general procedure A was followed. The resultant product was purified via flash chromatography (3:97 MeOH: DCM) to yield an oil (158 mg, 29%). <sup>1</sup>H NMR (CDCl<sub>3</sub>) δ 7.22 (dd, *J* = 8.1, 2.0 Hz, 1H), 7.16 – 7.14 (m, 1H), 6.95 (d, *J* = 8.2 Hz, 1H), 4.55 (s, 1H), 3.56 (s, 2H), 3.35 (s, 2H), 2.82 (t, *J* = 5.8 Hz, 2H), 2.69 (t, *J* = 5.9 Hz, 2H), 2.53 – 2.46 (m, 2H), 2.01 – 1.92 (m, 2H), 1.82 – 1.71 (m, 2H), 1.48 – 1.36 (m, 11), 1.14 – 0.95 (m, 4H). <sup>13</sup>C NMR (CDCl<sub>3</sub>) δ 155.3 (C), 137.0 (C), 133.3 (C), 130.3 (CH), 129.3 (CH), 129.1 (CH), 119.1 (C), 78.9 (C), 60.3 (CH<sub>2</sub>), 56.0 (CH<sub>2</sub>), 55.6 (CH<sub>2</sub>), 50.6 (CH<sub>2</sub>), 49.8 (CH), 39.6 (CH<sub>2</sub>), 35.3 (CH), 33.9 (CH<sub>2</sub>), 33.4 (CH<sub>2</sub>), 31.9 (CH<sub>2</sub>), 31.8 (CH<sub>2</sub>), 28.4 (CH<sub>3</sub>). LCMS (*m/z*): [M+H]<sup>+</sup> 438.9.

**tert-Butyl ((trans)-4-(2-(7-cyano-3,4-dihydroisoquinolin-2(1H)-yl)ethyl)cyclohexyl)carbamate (14)**<sup>47</sup>

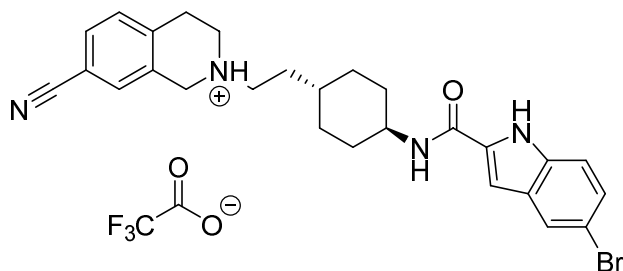
Refer to compound **8b** in Chapter 3.

**2-(2-((*trans*)-4-Aminocyclohexyl)ethyl)-1,2,3,4-tetrahydroisoquinoline-7-carbonitrile (15)<sup>47</sup>**

Refer to compound **9b** in Chapter 3.

**2-(2-((*trans*)-4-(1*H*-Indole-2-carboxamido)cyclohexyl)ethyl)-7-bromo-1,2,3,4-tetrahydroisoquinolin-2-ium 2,2,2-trifluoroacetate (16)<sup>47</sup>**

Using *tert*-butyl ((*trans*)-4-(2-(7-bromo-3,4-dihydroisoquinolin-2(1*H*)-yl)ethyl)cyclohexyl)carbamate as the protected amine, general procedure C was followed. Upon confirmation of *tert*-butyl carbamate deprotection via TLC, the amide coupling procedure was carried out. The resultant precipitate was purified using preparative HPLC which yielded the TFA salt as a pale yellow solid (37.4 mg, 31%). <sup>1</sup>H NMR (*d*<sub>6</sub>-DMSO) δ 11.49 (s, 1H), 8.17 (d, *J* = 8.0 Hz, 1H), 7.58 (d, *J* = 8.0 Hz, 1H), 7.41 (dd, *J* = 8.2, 0.7 Hz, 1H), 7.35 – 7.23 (m, 2H), 7.18 – 7.11 (m, 2H), 7.08 – 6.98 (m, 2H), 3.81 – 3.69 (m, 1H), 3.53 (s, 2H), 2.75 (t, *J* = 5.6 Hz, 2H), 2.63 (t, *J* = 5.8 Hz, 2H), 2.47 (t, *J* = 7.5 Hz, 2H), 1.92 – 1.77 (m, 4H), 1.44 (dd, *J* = 14.4, 6.8 Hz, 2H), 1.40 – 1.29 (m, 3H), 1.15 – 0.99 (m, 2H). <sup>13</sup>C NMR (101 MHz, *d*<sub>6</sub>-DMSO) δ 160.2 (C), 137.8 (C), 136.3 (C), 133.8 (C), 132.0 (C), 130.6 (CH), 129.0 (CH), 128.7 (CH), 127.1 (C), 123.1 (CH), 121.4 (CH), 119.6 (CH), 118.2 (C), 112.2 (CH), 102.4 (CH), 55.3 (CH<sub>2</sub>), 55.0 (CH<sub>2</sub>), 50.2 (CH<sub>2</sub>), 48.2 (CH), 34.7 (CH), 33.6 (CH<sub>2</sub>), 32.3 (CH<sub>2</sub>), 31.7 (CH<sub>2</sub>), 28.1 (CH<sub>2</sub>). LCMS (*m/z*): [M+H]<sup>+</sup> 481.1.

**2-(2-((*trans*)-4-(5-Bromo-1*H*-indole-2-carboxamido)cyclohexyl)ethyl)-7-cyano-1,2,3,4-tetrahydroisoquinolin-2-ium 2,2,2-trifluoroacetate (17)**

Using 2-(2-((*trans*)-4-aminocyclohexyl)ethyl)-1,2,3,4-tetrahydroisoquinoline-7-carbonitrile as the amine and 5-bromo-1*H*-indole-2-carboxylic acid, general procedure B was followed. The resultant yellow precipitate was then purified using preparative HPLC to yield the TFA salt as a yellow solid (47.5 mg, 41%). <sup>1</sup>H NMR (*d*<sub>6</sub>-DMSO) δ 11.75 (d, *J* = 1.5 Hz, 1H), 10.27 (s, 1H), 8.33 (d, *J* = 8.0 Hz, 1H), 7.83 (d, *J* = 1.8 Hz, 1H), 7.76 (d, *J* = 6.0 Hz, 2H), 7.48 (d, *J* = 8.5 Hz, 1H), 7.38 (d, *J* = 8.7 Hz, 1H), 7.28 (dd, *J* = 8.7, 1.9 Hz, 1H), 7.14 (d, *J* = 1.4 Hz, 1H), 4.70 – 4.54 (m, 1H), 4.39 – 4.23 (m, 1H), 3.89 – 3.69 (m, 2H), 3.60 (br s, 3H), 3.31 – 3.24 (m, 1H), 3.22 – 3.16 (m, 1H), 1.95 – 1.77 (m, 4H), 1.71 – 1.63 (m, 2H), 1.42 – 1.27 (m, 3H), 1.17 – 1.02 (m, 2H). <sup>13</sup>C NMR (*d*<sub>6</sub>-DMSO) δ 160.3 (C), 138.0 (C), 135.4 (C), 133.8 (C), 131.5 (CH), 131.2 (CH), 130.3 (CH), 129.3 (C), 126.2 (CH), 124.0 (CH), 119.0 (C), 114.8 (CH), 112.6 (C), 109.9 (C), 102.4 (CH), 54.0 (CH<sub>2</sub>), 51.6 (CH<sub>2</sub>), 48.8 (CH<sub>2</sub>), 48.5 (CH), 34.7 (CH), 32.4 (CH<sub>2</sub>), 31.7 (CH<sub>2</sub>), 30.7 (CH<sub>2</sub>), 25.6 (CH<sub>2</sub>). LCMS (*m/z*): [M+]<sup>+</sup> 504.9, [M+2]<sup>+</sup> 506.9.

**Pharmacology**

**Cell Lines and Transfection.** FlpIn CHO cells stably expressing the wild-type D<sub>2L</sub>R were transfected and maintained in the conditions stated by Szabo *et al.*<sup>44</sup>

For FlpIn CHO cells stably expressing both the wild-type D<sub>2L</sub>R and the YFP-Epac-RLuc biosensor (CAMYEL), FlpIn CHO cells were both transfected with pGO44 (Invitrogen Life Technology) and the D<sub>2L</sub>R gene cloned in pEF5/FRT/*v*-dest plasmid (Invitrogen Life Technology) and selected with 700 μg/ mL Hygromycin B Gold (Invivogen). The cells stably expressing the D<sub>2L</sub>R were then transfected with the CAMYEL construct<sup>52</sup> and selected as a monoclonal cell line using both Hygromycin B Gold and G418 (Gibco Life Technology) at a concentration of 700 μg/ mL.

**Membrane Preparation.** FlpIn CHO cells stably expressing the wild-type D<sub>2</sub>L<sub>R</sub> were grown to confluency using 500 cm<sup>2</sup> cell culture plates. The cells were harvested in PBS containing 2 mM EDTA and centrifuged at 300g for 3 min at 4 °C. The resulting pellet was resuspended in ice cold assay buffer (20 mM HEPES, 100 mM NaCl, 6 mM MgCl<sub>2</sub>, 1 mM EGTA and 1 mM EDTA, pH 7.4) and the centrifugation was repeated. The intact cell pellet was then resuspended in assay buffer and homogenised using a Polytron homogeniser. After centrifugation (300g, 5 min, 4 °C), the supernatant was centrifuged at 30,000g for 1 h at 4 °C using a Sorval Evolution RC ultracentrifuge (Thermo Scientific). The resulting pellet was resuspended in the assay buffer and stored in 250 µL aliquots at -80 °C. Membrane protein concentration was determined using the Bradford method.

**[<sup>3</sup>H]Spiperone Competitive Binding Assays.** All radioligand binding experiments were conducted in a 1 mL reaction volume in assay buffer (20 mM HEPES, 100 mM NaCl, 6 mM MgCl<sub>2</sub>, 1 mM EGTA and 1 mM EDTA, pH 7.4). In all cases non-specific binding was determined in the presence of 1 µM haloperidol. To obtain affinity estimates of unlabelled ligands, competition binding experiments were performed at equilibrium to measure the ability of increasing concentrations of the test ligands to compete 0.1 nM [<sup>3</sup>H]spiperone for binding at the D<sub>2</sub>L<sub>R</sub> (wild-type). The membranes (5 µg, unless otherwise stated) were incubated with the drugs for 3 h at 37 °C ([<sup>3</sup>H]spiperone). Following incubation, bound and free radioligand were separated by fast-flow filtration through GF/B filters using a Brandel harvester followed by three washes with ice cold NaCl (0.9% (m/v)). Filter-bound radioactivity was measured by scintillation spectrometry after the addition of 3.5 mL of Ultima Gold (PerkinElmer) using a Tri-Carb 2900TR liquid scintillation counter (PerkinElmer).

**Bioluminescence Resonance Energy Transfer (BRET) cAMP assay.** Flp-In-CHO cells stably expressing wild-type D<sub>2</sub>L<sub>R</sub> and the CAMYEL biosensor were plated at a density of 50,000 cells per well into 96-well CulturPlates (PerkinElmer) and grown overnight. The cells were equilibrated in Hank's balanced salt solution (HBSS) at 37 °C before commencing the experiment. The cells were co-stimulated with the ligands, dopamine and 10 µM (final concentration) forskolin for 30 min prior to BRET measurement. Coelenterazine (Promega) was added at a final concentration of 5 µM at least 5 min prior to measurement. The signals were detected at 445–505 and 505–565 nm using a LUMIstar Omega instrument (BMG LabTech, Offenburg, Germany).

**Evaluation of Irreversible Ligands.** *Pre-incubation of Control and Test Ligands.* FlpIn CHO cells stably expressing the wild-type D<sub>2L</sub>R were grown to confluency in 175 cm<sup>2</sup> cell culture flasks. The cells were harvested in PBS containing 2 mM EDTA and centrifuged at 300g for 3 min at 4 °C. The resulting pellet was resuspended in 10 mL ice cold assay buffer (20 mM HEPES, 100 mM NaCl, 6 mM MgCl<sub>2</sub>, 1 mM EGTA and 1 mM EDTA, pH 7.4) supplemented with saponin (50 µg/mL). The cells were then dispensed into Eppendorf tubes at a density of 2,000,000 cells per tube and each tube was made up to a final volume of 1 mL using ice cold saponin-supplemented assay buffer and maintained at 4 °C. 200 µL of the test or control ligands were added to the necessary Eppendorf tubes (10 µM final concentration) and the tubes were then left to equilibrate at 37 °C for 1 h in a waterbath. The tubes were immediately placed on ice for 5 min, after which, tubes requiring UV-exposure were exposed to 254 nm UV light for 30 min at 4 °C. The tubes were then centrifuged for 10 min (4 °C, 21,000 rpm). The supernatant was discarded and the cells were resuspended in cold saponin-supplemented assay buffer (1 mL) and centrifuged again for 5 min (4 °C, 21,000 rpm). This process was carried out a further two times. The supernatant was finally discarded and cold un-supplemented assay buffer was added to each tube (500 µL). The cells were then lysed and homogenised via ultrasonication and the protein concentration was determined using the Bradford method. The required amount of cold un-supplemented assay buffer was then added to each treatment tube to bring the concentration of each to 50 µg/mL.

*Assay Protocol.* All radioligand binding experiments were conducted in a 1 mL reaction volume in assay buffer (20 mM HEPES, 100 mM NaCl, 6 mM MgCl<sub>2</sub>, 1 mM EGTA and 1 mM EDTA, pH 7.4). In all cases non-specific binding was determined in the presence of 1 µM haloperidol. To obtain estimates of maximal binding, binding experiments were performed at equilibrium to measure the ability of 0.1 nM [<sup>3</sup>H]spiperone to compete for binding at the D<sub>2L</sub>R (wild-type) against the test ligands which had, or had not, been exposed to UV irradiation. The cell lysates (5 µg) were incubated with the [<sup>3</sup>H]spiperone for 3 h at 37 °C. Following incubation, bound and free radioligand were separated by fast-flow filtration through GF/B filters using a Brandel harvester followed by three washes with ice cold NaCl (0.9% (m/v)). Filter-bound radioactivity was measured by scintillation spectrometry after the addition of 3.5 mL of Ultima Gold (PerkinElmer) using a Tri-Carb 2900TR liquid scintillation counter (PerkinElmer).

**Data Analysis.** The results obtained were analysed using Prism 6.01 (GraphPad Software Inc., San Diego, CA). For the displacement of [<sup>3</sup>H]spiperone data were fit to a one-site model with a variable Hill slope:

$$Y = \frac{(top-bottom)x^{n_H}}{x^{n_H} + IC_{50}^{n_H}} \quad (1)$$

where Y denotes the percent specific binding; top and bottom denote the maximal and minimal asymptotes, respectively; x denotes the inhibitor potency (mid-point location) parameter;  $n_H$  denotes the Hill slope factor. With the assumption of simple competition,  $IC_{50}$  values were converted to  $K_i$  values via the Cheng-Prusoff equation.<sup>53</sup> Competition-binding curves between [<sup>3</sup>H]spiperone and **6** (and its analogues) could be fit to the allosteric ternary complex model using the following equation:<sup>54</sup>

$$Y = \frac{\frac{[A]}{K_A}}{\frac{[A]}{K_A} + \left( \frac{1 + \frac{[B]}{K_B}}{1 + \alpha \frac{[B]}{K_B}} \right)} \quad (2)$$

where Y is percentage (vehicle control) binding; [A] and [B] are the concentrations of [<sup>3</sup>H]spiperone and **6**, respectively;  $K_A$  and  $K_B$  are the equilibrium dissociation constants of [<sup>3</sup>H]spiperone and **6**, respectively;  $\alpha$  is the cooperativity between **6** and [<sup>3</sup>H]spiperone. Values  $\alpha > 1$  denote positive cooperativity; values of  $< 1$  (but  $> 0$ ) denote negative cooperativity, and values of 1 denote neutral cooperativity.

A logistic equation of competitive agonist-antagonist interaction was fitted globally to data from functional experiments measuring the interaction between dopamine and all analogues of **6**:

$$response = bottom + \frac{(E_{max} - bottom)}{1 + \left( \frac{10^{-pEC_{50}} \left[ 1 + \left( \frac{[B]}{10^{-pA_2}} \right)^s \right]^{n_H}}{[A]} \right)} \quad (3)$$

where s represents the Schild slope for the antagonist and  $pA_2$  represents the negative logarithm of the molar concentration of the antagonist at which double the concentration of the agonist is needed to elicit the original submaximal response obtained in the absence of the antagonist.

Functional data describing the interaction between all analogues of **6** and dopamine are analysed according to the allosteric ternary complex model:

$$E = \frac{E_m[A]^{nH}}{[A]^{nH} + [EC_{50}]^{nH} \left( \frac{1 + \frac{[B]}{K_B}}{1 + \frac{\alpha\beta[B]}{K_B}} \right)} \quad (4)$$

where  $E_m$  is the maximal cellular response possible, [A] and [B] are the concentrations of orthosteric and allosteric ligands, respectively,  $K_B$  is the equilibrium dissociation constant of the orthosteric and allosteric ligands,  $\alpha\beta$  is the composite cooperativity parameter between orthosteric and allosteric ligands that includes effects upon the affinity and efficacy of the orthosteric ligand, and  $nH$  is the Hill slope of the orthosteric agonist concentration-response curves. Values of  $\alpha$  and/ or  $\beta$  greater than 1 denote allosteric potentiation, whereas values less than 1 (but greater than 0) denote allosteric inhibition.

## 4.6 References

1. Kopinathan, A.; Scammells, P. J.; Lane, J. R.; Capuano, B. Multivalent approaches and beyond: novel tools for the investigation of dopamine D<sub>2</sub> receptor pharmacology. *Future Med. Chem.* **2016**, *8*, 1349-1372.
2. Jorg, M.; Scammells, P. J. Guidelines for the Synthesis of Small-Molecule Irreversible Probes Targeting G Protein-Coupled Receptors. *ChemMedChem* **2016**, *11*, 1488-1498.
3. Shonberg, J.; Kling, R. C.; Gmeiner, P.; Lober, S. GPCR crystal structures: Medicinal chemistry in the pocket. *Bioorg. Med. Chem.* **2015**, *23*, 3880-3906.
4. Weichert, D.; Gmeiner, P. Covalent molecular probes for class A G protein-coupled receptors: advances and applications. *ACS Chem. Biol.* **2015**, *10*, 1376-1386.
5. Nijmeijer, S.; Engelhardt, H.; Schultes, S.; van de Stolpe, A. C.; Lusink, V.; de Graaf, C.; Wijtmans, M.; Haaksma, E. E. J.; de Esch, I. J. P.; Stachurski, K.; Vischer, H. F.; Leurs, R. Design and pharmacological characterization of VUF14480, a covalent partial agonist that interacts with cysteine 983.36 of the human histamine H<sub>4</sub> receptor. *Br. J. Pharmacol.* **2013**, *170*, 89-100.
6. Krishnan, S.; Miller, R. M.; Tian, B.; Mullins, R. D.; Jacobson, M. P.; Taunton, J. Design of reversible, cysteine-targeted Michael acceptors guided by kinetic and computational analysis. *J. Am. Chem. Soc.* **2014**, *136*, 12624-12630.
7. Pitha, J.; Buchowiecki, W.; Milecki, J.; Kusiak, J. W. Affinity labels for  $\beta$ -adrenoceptors: preparation and properties of alkylating  $\beta$ -blockers derived from indole. *J. Med. Chem.* **1987**, *30*, 612-615.
8. Baraldi, P. G.; Cacciari, B.; Moro, S.; Romagnoli, R.; Ji, X.-d.; Jacobson, K. A.; Gessi, S.; Borea, P. A.; Spalluto, G. Fluorosulfonyl- and Bis-( $\beta$ -chloroethyl)amino-phenylamino Functionalized Pyrazolo[4,3-*e*]1,2,4-triazolo[1,5-*c*]pyrimidine Derivatives: Irreversible Antagonists at the Human A<sub>3</sub> Adenosine Receptor and Molecular Modeling Studies. *J. Med. Chem.* **2001**, *44*, 2735-2742.
9. Kruse, A. C.; Ring, A. M.; Manglik, A.; Hu, J.; Hu, K.; Eitel, K.; Hubner, H.; Pardon, E.; Valant, C.; Sexton, P. M.; Christopoulos, A.; Felder, C. C.; Gmeiner, P.; Steyaert, J.; Weis, W. I.; Garcia, K. C.; Wess, J.; Kobilka, B. K. Activation and allosteric modulation of a muscarinic acetylcholine receptor. *Nature* **2013**, *504*, 101-106.
10. Davie, B. J.; Valant, C.; White, J. M.; Sexton, P. M.; Capuano, B.; Christopoulos, A.; Scammells, P. J. Synthesis and Pharmacological Evaluation of Analogues of Benzyl Quinolone Carboxylic Acid (BQCA) Designed to Bind Irreversibly to an Allosteric Site of the M-1 Muscarinic Acetylcholine Receptor. *J. Med. Chem.* **2014**, *57*, 5405-5418.

11. Rosenbaum, D. M.; Zhang, C.; Lyons, J. A.; Holl, R.; Aragao, D.; Arlow, D. H.; Rasmussen, S. G.; Choi, H. J.; Devree, B. T.; Sunahara, R. K.; Chae, P. S.; Gellman, S. H.; Dror, R. O.; Shaw, D. E.; Weis, W. I.; Caffrey, M.; Gmeiner, P.; Kobilka, B. K. Structure and function of an irreversible agonist-beta(2) adrenoceptor complex. *Nature* **2011**, 469, 236-240.
12. Yan, F.; Bikbulatov, R. V.; Mocanu, V.; Dicheva, N.; Parker, C. E.; Wetsel, W. C.; Mosier, P. D.; Westkaemper, R. B.; Allen, J. A.; Zjawiony, J. K.; Roth, B. L. Structure-based design, synthesis, and biochemical and pharmacological characterization of novel salvinorin A analogues as active state probes of the kappa-opioid receptor. *Biochemistry* **2009**, 48, 6898-6908.
13. Appavu, C.; Li, S.; Susan, L.; Aram, O.; Jianyao, W.; JoAnn, S. Reversible Covalent Binding of Neratinib to Human Serum Albumin In Vitro. *Drug Metab. Lett.* **2010**, 4, 220-227.
14. Winkler, J. D.; Thermos, K.; Weiss, B. Differential effects of fluphenazine-N-mustard, on calmodulin activity and on D<sub>1</sub> and D<sub>2</sub> dopaminergic responses. *Psychopharmacology* **1987**, 92, 285-291.
15. Chen, J. F.; Aloyo, V. J.; Qin, Z.-H.; Weiss, B. Irreversible blockade of D<sub>2</sub> dopamine receptors by fluphenazine-N-mustard increases D<sub>2</sub> dopamine receptor mRNA and proenkephalin mRNA and decreases D<sub>1</sub> dopamine receptor mRNA and mu and delta opioid receptors in rat striatum. *Neurochem. Int.* **1994**, 25, 355-366.
16. Xu, S. X.; Hatada, Y.; Black, L. E.; Creese, I.; Sibley, D. R. N-(p-isothiocyanatophenethyl)piperone, a selective and irreversible antagonist of D<sub>2</sub> dopamine receptors in brain. *J. Pharm. Exp. Ther.* **1991**, 257, 608-615.
17. Thompson, T. L.; Bridges, S. R.; Weirs, W. J. Alteration of dopamine transport in the striatum and nucleus accumbens of ovariectomized and estrogen-primed rats following N-(p-isothiocyanatophenethyl) spiperone (NIPS) treatment. *Brain Res. Bull.* **2001**, 54, 631-638.
18. McDougall, S. A.; Rudberg, K. N.; Veliz, A.; Dhargalkar, J. M.; Garcia, A. S.; Romero, L. C.; Gonzalez, A. E.; Mohd-Yusof, A.; Crawford, C. A. Importance of D<sub>1</sub> and D<sub>2</sub> receptor stimulation for the induction and expression of cocaine-induced behavioral sensitization in preweanling rats. *Behav. Brain Res.* **2017**, 326, 226-236.
19. Nilsson, C. L.; Ekman, A.; Hellstrand, M.; Eriksson, E. Inverse Agonism at Dopamine D<sub>2</sub> Receptors. *Neuropsychopharmacology* **1996**, 15, 53-61.

20. Weichert, D.; Kruse, A. C.; Manglik, A.; Hiller, C.; Zhang, C.; Hübner, H.; Kobilka, B. K.; Gmeiner, P. Covalent agonists for studying G protein-coupled receptor activation. *PNAS* **2014**, 111, 10744-10748.
21. Davie, B. J.; Sexton, P. M.; Capuano, B.; Christopoulos, A.; Scammells, P. J. Development of a photoactivatable allosteric ligand for the M<sub>1</sub> muscarinic acetylcholine receptor. *ACS Chem. Neurosci.* **2014**, 5, 902-907.
22. Dormán, G.; Prestwich, G. D. Using photolabile ligands in drug discovery and development. *Trends Biotechnol.* **2000**, 18, 64-77.
23. Xu, B.; Wu, L. Analysis of receptor-ligand binding by photoaffinity cross-linking. *Sci. China Chem.* **2014**, 57, 232-242.
24. Lapinsky, D. J. Tandem photoaffinity labeling-bioorthogonal conjugation in medicinal chemistry. *Bioorg. Med. Chem.* **2012**, 20, 6237-6247.
25. Smith, E.; Collins, I. Photoaffinity labeling in target- and binding-site identification. *Future Med. Chem.* **2015**, 7, 159-183.
26. Grunbeck, A.; Sakmar, T. P. Probing G protein-coupled receptor-ligand interactions with targeted photoactivatable cross-linkers. *Biochemistry* **2013**, 52, 8625-8632.
27. Brune, S.; Pricl, S.; Wunsch, B. Structure of the sigma<sub>1</sub> receptor and its ligand binding site. *J. Med. Chem.* **2013**, 56, 9809-9819.
28. Gomes, I.; Jordan, B. A.; Gupta, A.; Rios, C.; Trapaidze, N.; Devi, L. A. G protein coupled receptor dimerization: implications in modulating receptor function. *J. Mol. Med.* **2001**, 79, 226-242.
29. Benovic, Jeffrey L. G-Protein-Coupled Receptors Signal Victory. *Cell* **2012**, 151, 1148-1150.
30. Niznik, H. B.; Guan, J. H.; Neumeyer, J. L.; Seeman, P. A photoaffinity ligand for dopamine D<sub>2</sub> receptors: azidoclebopride. *Mol. Pharmacol.* **1985**, 27, 193-199.
31. Wouters, W.; Vandun, J.; Laduron, P. M. Photoaffinity-Labeling of Human-Brain Dopamine-Receptors. *Biochem. Pharmacol.* **1984**, 33, 3517-3520.
32. Amlaiky, N.; Caron, M. G. Photoaffinity labeling of the D<sub>2</sub>-dopamine receptor using a novel high affinity radioiodinated probe. *J. Biol. Chem.* **1985**, 260, 1983-1986.
33. Nishikori, K.; Noshiro, O.; Sano, K.; Maeno, H. Characterization, solubilization, and separation of two distinct dopamine receptors in canine caudate nucleus. *J. Biol. Chem.* **1980**, 255, 10909-10915.
34. Neumeyer, J. L.; Guan, J. H.; Niznik, H. B.; Dumbrille-Ross, A.; Seeman, P.; Padmanabhan, S.; Elmaleh, D. R. Novel photoaffinity label for the dopamine D<sub>2</sub> receptor: synthesis of 4-amino-5-iodo-2-methoxy-N-[1-(phenylmethyl)-4-

- piperidinyl]benzamide (iodoazidocleboopride, IAC) and the corresponding <sup>125</sup>I-labeled analog (<sup>125</sup>IAC). *J. Med. Chem.* **1985**, 28, 405-407.
35. Niznik, H. B.; Dumbrille-Ross, A.; Guan, J. H.; Neumeyer, J. L.; Seeman, P. Dopamine D<sub>2</sub> receptors photolabeled by iodo-azido-cleboopride. *Neurosci. Lett.* **1985**, 55, 267-272.
  36. Kanety, H.; Fuchs, S. Immuno-photoaffinity labeling of the D<sub>2</sub>-dopamine receptor. *Biochem. Bioph. Res. Co.* **1988**, 155, 930-936.
  37. Redouane, K.; Sokoloff, P.; Schwartz, J.-C.; Hamdi, P.; Mann, A.; Wermuth, C. G.; Roy, J.; Morgat, J.-L. Photoaffinity labeling of D-2 dopamine binding subunits from rat striatum, anterior pituitary and olfactory bulb with a new probe, [<sup>3</sup>H] azidosulpride. *Biochem. Bioph. Res. Co.* **1985**, 130, 1086-1092.
  38. Niznik, H. B.; Grigoriadis, D. E.; Seeman, P. Photoaffinity labelling of dopamine D<sub>2</sub> receptors by [<sup>3</sup>H]azidomethylspiperone. *FEBS Lett.* **1986**, 209, 71-76.
  39. Chien, E. Y.; Liu, W.; Zhao, Q.; Katritch, V.; Han, G. W.; Hanson, M. A.; Shi, L.; Newman, A. H.; Javitch, J. A.; Cherezov, V.; Stevens, R. C. Structure of the human dopamine D<sub>3</sub> receptor in complex with a D<sub>2</sub>/D<sub>3</sub> selective antagonist. *Science*. **2010**, 330, 1091-1095.
  40. Shi, L.; Javitch, J. A. The binding site of aminergic G protein-coupled receptors: the transmembrane segments and second extracellular loop. *Annu. Rev. Pharmacol. Toxicol.* **2002**, 42, 437-467.
  41. Newman, A. H. B., T.; Banala, A. K.; Donthamsetti, P.; Pongetti, K.; LaBounty, A.; Levy, B.; Cao, J.; Michino, M.; Luedtke, R. R.; Javitch, J. A.; Shi, L. Molecular Determinants of Selectivity and Efficacy at the Dopamine D<sub>3</sub> Receptor. *J. Med. Chem.* **2012**, 55, 6689-6699.
  42. Shonberg, J.; Herenbrink, C. K.; Lopez, L.; Christopoulos, A.; Scammells, P. J.; Capuano, B.; Lane, J. R. A structure-activity analysis of biased agonism at the dopamine D<sub>2</sub> receptor. *J. Med. Chem.* **2013**, 56, 9199-221.
  43. Weichert, D.; Banerjee, A.; Hiller, C.; Kling, R. C.; Hübner, H.; Gmeiner, P. Molecular Determinants of Biased Agonism at the Dopamine D<sub>2</sub> Receptor. *J. Med. Chem.* **2015**, 58, 2703-2717.
  44. Szabo, M.; Klein Herenbrink, C.; Christopoulos, A.; Lane, J. R.; Capuano, B. Structure-Activity Relationships of Privileged Structures Lead to the Discovery of Novel Biased Ligands at the Dopamine D<sub>2</sub> Receptor. *J. Med. Chem.* **2014**, 57, 4924-4939.
  45. Lane, J. R.; Donthamsetti, P.; Shonberg, J.; Draper-Joyce, C. J.; Dentry, S.; Michino, M.; Shi, L.; Lopez, L.; Scammells, P. J.; Capuano, B.; Sexton, P. M.; Javitch, J. A.;

- Christopoulos, A. A new mechanism of allostery in a G protein-coupled receptor dimer. *Nat. Chem. Biol.* **2014**, 10, 745-752.
46. Ballesteros, J. A.; Weinstein, H. [19] Integrated methods for the construction of three-dimensional models and computational probing of structure-function relations in G protein-coupled receptors. In *Methods in Neurosciences*, Stuart, C. S., Ed. Academic Press: 1995; Vol. 25, pp 366-428.
47. Shonberg, J.; Draper-Joyce, C.; Mistry, S. N.; Christopoulos, A.; Scammells, P. J.; Lane, J. R.; Capuano, B. Structure-Activity Study of *N*-((trans)-4-(2-(7-Cyano-3,4-dihydroisoquinolin-2(1*H*)-yl)ethyl)cyclohexyl)-1*H*-indole-2-carboxamide (SB269652), a Bitopic Ligand That Acts as a Negative Allosteric Modulator of the Dopamine D<sub>2</sub> Receptor. *J. Med. Chem.* **2015**, 58, 5287-5307.
48. Bräse, S.; Gil, C.; Knepper, K.; Zimmermann, V. Organic Azides: An Exploding Diversity of a Unique Class of Compounds. *Angew. Chem. Int.l Ed.* **2005**, 44, 5188-5240.
49. Andersen, J.; Madsen, U.; Bjorkling, F.; Liang, X. F. Rapid synthesis of aryl azides from aryl halides under mild conditions. *Synlett* **2005**, 2209-2213.
50. Leach, K.; Sexton, P. M.; Christopoulos, A. Allosteric GPCR modulators: taking advantage of permissive receptor pharmacology. *Trends Pharmacol. Sci.* **2007**, 28, 382-389.
51. Christopoulos, A. Assessing the distribution of parameters in models of ligand-receptor interaction: to log or not to log. *Trends Pharmacol. Sci.* **1998**, 19, 351-357.
52. Jiang, L. I.; Collins, J.; Davis, R.; Lin, K.-M.; DeCamp, D.; Roach, T.; Hsueh, R.; Rebres, R. A.; Ross, E. M.; Taussig, R.; Fraser, I.; Sternweis, P. C. Use of a cAMP BRET Sensor to Characterize a Novel Regulation of cAMP by the Sphingosine 1-Phosphate/G<sub>13</sub> Pathway. *J. Biol. Chem.* **2007**, 282, 10576-10584.
53. Cheng, Y.; Prusoff, W. H. Relationship between the inhibition constant (K<sub>1</sub>) and the concentration of inhibitor which causes 50 per cent inhibition (I<sub>50</sub>) of an enzymatic reaction. *Biochem. Pharmacol.* **1973**, 22, 3099-108.
54. May, L. T.; Leach, K.; Sexton, P. M.; Christopoulos, A. Allosteric modulation of G protein-coupled receptors. *Annu. Rev. Pharmacol. Toxicol.* **2007**, 47, 1-51.

---

## **Chapter 5**

# **Thesis Outcomes and Future Directions**

---

The overarching aim of this thesis has been to demonstrate the utility of multivalent ligands as chemical probes for the investigation of dopamine D<sub>2</sub> receptor (D<sub>2</sub>R) pharmacology using the extended scaffolds of aripiprazole and SB269652. As such, through the use of common medicinal chemistry strategies such as traditional and retrospective fragment-based structure-activity relationship (SAR) studies, we have been able to investigate the molecular determinants of efficacy and allostery at the D<sub>2</sub>R. Affinity labelling strategies were also employed in the development of photoactivatable tools for the investigation of both bitopic and allosteric receptor-ligand interactions at the D<sub>2</sub>R.

## Chapter 2: Probing Efficacy at the Dopamine D<sub>2</sub> Receptor

Chapter 2 demonstrated the use of multivalent ligands as a tool for investigating the molecular determinants of efficacy at the D<sub>2</sub>R. Sub-chapter 2.1 in particular, focussed on the synthesis and pharmacological evaluation of progressively fragmented synthons of aripiprazole in a bid to determine key structural attributes that are important for its efficacy at the D<sub>2</sub>R. From this study it was determined that the 1,2,3,4-tetrahydroquinolin-2-one (THQ) tail of aripiprazole was a key determinant of functional affinity ( $K_A = 12.8$  nM, 777-fold) and efficacy ( $\tau = 0.940$ , 3-fold), causing enhancements in both parameters upon attachment to the orthosterically-binding 1-(2,3-dichlorophenyl)piperazine (DCPP) head group ( $K_A = 9941$  nM;  $\tau = 0.365$ ). Intriguingly, attachment of the THQ moiety (**14**) to a series of pharmacologically-diverse, orthosterically-engaging D<sub>2</sub>R molecules also caused enhancements in affinity and a trend towards increased efficacy, particularly for agonist structures. Furthermore, using these hybrid structures, mutagenesis studies revealed that the nature of secondary binding interactions within the extracellular regions of transmembrane helices (TMs) 1 and 2 of the D<sub>2</sub>R were able to modulate the efficacy of extended ligands in differing directions. Accordingly, Sub-chapter 2.2 evaluated the notion of modulating efficacy at the D<sub>2</sub>R using differing tail structures. In a preliminary investigation, a series of hybrid molecules incorporating the 7-azaindole-2-carboxamide tail of the highest affinity SB269652 analogue from our previous SAR study, were synthesised and displayed potency-enhancing properties at the D<sub>2</sub>R. Changes in efficacy, however, were not observed. From these results it is clear that the potency and efficacy of these extended structures is dependent on the nature and composition of the tail moiety.

As a direct follow-up to the preliminary work presented in Sub-chapter 2.2, further evaluation of the functional affinity ( $K_A$ ) and efficacy ( $\tau$ ) of these hybrid ligands is required in order to determine their impact on D<sub>2</sub>R pharmacology. Furthermore, given the indole-2-

carboxamide tail of SB269652 is considered a key structural determinant of its negative cooperativity, it would be judicious to also evaluate whether these 7-azaindole-2-carboxamidoalkyl-containing hybrid molecules are able to exert cooperativity in the presence of dopamine. Overall, while a crystal structure of the D<sub>2</sub>R remains elusive, future prospects for probing the molecular determinants of efficacy at the D<sub>2</sub>R lie in the evaluation of other extended D<sub>2</sub>R structures with structurally diverse tail moieties (e.g. ziprasidone, risperidone and bifeprunox, Figure 1). Retrospective fragment-based SAR analysis in conjunction with mutagenesis and computational efforts, could potentially aid the development of a suite of tail moieties which could be used to tune efficacy at the D<sub>2</sub>R. This in turn could aid the rational design of high affinity D<sub>2</sub>R-acting ligands with desired efficacies or, the redevelopment of existing therapeutics in a bid to lower their propensity for causing unwanted side-effects.

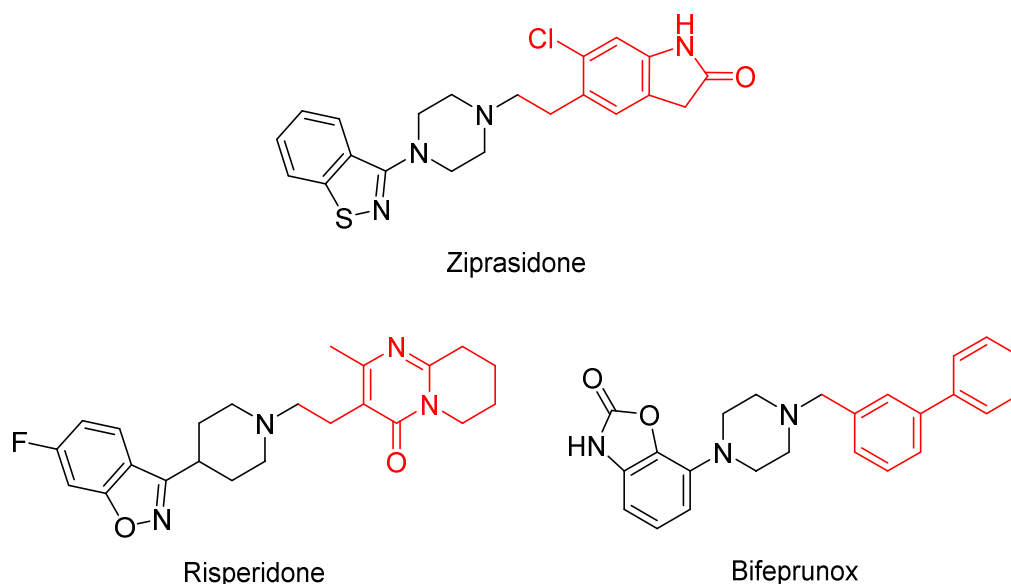


**Figure 1.** The chemical structures of D<sub>2</sub>R ligands with extended structures; ziprasidone, risperidone and bifeprunox (tail moieties which extend away from the orthosteric binding site are highlighted in red).

### Chapter 3: Probing Allostery at the Dopamine D<sub>2</sub> Receptor

Chapter 3 centred on utilising multivalent ligands as a chemical probe for the investigation of allostery at the D<sub>2</sub>R. Herein, a traditional SAR investigation of SB269652 was conducted and structural modifications of the allosterically-binding indole-2-carboxamide tail yielded a number of analogues displaying a spectrum of negative cooperativities. Key SAR findings include that fluorine-substitution around the benzo portion of the indole-2-carboxamide ring yielded relatively high affinity analogues which were able to modulate cooperativity at the D<sub>2</sub>R. The methoxy-substituted derivatives in general, however, proved to be detrimental to negative

cooperativity. Furthermore, incorporation of a second nitrogen atom within the indole-ring, and the subsequent repositioning of the carboxamide attachment point (2- versus 3-substitution) was very well tolerated and yielded two analogues which displayed both high affinity and negative cooperativity. As such, we discovered a first-in-class analogue of SB269652 that demonstrated sub-nanomolar functional affinity for the D<sub>2</sub>R and could modulate both the affinity and efficacy of dopamine (**15e**, Chapter 3, Figure 2). Finally, the N-methylated derivatives and the “best of” SB269652 analogues derived from our initial SAR study highlighted the difficulty in developing SAR for bitopic allosteric modulators and provided a timely reminder that SAR is not necessarily an additive phenomenon.

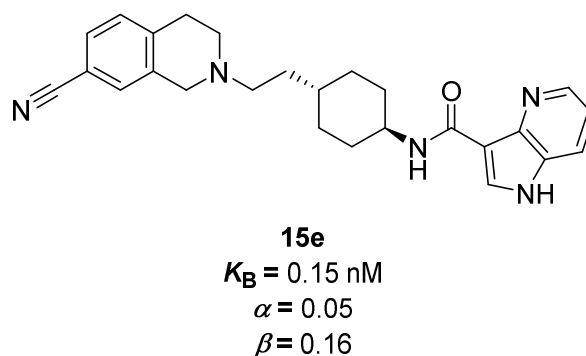


**Figure 2.** Compound **15e** is a first-in-class analogue of SB269652 which can modulate both the affinity (20-fold) and efficacy (6-fold) of dopamine at the D<sub>2</sub>R.

Future prospects for this work include further investigation of ring activating (e.g. OH or alkyl) or deactivating (e.g. Cl, Br or I) substituted tail moieties and their effect on negative cooperativity at the D<sub>2</sub>R. This would enable us to determine whether electron-withdrawing moieties are beneficial for negative cooperativity or if it may be related to the relative sizes of the substituents. Re-positioning of the indole-carboxamide tail may also be a worthwhile pursuit given that the indole-3-carboxamide analogues led to the discovery of a high affinity analogue with a novel pharmacological profile. Furthermore, based on the analogues generated in Chapter 3 and those investigated in our initial SAR investigation, we have now generated a wide variety of analogues with a spectrum of negative cooperativities. As such, preliminary *in vivo* investigations in behavioural animal models would provide insight into whether D<sub>2</sub>R negative allosteric modulators (NAMs) with low or high negative cooperativities may have therapeutic utility in treating CNS disorders such as schizophrenia.

#### **Chapter 4: Probing Receptor-ligand Interactions at the Dopamine D<sub>2</sub> Receptor**

Finally, Chapter 4 illustrated the successful design, synthesis and preliminary evaluation of photoactivatable azide derivatives of SB269652. Due to the lack of literature surrounding receptor-ligand interactions of bitopic and allosterically-engaging D<sub>2</sub>R ligands, the encouraging results observed in Chapter 4 demonstrate that irreversible analogues of extended D<sub>2</sub>R structures are capable of selectively capturing the binding site of interest. However, the development of such ligands requires sound SAR knowledge of the ligand of interest in order to determine ideal attachment points for photoactivatable or chemoreactive moieties. Due to time constraints, the optimisation of crosslinking experiments to deduce whether the 5-azidoindole-2-carboxamide derivative was an irreversible ligand was not carried out. Nonetheless, the results obtained in Chapter 4 demonstrate that irreversible probes may be an ideal strategy to employ in order to further our knowledge of a receptor-target which plays such a pivotal role in the symptoms of diseases such as schizophrenia.

Since the results presented in Chapter 4 are an initial effort toward developing multivalent irreversible probes for the D<sub>2</sub>R, further refinement in experimental procedures is required. Kinetic binding studies of SB269652 and the photoactivatable probes synthesised, would enable the optimisation of crosslinking experiments and confirm whether kinetics played a role in the results observed in Chapter 4. Other future prospects for this work may also include the development of alternative irreversible SB269652 analogues comprising other photoactivatable or chemoreactive moieties. Given its relative similarity in size and structure to the azide moiety, it could be envisaged that derivatives of SB269652 containing an isothiocyanate functional group could successfully yield a series of chemoreactive D<sub>2</sub>R probes (Figure 3). Furthermore, it would be worthwhile to determine whether these ligands are able to trigger ligand-induced thermostability upon irreversibly binding the D<sub>2</sub>R. The 7-azido-1,2,3,4-tetrahydroisoquinoline derivative, in particular, may have the ability to constrain the D<sub>2</sub>R in a conformation that is favourable for crystallisation since it is able to engage both the orthosteric and allosteric binding site of the D<sub>2</sub>R in a similar manner to SB269652.

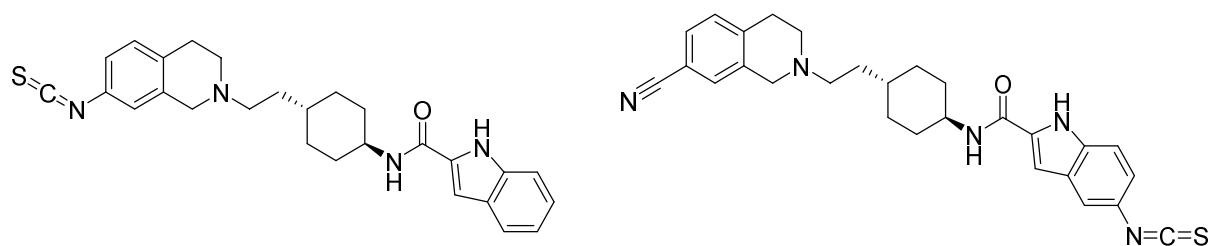


**Figure 3.** The proposed chemical structures of chemoreactive derivatives of SB269652 containing the isothiocyanate functional group.

This body of work clearly demonstrates that multivalent ligands have a great deal of value as chemical probes for the investigation of the D<sub>2</sub>R. Through the strategic use of medicinal chemistry techniques and pharmacological evaluation, we have been able to gain insight into the molecular determinants of efficacy and negative cooperativity at the D<sub>2</sub>R, and develop a tool that could provide insight into bitopic and allosteric receptor-ligand interactions without the aid of a crystal structure. Although this work may be considered time-intensive, it has provided information into previously unexplored aspects of D<sub>2</sub>R pharmacology and provides a new strategy for the investigation of other receptors that cannot be crystallised using current methodologies.

---

---

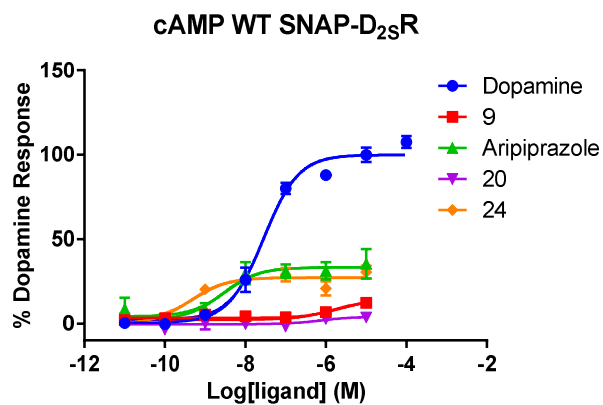
# Appendices

---

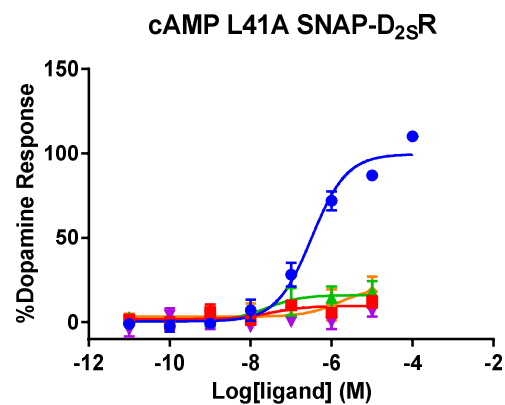
---

## Appendix 1. Chapter 2 Supplementary Material

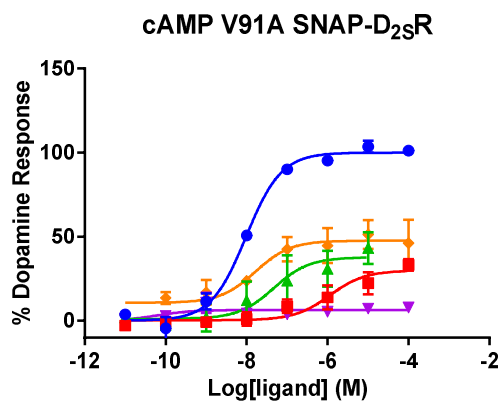
A



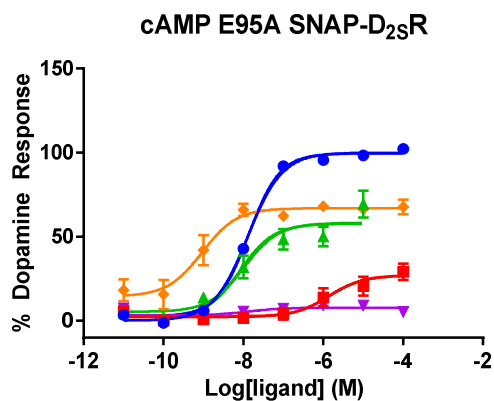
B



C



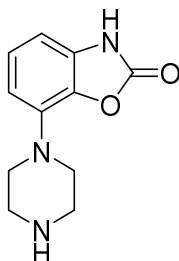
D



**A1.1** Apparent changes in efficacy were observed for the phenylpiperazine-containing hybrids and their privileged scaffolds.

**A1.2** Synthesis procedure for a key intermediate required for the synthesis of **55**.

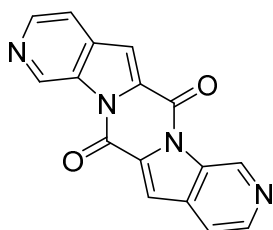
**7-(Piperazin-1-yl)benzo[d]oxazol-2(3H)-one**



Bis(2-chloroethyl)amine (4.31 g, 30.3 mmol) was taken up in 1,4-dioxane (80 mL), and to this a solution of 7-aminobenzo[d]oxazol-2(3H)-one (3.80 g, 25.3 mmol) in a minimum amount of 1,4-dioxane was added. The mixture was stirred at reflux for 72 h. The reaction solvent was decanted from the reaction vessel, leaving behind a dark residue. The residue was washed with 1,4-dioxane (3 x 50 mL) and purified using preparative HPLC. This yielded the product as a pale brown solid (301 mg, 5%). <sup>1</sup>H NMR (D<sub>2</sub>O) δ 7.16 (t, *J* = 8.1 Hz, 1H), 6.88 (d, *J* = 7.9 Hz, 1H), 6.81 (d, *J* = 8.4 Hz, 1H), 3.47 (dd, *J* = 7.0, 3.4 Hz, 4H), 3.41 (dd, *J* = 7.0, 3.4 Hz, 4H). <sup>13</sup>C NMR (D<sub>2</sub>O) δ 156.3 (C), 134.4 (C), 133.5 (C), 130.6 (C), 125.1 (CH), 111.3 (CH), 105.2 (CH), 46.4 (CH<sub>2</sub>), 43.1 (CH<sub>2</sub>).

## Appendix 2. Chapter 3 Supplementary Material

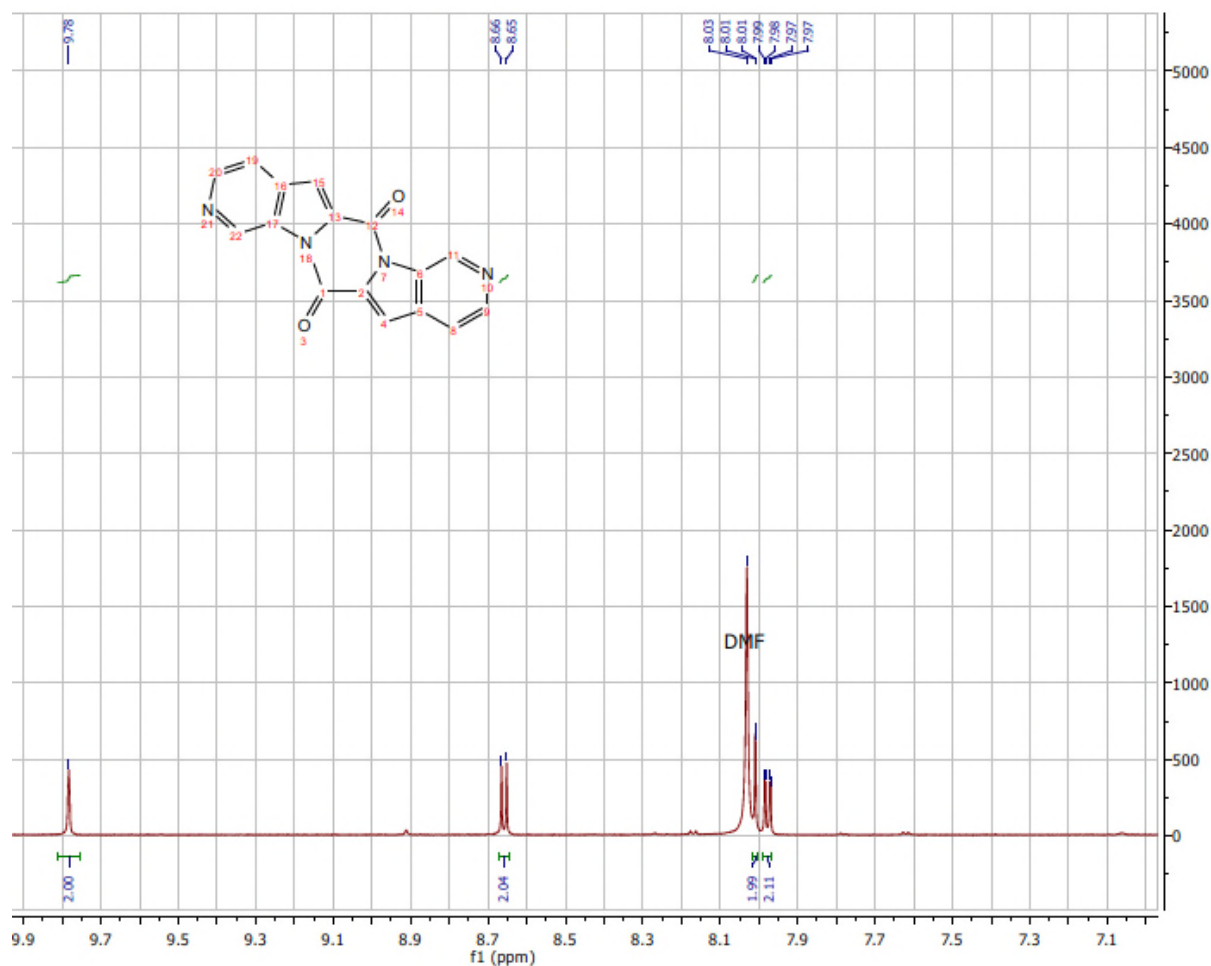
A2.1 The structure and  $^1\text{H}$  NMR spectrum (A), and LCMS spectrum (B) of the self-dimerised by-product yielded in an amide coupling of 1*H*-pyrrolo[2,3-*c*]pyridine-2-carboxylic acid



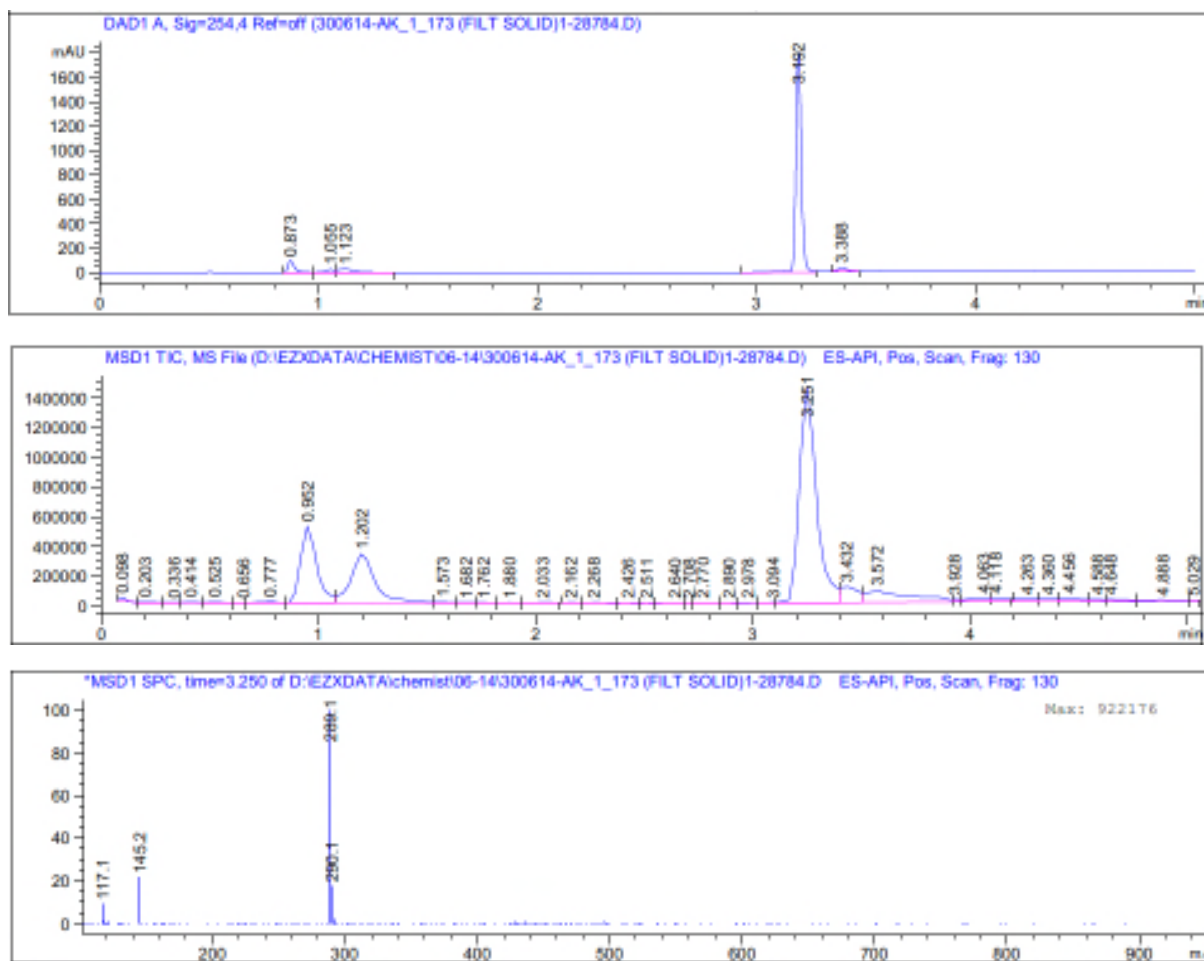
Chemical Formula:  $\text{C}_{16}\text{H}_8\text{N}_4\text{O}_2$

Molecular Weight: 288.27

A)



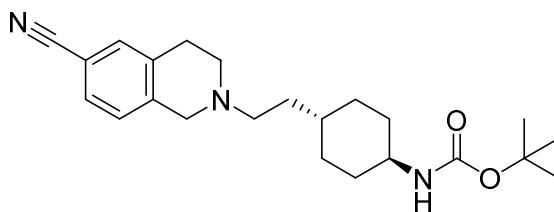
B)

LCMS ( $m/z$ ):  $[M+H]^+$  289.1

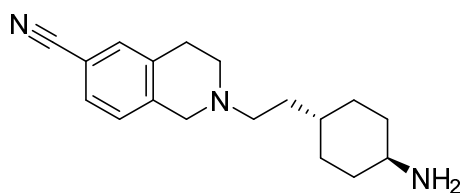
## A2.2 Synthesis and pharmacological evaluation of an SB269652 analogue (**40**) containing the head moiety of SB277011-A.

We synthesised an analogue containing the head group of SB277011-A, a D<sub>3</sub>R-selective antagonist discovered by SmithKlein Beecham in the same study as **1** to evaluate the effect of 6-substituted head groups on negative cooperativity at the D<sub>2</sub>R.<sup>1</sup> Compound **40** demonstrated 9-fold weaker negative cooperativity and similar functional affinity compared to **1** at the D<sub>2</sub>R. As such, it was determined that small substituents at the 7-position of the head moiety was optimal for NAM activity at the D<sub>2</sub>R.

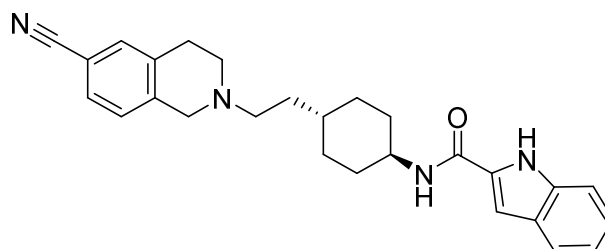
### *tert*-Butyl ((*trans*)-4-(2-(6-cyano-3,4-dihydroisoquinolin-2(1*H*)-yl)ethyl)cyclohexyl)carbamate<sup>2</sup>



Using 1,2,3,4-tetrahydroisoquinoline-6-carbonitrile as the amine and *tert*-butyl ((*trans*)-4-(2-oxoethyl)cyclohexyl)carbamate as the aldehyde, General Procedure A was followed. The resultant product obtained was a pale yellow oil (38.2 mg, 48%). <sup>1</sup>H NMR (CDCl<sub>3</sub>) δ 7.41 (m, 2H), 7.13 (d, *J* = 8.0 Hz 1H), 4.29 (br s, 1H), 3.76 (s, 2H), 3.30 (br, s, 1H), 3.11- 2.26 (m, 6H), 2.03-1.84 (m, 2H), 1.78-1.65 (m, 2H), 1.63- 1.42 (m, 5H), 1.37 (s, 9H), 1.04- 0.99 (m, 2H); <sup>13</sup>C NMR (CDCl<sub>3</sub>) δ 155.3 (C), 140.3 (C), 135.8 (C), 132.5 (CH), 129.2 (CH), 127.4 (CH), 119.1 (C), 110.0 (C), 79.1 (C), 56.1 (CH<sub>2</sub>), 56.0 (CH<sub>2</sub>), 50.2 (CH<sub>2</sub>), 49.8 (CH), 35.2 (CH), 33.9 (CH<sub>2</sub>), 33.4 (CH<sub>2</sub>), 31.9 (CH<sub>2</sub>), 28.7 (CH<sub>2</sub>), 28.4 (CH<sub>3</sub>). LCMS (*m/z*): C<sub>23</sub>H<sub>33</sub>N<sub>3</sub>O<sub>2</sub> requires [M+H]<sup>+</sup> 384.3; found 384.3.

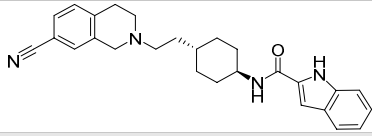
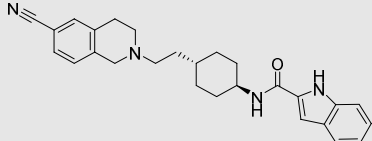
2-(2-((*trans*)-4-Aminocyclohexyl)ethyl)-1,2,3,4-tetrahydroisoquinoline-6-carbonitrile<sup>2</sup>

Using *tert*-butyl ((*trans*)-4-(2-(6-cyano-3,4-dihydroisoquinolin-2(1*H*)-yl)ethyl)cyclohexyl)carbamate as the protected amine, General Procedure B was followed to yield a yellow oil in quantitative yields (59.9 mg). <sup>1</sup>H NMR (CDCl<sub>3</sub>) δ 7.38 – 7.30 (m, 2H), 7.08 (d, *J* = 8.1 Hz, 1H), 3.61 (s, 2H), 2.88 (app t, *J* = 6.0 Hz, 2H), 2.73 – 2.39 (m, 6H), 1.85 (m, 4H), 1.51 – 1.39 (m, 3H), 1.34 – 1.17 (m, 1H), 1.16 – 0.88 (m, 4H). <sup>13</sup>C NMR (CDCl<sub>3</sub>) δ 140.6 (C), 135.9 (C), 132.4 (CH), 129.1 (CH), 127.4 (CH), 123.8 (CH), 119.1 (C), 109.9 (C), 56.2 (CH<sub>2</sub>), 56.1 (CH<sub>2</sub>), 50.3 (CH<sub>2</sub>), 35.2 (CH), 34.1 (CH<sub>2</sub>), 31.97 (CH<sub>2</sub>), 29.0 (CH<sub>2</sub>), 28.8 (CH<sub>2</sub>). LCMS (*m/z*): [M+H]<sup>+</sup> found 284.2.

*N*-((*trans*)-4-(2-(6-Cyano-3,4-dihydroisoquinolin-2(1*H*)-yl)ethyl)cyclohexyl)-1*H*-indole-2-carboxamide<sup>1</sup>

2-(2-((*trans*)-4-Aminocyclohexyl)ethyl)-1,2,3,4-tetrahydroisoquinoline-6-carbonitrile (58.6 mg, 206 μmol) was added to an rbf containing DCM. To this, 1*H*-indole-2-carboxylic acid (37.0 mg, 230 μmol) and (Benzotriazol-1-yl)oxytris(dimethylamino)phosphonium hexafluorophosphate (BOP) (152 mg, 344 μmol) were added along with an excess of DIPEA. The reaction mixture was stirred at rt for 3 h, after which, precipitate had formed. The precipitate was collected *via* vacuum filtration and washed with cold water and DCM and left to dry. The resultant product was off-white solid which was obtained in good yield (31.5 mg, 31.2%). <sup>1</sup>H NMR (*d*<sub>6</sub>-DMSO) δ 11.51 (s, 1H), 8.19 (d, *J* = 8.0 Hz, 1H), 7.62 – 7.55 (m, 3H), 7.42 (d, *J* = 8.2 Hz, 1H), 7.29 (d, *J* = 8.0 Hz, 1H), 7.19 – 7.11 (m, 2H), 7.02 (m, 1H), 3.75 (m, 3H), 2.86 (m, 2H), 2.70 (br s, 1H), 2.55 (m, 2H), 1.98 – 1.72 (m, 4H), 1.55 – 1.07 (m, 8H). <sup>13</sup>C NMR (*d*<sub>6</sub>-DMSO) δ 160.6 (C), 136.8 (2 C), 136.5 (C), 132.7 (CH), 132.5 (C), 129.5 (CH), 128.2 (CH), 127.5 (C), 123.6 (CH),

121.9 (CH), 120.1 (CH), 119.5 (C), 112.7 (CH), 109.2 (C), 102.9 (CH), 55.8 (CH<sub>2</sub>), 50.2 (CH<sub>2</sub>), 48.6 (CH), 35.2 (CH), 32.8 (CH<sub>2</sub>), 32.2 (CH<sub>2</sub>), 28.6 (CH<sub>2</sub>). HPLC: *t*<sub>R</sub> 6.22 min, >95% purity. HRMS (*m/z*): C<sub>27</sub>H<sub>31</sub>N<sub>5</sub>O requires [M+H]<sup>+</sup> 427.2426; found 427.2499.

Compound	Structure	p <i>K</i> <sub>B</sub> ± SEM ( <i>K</i> <sub>B</sub> , nM)	Log <i>αβ</i> ± SEM ( <i>αβ</i> ) <sup>a</sup>
1		6.11 ± 0.02 (776)	-1.23 ± 0.14 (0.06)
40		6.28 ± 0.24 (524)	-0.29 ± 0.05* (0.51)

Determined by ERK1/2 phosphorylation studies in the presence of dopamine. Data represents the mean ± SEM of three individual experiments conducted in duplicate; <sup>a</sup> Compound demonstrated a Schild slope significantly different from unity, therefore, the compound demonstrated negative cooperativity. (\*) Statistically different from the corresponding parameters for **1** (*p* < 0.05, one-way ANOVA, Dunnett's post-hoc test).

## References

1. Branch, C. L.; Johnson, C. N.; Stemp, G.; . Preparation of tetrahydroisoquinolines as modulators of dopamine D<sub>3</sub> receptors. WO1997043262 A1, 1999.
2. Stemp, G.; Ashmeade, T.; Branch, C. L.; Hadley, M. S.; Hunter, A. J.; Johnson, C. N.; Nash, D. J.; Thewlis, K. M.; Vong, A. K. K.; Austin, N. E.; Jeffrey, P.; Avenell, K. Y.; Boyfield, I.; Hagan, J. J.; Middlemiss, D. N.; Reavill, C.; Riley, G. J.; Routledge, C.; Wood, M. Design and synthesis of *trans*-*N*-[4-[2-(6-cyano-1,2,3,4-tetrahydroisoquinolin-2-yl)ethyl]cyclohexyl]-4-quinolinecarboxamide (SB-277011): A potent and selective dopamine D<sub>3</sub> receptor antagonist with high oral bioavailability and CNS penetration in the rat. *J. Med. Chem.* **2000**, 43, 1878-1885.

---

## List of Publications

**Kopinathan, A.**; Scammells, P. J.; Lane, J. R.; Capuano, B., Multivalent approaches and beyond: Novel tools for the investigation of the dopamine D<sub>2</sub> receptor pharmacology, *Future Med. Chem.*, **2016**, 8 (11), 1349-1372.

## Awards

Jun 2017      Postgraduate Publication Award  
May 2016      CTx Postgraduate and MGE Student Travel Award  
Jun 2015      Faculty of Pharmacy and Pharmaceutical Sciences 3-Minute Thesis, 1<sup>st</sup> place  
Jan 2012      Monash Honours Jubilee Scholarship

## Conference Presentations

**Kopinathan, A.**, *et al.* Elucidating the Structural Determinants of Agonist Efficacy at The Dopamine D<sub>2</sub> Receptor.

- Bayer Pharmaceuticals, Berlin, Germany. 8<sup>th</sup> September 2016. (Oral Presentation)
- Juniper Pharma Services, Nottingham, United Kingdom. 5-6<sup>th</sup> September 2016. (Oral Presentation)
- Centre for Biomolecular Sciences, Nottingham, United Kingdom. 2<sup>nd</sup> September 2016. (Oral presentation)

**Kopinathan, A.**, *et al.* The 7-Substituted 1,2,3,4-Tetrahydroquinolin-2-one Moiety of Aripiprazole is a Key Determinant of Efficacy at the Dopamine D<sub>2</sub> Receptor.

- EFMC-ISMC 24<sup>th</sup> International Symposium on Medicinal Chemistry, Manchester, United Kingdom. 28<sup>th</sup> August – 1<sup>st</sup> September 2016. (Poster Presentation)
- CTx Annual Postgraduate Student Research Symposium, CSIRO, Parkville, Melbourne, Australia. 15<sup>th</sup> June 2016. (Poster Presentation)

**Kopinathan, A.**, *et al.* Fragment-based SAR Investigation of Aripiprazole, MIPS Postgraduate Symposium, Monash University, Parkville, Melbourne, Australia. 1<sup>st</sup> October 2015. (Oral Presentation)